Molecular and Imaging Biomarkers of Radioresistance in Head and Neck Squamous Cell Carcinoma

Suh, Yae-Eun

Awarding institution:
King's College London

Molecular and Imaging Biomarkers of Radioresistance in Head and Neck Squamous Cell Carcinoma

A thesis presented for the degree of Doctor of Philosophy at King's College London

Yae-eun Suh

Molecular Oncology, Clinical Oncology and Imaging Sciences

Department of Mucosal & Salivary Biology

King's College London

2016

Abstract

The development of individualised treatments in head and neck squamous cell carcinoma (HNSCC) requires understanding of the molecular biology of cancer and the ability to translate this into therapy. Due to the heterogeneity of HNSCCs biomarkers are needed to identify the mechanisms of tumourigenesis and treatment resistance to improve outcome. Radioresistance is a major cause of treatment failure and early identification is key to the development of treatment strategies to overcome resistance and improve disease control.

MicroRNAs are small endogenous non-coding RNAs that regulate gene expression at the post-transcriptional level, and are a potential source of biomarkers. Altered expression has been reported in almost all types of cancer and directly implicated in tumourigenesis. We found miR-196a to be upregulated in a group of patients with HNSCC with recurrent disease after radical treatment. In HNSCC cell lines miR-196a exerted an oncogenic phenotype through targeting the protein annexin A1. In addition miR-196a overexpression resulted in resistance to irradiation, suggesting that it may represent both a prognostic and predictive biomarker in HNSCC.

Hypoxia is a well established biomarker of radioresistance in HNSCC and the association with poor outcome is well known. Many therapeutic strategies to overcome hypoxia have been developed, but accurately detecting tumour hypoxia has limited the translation of hypoxia modification strategies into routine practice. ^{64}Cu-ATSM PET is currently a research tool used to image hypoxia, and in combination with gene expression profiling of diagnostic biopsy samples, could provide early identification as well as the quantification and spatial distribution of hypoxia. We performed a pilot study in 15 patients with locally advanced oropharyngeal squamous cell carcinoma and demonstrated that increasing hypoxic volume defined by ^{64}Cu-ATSM PET was significantly associated with published hypoxia gene signatures in corresponding biopsy samples. We developed a ^{64}Cu-ATSM hypoxic volume specific gene signature, which can be applied prospectively to future samples and correlated with long term follow up to investigate its role as a biomarker. In addition, circulating miR-196a levels in patient plasma samples correlated with increasing tumour volume.

In conclusion, miR-196a may represent a biomarker of aggressive and radioresistant disease, partly through targeting annexin A1. ^{64}Cu-ATSM-defined hypoxic volume correlates with published hypoxia gene signatures, and in conjuction with gene signatures from biopsy samples, may represent a method for early identification of patients with radioresistant disease at a stage when management could be altered to improve outcome.

Table of contents

List of figures

List of tables

Acknowledgments

This work was carried out with the support of grants from the Comprehensive Cancer Imaging Centre, King's Health Partners and the Rosetrees Trust.

I would like to thank my supervisors Professor Mahvash Tavassoli and Dr Teresa Guerrero Urbano for taking me on as their student and for their continued guidance and support.

I would also like to thank Dr Joop Gäken at the Rayne Institute for providing reagents and training, Professor Eddy Odell and Rhonda Henley-Smith in Oral Pathology, Dr Sally Barrington, Lucy Pike, Joemon John and the techs in the Clinical PET Centre, and Dr Katherine Lawler who carried out the bioinformatics analyses. I would not have been able to complete this work without their help and expertise.

Thank you also to my fellow students and colleagues in the lab who helped fast track my lab skills and made life a lot more fun.

Finally, a huge thank you to my family, especially my parents and Simon, for putting up with me and encouraging me over the last few years, and for their endless support.

List of abbreviations

AGO2	Argonaute 2
AMPK	Adenosine monophosphate-activated protein kinase
ANXA1	Annexin A1
APS	Ammonium persulphate
ARCON	Accelerated radiotherapy with carbogen and nicotinamide
ATM	Ataxia telangiectasia mutated
ATP	Adenosine triphosphate
ATR	Ataxia telangiectasia and Rad3 related
ATR	Ataxia telangiectasia and Rad3-related protein
BNIP3	BCL2/adenovirus E1B 19kDa interacting protein 3
BSA	Bovine serum albumin
BTV	Biological target volume
CA9	Carbonic anhydrase
CCND1	Cyclin D1
CDK	Cyclin-dependent kinase
cDNA	Complementary DNA
chemoRT	Chemoradioation
CoA	Coenzyme A
CON	Carbogen and nicotinamide
COX	Cyclooxygenase
Ct	Cycle threshold
CT	Computed tomography
Cu-ATSM	Copper(II)-diacetyl-bis(N^4-methylthio-semicabazone)
Cu-PTSM	Copper(II)-pyruvaldehyde-bis(N^4-methylthio-semicabazone)
DAHANCA	Danish Head and Neck Cancer Group
DAPI	4',6-diamidino-2-phenylindole
DDR	DNA damage response
DFS	Disease free survival
DGCR8	DiGeorge syndrome critical region 8
dH_2O	Distilled water
DMEM	Dubecco's modified eagle media
DMSO	Dimethyl sulfoxide
DNA-PKcs	DNA-dependent protein kinase catalytic subunit
DSB	Double strand DNA break
DSS	Disease specific survival
E.Coli	Esherichia coli
ECL	Enhanced chemiluminescence
EDTA	Ehtylenediaminetetraacetic acid
EF5	Pentafluorinated etanidazole
EGFR	Epidermal growth factor receptor
EGTA	Ethylene glycol tetraacetic acid
EMT	Epithelial mesenchymal transition
ER	Endoplasmic reticulum
ERBB2/HER2	Human epidermal growth factor 2
ERG	ETS-related gene
ERK	Extracellular signal-regulated kinase
ETC	Electron transport chain
FBS	Foetal bovine serum
^{18}F-FAZA	^{18}Fluorine-fluoroazomycin arabinofuranoside
^{18}F-FDG	^{18}Fluorine-fluorodeoxyglucose
^{18}F-FLT	^{18}fluorine-fluorothymidine
^{18}F-FMISO	^{18}Fluorine-fluoromisonidazole
FFPE	Formalin fixed paraffin embedded
FIH	Factor-inhibiting hypoxia-inducible factor
FITC	Fluorescein isothiocyanate
FOX	Forkhead box
5-FU	5-fluorouracil

GAPDH	Glyceraldehyde-3-phosphate dehydrogenase
GBM	Glioblastoma
GFP	Green fluorescent protein
GLUT	Glucose transporters
GTP	Guanosine triphosphate
GTV	Gross tumour volume
Gy	Gray
Hb	Haemoglobin
HEBS	HEPES-buffered saline
HEPES	1-(2-hydroxyethyl)-1-piperanzineethanesulfonic acid
HF	Hypoxic fraction
HIF	Hypoxia-inducible factor
HMGA2	High mobility group AT-hook 2
HNSCC	Head and neck squamous cell carcinoma
HOX	Homeobox
HOX	Homeobox
HPV	Human papillomavirus
HRE	Hypoxia-responsive elements
HRP	Horseradish peroxide
HV	Hypoxic volume
IgG	Immunoglobulin G
IHC	Immunohistochemistry
IMRT	Intensity modulated radiotherapy
ING5	Inhibitor of growth 5
IκBα	Inhibitor of kappa B
JAK	Janus kinases
KD	Knockdown
KT5	Keratin 5
LB	Luria-Bertani
LDH	Lactate dehydrogenase
LRC	Locoregional control
LRC	Locoregional control
LSB	Lamelli sample buffer
LSB	Lamelli sample buffer
MAPK	Mitogen-activated protein kinase
MDM2	Mouse double minute 2 homolog
MDR	Multidrug resistance
MEK	Mitogen-activated protein kinase kinase
MET	Mesenchymal epithelial transition factor
miRNA	MicroRNA
MRI	Magnetic resonance imaging
mRNA	Messenger RNA
mTORC	Mammalian target of rapamycin complex
MTT	3-(4,5-Dimethylthiazol-2-yl)-2,5-diphenyltetrazolium bromide
NAD	Nicotinamide adenine dinucleotide
NADH	Nicotinamide adenine dinucleotide hydrogen
NF-κB	Nuclear factor kappa B
NPC	Nasopharyngeal cancer
NSCLC	Non-small cell lung cancer
OPN	Osteopontin
OPSCC	Oropharyngeal squamous cell carcinoma
OS	Overall survival
PAGE	Polyacrylamide gel electrophoresis
PARP	Poly ADP ribose polymerase
PBS	Phosphate-buffered saline
PDGF	Platelet-derived growth factor
PDH	Pyruvate dehydrogenase
PDK	Pyruvate dehydrogenase kinase
PE	Plating efficiency
PERK	Protein kinase R-like endoplastic reticulum kinase

PET	Positron emission tomography
PFA	Paraformaldehyde
PHD	Propyl hydroxylase
PI3K	Phosphatidylinositol 3-kinase
PIK3CA	Phosphatidylinositol-4,5-bisphosphate 3-kinase
PMSF	Phenylmethylsulfonyl fluoride
pO_2	Oxygen partial pressure
PTEN	Phosphatase and tensin homolog
qRT-PCR	Quantitative real time polymerase chain reaction
Rb	Retinoblastoma
RFP	Red fluorescent protein
RFS	Recurrence free survival
RISC	RNA-induced silencing complex
ROS	Reactive oxygen species
ROI	Region of interest
RT	Radiotherapy
RT-PCR	Reverse transcription polymerase chain reaction
S100A9	S100 calcium-binding protein A9
SCC	Squamous cell carcinoma
SDS	Sodium docecyl sulphate
SF	Survival fraction
shRNA	Small hairpin RNA
SNP	Single nucleotide polymorphism
SPRR2C	Small proline-rich protein 2C
STAT	Signal transducer and activator of transcription
SUV	Standardised uptake value
SUV_{max}	Maximum standardised uptake value
SUV_{mean}	Mean standardised uptake value
SUV_{peak}	Peak standardised uptake value
SV40	Simian virus 40
TBR	Tumour to background ratio
TBS	Tris-buffered saline
TBS-T	Tris-buffered saline-Tween
TCA	Tricarboxylic acid
TE	Tris-EDTA
TEMED	Tetramethylethylenediamine
TGF-β	Transforming growth factor β
TK1	Thymidine kinase 1
TLR8	Toll-like receptor 8
TMR	Tumour to muscle ratio
TPZ	Tirapazamine
TRAIL	Tumour necrosis factor-related apoptosis inducing ligand
Tris	Tris(hydroxymethyl)aminomethane
TSC	Tuberous sclerosis
TSG	Tumour suppressor gene
UPR	Unfolded protein response
UTR	Untranslated region
VEGF	Vascular endothelial growth factor
VHL	Von Hippel Lindau
VOI	Volume of interest
VSV-G	Glycoprotein G of the vesicular stomatitis virus
w/v	Weight/volume
ZEB	Zinc finger E-box binding homeobox

Chapter 1

Biomarkers in Head and Neck Squamous Cell Carcinoma

1.1 Introduction

There is an urgent need for biomarkers in head and neck cancer to improve the management and outcome of this patient population. The first half of the thesis (chapter 2) explores the early stages of molecular biomarker discovery in vitro in head and neck cancer, specifically microRNA-196a. The second half (chapter 3) focuses on hypoxia, a well known biomarker of radioresistance and poor outcome in head and neck cancer, and investigates the combination of molecular and novel imaging biomarkers to improve detection and translation into clinical practice. This first chapter summarises the current management of head and neck squamous cell carcinomas (HNSCC) and the need for biomarkers in this group of patients. Established and important molecular and imaging biomarkers under investigation will be reviewed followed by a review of microRNAs, hypoxia and ^{64}Cu-ATSM, the imaging biomarker investigated in the thesis.

1.2 Clinical background

Head and neck cancers encompass a heterogeneous group of tumours which, in general, are biologically aggressive in nature. They include the following subsites: oral cavity, oropharynx, hypopharynx, larynx, paranasal sinuses, nasal cavity, nasopharynx and salivary glands. Over 90% are squamous cell carcinomas arising from the epithelial cells that line the mucosal surfaces of the head and neck.[1] These cancers remain difficult to treat as they are often situated near critical anatomical structures that are sensitive to treatment-induced damage. Both tumour and treatment can cause severe, long-term and permanent adverse effects.

For patients who do not achieve locoregional control by surgery and/or (chemo)radiotherapy, there are few effective treatment options. Targeted therapies and predictive biomarkers are needed in order to improve the management and minimise the treatment toxicity, and to allow the selection of patients who are likely to benefit from conventional or novel therapies.

1.2.1 Incidence and risk factors

There were an estimated 686000 new cases of head and neck cancers worldwide in 2012, accounting for 4.8% of all malignancies, and an estimated 376000 deaths, equating to 4.6% of all cancer mortality.[2] In the UK in 2012 there were 9127 new cases and 2903 deaths of oral (lip, tongue, mouth, oropharynx, piriform sinus, hypopharynx) and larynx cancers.[3]

More than 75% of cases of head and neck squamous cell carcinomas are attributable to tobacco smoking and alcohol consumption. Smoking increases the risk by approximately 10-fold compared with never smokers, and heavy alcohol intake is an independent risk factor.[4] The combined effect of tobacco and alcohol causes a greater than multiplicative risk.[5] Public health measures have been successful in reducing the use of tobacco, and therefore the incidence of HNSCC overall has been decreasing over the last 30 years in developed countries. However, there has been a dramatic increase in the incidence rates of oropharyngeal (tonsil and base of tongue) cancers, predominantly in developed countries and at younger ages, due to infection with high-risk human papillomavirus (HPV).[6-8] Other cultural and habitual risk factors include chewing tobacco or Betel nut in South East Asia and drinking mate in South America.[9] A high incidence of aggressive HNSCC at a young age is seen in Fanconi's anaemia, a rare autosomal recessive disorder associated with chromosomal instability.[10]

1.2.2 Stage and treatment

The subsite and stage at presentation are predictive of survival and guides management. The treatment of an individual cancer is typically determined in a multidisciplinary setting, with additional tumour information, such as the histological subtype, and patient characteristics, such as fitness, baseline swallow and airway function, guiding optimal treatment strategies.

1.2.2.1 Early stage disease

Approximately one third of patients present with early stage (stage I and II) disease and in general have small primary tumours with no cervical nodal involvement. These patients are treated with either surgery and postoperative radiotherapy (RT) or primary radiotherapy depending on the primary tumour site, patient factors and patient choice, with cure rates of 70-90%.[11]

1.2.2.2 Locally advanced disease

The majority of patients present with locally advanced (stage III and IV) disease. Radical treatment in this situation requires multimodality therapy with surgery, commonly followed by postoperative RT or chemoradiotherapy (chemoRT), or organ preserving primary RT with or without concomitant chemotherapy with reduced cosmetic compromise.[12] Multimodality treatments are intensive and associated with severe acute toxicity, such as mucositis, dermatitis, and dysphagia, and long-term sequelae, for example sensorineural hearing loss, permanent xerostomia and altered swallowing function. The choice of treatment again depends on many factors and is determined on a case-by-case basis.

Resectable disease describes tumours that can be removed without causing unacceptable cosmetic and functional morbidity. Postoperative RT is standard treatment for patients with locally advanced tumours as they are at high risk of locoregional failure after surgery. Aggressive features of high risk of relapse include tumours with microscopically positive resection margins and extracapsular nodal disease.[13,14] Multiple involved nodes, close resection margins, T stage 3/4 disease, perineural and lymphovascular invasion are also factors that are be taken into consideration. In 2004, two mulit-centre randomised studies demonstrated that the addition of cisplatin chemotherapy to postoperative radiotherapy in high risk groups significantly improved outcomes and therefore postoperative chemoRT became the standard of care for patients with high risk pathological features.[13,15]

Locally advanced resectable and unresectable HNSCC can be treated with primary RT using doses of 70 Gy (2 Gy per fraction) to the primary tumour and involved nodes, and 44 to 50 Gy (2 Gy per fraction) to low/intermediate risk sites.[16] The addition of cisplatin chemotherapy to RT to increase the efficacy of RT has improved the survival in HNSCC and is currently the standard of care. A meta-analysis of 87 trials showed that the addition of chemotherapy improved survival, whether given as adjuvant, induction or concomitant, with an absolute benefit of 4.5% at 5 years. Concomitant chemoRT yielded the greatest absolute benefit of 6.5% at 5 years,[12] and platinum-based regimes were more effective[17] but with increased mucositis[18] and late toxicity.[19] Cetuximab is a monoclonal antibody against epidermal growth factor receptor (EGFR), which is overexpressed in HNSCC and associated with poor outcome.[20] Radiation increases the expression of EGFR in cancer cells and blocking the EGFR signalling pathway with cetuximab has been shown to enhance the effects of RT.[21] Cetuximab concomitant with RT is superior to RT alone in patients with locally advanced HNSCC,[22] and is an alternative option to platinum chemotherapy in patients medically unfit for chemoRT.

Altered fractionation schemes have been investigated to overcome accelerated repopulation. As tumours reduce in size during a course of RT the clonogenic surviving cells compensate by dividing rapidly. An estimated dose increment of 0.6 Gy per day approximately 28 days after the start of RT is required to compensate for this repopulation in HNSCC.[23] Accelerated RT delivers the total dose of radiation over a shorter period of time, decreasing the chance for tumour cells to regenerate during treatment. Hyperfractionation delivers more than one fraction of RT a day in smaller doses per fraction, given over the same period of time as standard RT, allowing the increased total dose delivery as late responding normal tissues are less sensitive to smaller doses per fraction. These strategies have been shown in randomised trials to significantly increased locoregional control (LRC) but with increased toxicity,[24,25] and a meta-analysis from 15

randomised trials of altered fractionation in HNSCC demonstrated an absolute survival benefit of 3.4% at 5 years.[26] The benefit was significantly higher with hyperfractionated RT (8% benefit at 5 years). The use of chemotherapy with altered fractionation has been shown to be more efficacious than altered fractionation alone without increased toxicity,[27] but has not shown a benefit over concomitant chemotherapy with standard RT.[28]

Radioresistance is a major cause of treatment failure and is influenced by many factors including accelerated repopulation, intrinsic radiosensitivity and tumour hypoxia. Despite recent advances in both surgical and radiotherapy delivery techniques up to 50% of locally advanced tumours relapse, usually within the first 2 years after treatment. There are limited options for salvage surgery or re-irradiation, which are associated with high risk of complications.[12]

1.2.2.3 Metastatic disease

The outcome of patients with recurrent of metastatic disease with conventional treatments is very poor, and options are often limited by the performance status of patients who frequently have morbidity due to previous therapy.

Several chemotherapy agents can be used for inoperable recurrences or metastatic disease, with response rates of only 10-35% and median survival of 6-12 months.[29] The commonly used chemotherapy combination is cisplatin or carboplatin with 5-fluorouracil (5-FU), which has been shown to produce higher response rates and better quality of life than single agent treatment such as methotrexate, but with no difference in OS.[30] Cetuximab has been investigated in the palliative setting and has a response rate of 13% as a single agent after previous platinum therapy.[31] An improved response rate of 26% was seen in combination with cisplatin compared with a response rate of 10% with cisplatin alone,[32] and a phase III trial demonstrated significantly improve median survival when cetuximab was combined with cisplatin/5-FU versus cisplatin/5-FU (10.1 versus 7.4 months), with response rates of 36% and 20% respectively.[33]

1.3 Biomarkers in HNSCC

Locally advanced disease in HNSCC represents tumours with multiple genetic aberrations that have allowed the tumour to proliferate, grow and locally metastasise. They have an aggressive phenotype and are characterised by complex molecular changes that lead to RT resistance. Despite the progress in improving current treatments and developing novel targeted therapies, there have only been modest improvements in the outcome for this

group of patients over the last 30 years. Therefore, there is an urgent clinical need to understand the mechanisms of treatment resistance and identify those at risk of treatment failure. As HNSCC is such a heterogeneous disease improved patient stratification and selection to develop more individualised treatment strategies would improve the therapeutic ratio and achieve better disease control.

Biomarkers, which include molecular and imaging markers of biological processes, are increasingly being evaluated to aid diagnosis, prognosis and prediction of treatment response. Prognostic biomarkers are associated with outcomes independent of a given treatment, whereas predictive biomarkers are associated with outcomes to a specific treatment. Predictive biomarkers are in clinical use, such as the identification of *EGFR* mutation in lung cancer to determine response to erlotinib[34] and *BRAF* mutation in melanoma to predict response to vemurafenib.[35] Genetic and molecular advances in HNSCC have revealed new genes and pathways involved in tumourigenesis, creating opportunities to explore novel therapeutic targets. In addition, imaging technologies are continually in development, providing further strategies to classify patients into prognostic groups. In HNSCC established prognostic biomarkers include HPV in oropharyngeal squamous cell carcinoma (OPSCC) and ^{18}Fluorine-flourodeoxyglucose positron emission tomography.

1.3.1 Established prognostic biomarkers in HNSCC

1.3.1.1 Human Papillomavirus (HPV)

HPV infection in OPSCC is now recognised as an aetiological agent, responsible for the significant increase in incidence in Western countries.[7,8] An estimated 60 to 70% of newly diagnosed oropharyngeal cancers in the US and Western Europe are associated with HPV.[6] These cancers represent a distinct subgroup characterised by specific biological and clinical profiles. Patients with HPV-associated OPSCC tend to be white males, on average 5 years younger than HPV-negative patients, have higher socioeconomic status and are less likely to smoke or drink alcohol.[6] HPV is detected in other subsites such as larynx and nasopharynx but no causal relationship or association with outcome has been established, and the significance in non-oropharyngeal head and neck tumours is unclear.[36]

HPVs are small, non-enveloped, double stranded DNA viruses. The genome encodes for early genes (E1-7) and late structural genes (L1, L2). E1 and 2 encode regulatory proteins and E5-7 encode oncoproteins. HPVs enter the host via wounds or abrasions in the mucosa and infect basal epithelial cells, where the host cell DNA replication machinery is used for viral replication.[37] The E6 protein interacts with E6-associated protein (E6-AP) resulting in a rapid degradation of tumour suppressor p53 via the ubiquitin-proteosome

pathway. This leads to inhibition of the proapoptotic functions of p53 and bypassing of the p53-mediated checkpoints.[38] The E7 protein competes with E2F1 transcription factor for binding to the pRb tumour suppressor, displacing E2F1. E2F1 activates genes responsible for cell cycle progression through the G_1 to S phase, promoting cellular proliferation and transformation.[39] pRb is a negative regulator of the cyclin-dependent kinase inhibitor $p16^{INK4A}$, and therefore inactivation of pRb results in $p16^{INK4A}$ upregulation. This can be detected using immunohistochemistry in HPV-associated tumour samples and represents a biologically significant surrogate marker for HPV oncoprotein expression.[40]

Locally advanced OPSCC is treated with concomitant chemoRT and at present, treatment is the same regardless of HPV status outside the context of a clinical trial. HPV-associated OPSCC has a favourable prognosis, with a 60-80% reduction in the risk of death compared with HPV-negative OPSCC after standard therapy,[41,42] highlighting the need for different treatment strategies to reduce the morbidity associated with current treatment. Locally advanced HPV-negative OPSCC continues to have a poor prognosis and a significant proportion of these patients develop recurrent disease. Therefore HPV-negative OPSCC patients would benefit from markers predictive of response from current treatment, as well as the development of treatment intensification strategies and novel targeted agents. The research into HPV as a biomarker in OPSCC has translated into several phase III studies currently recruiting to investigate the replacement of standard cisplatin in concomitant chemoRT with cetuximab, or assessing de-escalating treatment strategies such as using induction chemotherapy followed by reduced dose radiation.[43] HPV vaccines are under development, as both preventative and therapeutic applications. Gardasil and Cervarix are HPV vaccines in use for the prevention of cervical cancer, but could afford protection against oral HPV16/18 infection. Reduced prevalence of oral HPV infection was found in women recruited to investigate the efficacy of HPV vaccination against cervical cancer.[44] These vaccines may also cause induction of cell mediated immunity against HPV positive tumours and phase I studies are ongoing investigating the ability to deliver HPV16 E7 antigen using recombinant listeria-based vaccine or a DNA-based vector.[45] Tumour infiltrating lymphocytes in HPV-positive OPSCC express high levels of programmed cell death protein 1 (PD-1) receptor and its ligand PD-L1. The interaction of PD-L1 with PD-1 receptor results in negative T cell regulation and immune inhibition, and in normal tissues this is a mechanism to protect against excessive tissue destruction. Localised expression of PD-L1 has been demonstrated in the deep crypts of normal tonsils where initial HPV infection takes place, suggesting a protected site where the virus can evade immune recognition.[46] PD-L1 has been shown to be induced by the activation of the PI3K/AKT pathway through the loss of *PTEN*,[47] which is a common mutation in HPV-positive but not

HPV-negative SCC.[48,49] Anti-PD-1 and anti-PD-L1 phase I studies have been carried out in solid tumours with objective responses.[50,51]

1.3.1.2 ^{18}Fluorine-fluorodeoxyglucose positron emission tomography

Positron emission tomography (PET) is a molecular imaging technique that can visualise and quantify tumours and their microenvironment. Different biological tumour characteristics can be imaged depending on the radiotracer used, including those relevant to radioresistance such as increased metabolism, accelerated repopulation or proliferation, and hypoxia. As it is non-invasive and visualises whole tumours and metastatic lesions simultaneously, patients can potentially receive serial imaging to monitor response to treatment, with the patient serving as their own control, and therefore has important roles in treatment selection and possible treatment adaptation.

The most commonly used radiotracer is ^{18}Fluorine (^{18}F) labelled fluorodeoxyglucose (FDG), which is a glucose analogue that is taken up by cells with increased glucose metabolism. ^{18}F-FDG enters cells via glucose transporters and is phosphorylated by hexokinase to ^{18}F-fluoro-2-deoxyglucose-6-phosphate, which becomes trapped within the cell. ^{18}F undergoes radioactive decay and emits positrons. These positrons interact with electrons in an annihilation reaction to emit two 511 KeV photons in opposite directions, which are detected by scintillation crystals of the PET scanner, converted to light and a 3D image is reconstructed. PET is combined with a computed tomography (CT) imaging in a single scanner to provide both quantitative functional and anatomical information.

^{18}F-FDG PET in HNSCC is used for improved diagnosis and staging, tumour volume assessment to aid RT planning, and response assessment. High uptake has been correlated with more advanced tumour stage, poorer differentiation and perineural and extracapsular invasion,[52] and has been shown to have prognostic value. Two meta-analyses have demonstrated that the semi-quantitative measure of the normalised concentration of radioactivity in a tumour SUV_{max} (maximum standardised uptake value) before treatment is associated with outcome.[53,54] Low pre-treatment SUV_{max} of primary tumours were associated with reduced risk of progression, recurrence and death, although the definition of low/high SUV_{max} was variable. Post-treatment ^{18}F-FDG PET is used routinely for response assessment after primary (chemo)RT, to guide whether further surgical management is required.[55] A meta-analysis of PET in the post-treatment setting demonstrated high negative predictive value for the primary tumour and neck metastases.[56] It can be used to avoid post-treatment neck dissection but the positive predictive value can be as low as 38% due to inflammation related uptake after RT.[57]

Mid-treatment ^{18}F-FDG PET has also been investigated in small studies and shown potential for early treatment response assessment, either after induction chemotherapy[58] or 1-2 weeks after the start of chemoRT,[59] with a SUV_{max} reduction of > 50% associated with complete clinical response and better OS. Mid-treatment ^{18}F-FDG PET therefore has the potential to identify patients who may benefit from treatment modification. Integration of ^{18}F-FDG PET into RT planning is currently an active area of research. ^{18}F-FDG PET can be used as an aid to tumour volume definition for RT as it can potentially define tumours more accurately compared with CT or MRI,[60] and has demonstrated frequent tumour extension outside CT-based tumour volumes.[61] In addition a significant proportion of recurrences after treatment have been shown to occur in the pre-treatment ^{18}F-FDG PET region and therefore coverage of this region in the high dose RT volume is essential.[62] However the direct PET-based RT planning is not carried out outside of clinical trials mainly due to the uncertainties regarding optimal tumour segmentation. Preclinical autoradiography studies have been found discrepancies between PET images and microregional distributions of ^{18}F-FDG due to the finite resolution of PET,[63] and the discrimination of uptake from background tissues remain unclear.

1.3.2 Biomarkers under investigation in HNSCC

Gene expression profiling using microarray based assays has allowed the evaluation of the expression of tens of thousands of genes at once, enabling lists of genes, or signatures that are over- or underexpressed to be assessed. Next-generation sequencing now provides the platform to carry out the evaluation of the whole exome, genome, transcriptome and copy number variations to provide a comprehensive assessment of the genetic alterations underlying HNSCC, which can potentially provide information that can be used to change patient management.

Genomic data from 3 large genome-wide sequencing studies have demonstrated that the majority of HNSCC tumours have loss of function mutations in tumour suppressor genes (TSGs) and only a few functionally activating gene mutations (Table 1.1).[48,49,64] Unfortunately targeting TSGs or their pathways to restore or reactivate their function is difficult compared with targeting oncogenes with specific inhibitors. Therefore elucidating the genetic basis of tumours, as well as exploring other novel biomarkers, such as microRNAs, and further developing established biomarkers, such as hypoxia, are important steps towards indiviualised management of HNSCC.

Table 1.1 Mutation rates of genes found to be commonly mutated in 3 gene sequencing studies in HNSCC. Adapted from Sun et al.[65]

Gene	Type of gene	Cancer Genome Atlas[64] (n=279)	Agrawal et al[48] (n=120)	Stransky et al[49] (n=74)
TP53	TSG	72%	47%	62%
CDKN2A	TSG	22%	9%	12%
NOTCH1	Both	19%	15%	14%
PIK3CA	Oncogene	21%	6%	8%
FBXW7	TSG	5%	5%	5%
HRAS	Oncogene	4%	4%	5%

1.3.2.1 p53/Retinoblastoma (pRb)

Tumour suppressor protein p53 plays a key role in the regulation of genes involved in cell cycle and growth arrest, DNA repair or apoptosis, thereby maintaining genomic stability.[66] In response to DNA damage p53 can arrest the cell cycle and activate repair or initiate apoptosis. The level of p53 is regulated by Mouse double minute 2 homolog (MDM2), an E3 ubiquitin-protein ligase, which binds to p53 and causes its degradation. MDM2 is inhibited by $p14^{ARF}$, which is encoded by the gene *CDKN2A*, protecting p53 from degradation. Tumour suppressor protein pRb controls the expression of genes involved in cell cycle progression through the G1 restriction point. pRb binds and inhibits E2F1 transcription factors, which induce expression of S phase genes and cell proliferation. Mitogenic signals activate cyclin D1/CDK4/CDK6 complexes, which phosphorylate pRb resulting in the release of E2F1. The cyclin D1-CDK4/6 complexes are inhibited by $p16^{INK4A}$, encoded by the gene *CDKN2A,* and p21 (cyclin-dependent kinase inhibitor 1/CDKN1).[67] Mutations in p53 and pRb pathways result in limitless replicative potential and immortalisation.

Mutation of the TP53 tumour suppressor gene is one of the earliest and most frequently detectable genetic alterations in HNSCC, reported in 50-80% of cases.[48,68] In p53 wild type tumours, p53 function may be inactivated by other mechanisms, such as HPV infection, overexpression or amplification of MDM2 and deletion of the $p14^{ARF}$ gene.[66] pRb is targeted early carcinogenesis through inactivation of the tumour suppressive *CDKN2A* gene, with mutations seen in 9-22% and copy number losses in a further 20-30% of cases.[48,49,64] The *CCND1* gene, which encodes cyclin D1, has been found to be amplified or overexpressed in over 80% of HNSCC.[69] In addition E2F1 activating mutations were observed in 20% of The Cancer Genome Atlas tumours, particularly in HPV-positive samples. *TP53* mutation, loss of $p16^{INK4A}$ and overexpression of cyclin D1 are all associated with reduced survival.[68] *TP53* mutation is predictive of poor response to

chemotherapy and locoregional recurrence following radiotherapy,[70] and cyclin D1 deregulation has been associated with EGFR-inhibitor resistance.[71]

Restoring or modulating p53 as targeted therapy, for example with gene therapy, has been an area of intensive research for decades, with limited success. A phase I study of dendritic cell p53 peptide vaccine therapy recently reported the feasibility and safety in the adjuvant setting.[72] p53-reactivating small molecules are currently under investigation in HNSCC cell lines,[73] and other strategies include targeting *CDKN2A* to reactivate $p16^{INK4A}$ and CDK inhibitors.

1.3.2.2 Epidermal growth factor receptor

EGFR (ErbB1) is a member of the ErbB/HER2 family of transmembrane receptor tyrosine kinases, which play a major role in cell proliferation, differentiation, survival and migration. EGFR is activated by a number of ligands such as EGF, resulting in downstream signal transduction cascades including the Ras/Raf/mitogen-activated protein kinase (MAPK), phosphoinositide 3-kinase (PI3K)/AKT and Janus kinases (JAK)/signal transducers and activators of transcription 3 (STAT3) pathways (Figure 1.1).[74] EGF-bound EGFR can also translocate to the nucleus to function as a transcription factor. One of the nuclear targets is *CCND1*, which encodes cyclin D1 protein involved in cell cycle progression.[75]

EGFR is overexpressed in 80-90% of HNSCC[76] and in dysplasic lesions,[77] indicating that EGFR is an early event in HNSCC carcinogenesis. EGFR overexpression is mainly at the transcriptional level as there are few EGFR activating mutations in HNSCC.[64,76] The intensity of expression, as assessed by immunohistochemistry, and increased gene copy number has been shown to indicate poor outcome.[20,78] However, variations in EGFR antibody staining protocols and interpretation, and the lack of association with the efficacy of EGFR-directed therapy has limited its clinical utility.[79] EGFR can be targeted either by inhibition of the extracellular ligand binding using monoclonal antibodies, such as cetuximab, or by inhibition of the tyrosine kinase domain with a small molecule (TKIs), such as gefitinib and erlotinib, but despite the high expression, EGFR inhibition has only a modest effect. Gefitinib and erlotinib inhibit only EGFR and have shown disappointing results in HNSCC.[80,81] Afatinib irreversibly blocks EGFR, HER2 and ErbB4 and is under investigation in HNSCC.

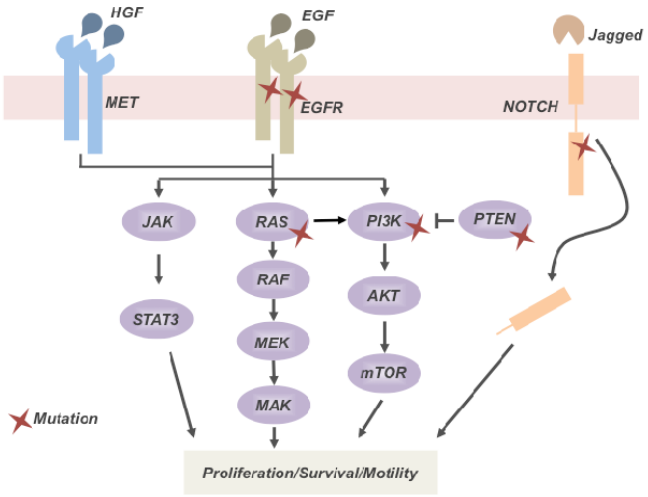

Figure 1.1 RTK signalling cascade.
Activation of RTKs result in the signalling of a number of pathways involved in cell survival.

1.3.2.3 NOTCH

NOTCH1 signalling is involved in a number of biological functions, including regulation of self-renewal capacity, survival, and promoting terminal differentiation. The NOTCH pathways consists of four receptors bound to the cell membrane, NOTCH 1-4, and two families of ligands, Delta-like (1, 3, and 4) and Jagged (JAG1 and 2). Ligand binding leads to two cleavages of NOTCH1 by TNFα-converting enzyme (TACE) and γ-secretase resulting in release of the NOTCH1 intracellular domain (NCID). NCID translocates to the nucleus and interacts with nuclear co-activating MAML proteins to promote transcription of its target genes. NOTCH1 is regulated partly by ubiquitination and degradation, which involves FBXW7.[82]

NOTCH1 and *FBXW7* mutations in HNSCC were novel findings in whole-exome sequencing studies.[48,49] Chromosomal aberrations in *JAG1*, *JAG2* and *MAML1* have also been reported.[69] The majority of *NOTCH1* mutations were nonsense mutations, predicted to result in truncated NOTCH1 proteins lacking the transcriptional activation domains, therefore suggesting a tumour suppressor role for this pathway in HNSCC. However recent reports have suggested a subset of HNSCC with activating *NOTCH1* mutation,[83] supported by in vitro functional studies in HNSCC cell lines.[84] The role of NOTCH1 in HNSCC tumourigenesis needs to be further investigated, but could potentially represent another therapeutic target. Both NOTCH1 pathway inhibitors, such as γ-secretase inhibitors,[85] and NOTCH1 pathway activators, via inhibition of histone deacetylase, are currently in clinical development.

1.3.2.4 PI3K/AKT/mTOR

PI3Ks are a family of enzymes that have important roles in promoting cell growth, differentiation and survival. PI3Ks are heterodimers and composed of a 110 kDa catalytic subunit and an 85 kDa regulatory subunit. Activation by RTKs results in the phosphorylation of phosphatidylinositol1,4-bisphosphate (PIP_2) by the catalytic subunit to form phosphatidylinositol1,4,5-triphosphate (PIP_3). PIP_3 recruits AKT to the plasma membrane resulting in phosphorylation and activation of AKT by mammalian target of rapamycin complex 2 (mTORC2). Activated AKT phosphorylates proteins involved in cell growth and survival, including MDM2, NF-κB via IκB kinase, and inactivation of the pro-apoptotic protein BAD. AKT also stimulates cell proliferation by inactivating p21 and stabilising cyclin D1. The tumour suppressor phosphatase and tensin homology (PTEN) mediates the conversion of PIP_3 to PIP_2, counteracting the activation of AKT.[86] Mammalian target of rapamycin (mTOR) is a protein kinase that acts downstream of PI3K and AKT and plays an important role in cell growth, survival, protein synthesis and autophagy. mTORC1 activates ribosomal protein S6 kinase 1 (S6K1) and inactivates eukaryotic translation initiation factor 4E-binding protein 1 (4E-BP1), resulting in protein translation and cell growth.

Genetic aberrations of the PI3K pathway are common in HNSCC. The 110 kDa catalytic subunit, p110α, is encoded by the *PIK3CA* gene, which is mutated in 6-30% of HNSCC, resulting in constitutive activation of the pathway.[48,49,87] It has been found to be particularly common in HPV-positive HNSCC cases, where the mutation is in the helical domain of the *PIK3CA* gene. HPV-negative tumours have mutations throughout the gene, but demonstrate specific mutations, such as H1047R in exon 20 in the kinase domain, which may predict higher response rates to treatment with PI3K pathway inhibitors.[88] In addition, *PTEN* mutations have been reported in 7% of HNSCC, and the mTOR pathway is frequently activated, independent from activation of EGFR or the presence of mutant p53, particularly in HPV positive tumours.[49,89,90] The PI3K pathway is an important therapeutic target for cancers and the activation has been implicated in radioresistance.[91] HNSCC xenografts with *PIK3CA* mutation demonstrated selective sensitivity to mTOR/PI3K inhibition compared with wild type tumours[87] and differential sensitivity to PI3K inhibition over AKT inhibition in HPV-positive tumours.[92] The mTOR inhibitors everolimus and temsirolimus are in clinical use in different tumour types, and have been investigated in HNSCC in phase I and II trials in combination with chemotherapy and EGFR inhibition.[93] PI3K and AKT inhibitor early phase studies are ongoing. Bortezomib is a protease inhibitor which also inhibits the activation of NF-κB and induces PTEN expression. A phase I study in combination with chemoRT in locally advanced or recurrent HNSCC, demonstrated a median survival of 24.7 months.[94]

1.3.2.5 RAS

Ras is a guanosine nucleotide binding protein localised on the plasma membrane. There are three Ras genes: *HRAS*, *KRAS* and *NRAS*. In the inactivated state Ras is bound to guanosine diphosphate (GDP). Activation converts Ras to the guanosine triphosphate (GTP) bound form, which binds to and activates Raf-1. The targets for phosphorylation of Raf-1 include the kinases MEK1 and MEK2, which in turn activate the MAP kinases ERK1 and ERK2. These translocate to the nucleus and target genes involved in cell growth, proliferation and survival. Ras can also activate the PI3K signalling cascade.[95] Activating HRAS mutations have been found in 4-5% of HNSCC cases.[48,49] KRAS in colorectal cancers are predictive of poor response to EGFR inhibitors,[96] but the predictive value in HNSCC remains unclear. Sorafenib is a tyrosine kinase inhibitor, which has multiple targets including Raf and VEGF (vascular endothelial growth factor receptor) and in combination with chemotherapy has shown a response rate of 55% and median overall survival of 22.6 months in one phase II trial in HNSCC.[97] The MEK inhibitor trametinib has recently been approved for use in metastatic melanoma and is under investigation in combination with AKT inhibition in solid tumours including HNSCC.

1.3.2.6 MET

The proto-oncogene *c-MET* encodes mesenchymal epithelial transition factor (MET), which is an RTK activated by hepatocyte growth factor (HGF). Ligand binging activates signalling cascades resulting in cell morphogenesis, motility, growth and survival. MET and HGF have been found to be overexpressed in over 80% of HNSCC and increased *MET* copy numbers in 13% of HNSCC tumour samples.[98,99] MET expression has been suggested to be a prognostic biomarker in HPV-negative HNSCC with overexpression correlating with reduced disease-free and overall survival.[100] It has also been implicated in resistance to radiation, cisplatin and cetuximab.[101-103] Foretinib is a multi-tyrosine kinase inhibitor that binds to the ATP pocket of the MET receptor. It has been tested in a phase II study in recurrent/metastatic HNSCC which showed disease stabilisation.[104]

1.3.2.7 JAK/STAT

The Janus kinases (JAKs) are part of a family of non-receptor tyrosine kinases that phosphorylate signal transducer and activator of transcription (STAT) and promote cell growth and survival, angiogenesis and suppression of immune surveillance.[105] STAT proteins are important in mediating EGFR signalling and STAT3 is overexpressed in HNSCC.[106] In HNSCC tumour models inhibition of STAT3 resulted in increased apoptosis,[106] and STAT3 knockdown HNSCC cells demonstrated increased radiosensitivity and cetuximab sensitivity.[107] Direct targets of STAT3 include members of the Bcl-2 family, genes involved in cancer inflammation such as interleukin-6, matrix metalloproteinases,

hypoxia-regulated factor-1 (HIF-1) and vascular endothelial growth factor (VEGF).[108] Ruxolitinib is a JAK inhibitor being investigated in phase I studies in combination with chemotherapy in advanced solid tumours. A phase 0 trial of a STAT decoy oligonucleotide injected into HNSCC tumours before surgery demonstrated downregulation of STAT3 target gene expression warranting further investigation of this target in HNSCC.[109]

1.3.2.8 Gene expression profiling

Gene expression profiling using microarrays have been investigated to predict outcome. Using samples from patients with clinical data, supervised analysis can identify genes that are most strongly associated with clinical outcomes. Signatures to predict with recurrence,[110] lymph node metastases,[111] hypoxia[112] and outcome after chemoRT[113] have been described using both fresh frozen and formalin fixed paraffin embedded (FFPE) samples. More recently a meta-analysis of 9 microarray gene expression datasets of HNSCC demonstrated a 172 gene signature highly prognostic of risk of relapse, independent from HPV status, and was validated in 6 independent datasets.[114]

Gene expression profiling has also demonstrated that HNSCC can be characterised based on their gene expression profile. Chung et al[115] assayed 60 HNSCC samples and found that the gene expression patterns allowed categorisation into 4 distinct subtypes, which showed significant differences in recurrence free survival. In addition they identified a signature from the primary tumour diagnostic biopsy sample that could predict the presence of lymph node metastases. The subtypes were validated by Walter et al using integrated genomic analysis,[116] and classified as basal, mesenchymal, atypical and classical, and confirmed more recently by The Cancer Genome Atlas Network.[64] For example, the atypical subtype was characterised by lack of chromosome 7p amplifications, which contains *EGFR*, and enrichment of HPV-positive tumours with activating mutations in the *PIK3CA* helical domain. The classical subtype included *TP53* mutations, loss of chromosome 9p containing *CDKN2A* and a heavy smoking history. Studies have also identified clear differences between HPV-negative and positive tumours. HPV-negative tumours harbor *TP53* loss in almost all cases and high rates of *CDK2NA* loss, altering the pRB pathway. They also demonstrated amplification of *EGFR* and *CCND1*, and deletions in *NOTCH1*. HPV-positive tumours have infrequent *TP53* and *CDKN2A* mutations and more frequent *PIK3CA* activating mutations.[87,117]

1.3.2.9 Other PET biomarkers

Other PET-based imaging biomarkers of radioresistance are under investigation, including radiotracers to detect proliferation and hypoxia. Hypoxia imaging is further discussed in section 1.5.4.

Compensatory enhanced proliferation during RT is a recognised mechanism for resistance and treatment failure in HNSCC.[118] ^{18}F-fluorothymidine (FLT) is a PET tracer that is taken up into cells by nucleoside transporters, phosphorylated and trapped by the cytosolic enzyme thymidine kinase 1 (TK1), the activity of which increased nearly 10-fold during DNA synthesis. ^{18}F-FLT retention is therefore a measure of cellular TK1, which is closely related to cellular proliferation.[119] In HNSCC pre-treatment high uptake has been shown to be predictive of poor outcome, and patients with high SUV_{max} treated with chemoRT had better outcome compared with RT alone.[120] Serial PET before and during RT has demonstrated a decrease in proliferative activity during therapy,[121] with greater decline indicative of better long-term outcome.[120,122] ^{18}F-FLT PET therefore has the potential to identify patients who are not responding adequately to treatment at a stage when there is a possibility for treatment intensification.

Another imaging target in HNSCC is EGFR, which could monitor and predict EGFR-targeted treatment response. Cetuximab has been labelled with several radionuclides and investigated in animal models, for example ^{89}Zr and ^{64}Cu.[123] Uptake in tumours have been correlated with EGFR expression assessed by IHC.[124] In addition ^{111}In-cetuximab has been shown to visualise EGFR accessibility and radiation-induced changes in EGFR HNSCC xenografts,[125] demonstrating the potential clinical value of this tracer.

1.4 MicroRNAs as biomarkers

MicroRNAs (miRNAs) are endogenous, small, non-coding RNAs, 18 to 25 nucleotides in length. They are evolutionarily highly conserved in eukaryotic organisms and regulate and refine gene expression at the post-transcriptional level.[126] Over 2500 mature miRNAs have been identified to date (miRBase.org), with each miRNA influencing the expression of hundreds of genes and a single messenger RNA (mRNA) being targeted by multiple miRNAs. It is estimated that over one third of human genes are conserved targets of miRNAs.[127] They are involved in a wide variety of critical biological processes including cell cycle regulation, differentiation, development, metabolism and death.[128] MiRNAs have been described as micromanagers of protein output within a complex interactive network,

fine-tuning the expression of many genes, with alteration of a single miRNA likely to result in subtle phenotypic consequences.[129] MiRNAs were first discovered in 1993 by Ambros et al.[130] During their study of the nematode Caenorhabditis elegans gene *lin-4*, they found that this gene did not encode a protein but produced a small RNA. This small RNA repressed the expression of its target LIN-14 through base pairing with the 3'-untranslated region (3'-UTR) of the *lin-14* mRNA. However the significance of this discovery was only realised when the second miRNA, let-7, was characterised in 2000,[131] and subsequently found to be conserved in many species. Since the discovery of miRNAs there has been huge interest in their role in tumourigenesis, and their potential as biomarkers and possible therapeutic targets.

1.4.1 Biogenesis

Thirty percent of miRNA genes are located in intergenic regions, or in their own transcription units, and therefore transcribed as independent units.[132] The rest are located within the introns or exons of non-coding or protein-coding genes.[133] These miRNAs are usually expressed with the transcription of the host gene, suggesting that they may be regulated together and derive from a common transcript.[134] MiRNAs can be organised as individual genes or located close to each other and transcribed as clusters, with common function and sequence.[135]

MiRNAs are transcribed by RNA polymerase II into an initial miRNA precursor called pri-miRNA, which are several kilobases in length and fold into hairpin structures containing imperfectly base-paired stems. The pri-miRNA is processed in the nucleus by the ribonucleases Drosha and DiGeorge syndrome critical region 8 (DGCR8), which forms the microprocessor complex, to become a precursor of about 70 to 100 nucleotides, called pre-miRNA. Pre-miRNA is exported to the cytoplasm by exportin 5,[136] where it undergoes further processing by another ribonuclease, Dicer, into a mature 18 to 24 nucleotide double strand miRNA. Only one strand (the 'guide' strand) is incorporated into a large protein complex called RNA-induced silencing complex (RISC), which is constituted by Argonaute family protein members, whilst the other strand (the 'passenger' strand or miRNA*) is removed and degraded. The mature miRNA will recognise the complementary sequences in the target mRNA and guide the miRNA-RISC complex to cleave the mRNA or inhibit protein translation (Figure 1.2).[137]

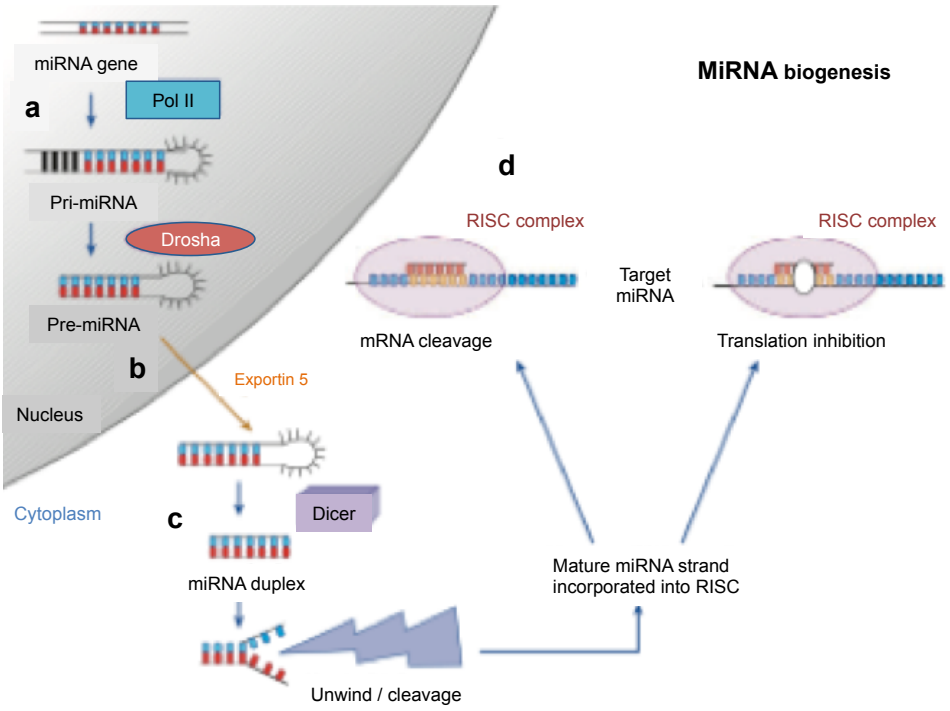

Figure 1.2 MiRNA biogenesis.
a) MiRNA transcription by RNA polymerase II into pri-miRNA, which is cleaved by the enzyme Drosha to form a hairpin precursor pre-miRNA. **b)** Pre-miRNA is exported to the cytoplasm by exportin 5. **c)** Pre-miRNA is processed in the cytoplasm by the enzyme Dicer to form a transient miRNA duplex. One strand is incorporated into the protein complex RISC. **d)** The mature miRNA leads the RISC to degrade the mRNA or induce translational repression, depending on the degree of complementarity between the miRNA and mRNA target. Adapted from Garzon et al 2009.[137]

The main function of miRNAs is to inhibit protein synthesis, either by inhibition of translation or mRNA degradation by base pairing with their mRNA targets. The specificity depends on the degree of base pairing between the nucleotide positions 2 to 8 of the 5'-UTR of the mature miRNA, which is known as the seed region, with the 3'-UTR of the target mRNA.[127] MiRNAs with the same 2 to 8 nucleotide sequences belong to the same family.[138] In plants most miRNAs base pair to mRNA with nearly perfect complementarity, resulting in mRNA degradation.[139] This is rare in animals, where imperfect miRNA-mRNA base pairing leads to post-translational inhibition,[140] including inhibition of translation initiation or post-initiation, mRNA destabilisation and decay, or co-translational protein degradation.

MiRNA biogenesis and function in animals are complex and do not always follow this pathway. They have been reported to target the 5'-UTR and coding regions of target mRNAs, with association of miRNAs with 5'-UTR target sites sometimes resulting in activation rather than repression of translation.[141] Some miRNAs mature by mRNA splicing with or without exonuclease trimming of strands, independent of the enzymes Drosha and Dicer, giving rise to miRtrons.[142] Furthermore, in addition to gene silencing activity, miRNAs

have been reported to also have decoy activity that interferes with the function of regulatory proteins, acting as molecular decoys for RNA-binding proteins.[143]

1.4.2 MicroRNAs in cancer

The first report of the role of miRNAs in cancer was published in 2002, when it was demonstrated that in more than 65% of cases of chronic lymphocytic leukaemia, a small region in chromosome 13q14 was deleted. This region did not contain a protein-coding tumour suppressor gene but two microRNAs, miR-15 and miR-16.[144] Since then altered miRNA expression has been reported in almost all types of cancer.[145] MiRNA deregulation can be caused by a variety of mechanisms, including genomic deletion, mutation or amplification,[146] single nucleotide polymorphisms,[147] and epigenetic instability such as promoter hypermethylation and histone deacetylation.[148] Transcription factors, known to be deregulated in cancer, can also influence the regulation of miRNA transcription. For example MYC, a well established oncogenic transcription factor, has been shown to promote the transcription of the miR-17-92 cluster of oncogenic miRNAs.[149] In addition, miRNA expression is under tight regulatory control and alterations to the enzymes in their biogenesis pathway can also affect tumorigenesis.[150]

MiRNAs are directly implicated in the tumorigenesis of cancer by acting as oncogenes or tumour suppressor genes (TSGs). They have been found to be involved in a variety of pathways in cancer development and progression, such as proliferation, apoptosis,[151] angiogenesis,[152] maintenance of the cancer stem cell and metastasis.[153] In some cases the same miRNA can act as an oncogene in one cell type and a TSG in other, by acting on different targets or by functioning under differing transcriptional regulation. For example, miR-7 in head and neck cancer cell lines was shown to regulate EGFR expression and AKT activity and therefore has a tumour suppressor function. On the other hand miR-7, along with miR-21, has been associated with keratinisation of oral tumours and poor prognosis, suggesting a possible oncogenic role.[154]

Improved understanding of the role of miRNAs in both physiological and pathological processes has revealed their huge clinical potential, especially as they have been found to be are stable even after many years in FFPE samples and in body fluids.[155,156] The biogenesis of miRNAs is tightly regulated and very sensitive to endogenous and exogenous stimuli, resulting in differing expression profiles between cell types and cell conditions. Global miRNA gene profiling of normal and tumour tissues has been carried out to assess whether miRNA signatures could be used as clinical biomarkers of diagnosis, classification, prognosis, and treatment response prediction. For example, miRNA expression profiling can differentiate between normal and diseased tissue and identify

tissues of origin accurately.[145] They have also been shown to be able to discriminate different subtypes of a particular cancer, such as basal and luminal breast cancer subtypes.[157] MiRNA profiling has revealed patterns of expression associated with disease outcome, such as miR-155 overexpression and let-7a downregulation in lung cancer, which predicts for poor disease outcome,[158] supporting the potential of miRNAs as prognostic biomarkers. A more important potential role for miRNA signatures is the ability to predict the response to specific drugs or radiotherapy. For example, high miR-21 expression has been shown to predict poor response to adjuvant chemotherapy in pancreatic and colon cancer,[159] and radioresistance in lung cancer.[160]

MiRNAs represent potential therapeutic targets for the diseases in which they are deregulated. MiRNAs that are overexpressed can be targeted using a class of anti-miRNA antisense oligonucleotides called antagomirs. In tumours where miRNAs are downregulated and function as TSGs, miRNAs can be replaced using synthetic miRNAs, which mimic the expression of the protective miRNAs, or genes coding for downregulated miRNAs could be inserted into viral constructs. However, their development has the challenges of delivery and retention, safety and potential off target effects.[161] MicroRNAs are increasingly being integrated into clinical trials but these are mainly looking at the expression signatures as biomarkers for diagnosis, prognosis or treatment response. However there are currently two clinical studies, one phase 2 trial of miravirsen, a miR-122 inhibitor for hepatitis C infection,[162] and one phase one study to assess the safety of a miR-34 mimic in patients with primary liver cancer or liver metastases.[163]

1.4.3 MicroRNAs in head and neck cancer

Several mechanisms for miRNA deregulation have been identified in the pathogenesis of HNSCC. For example, single nucleotide polymorphism (SNP) in miR-885-5p[164] and in the 3'-UTR of Dicer, affecting the binding of miRNAs to Dicer,[150] have been associated with HNSCC susceptibility. In addition, miR-137 and miR-193a tumour suppressor miRNAs have been found to be epigenetically silenced during oral carcinogenesis.[165]

Expression profiling of miRNAs has been performed in head and neck, but with variable results due to differences in the HNSCC subtype investigated, condition of samples used and their processing, as well as data analysis methods. However there are some consistently upregulated miRNAs (Table 1.2).

Table 1.2 Examples of consistently altered miRNAs in HNSCC.

MicroRNA	Targets	Reference
Upregulated		
miR-21	*PTEN, PDCD4*	166
miR-31	FIH	167
miR-106b-25	p21	168,169
miR-155	SOSC1-STAT3, *CDC73*	170,171
Downregulated		
let-7	*KRAS*	172,173
miR-125a/b	ErbB2	174
miR-133a/b	PKM2, ARPC5	175,176
miR-200a	ZEB1, ZEB2	177

Upregulation of miR-21 is one of the commonest findings in human cancers, where it is implicated in cell proliferation, invasion and metastases, and is consistently upregulated in head and neck cancer.[168,178] MiR-21 upregulation in HNSCC is associated with poor prognosis and correlated with tumour suppressor targets such as *PTEN* and the programmed cell death 4 (*PDCD4*) gene.[166] MiR-31 enhances oncogenesis via targeting factor-inhibiting hypoxia-inducible factor (FIH), which inhibits the activation of ability of HIF-1 regulated genes.[167] The miR-106b-25 cluster of miRNAs negatively regulates the p21 CDK inhibitor, can promote cell proliferation by deregulating cell cycle check points,[169] with knockdown of this cluster resulting in G1 cell cycle arrest.[168] MiR-155 promotes proliferation and invasion through targeting suppressor of cytokine signalling 1 (SOSC1)-STAT3 pathway in laryngeal cancers and *CDC73* gene,[171] which negatively regulates cyclin D1 and MYC, in oral cancers.[170]

Consistently downregulated microRNAs include let-7, which negatively regulates KRAS, and reduced expression is associated with poor prognosis.[172,173] MiR-125a/b is also downregulated in independent studies and thought to target the oncogene *ERBB2*,[174] as is miR-133a/b which targets pyruvate kinase M2 (PKM2), a key regulator of cancer metabolism.[175] MiR-133a also directly regulates the actin-related protein complex 5 (ARPC5) with inhibition of cell migration and invasion when miR-133a is restored or ARPC5 is repressed.[176] Downregulation of the tumour suppressive miR-200a is seen in both saliva and tissue samples of HNSCC patients and is known to target ZEB1 and ZEB2, which repress the transcription of E-cadherin and mediate epithelial-mesenchymal transition and cell migration.[177]

MicroRNAs have a role in the response to therapy in HNSCC. For example, miR-21 inhibition was found to induce sensitivity of OSCC cells to cisplatin, with cells transfected with *PDCD4* siRNA, a known target of miR-21, becoming more resistant to cisplatin. Suppression of miR-21 promoted cisplatin-induced apoptosis, whereas PDCD4

suppression reduced apoptosis.[179] Cisplatin resistant oral cancer cell lines are associated with miR-181a downregulation and TWIST1 upregulation, with enhanced epithelial-mesenchymal transition and metastatic potential. MiR-181a upregulation reversed chemoresistance, as did TWIST1 knockdown.[180] In addition miR-200b and miR-15b downregulation was found in cisplatin-resistant tongue SCCs, and ectopic expression of these miRNAs reversed chemoresistance and reduced motility and invasiveness.[181]

1.4.4 MicroRNAs and radiotherapy

MiRNAs are implicated in the response of tumours to radiotherapy. Ionising radiation induces DNA damage, which triggers the DNA damage response (DDR) pathway. The DDR initially responds to radiation by recruiting a large number of proteins to the site of DNA damage to form ionising radiation induced foci. Repair pathways include base excision repair, single-strand break repair and double-strand break repair, which occur through homologous recombination or non-homologous end-joining. Phosphorylation of the protein gamma H2AX is an early event, which occurs through the activation of ataxia telangiectasia mutated (ATM), DNA-dependent protein kinase catalytic subunit (DNA-PKcs) and AT and Rad3-related (ATR) kinases. In double-stranded damage this activation and phosphorylation recruits and phosphorylates other proteins, such as sensor proteins BRCA1, RAD50, NBS1, which act as signals to activate downstream effectors of the DDR, such as XRCC4, Ku70-Ku80, RAD 51/52, and BRACA1/2, resulting in cell cycle arrest followed by repair or apoptosis if too much damage has occurred.[182]

MiRNAs can influence and regulate the proteins involved in the DDR pathway, and DNA damage can induce the transcription of specific miRNAs. For example, the miR-34 family is induced by DNA damage in a p53-dependent manner, with ectopic miR-34a expression inducing cell cycle arrest and promoting apoptosis.[183] ATM and ATR have been shown to be direct targets of miR-185, with miR-185 overexpression enhancing radiation-induced apoptosis via the ATR pathway.[184] MiR-421 has also been shown to suppress ATM expression and ectopic expression resulted in S-phase cell cycle checkpoint deficiency and increased radiosensitivity. In addition, MYC transcription factor overexpression induced miR-421 expression, which in turn regulated ATM,[185] and miR-24 overexpression downregulated histone H2AX resulting in increased sensitivity to irradiation secondary to reduced capacity to recruit proteins to repair DNA double strand breaks.[186]

MiRNA microarrays have been used to show altered miRNA expression profiles before and after irradiation, particularly in genes involved in DNA repair, stress response and cell cycle control.[187] In lung cancer cell lines the let-7 family of miRNAs, which is associated with poor

outcome in low levels, has been shown to be downregulated in response to irradiation. Overexpression of let-7 resulted in radiosensitivity and decreasing the levels caused radioresistance.[188] MiR-521 levels were significantly decreased and miR-34c levels increased in prostate cancer cells in response to irradiation. MiR-521 overexpression sensitised the cells, whereas inhibition caused radioresistance by suppressing the expression of Cockayne syndrome protein A, a DNA repair protein.[189] MiR-302 has been reported to be involved in radioresistance of breast cancer via the modulation of AKT1 and RAD52, and enforced expression sensitised resistant breast cancer cells in vitro and in vivo.[190]

In HNSCC miRNA expression has been profiled after irradiation and miR-1284, which negatively regulates p53 TSG, has been found to be significantly upregulated.[191] In oral cancer cell lines miR-1125b transfection resulted in decreased proliferation rate and enhanced radiosensitivity to high doses of irradiation.[192] Gene expression has been profiled in radioresistant versus radiosensitive oral squamous cell carcinoma cell (SCC) lines, with different signatures being identified.[193] Some of these genes have been shown to be downregulated in oral SCC transfected with miR-100, suggesting it is involved in radiation response.[194] A recent study profiled miRNA expression of a large panel of radioresistant and radiosensitive HNSCC cell lines to identify a biomarker for intrinsic radioresistance. Low expression of epithelial-mesenchymal transition (EMT) inhibiting miRNAs, especially miR-203, were found to be important determinants of radioresistance, and induction of EMT reduced radiosensitivity.[195] HNSCC samples from the Cancer Genome Atlas database was used to validate a five miRNA signature that can could predict radiation responsiveness, which correlated with the expression level of ATM.[196] MiRNAs therefore have the potential to predict radiosensitivity/radioresistance and modulation can alter the sensitivity, indicating the possibility of combining miRNA-based therapy and radiotherapy to improve outcome.

1.5 Hypoxia as a biomarker

Tissue hypoxia occurs when the oxygen level in tissues falls below physiological levels resulting from the inadequate supply of oxygen to meet demand.[197] It arises in tumours due to the high metabolic demand of rapidly proliferating cancer cells and also due to disruption in the blood supply. Tumours develop aberrant and chaotic microvasculature, which are structurally immature and leaky, resulting in ineffective oxygen delivery.[198] Fluid accumulation and increased tumour interstitial pressure restricts and compresses intratumoural blood vessels, further reducing the blood supply. Hypoxia is common in solid

tumours and is associated with poor prognosis. Hypoxia leads to increased risk of tumour progression, metastases, resistance to anti-cancer therapies and recurrence due of a wide range of hypoxia-related consequences, resulting in metabolic and genetic changes that promote an aggressive tumour phenotype.[199] Hypoxia drives tumour progression by selecting clones that can best adapt to the stress of inadequate perfusion and nutrient deprivation, which then expand and develop into a more malignant phenotype.

Hypoxia has been extensively investigated in HNSCC and the association with poor outcome is well known. However it is difficult to assess as intratumoural hypoxia is heterogeneous and dynamic, due to continuing tumour and vessel growth, and constant fluctuations in blood flow. Different biological effects are triggered at different levels of oxygen partial pressure (pO_2) in tissues. There is no consensus for hypoxic thresholds in tumours but at pO_2 < 25-30 mmHg radiosensitivity progressively decreases,[197,200] and at pO_2 < 10-15 mmHg changes in gene expression under the control of the hypoxia regulated transcription factor HIF-1 are demonstrated. At pO_2 < 10 mmHg Vaupel et al[201] demonstrated intracellular acidosis and adenosine triphosphate (ATP) depletion in murine fibroblasts and this level represents a critical threshold for energy metabolism. There is also decreased protein synthesis and oxygen consumption to increase tolerance to hypoxia. At pO_2 < 1 mmHg there is increased apoptosis, reduced oxidative phosphorylation and cells switch to glycolysis to maintain adequate energy levels. Lower levels of pO_2 of 0.2-1 mmHg lengthen G_1 phase of the cell cycle or arrest cells in G_1 and anoxia causes immediate cell cycle arrest.[197]

1.5.1 Classification

Hypoxia can be broadly divided into two basic types: chronic and acute. However there are no clear cutoffs between the two types and there are typically mixed heterogeneous patterns throughout the tumour. Chronic, or diffusion-limited hypoxia, was first described by Thomlinson and Gray in 1955, and is caused by consumption of oxygen by cells close to the blood vessels, leaving an inadequate supply of oxygen and nutrients to the cells further away from the vessels. A distance of approximately 180 μm from vascularised stroma was shown to be the diffusion distance of soluble oxygen.[202] It can also be caused by reduced oxygen content in the blood, such as in anaemia, which may be caused by tumour-related factors as well as anti-cancer therapy or carboxyhaemoglobin formation in heavy smokers, and by compromised perfusion of leaky microvessels. Chronic hypoxia usually occurs after several hours to days of hypoxia, long enough to induce changes in gene expression.[203] Acute hypoxia, otherwise known as cycling, transient, intermittent, or perfusion-limited hypoxia, occurs as a result of fluctuations in the perfusion of tumour vasculature. This results in time periods of better or worse oxygenation of tumour areas. This type of hypoxia

may be ischaemic due to transient occlusion of blood flow by blood clots or tumour cells, or hypoxaemic due to transient reduction in the oxygen content within microvessels.[204] Acute hypoxia may have greater effects than chronic hypoxia on the development of an invasive phenotype with hypoxia-reoxygenation episodes resulting in genomic instability, accelerated growth and metastases.[205]

1.5.2 Biological consequences

Tumour cells exposed to hypoxia activate many signalling pathways, which act in an integrated network affecting common downstream pathways and working together to ensure adaptation to overcome the lack of oxygen and nutrients. They induce changes such as angiogenesis, glycolysis, inhibition of apoptosis and downregulation of cell adhesion molecules resulting in tumour cell detachment, all of which lead to the development and selection of more aggressive clones of tumour cells.

1.5.2.1 Metabolism

Glucose is the main source of energy for cells and enters the cell through a family of glucose transporters (GLUT1 to 4). Energy in the form of ATP is generated under aerobic conditions via glycolysis or the tricarboxylic (TCA) cycle. During glycolysis glucose is metabolised to pyruvate in the cytosol to produce 2 ATPs from each molecule of glucose. Pyruvate enters the mitochondria and is oxidised by pyruvate dehydrogenase (PDH) to produce acetyl coenzyme A (CoA), which enters the TCA cycle. Acetyl CoA is metabolised through a series of reactions generating nicotinamide adenine dinucleotide hydrogen (NADH), a reducing agent used by the oxidative phosphorylation pathway in mitochondria. NADH passes electrons derived from the TCA cycle to the electron transport chain (ETC) in mitochondria, and combines with oxygen to produce water and a proton gradient that is used to generate 36 ATPs per glucose. In the mitochondria ETC, electrons transfer steps are cataylsed at Complex I (NADH dehydrogenase or ubiquinone oxidoreductase) and III (coenzyme Q or cytochrome c reductase) and is transferred to O_2 at Complex IV (cytochrome c oxidase). Each step is coupled with proton translocation across the inner mitochondrial membrane, driving ATP synthesis at Complex V. Electrons can escape the ETC and be captured by O_2, forming reactive oxygen species (ROS) and resulting in oxidative stress.[206]

Under anaerobic conditions the lack of oxygen to act as the final electron acceptor at complex IV in the ETC prevents aerobic metabolism from progressing. Pyruvate is not used in the TCA cycle, but converted to lactate in the cytosol by lactate dehydrogenase (LDH) to regenerate nictotinamide adenine dinucleotide (NAD^+) from reduced NADH, which is

required by glyceraldehyde-3-phosphate dehydrogenase (GAPDH) for additional cycles of glycolysis. PDH is phosphorylated and inactivated by pyruvate dehydrogenase kinase (PDK).[207] Cancer cells have a high rate of glucose consumption even in the presence of oxygen, known as the Warburg effect or aerobic glycolysis.[208] ATP production via glycolysis is much faster but less efficient and cancer cells avidly consume glucose to meet their increased energy and biosynthesis needs. A constant high rate of glycolysis in tumour cells uses up the NAD^+ pool and glycolysis cannot be sustained unless NAD^+ is regenerated, which is achieved by increasing lactate production.

1.5.2.2 Hypoxia-inducible factor-1 signalling pathway

Tumour cell responses to hypoxia are initiated through activation of the hypoxia inducible factor (HIF) family of transcription factors, the most important of which is HIF-1. HIF-1 is a heterodimeric protein consisting of an oxygen-regulated α subunit and a constitutively expressed oxygen-independent β subunit. Under conditions of normal oxygen HIF-1α is rapidly degraded by the Von Hippel Lindau (VHL) tumour suppressor protein via the ubiquitin-proteasome pathway. The α subunits of HIF are hydroxylated at conserved proline residues by propyl hydroxylase (PHD), which use oxygen as a co-substrate, resulting in recognition and ubiquitination by the VHL E3 ligase, labelling them for degradation by the proteasome. HIF-1α accumulation is also prevented under normoxia by factor inhibiting HIF-1 (FIH), which hydroxylates the transactivation domain of HIF-1α. This inhibits the binding of CREB binding protein (CBP) and p300 transcription co-factors to the HIF-1 complex (Figure 1.3).[209]

Hypoxia inhibits hydroxylation of HIF-1α by PHD and FIH, which results in stabilisation and accumulation of HIF-1α. HIF-1α translocates to the nucleus where it heterodimerises with constitutively expressed HIF-1β, and binds to the hypoxia-responsive elements (HREs) in the promotors of target genes. Genes that help overcome hypoxia, such as those involved in cell survival under oxidative stress, erythropoiesis, angiogenesis, glucose metabolism and pH regulation are upregulated, resulting in the upregulation of more than 100 proteins that promote survival and increased aggressiveness of hypoxic tumour cells.[209] Vascular endothelial growth factor (VEGF) is upregulated by HIF-1α in hypoxia and is the strongest inducer of angiogenesis, stimulating the proliferation of endothelial cells and the formation of new blood vessels. VEGF also acts as a tumour cell survival factor, inhibiting cell apoptosis by inducing the anti-apoptotic protein Bcl-2.[210]

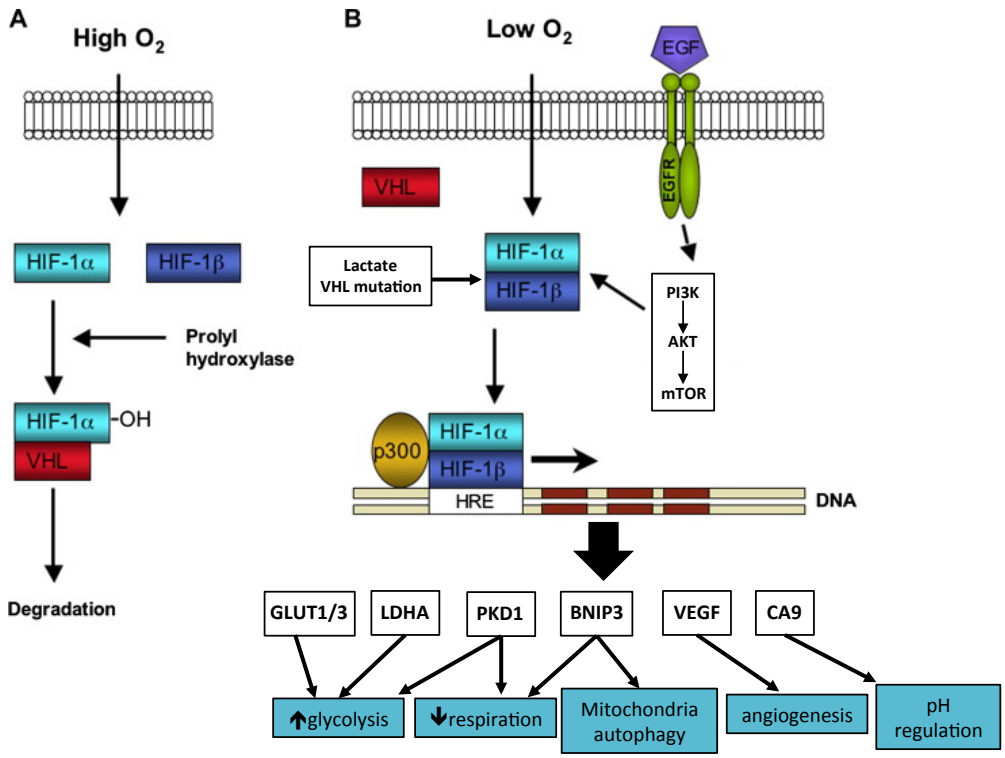

Figure 1.3 HIF-1 activation pathway.
A) Under normoxia HIF-1α is hydroxylated by propyl hydroxylase and is degraded by VHL via the ubiquitin-proteosome pathway. B) Under hypoxia propyl hydroxylase and FIH are inhibited and HIF-1α is stabilised, allowing heterodimerisation with HIF-1β and subsequent binding to the hypoxia-responsive elements in target genes. This results in the upregulation of proteins that promote cell survival. HIF-1α can expression can also be upregulatd by EGFR and PI3K signaling pathways. Adapted from Rademaker 2008.[200]

Under hypoxia HIF-1α mediates a switch from oxidative to glycolytic metabolism.[207] HIF-1α activation affects cellular glucose metabolism by inducing the transcription of genes involved in increased glucose uptake, such as the glucose transporters GLUT1 and GLUT3, and stimulation of glycolytic enzymes that breakdown intracellular glucose. HIF-1α induces lactate dehydrogenase A (LDHA), increasing the conversion of pyruvate to lactate. In addition, HIF-1α activates pyruvate dehydrogenase kinase (PDK), which inactivates pyruvate dehydrogenase (PDH), actively shunting pyruvate away from the mitochondria. This reduces flux through the TCA cycle, reducing delivery of NADH to the ETC. Mitochondrial function is therefore reduced, decreasing oxygen demand in hypoxic cells. In addition HIF-1α induces BCL2/adenovirus E1B 19kDa interacting protein 3 (BNIP3) expression, which triggers mitochondrial autophagy, decreasing mitochondrial mass and oxygen consumption.[206] HIF-1α also diverts pyruvate to be phosphorylated by hexokinase to glucose-6-phosphate, which is used in anabolic pathways such as the pentose phosphate pathway, by upregulating hexokinase. This pathway generates the precursors of nucleotides and amino acids required for the rapid tumour cell growth and proliferation. Hypoxia also triggers the generation of reactive oxygen species (ROS) by the ETC, which

is released into the cytosol where they inhibit PHDs, resulting in stabilisation of HIF-1α.[211] Glycolytic metabolism results in acidosis of the tumour microenvironment due to increased lactate and carbon dioxide levels, which are actively expelled from the tumour cells into the extracellular matrix. HIF-1α upregulates monocarboxylate transporter 4 (MCT4), which removes lactate from the cell, carbonic anhydrase 9 (CA9), which catalyses the conversion of carbon dioxide released during the pentose phosphate pathway to carbonic acid, and sodium-hydrogen exchanger (NHE1), which maintains an alkaline intracellular pH and acidic extracellular pH. Acidosis induces the secretion of matrix-degrading hyaluronidase and metalloproteinases by tumour-associated fibroblasts, creating a tumour microenvironment favourable for invasion and migration.[212] In addition it reduces anti-tumour immunity, inhibiting the activity of dendritic cells and T cells, and the efficacy of drug uptake by tumours, further driving tumour progression.[213]

HIF-1α activation has many other downstream effects including the expression of several proteins important in epithelial-mesenchymal transition, preparing tumour cells for invasion and migration, such as SNAIL, SLUG, TWIST,[214] and inhibition of E-cadherin.[215] It has also been implicated in the regulation of cancer stem cells, through activation of NOTCH1, and tumour-mediated immune suppression through attenuation of T cell function.[216] HIF-1α is also involved in the activation of tumour-associated inflammatory signalling in conjunction with nuclear factor-kappa B (NF-κB),[217] which activates genes that promote cell proliferation and cell survival, and STAT3, which also works with HIF1α to activate VEGF.[218] In addition miRNAs are also activated, with direct binding of HIF-1α to a HRE on the proximal miR-210 promotor.[219]

Factors other than hypoxia can activate HIF-1α, such as pyruvate and lactate, indicating a positive feedback mechanism. HIF-1α expression can also be upregulated under conditions of normoxia, such as through activation of the receptors of the tyrosine kinase family including EGFR, activation of the PI3K-AKT-mTOR pathway, and genetic mutations including VHL inactivation, loss of PTEN and p53 tumour suppressors.[220]

1.5.2.3 mTOR signalling

mTOR activation results in stimulation of protein synthesis and cell growth. Mild to moderate hypoxia levels suppress mTOR through a HIF-1 independent pathway involving the activation of tuberous sclerosis protein 1(TSC1)-TSC2 complex via adenosine monophosphate-activated protein kinase (AMPK) or via transcriptional regulation of REDD1. mTOR is a principle regulator of autophagy under nutrient depleted conditions, which is regulated by BNIP3 and AMPK during hypoxia. In addition mTOR interacts with HIF-1α, promoting the rate of HIF-1α mRNA translation. In tumour cells hypoxia has been

shown to be less effective at inhibiting mTOR through mechanisms such as constitutive mTOR activity or loss of function of TSC2 or PTEN, the negative regulator of this pathway.[221]

1.5.2.4 The unfolded protein response (UPR)

Messenger RNA translation, post-translational modifications and protein folding takes place in the endoplasmic reticulum (ER). Under conditions of stress, such as severe hypoxia, misfolding of proteins occur which accumulate in the ER, resulting in ER stress. This activates the unfolded protein response, which aims to relieve this stress and increase cell survival by activating the ER stress sensors such as protein kinase R-like endoplasmic reticulum kinase (PERK). PERK activation results in inhibition of global mRNA translation and protein synthesis to reduce the load of misfolded proteins and lower energy demands. It also upregulates the expression of genes involved in resistance to oxidative stress and amino acid metabolism to promote cell survival, and enhances HIF-1α transcriptional activity. ER-associated degradation and autophagy occur to remove misfolded proteins, further reducing ER stress.[222] ER stress also modulates the expression of VEGF, stimulating angiogenesis and promoting cell survival of rapidly growing cells. In addition VEGF signalling can activate the UPR in endothelial cells in the absence of ER stress via mTOR signalling, further promoting angiogenesis.[223] The UPR is upregulated in tumours and is an important survival response in conditions of prolonged hypoxia, increasing the threshold for apoptosis. Tumours cells with abrogated PERK activity show significantly reduced clonogenic survival and decreased ability to tolerate moderate to extreme hypoxia, with higher levels of apoptosis in hypoxic areas.[224]

1.5.2.5 MicroRNAs

Several studies have demonstrated through genome-wide miRNA profiling that miRNA expression in tumour cells is altered in response to hypoxia.[152,225-229] However due to differences in tumour cell lines, variations in exposure to hypoxia severity and duration, as well as differences in microarray hybridisation platforms resulting in different ranges of miRNAs screened, there has been limited overlap in the patterns of miRNA up- and downregulation. Next generation sequencing techniques have revealed a greater number of previously not identified miRNAs, highlighting the complexity of miRNA response to hypoxia.[230] MiR-210, however, has been robustly and consistently induced by hypoxia, in both normal and cancer cells. It has also been shown to be overexpressed in a variety of solid tumours and patient plasma or serum, including HNSCC, where it is generally associated with poor clinical outcome.[231,232] Under hypoxic conditions miR-210 is induced independently and directly by HIF-1α through interaction with its promotor sequence, and

targets genes involved cell cycle regulation, mitochondrial function, apoptosis, angiogenesis and metastases. MiR-210 promotes stabilisation of HIF-1α and inhibit PHDs preventing the degradation of HIF-1α.[233]

1.5.3 Clinical consequences in HNSCC

1.5.3.1 Clinical studies using Eppendorf polarographic needle electrodes

Approximately 50-60% of human tumour contain hypoxic and/or anoxic tissue regions that are heterogeneously distributed within the tumour.[234] Many clinical studies, mainly in HNSCC and cervix cancers, using Eppendorf polarographic needle electrode histography have directly demonstrated that tumour hypoxia predicts for decreased local control, increased disease recurrence and reduced overall survival. This technique involves inserting an electrode into multiple sites in a tumour and measuring the pO_2 at several points per needle track and data from all tracks form a histogram. In head and neck cancers the pO_2 measurements between the primary tumour and metastatic lymph nodes have shown little difference, and nodal measurements have been used to represent the hypoxic status of the patient.[235]

In head and neck cancer, Gatenby et al[236] in 1988 measured the oxygen tension in 31 lymph node metastases from HNSCC patients, and demonstrated a significant relationship between low mean pO_2 measurements and poor response to radiotherapy. The volume of tumour containing low oxygen levels was also found to be important. Nordsmark et al[237] measured the pretreatment oxygenation status initially in 34 lymph nodes and one primary using the Eppendorf polarographic needle electrode histography and evaluated the tumour oxygenation status as the percentage of pO_2 values ≤ 2.5 mmHg (hypoxic fraction 2.5, HF2.5). The median HF2.5 of 15% was used to define hypoxia and these patients had significantly poorer locoregional control (LRC). This was confirmed by the same group in a further 35 patients.[238] Brizel et al[239,240] assessed 63 patients for pretreatment tumour oxygenation using the primary site or metastatic lymph node. A preliminary study had shown significantly worse disease free survival (DFS) at 12 months for patients with a median pO_2 < 10 mmHg, and this was used to define hypoxic tumours. Whether the measurement was taken at the primary or nodal site did not affect the DFS and hypoxic tumours had significantly worse 3 year LRC, DFS and overall survival (OS), independent of tumour stage. However a small study of 25 patients did not find an association between pretreatment oxygen levels and LRC or OS.[241]

Stadler et al[242] identified the importance of the hypoxic subvolume, defined as the percentage of pO_2 values < 5 mmHg multiplied by the total tumour volume. Fifty-nine

HNSCC primaries and nodes were assessed and the median pO2 was 16 mmHg, with no difference between the sites. On multivariate analysis the hypoxic subvolume and the HF5 were significant prognostic factors for survival. This was confirmed in a further 125 patients, where hypoxic tumour volume was a strong and independent prognostic factor for survival.[243] Rudat et al[244] evaluated the repeatability and predictive value of pO_2 Eppendorph electrode histography in HNSCC. High variability was seen in patients who had 2 repeated independent measurement of the same tumour. In 41 patients with follow up data, locally advanced HNSCC the fraction of $pO_2 \leq 2.5$ mmHg was a significant prognostic factor for survival.

A joint analysis of prospectively collected Eppendorf pO_2 measurements from multiple centres was performed, which consisted of 397 patients with HNSCC.[245] Median tumour pO_2 was 9 mmHg and multivariate analysis demonstrated that HF2.5 greater than population median (19%) was associated with poorer OS at 3 years, providing strong evidence that tumour hypoxia has a significant role in HNSCC. Table.1.3 summaries the clinical data from HNSCC.

Table.1.3 Summary of Eppendorf electrode histography studies in HNSCC.

No. of patients	Outcome	Ref
31	Mean pO_2 20.6 mmHg in complete responders vs 4.7 mmHg in non-responders to radiotherapy.	236
35	Median pO_2 14 mmHg. Median HF2.5 > median (15%) significantly worse LRC.	237
31	Median pO_2 12 mmHg, median HF2.5 30%. Median HF2.5 > median (15%) significantly worse LRC.	238
63	Median pO_2 4.8 mmHg for 24 primary sites. Median pO_2 4.3 mmHg for 39 nodes. Median pO_2 < 10 mmHg significantly worse LRC, DFS, OS.	239,240
41	Median pO_2 10 mmHg. HF2.5 > median (21%) worse OS.	244
397	Joint analysis of prospectively collected data in HNSCC. Median tumour pO_2 9 mmHg. HP2.5 > median (19%) associated with poorer OS.	245
25	Mean pO_2 20.2 mmHg. No prognostic impact on outcome.	241
59	Median pO_2 16mmHg. Hypoxic subvolume > 6 cm3, HF5 > median (30%) worse overall survival.	242
125	Median pO_2 9.4 mmHg. Hypoxic volume prognostic factor for OS.	243

1.5.3.2 Resistance to radiotherapy

Radiosensitvity rapidly decreases when the pO_2 in a tumour is less than 25 to 30 mmHg.[197] In 1953 Gray et al[246] determined the radiation dose required to achieve the same biological

effect is 2.8 to 3 times higher in the absence of oxygen. When ionising radiation is absorbed in tissue, free radicals are produced as a result of ionisations either directly in the DNA itself, or indirectly in other molecules such as water. Free radicals break chemical bonds and initiate a chain of events that result in DNA damage. Oxygen molecules are able to react with the free radicals and create a stable change in the chemical composition of the DNA damage. Oxygen therefore enhances the damage by "fixing" or making the damage permanent. In the absence of oxygen the target is chemically restored and the damage is repaired. In order for oxygen to consolidate radiation-induced damage it needs to be present at the time of irradiation or within a few milliseconds.[247] Other hypoxia-induced mechanisms also contribute to radioresistance including glycolytic metabolism and lactate accumulation, which act as antioxidants and scavenge free radicals.[248,249]

The changes in hypoxia heterogeneity during a course of fractionated RT can affect the response. During the early stages of treatment cell density decreases as the well-oxygenated tumour cells are killed. This results in reduced intratumoural pressure and increased vascular density leading to tumour reoxygenation.[250] This reoxygenation does not increase HIF-1α degradation, but the increase in ROS formation stabilises HIF-1α and increases the expression in a hypoxia-independent manner.[251] This, together with accelerated repopulation that occurs at the later stages of RT, means that the entire cumulative dose of RT needs to be delivered.

1.5.3.3 Resistance to chemotherapy

Some chemotherapeutic agents, such as etoposide, are dependent on the presence of oxygen for maximum cytotoxic effect.[252] The disordered and leaky blood vessels in hypoxic tumours prevent efficient delivery of chemotherapy drugs. Hypoxic cells are distant from blood vessels and therefore not adequately exposed to drugs.[253] Alkylating agents, such as cisplatin, and anti-metabolites, such as 5-FU, act during DNA synthesis by damaging DNA and initiating apoptosis. Cellular proliferation and DNA synthesis decreases as a function of distance from blood vessels and hypoxia selects for cells that have lost sensitivity to p53 mediated apoptosis, reducing the cytotoxic effect. Hypoxia upregulates genes involved in drug resistance, such as multidrug resistance 1 (MDR1) leading to the increased expression of P-glycoprotein, which is associated with tumour resistance to chemotherapeutics.[254] The acidic tumour microenvironment creates a pH gradient between the tumour cell and extracellular space, inhibiting the accumulation of drugs that are weak bases, such as doxorubicin.[255]

1.5.3.4 Therapeutic approaches to overcome hypoxia radioresistance in HNSCC

Hypoxia represents a potential target for therapy. Various strategies have been used to overcome hypoxia in HNSCC, summarised in Table.1.4. A meta-analysis of 32 clinical trials of various strategies of hypoxic modification demonstrated a small but significant improvement in LRC, disease specific survival (DSS) and OS in HNSCC treated with primary RT.[256] Hypoxia stratification is required to identify patients at risk of treatment failure but also patients with normoxic tumours, who do not gain benefit from additional treatment, who can avoid any additional toxicity.

Table.1.4 Summary of methods investigated to overcome hypoxic radioresistance.

Method	Example
Increasing oxygen availability	Hyperbaric oxygen ARCON Blood transfusion, erythropoeitn
Radiosensitisers	Nimorazole
Hypoxia cytotoxin	Tirapazamine
Increasing radiotherapy dose	Dose painting
Other	Anti-angiogenic agents with RT HIF-1 targeting

Improving haemoglobin (Hb) levels

Many studies have demonstrated that low haemoglobin level prior to treatment associated with significant reduction in survival and increase in locoregional failure in HNSCC after RT or CRT.[257,258] Over 1000 patients pooled from 2 studies demonstrated that high Hb was significantly associated with higher OS and the administration of blood during therapy increased Hb level. However blood transfusions had no impact on LRC, DSS or OS.[259] Exogenous erythropoietin administration to stimulate red blood cell production and correct anaemia has been investigated. However this did not improve tumour control or survival as demonstrated in 2 meta-analyses, but suggested an increase in mortality.[77,260]

Increasing oxygen availability

Hyperbaric oxygen is the administration of 100% oxygen at higher than normal atmospheric pressure. This elevated pressure results in increased pO_2 in tissues and has been delivered in hyperbaric oxygen chambers with RT. This strategy has been shown to significantly improve tumour control and mortality, but also causes an increased rate of severe radiation tissue injury and chance of oxygen toxic seizures during therapy.[261]

Carbogen (95% oxygen and 5% carbon dioxide) breathing before RT did not improve tumour control,[262] but combined with accelerated radiotherapy and nicotinamide (ARCON,

accelerated radiotherapy with carbogen and nicotinamide) has been shown to result in high LRC in advanced larynx and oropharynx SCC.[263] This combination aims to limit clonogenic repopulation during therapy by reducing the overall duration of RT by delivering more than one fraction a day, decrease diffusion-limited hypoxia with inhalation of carbogen, and decrease perfusion-limited hypoxia by administering nicotinamide, a vasoactive vitamin B_6 analogue. A more recent study compared accelerated RT with ARCON in larynx SCC and did not demonstrate a benefit. However a subgroup of patients had their hypoxic status assessed with pimonidazole IHC, which stains regions of hypoxia, and significant improvement in regional control and DFS was found in the high pimonidazole staining group treated with ARCON.[264]

Radiosensitisers

Cellular sensitivity to RT can be improved by increasing the apparent cellular pO_2 levels using radiosensitisers. Nitromidazoles are chemical compounds that mimic the radiosensitising effect of oxygen by inducing and stabilsing free-radical mediated double-stranded DNA breaks. The benefit of the addition of a nitroimidazole compound to RT was carried out in many studies, without clinical benefit.[265,266] However these studies used the older generation of the drug which is limited by neurotoxicity. Overgaard et al[267] carried out a meta-analysis of over 7000 patients treated with nitroimidazole-based radiosensitisers in various tumour types of unknown hypoxia status and found an improvement in LRC and OS, with the greatest benefit in HNSCC. This was followed by the DAHANCA 5 study which randomized over 400 HNSCC patients to receive RT with nimorazole or RT with placebo. LRC and DSS were significantly higher with the addition of nimorazole.[268] A phase II study investigated accelerated RT with nimorazole and cisplatin in 227 patients with locally advanced HNSCC and recently reported a high 5-year OS of 75%.[269]

Hypoxic cytotoxins

This group of drugs, of which tirapazamine is the most widely investigated, have a direct cytotoxic effect on hypoxic cells. Tirapazamine (TPZ) is a prodrug that requires one-electron reduction to a radical by intracellular reductases. In normoxia the unpaired electron in the radical is rapidly transferred to molecular oxygen, forming superoxide and regenerating the initial prodrug. In hypoxic conditions the radical accumulates and induces DNA damage, in part due to poisoning of topoisomerase II.[270]

TPZ combined with cisplatin and RT in HNSCC has shown to be well tolerated in phase I and II studies.[271,272] Rischin et al carried out a phase II randomised trial of this combination versus cisplatin and RT and demonstrated a trend towards improved 3-year survival with acceptable toxicity.[273] However, further studies have not shown a benefit in survival or

quality of life from the addition of TPZ.[274] Rischin et al also carried out a substudy of 45 patients who had their tumour hypoxic status assessed by ^{18}F-fluoromisonidazole, a hypoxic radiotracer, PET scans. Hypoxic patients performed poorly in the absence of TPZ augmentation, whereas the rate of complete response in the hypoxic group receiving TPZ was nearly as high as the rate for normoxic chemoRT patient. Patients with hypoxic tumours were more likely to develop distant metastatic disease compared with normoxic patients.[275]

Hypoxia image-guided radiotherapy

Intensity modulated radiotherapy (IMRT) is used in the treatment of HNSCC. The intensity of the radiation beam can be modulated to reduce doses to normal structures without compromising the doses to the tumour. Tumour recurrence after compete response to radiotherapy has been shown to occur predominantly in high radiation dose regions, implying that tumours have radioresistant subvolumes, potentially due to hypoxia, within this region.[276] IMRT dose painting is a method of assigning different dose levels to structures within the same treatment fraction, resulting in the potential for higher total doses to selected targets.[277] Dose painting requires functional imaging such as positron emission tomography to direct regions for dose escalation. Intensification of intratumoural subvolumes of hypoxia has been investigated as a strategy to improve outcome in RT planning studies and radiobiological modelling studies only, as this requires accurate and stable identification of hypoxia to guide target volume delineation.

Targeting angiogenesis

High VEGF expression levels has been associated with worse overall survival in HNSCC.[278] As tumour vasculature is abnormal, increased VEGF expression and microvascular density does not lead to increased blood flow and oxygen delivery. Targeting VEGF is a strategy to improve oxygenation by normalising the tumour vasculature and thereby increase response to RT. RT can lead to stimulation of angiogenesis through upregulation of VEGR and therefore anti-angiogenic therapy has been tested with RT.[279] Bevacizumab is a humanised monoclonal antibody against VEGF approved for use in colorectal cancer, and has been investigated in phase II studies concomitant with chemoRT in HNSCC with encouraging results.[280] It inhibits endothelial cell growth and function, disrupting the formation of capillary networks, and has been shown to enhance RT response in HNSCC xenograft models.[281] Anti-angiogenic agents can improve tumour oxygenation by reducing the number of oxygen consuming endothelial and tumour cells, and the number of inefficient blood vessels. This also results in less leaky vessels and decreased interstitial pressure, improving perfusion.[282]

Targeting HIF-1

Targeting HIF-1 is an attractive therapeutic strategy to overcome the effects of hypoxia. Drugs that inhibit HIF-1 activity are already in clinical use, such as the topoisomerase I inhibitor topotecan and mTOR inhibitors which decrease HIF-1 synthesis, the anthracycline doxorubicin which suppresses HIF-1 DNA binding, and the proteasome inhibitor bortezomib, which reduces HIF-1 transactivation.[283] Newer drugs have been developed, such as PX-478 that inhibits HIF-1 by inhibiting HIF-1 mRNA translation and HIF-1 dequbiquitination and is being investigated in a phase I trial. In HNSCC tumour models this drug provided significant radiosensitisation of hypoxic cell lines and xenograft tumours.[284]

1.5.4 Other methods to detect hypoxia in HNSCC

Accurately detecting and quantifying hypoxic tumours is essential in identifying patients who have aggressive, treatment resistant disease and has been one of the limiting factors for translating hypoxia-modification strategies into routine practice. The use of Eppendorf oxygen electrode histography has been crucial to demonstrate the adverse effects of hypoxia on outcome in the clinical setting. It has the advantage of directly measuring absolute pO_2 values and has prognostic potential. However it has not been incorporated into routine clinical practice as it is an invasive procedure restricted to accessible tumours. It also requires an experiences operator but still exhibits large inter-observer variability,[285] and only provides information on the areas sampled. In addition it cannot differentiate between tumour and normal tissues.[234] Other methods that have been investigated are summarised in Table.1.5.

Table.1.5 Summary of methods used to detect hypoxia.

Method	Example
Direct detection	Eppendorf oxygen electrode histography
Exogenous markers	2-nitroimidazole – pimonidazole, EF5
Endogenous markers Tumour protein levels Circulating markers Gene expression signatures	 HIF-α1, CA9, osteopontin Osteopontin, miR-210 Hypoxia metagene, 15-gene classifier
Non-invasive imaging	DCE MRI, BOLD MRI PET – ^{18}F-FMISO, ^{64}Cu-ATSM

1.5.4.1 Exogenous markers of hypoxia

The most commonly used exogenous markers of hypoxia are 2-nitroimidazole compounds such as pimonidazole and pentafluorinated etanidazole (EF5).[286,287] They are irreversibly bioreduced by cellular nitroreductases and bind to thiol-containing proteins in viable hypoxic cells, forming stable adducts.[288] These adducts can then be detected by IHC

staining with specific antibodies. IHC staining can quantify hypoxia by visually or digitally estimating the fraction of stained cells and provides hypoxic measurements with high spatial resolution. Binding is commonly seen adjacent to regions of necrosis and at a distance from blood vessels, in keeping with diffusion-limited hypoxia.[286]

2-nitroimidazoles bind to tissue at a pO_2 level of < 10 mmHg and are more sensitive at lower pO_2 levels than microelectrodes.[289] The amount of bound marker is dependent on oxygen, the accumulation rate of individual hypoxic cells and intact nitroreductase enzymes in viable hypoxic cells.[290] Differences in the activity of the enzymes can affect level detected and the accumulation rate of pimonidazole is dependent on pH.[291] The main disadvantage to exogenous markers of hypoxia is that they have to be administered intravenously prior to tissue biopsy or surgical resection, to allow fixation of the adducts that form in hypoxic regions. Pimonidazole binding has shown good correlation with Eppendorf electrode measurements in mouse models,[289] but not in the clinical setting in cervix cancers.[292] Neither pimonidazole or Eppendorf electrode pO_2 were prognostic for outcome in 127 cervix cancer patients.[293]

The prognostic value of 2-nitroimidazoles has been shown in HNSCC. High pimonidazole binding in 43 biopsies was significantly associated with LRC and DFS at 2 years. This association was lost in the subgroup treated with ARCON, suggesting a predictive role for pimonidazole.[294] Pretreatment hypoxia using EF5 binding was investigated in 22 HNSCC patients and severe hypoxia, defined as maximum 30% EF5 binding which approximated to a pO_2 of 0.76 mmHg, was associated with shorter event free survival at 3 years.[295]

1.5.4.2 Endogenous markers of hypoxia

Endogenous markers are genes or gene products that are specifically upregulated under hypoxic conditions and can be measured in tumour specimens. HIF-1α, GLUT1 and 3, CA9 and osteopontin are detected by immunohistochemistry and can be assessed on formalin fixed paraffin embedded (FFPE) archival material, allowing correlation with outcomes. However the techniques of tissue processing and staining analysis have not been validated between different laboratories, limiting comparisons and clinical applications. Samples are usually from small biopsy specimens and therefore not representative of the hypoxia heterogeneity of entire tumour. In addition their expression may be affected by the type of hypoxia, for example HIF-1α is induced and repressed rapidly and reflect acute changes in hypoxia, whereas CA9 is slow to accumulate.[296] In general, studies using these markers show conflicting results, and the association between these markers and oxygen status of tissue is weak.

HIF-1α

HIF-1α is overexpressed in a wide variety of tumours. In HNSCC many studies have demonstrated an association with poor survival and poor response to chemoRT,[297,298] and has been found to be an independent prognostic factor in HNSCC. However there are also studies that show no association with prognosis,[299,300] and in one study in a surgically resected cohort of HNSCCs, HIF-1α expression was associated with significantly better DFS and OS.[301]

Glucose transporters (GLUT)

These glucose transporters are present in normal tissue but upregulated in tumours due to increased glucose requirements in anaerobic glycolysis.[302] In HNSCC GLUT-1 has been associated with poor treatment outcome in multiple retrospective series.[303,304] In 58 patients treated with ARCON GLUT-1 was associated with an increased rate of distant metastasis and worse OS but GLUT-3 was associated with better LRC.[305] Co-expression of HIF-1α and GLTU-1 significantly correlated with an increased risk of tumour-related death.[306]

Carbonic anhydrase 9 (CA9)

CA9 is a transmembrane enzyme and a downstream target of HIF-1. It catalyses the reversible hydration of carbon dioxide to carbonic acid and is involved in pH regulation. Elevated expression has been demonstrated at pO_2 < 20 mmHg.[307] Overexpression of CA9 has been found in different types of cancer including HNSCC but shows conflicting results as a prognostic marker. Strong CA9 expression was found to be related to poor complete response rate after treatment with chemoRT,[308] but positivity was associated with better LRC and freedom from distant metastases in 58 patients treated with ARCON,[305] or no association with LRC.[309] In the DAHANCA 5 study patients 320 samples were available for CA9 staining and the expression of CA9 did not correlate with any of the tumour or patient characteristics, was not a prognostic marker and did not correlate with nimorazole treatment.[310]

Osteopontin (OPN) in tissue and plasma

OPN is an extracellular matrix-associated integrin-binding glycoprotein induced by hypoxia, initially identified in non-collagenous bone matrix. Binding of OPN to cell surface receptors on tumour cells activates integrins and matrix metalloprotein signalling pathways, increasing the risk of tumour invasion and migration.[311] It is also involved in angiogenesis, promotes cell survival through PI3K/AKT and JAK/STAS3 signalling and regulation of NF-κB. It is upregulated through AKT activation, independent of HIF-1 under hypoxia.[312] High OPN levels in both tissue and plasma have been correlated with low tumour pO_2 in HNSCC and outcome.[309] A retrospective study of the DAHANCA 5 trial patients demonstrated that

high OPN plasma levels was associated with higher locoregional tumour failure and disease specific mortality.[313] Patients with high OPN levels who received nimorazole had better outcomes compared with patients with high OPN levels who did not receive nimorazole, whereas no effect was seen in the low/intermediate OPN group. Lim et al[314] investigated the predictive potential of OPN in patients who received tirapazamine but did not find that high levels were associated with poor prognosis and found no interaction between OPN and treatment. The difference in results compared with the DAHANCA study may be due to differences in treatment protocols, but also lack of standardisation for OPN thresholds between the studies.

Gene expression signatures of hypoxia

As hypoxia influences many biological pathways, a single marker is incapable of adequately describing this complex heterogeneous response. To improve hypoxia specificity combining several markers in gene expression signatures of hypoxia has been investigated. Different methods have been used to derive clinically applicable hypoxic gene signatures and are summarised in Table 1.6.

In vitro derived gene sets have been described by culturing tumour cell lines under normoxic and hypoxic conditions, then assessing the differences in gene expression. Koong et al[315] used FaDu HNSCC and SiHa cervical SCC cell lines to identify 9 genes exhibiting greater than 3-fold induction under hypoxic conditions when using the expression of VEGF as a cut off point for assessing hypoxia-induced genes. An 84 upregulated gene signature was generated by culturing normal and transformed keratinocytes at various different oxygen levels, which could be grouped into 6 functional groups, including as metabolism/transport, angiogenesis, tissue remodelling, apoptosis, proliferation/differentiation and gene expression.[316]

Chi et al[317] evaluated the gene expression in response to hypoxia in several primary cell lines in vitro using cDNA microarrays and found a wide variation in the response between cell and tissue types. However a 253 gene signature was identified which were concordant with gene expression data from a distinct subset of renal tumours, allowing classification by hierarchical clustering into 2 groups with high or low expression of the hypoxia response genes. The high expression group consisted of clear cell renal carcinomas, which typically have loss of function al VHL proteins, and the low group were other histological subtypes or normal samples. Similar classification grouped breast cancers in to ductal adenocarcinomas (high expression) and fibroadenomas or normal samples (low expression). In addition the gene signature was a strong predictor of clinical outcome in independent breast and ovarian cancer datasets.

Table 1.6 Summary of hypoxia gene expression signatures.

Source of signature	No. of genes in signature	Prognostic validation	Ref
FaDu, SiHa cell lines in vitro under hypoxia and normoxia	9	No	315
Normal cervical and dermal keratinocytes, normal stromal fibroblasts, SiHa, C33a, FaDu cells	84	No	316
Mammary and renal tubular epithelial cell lines under hypoxia or normoxia for 12 hours	253	2 breast cancer, 1 ovarian cancer datasets – prognostic for OS and RFS on univariate analysis; breast dataset - prognostic for OS on multivariate analysis	317
Mammary epithelial cell line under hypoxia; early (1-6 hours) or late (12-24 hours)	Early 15 Late 93	Early signature prognostic for DSS in breast cancer dataset on univariate analysis only; late signature not prognostic	318
59 HNSCC biopsy specimens Clustering around known hypoxia regulated genes	99 hypoxia metagene	Independent prognostic factor in head and neck for RFS and breast for OS and metastasis free survival	112
In silico generation of hypoxia co-expression networks using 3 head and neck and 5 breast cancer studies	51 common hypoxia metagene	Prognostic in breast, 2 lung, head and neck datasets	319
FaDu, UTSCC5, UTSCC 14, UTSCC15 cell lines under hypoxia and either normal or acidic pH	27	No	320
UTSCC33 , FaDu and SiHa tumour xenografts - hypoxic regions identified using FAZA hypoxia tracer; 58 HNSCC fresh frozen biopsies with oxygen electrode measurements	15	FFPE samples from DAHANCA5 trial – independent prognostic factor; more hypoxic tumours treated with nimorazole had reduced incidence of locoregional failure.	321
DU145, HT29, MCF7 cell lines exposed to normoxia and different times of severe hypoxia	7 temporal and 2 general signatures	Not prognostic in breast cancer dataset	322

Human mammary epithelial cells were cultured under hypoxic conditions at early and late time points to assess the time dependency of hypoxia-regulated gene expression.[318] The early response gene signature was characterised by genes related to growth, apoptosis, insulin and oestrogen receptor signalling, whereas the late response was characterised by genes involved in angiogenesis, glucose transport, proliferation, metastasis and apoptosis, and were similar to the genes identified by Chi et al. The early but not late signature was prognostic in univariate analysis, but not maintained in multivariate analysis in a breast cancer dataset. Sorensen et al[320] exposed 4 head and neck cell lines to different oxygen concentrations at normal or low pH, and analysed the gene expression to identify genes upregulated by hypoxia, independent of pH. Hypoxia induced pH independent genes were selected if they were common in 3 of the 4 head and neck cell lines, resulting in a 27 gene signature.

Winter et al[112] developed a hypoxia metagene from 59 HNSCC fresh frozen samples by clustering around the mRNA expression of 10 well-known hypoxia-regulated genes, such as CA9, GLUT1 and VEGF. Strongly correlated upregulated genes appearing in > 50% of clusters defined a signature comprising of 99 genes, which was found to be an independent prognostic factor for recurrence free survival (RFS) in an independent head and neck cancer and breast cancer dataset. The same group derived a common hypoxia metagene consisting of 51 genes by selecting genes that were consistently co-expressed with previously validated hypoxia-regulated genes.[319] By applying more training sets and co-expression networks a reduced metagene had prognostic significance in 4 independent datasets of breast, lung and head and neck cancers, and outperformed larger published signatures. The top 26 genes from this signature were retrospectively assessed in FFPE samples from laryngeal and bladder cancer patients treated with ARCON or CON (carbogen and nicotinamide) respectively.[323] Tumours were categorised into high and low hypoxia groups, and laryngeal tumours in the high hypoxia group showed greater benefit from ARCON than the low hypoxia group. The hypoxia signature did not predict benefit from CON in bladder cancer.

In contrast to previous studies on hypoxia gene expression, Toustrup et al[321] developed a classifier based on the hypoxic status of tumours. The hypoxia induced pH independent gene profile developed by Sorensen et al was validated in vivo in a xenograft study using ^{18}F-FAZA as an exogenous hypoxia radiotracer in autoradiographic studies. Hypoxic, non-hypoxic and mixed heterogeneous tumour areas defined by ^{18}F-FAZA positive and negative regions were demarcated and dissected. All the genes investigated were significantly upregulated in hypoxic tumour areas compared with non-hypoxic areas, and all but 3 were upregulated in samples from mixed heterogenous versus non-hypoxic areas. To identify the most informative genes, a training set of 58 hypoxia-evaluated HNSCC FFPE biopsies were analysed for gene expression. The oxygenation status of these tumours had previously been evaluated in accordance to the relative number of oxygen electrode measurements less than 2.5 mmHg in their metastatic cervical lymph nodes. A 15-gene expression classifier was generated containing 15 of the in vitro identified hypoxia-responsive genes, which could best discriminate between ‘more’ and ‘less’ hypoxic human HNSCCs. This was evaluated in an independent data set, where patients with HNSCC were randomised to receive either hypoxic modification with nimorazole or placebo concomitant with radiotherapy. Patients with ‘more’ hypoxic tumours defined by the classifier had significantly higher cumulative incidence of locoregional failure at 5 years compared with those with less hypoxic tumours. Within the ‘more’ hypoxic group, patients treated with nimorazole had significantly reduced incidence of failure compared with placebo, whereas in the ‘less’ hypoxic group there was no significant difference in outcome,

suggesting the classifier potentially has predictive value. Further subgroup analysis demonstrated that this benefit was only found in HPV-negative 'more' hypoxic tumours and not HPV-positive, whose outcome was unaffected by hypoxic modification.[324] The same frequencies of 'more' and 'less' hypoxic tumours were in HPV-negative and positive groups as assessed by the classifier. More recently the classifier was used to assess 55 patients recruited in a randomised trial of accelerated RT with or without nimorazole.[325] RT alone in 16 patients with 'more' hypoxic tumours was associated with higher locoregional tumour failure.

Further investigation into the time dependent gene expression changes in response to hypoxia has been carried out using prostate, colon and breast cancer cell lines exposed to hypoxia at 8 different time points between 0 and 24 hours.[322] Seven different signatures consisting of induced genes with distinct temporal profiles and 2 general hypoxia signatures were generated, but none were prognostic in a large breast cancer cohort. In contrast previously published in vivo derived signatures showed clear prognostic power, suggesting the importance of the tumour microenvironment in the response to hypoxia.

Classification of hypoxia gene expression has the potential to represent prognostic and predictive markers in cancer and has been demonstrated retrospectively to be applicable to unselected FFPE biopsy samples, and therefore translatable into clinical practice. However the 2 smaller gene signatures (15 and 26 gene signatures) which have demonstrated predictive value, have only 4 genes that overlap, suggesting that this method alone may not identify all hypoxic tumours. Prospective validation in clinical studies is required before further conclusions can be made.

1.5.4.3 Magnetic resonance imaging (MRI)

Dynamic contrast-enhanced MRI (DCE MRI)

In this technique fast repeated images are acquired before, during and after the rapid administration of a small hydrophilic gadolinium-based contrast agent, which diffuses through blood vessel walls and distributes into the extracellular space. The change in signal intensity reflects tumour perfusion, vessel permeability and the volume of extracellular space.[326] It does not correlate directly with tissue pO_2 levels but a small study in HNSCC found positive correlation between imaging parameters of poor perfusion and pimonidazole staining,[327] and with hypoxia defined by ^{18}F-fluoromisonidazole PET uptake in nodal metastases.[328]

Blood oxygen level-dependent MRI (BOLD MRI)

This is an indirect measure of visualising pO_2 in blood vessels and surrounding tissue based on the paramagnetic properties of deoxyhaemoglobin, which is related to tissue oxygenation. It does not provide quantitative information on oxygen concentration and the signal can be influenced by many factors such as blood flow and pH. However studies have shown correlation between this technique and polargraphic electrode pO_2 measurements and pimonidazole staining in prostate cancer, suggesting BOLD MRI may provide complementary information related to tissue oxygenation.[329]

1.5.4.4 Positron emission tomography (PET)

Several hypoxia-specific PET radiotracers have been developed and extensively investigated as it is a potentially useful non-invasive technique for identification, quantification of hypoxia and repeated measurements after intervention. The metabolic activity demonstrated by ^{18}F-FDG uptake is indirectly related to the proliferative activity and oxygenation status of tumours, but cannot reliably distinguish hypoxic tumours. A good hypoxia tracer should be able to detect pO_2 levels that are clinically relevant to therapy, and be able to distinguish between normoxia, hypoxia, anoxia and necrosis. The molecule should be small and lipophilic making it highly membrane permeable leading to rapid uptake into cells and rapid clearance from normoxic cells to allow a high tumour to background contrast. It should also have a good dosimetry profile with simple radiolabelling and production, and low radiation dose to the patient. Two main classes of hypoxia imaging radiotracers are in available in the clinical trial setting: one based on the nitroimidazole compounds and one based on a complex of copper with diacetyl-bis(N^4-methylsemicarbazone) (ATSM) ligands (section 1.6). A meta-analysis of published hypoxia imaging studies, which included PET and other imaging modalities of hypoxia, showed a uniform tendency for poor response to radiotherapy in tumours showing a higher uptake despite the heterogeneity of the image acquisition, data analysis and treatments.[330]

2-Nitroimidazole-based hypoxia tracers

^{18}F-fluoromisonidazole (^{18}F-FMISO)

^{18}F-FMISO is a derivative of the nitroimidazole group of compounds and is the most widely studied hypoxic radiotracer. It is moderately lipophilic and enters cells by passive diffusion across the cell membrane. The nitro group of the imidazole ring structure ($R\text{-}NO_2$) is reduced by intracellular reductases to $R\text{-}NO_2^-$, which is reoxidised in the presence of oxygen and the tracer can flow back into the extracellular compartment. In conditions of hypoxia $R\text{-}NO_2^-$ can be further reduced with progressive production of $R\text{-}NH_2$ compounds that bind covalently to intracellular molecules and the tracer becomes trapped. This occurs at pO_2 < 10 mmHg and therefore ^{18}F-FMISO detects clinically relevant hypoxia. The

process requires viable cells with functional nitroreductases and the tracer does not accumulate in necrotic cells.[331] The bioreductants involved in the mechanism is not clear but cytochrome P450, NADPH and xanthine oxidoreductase are implicated.[332,333]

^{18}F-FMISO distributes nearly equally between lipophilic tissues and hydrophilic blood and normoxic tissues show a tissue to blood ratio of almost 1.0. The optimal quantification of hypoxia is at 2-4 hours post-injection of tracer when normal tissues have equilibrated with plasma and hypoxic tissue continues to have selective retention. However even after this long uptake period tracer accumulation is still low with tumour to blood ratios of 1.2-1.4 indicative of hypoxia.[334,335] The tumour to blood ratio calculation increases the image contrast, compared with tumour to background muscle ratios, but requires a venous blood sample in the middle of the scan. The optimal timing is not entirely clear as a recent study in a preclinical tumour model demonstrated the tumour to blood ratio continued to increase up to 6 hours post-injection.[336] ^{18}F-FMISO is metabolised by the liver and excreted through the kidney and bladder and results in low radiation exposure compared with other radiopharmaceuticals.[337]

Clinical studies of ^{18}F-FMISO in HNSCC

Direct pO_2 measurements with polarographic electrodes in HNSCC patients showed greater ^{18}F-FMISO retention in hypoxic tumours, with a strong correlation between uptake and $pO_2 \leq 5$ mmHg[338] or HF2.5 and HF5,[339] but not with ^{18}F-FDG. However no correlation in HNSCC has also been reported[340] Rajendran et al[341] reported the largest study ^{18}F-FMISO, which involved 73 patients with HNSCC. Uptake was seen in 85% of patients and tumour to blood ratio and hypoxic volume showed a trend to be an independent prognostic measure. Rischin et al[275] demonstrated that pretreatment ^{18}F-FMISO was effective in determining hypoxic regions and tirapazamine was effective in patients with hypoxic tumours as assessed by ^{18}F-FMISO. Another group found that an SUV > 2 and tumour to muscle ratio (TMR) > 1.6 at 4 hours after injection were associated with disease recurrence after RT.[342] The same group also investigated the changes in ^{18}F-FMISO uptake during RT by performing a scan pretreatment and repeating at 30 Gy. The mean SUV and TMR significantly decreased during RT, indicating RT-induced reoxygenation. Lee et al[343] also performed a baseline and midtreatment scan and found 90% of 20 patients had hypoxia before treatment and only 2 had detectable hypoxia on their midtreatment scan, which did not correlate with outcome. Zips et al[344] carried out a baseline scan and 3 further scans during RT. The imaging parameters from scans at week 1 and 2 of RT strongly correlated with progression free survival, suggesting the prognostic value of imaging hypoxia at the start of RT rather than at baseline. Smaller studies have showed variable results, with ^{18}F-FMISO showing borderline significance for stratifying patients into treatment outcome

groups in 12 patients, and high SUV_{max} but not TMR correlating with poor DSS after RT or surgery in 17 patients.[345]

^{18}F-FMISO imaging has been used to assess the feasibility of hypoxia image-guided dose escalation. An additional 10 Gy to the hypoxic subvolume in HNSCC was estimated to increase the tumour control probability by 17% with acceptable increases in normal tissue complication probability in RT planning study.[276] Lee et al[334] also demonstrated the feasibility of this approach without compromising the dose to normal tissues, but the intratumoural distribution of hypoxia varied considerably and the hypoxic tumour volume delineated was not reproducible between 2 scans performed 3 days apart.[335] RT plans generated using the first scan were applied to the second scan which resulted in compromised coverage of the hypoxic tumour volumes.[346] However Okamoto et al[347] reported high reproducibility between ^{18}F-FMISO scans performed at 2 days apart in 11 patients, with 4 hour uptake parameters showing no significant difference in 10 of the 11 patients, concluding that ^{18}F-FMISO is promising for accurate RT planning. A further recent study again demonstrated high percentage tumour reoxygenation during RT shown by a reduction in uptake after 20 Gy, suggesting that dose escalation to hypoxic volumes may be inappropriate, but hypoxia imaging may be more useful in adaptive RT.[348]

^{18}F-FMISO is not a universal hypoxia tracer in cancer. It has shown minimal activity in pancreatic cancer patients[349] and high background uptake in the normal rectum in patients with colorectal cancer, as well as tracer diffusion through the bowel wall, making images difficult to interpret.[350] The low uptake of ^{18}F-FMISO in target tissue and slow clearance of unbound ^{18}F-FMISO from normoxic areas results in images of poor contrast. The relatively short half life of 110 minutes hampers late imaging that could enhance contrast between hypoxic and normoxic tissues. This has led to the development of other tracers with improved pharmacokinetics.

^{18}F-fluoroazomycin arabinofuranoside (^{18}F-FAZA)

This second generation 2-nitroimidazole is more hydrophilic than ^{18}F-FMISO and therefore has faster clearance from normal tissues and higher tumour to background ratios. Souvatzoglou et al[351] carried out an 11 patient pilot study in HNSCC and reported a higher contrast with non-target tissues compared to ^{18}F-FMISO, with an average TMR of 2.0 at 2 hours post injection. Mortensen et al[352] performed static ^{18}F-FAZA imaging in 40 oropharynx SCC patients. A hypoxic volume could be identified in 25 patients, with a median TMR of 1.5. The distribution of hypoxia among HPV positive and negative tumours was not significantly different and there was a significant difference in DFS in patients with

non-hypoxic tumours compared with hypoxic tumours. Tumours were ranked according to the expression of genes included in a 15-gene hypoxia classifier but no correlation was found between the hypoxic status as assessed by the classifier and ^{18}F-FAZA imaging, despite the gene profile being validated using ^{18}F-FAZA autoradiography in human tumour xenografts.[321]

1.6 Copper bis(thiosemicarbazone) complexes

In the 1960s dithiosemicarbazones were found to have anti-tumour properties that were enhanced when complexed with Cu(II).[353] The simplicity of the chemistry of the ligand and the availability of several positron emitting copper isotopes led to the further development of these complexes. Copper(II)-pyruvaldehyde-bis(N^4-methylthio-semicabazone) (Cu-PTSM) was initially developed as a perfusion tracer.[354] This complex rapidly diffuses into cells and becomes non-selectively bioreduced resulting in an unstable Cu(I) complex, from which the ligand dissociates, releasing the copper which is trapped within the cell. Manipulating the ligand backbone of the complexes altered their reduction potential, releasing/trapping Cu under specific intracellular conditions. Dearling et al[355,356] demonstrated that increasing the number of alkyl groups on the diketone backbone of bis(thiosemicarbazone) resulted in hypoxia selectivity by lowering the redox potential in vitro in EMT6 tumour cells. Several copper radionuclides are available for both PET and targeted radiotherapy, highlighting the versatility of this radiotracer (Table 1.7). ^{64}Cu is a good compromise as it has sufficiently long half-life, allowing the tracers to be produced and transported to over greater distances, with better intrinsic image resolution, and good production yield.[357] In addition ^{64}Cu emits Auger electrons as a result of electron capture, which have high linear energy transfer and short range, and can be potentially used for internal radiotherapy.[358]

Table 1.7 Properties of positron-emitting isotopes of copper.

Isotope	Half-life	Radioactivity	Range in tissue	Production
^{60}Cu	0.38 hours	β^+ 93% Electron capture 7%	4.4 mm	Cyclotron
^{61}Cu	3.32 hours	β^+ 62% Electron capture 38%	2.6 mm	Cyclotron
^{62}Cu	0.16 hours	β^+ 89% Electron capture 2%	6.6 mm	^{62}Zn/^{62}Cu generator
^{64}Cu	12.7 hours	β^+ 19% Electron capture 41% β^- 40%	1.4 mm 0.95 mm	Cyclotron
^{66}Cu	0.09 hours	β^- 100%	5.6 mm	Cyclotron
^{67}Cu	62.01 hours	β^- 100%	0.61 mm	Cyclotron

1.6.1 Copper(II)-diacetyl-bis(N^4-methylthiosemicarbazone) (Cu-ATSM)

Cu-ATSM was found to be a hypoxia selective complex.[356] Alkyl groups at the R1 and R2 positions of bis(thiosemicarbazone) determined the hypoxia selectivity and alkylation at the terminal amino R3 and R4 positions increased lipophilicity (Figure 1.4).

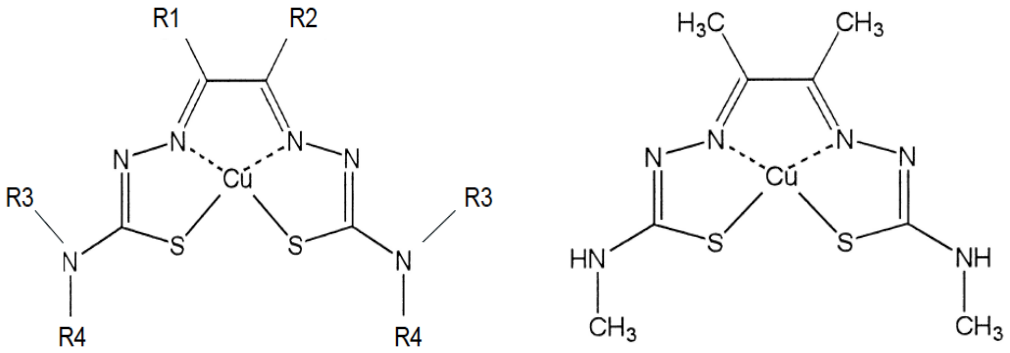

Figure 1.4 Structure of copper bis(thiosemicarbazone)s (left) and Cu-ATSM (right).

Cu-ATSM was developed to overcome some of the limitations of ^{18}F-FMISO imaging. It is an uncharged lipophilic molecule of low molecular weight and high membrane permeability. It has fast tumour uptake and clearance form normoxic tissues, allowing rapid imaging after injection and higher hypoxic-to-normoxic contrast. It is also simpler to synthesise and radiolabel compared with ^{18}F-FMISO, but the longer half-life results in a higher radiation dose to patients.[359] Radiation dosimetry calculated from rat biodistriution data and human imaging using 480 MBq ^{60}Cu-ATSM demonstrated that the liver is the dose-limiting organ and ^{64}Cu would remain in the liver for 8.25 ± 0.17 hours after injection.[360]

1.6.2 Mechanism

Several mechanisms for the hypoxia selectivity of Cu-ATSM have been suggested, all based on the bioreduction of Cu(II) to Cu(I). However the precise cellular retention mechanism is still unclear. The first mechanism was proposed by Fujibayashi et al;[361] Cu(II)-ATSM is reduced to Cu(I)-ATSM only within hypoxic cells due to the abnormally reduced state of their mitochondria, caused by the lack of oxygen as the final electron acceptor, and becomes irreversibly trapped following dissociation of Cu(I) from ATSM ligand. Using the Langendorff isolated rat ischaemic heart model, where the oxygen concentration can be controlled without changing blood flow, ^{62}Cu-ATSM showed low retention and rapid washout from normally perfused hearts, with a 3.5-fold increase in retention under hypoxic conditions within 15 minutes of tracer administration. They demonstrated that Cu-ATSM accumulation involved NADH-dependent enzymes of the mitochondrial ETC. Reduction only occurred in hypoxic cells and involved electron transfer

from hyper-reduced Complex I using NADH as a two-electron donor. The addition of NADH, which is known to increase in hypoxic tissues, increased Cu-ATSM reduction.[361] Obata et al[362] demonstrated that in tumour cells reduction was dependent on the presence of electron donors such as NADH and NADPH, and inhibition of the microsomal enzymes NADH-dependent cytochrome b5 reductase and NADPH-dependent cytochrome P450 reductase caused a 25-50% decrease in Cu(II)-ATSM reduction. This indicated that the retention may not entirely be dependent on oxygen concentration but also on the relative concentrations of intracellular reductants.

Dearling et al[356] observed that trapping of hypoxia selective complexes, such as Cu-ATSM, within the hypoxic cells was partially reversible, whereas trapping of the non-selective complexes, such as Cu-PTSM, was irreversible. They suggested that the reduction of Cu(II)-ATSM to Cu(I)-ATSM occurs in both normoxic and hypoxic cells, generating unstable anionic Cu(I)-ATSM. Cu(I) slowly dissociates from the ATSM ligand in cells with low oxygen concentration, becoming irreversibly trapped within the cell. In the presence of oxygen Cu(I)-ATSM oxidised back to neutral Cu(II)-ATSM and diffuses out of the cell. Cu(II)-PTSM is also reduced to Cu(I)-PTSM in all cells but is not readily oxidised back by oxygen due to its relatively high redox potential. It dissociates to become irreversibly trapped even if oxygen is available. The hypoxia selectivity therefore is a competition between dissociation and reoxidation of the reduced copper complexes, which is dependent on the oxygen concentration.[356,363]

Burgman et al[364] demonstrated efflux and reduction in the level of ^{64}Cu-ATSM in anoxic and hypoxic rodent prostate tumour cells after 30 minutes in vitro incubation, contradicting the models that suggest irreversibly trapping in conditions of low oxygen concentration. They proposed that following dissociation of Cu(I) and ATSM, Cu(I) is not trapped but absorbed into the intracellular Cu pool and is subject to cellular Cu metabolism. Cu is a co-factor in redox reactions of enzymes that carry out many normal physiological processes and its metabolism is tightly regulated. Cu uptake into cells is mediated by a plasma membrane protein CTR1, and ATP7A (Menkes protein) and ATP7B (Wilson protein) are Cu-transporting ATPases which export Cu to maintain intracellular levels. The uptake and efflux of Cu(I) from cells are suggested to be a result of active transport. The level of expression of these transporters vary in different cell types and regulation is cell specific,[365] which may explain the variations in Cu-ATSM retention.

Yoshii et al[366] observed that ^{64}Cu-ATSM accumulates in cells with over-reduced states caused by mitochondrial dysfunction, regardless of oxygen levels. Cell lines with mitochondrial DNA depletion or mutated mitochondria showed higher uptake compared

with control human osteosarcoma cells under normoxia, which did not increase under hypoxic conditions. ^{64}Cu-ATSM accumulation correlated with levels of the biological reductants NADH and NADPH, rather than increasing hypoxia. They suggested that ^{64}Cu-ATSM uptake reflects an over-reduced intracellular state, as indicated by the levels of NADH and NADPH, and would be a potential marker of disorders such as mitochondrial encephalomyopathies and Parkinson's disease, in which impairment of the respiratory chain generates excess electrons resulting in over-reduction and oxidative stress.[367,368] Similar results were demonstrated using cells with impaired mitochondrial ETC function, which accumulate NADH.[369] These cells showed increased Cu-ATSM retention, and the uptake did increase under hypoxic conditions. Hypoxia leading to NADH accumulation provides the cellular reduction potential to reduce Cu(II) to Cu(I) and dissociate from the ligand, resulting in increased retention.[369] Therefore the primary mechanism that drives cellular retention of Cu-ATSM may be the accumulation of NADH due to impaired activity of the mitochondrial ETC, resulting from conditions such as hypoxic tumours, myocardial ischaemia, mitochondrial encephalomyopathies, Parkinson's disease and other disorders that involve mitochondrial dysfunction.

Cu-ATSM uptake and retention has been associated with a number of other factors. Multidrug resistance protein 1 (MDR1) is a member of the ATP-binding cassette superfamily of membrane transport proteins and is involved in the mechanism of resistance to several chemotherapeutic drugs. Higher MDR1 expression is associated with poorer outcome after treatment and the expression varies in different tumours.[370] Liu et al[371] showed that cellular and tumoural retention of ^{64}Cu-PTSM and ^{64}Cu-ATSM were influenced by MDR1 expression, and knockdown of MDR1 resulted in increased cellular retention and decreased efflux. ^{64}Cu-ATSM has also been shown to be associated with $CD133^+$ cells. CD133 is used as a marker for cancer stem cells, which have been shown to increase in proportion when cancer cells are cultured under hypoxia compared with cell under normoxia.[372] ^{64}Cu-ATSM accumulation localised preferentially in regions with a high density of $CD133^+$ cells in mouse colon carcinoma cell lines, and when the proportion of $CD133^+$ cells was expanded by culturing under glucose starvation and hypoxia uptake was increased in these conditions.

Recent studies have reported that Cu itself plays a significant role in Cu-ATSM entrapment.[373] The in vitro and in vivo distribution of ^{64}Cu-ATSM and ^{64}Cu-acetate in EMT6 and CaNT mouse tumour models were compared, where ^{64}Cu-acetate, with no hypoxia selectivity, was used as a marker of cellular Cu processing. They demonstrated similar tumour uptake kinetics and biodistribution at 2 and 16 hours, both of which correlated with EF5 IHC at 16 hours only. Increasing inspired oxygen of anaethetised mice reduced the

uptake of both ^{64}Cu-ATSM and ^{64}Cu-acetate, and serum analysis indicated that ^{64}Cu-ATSM was partly metabolised to yield circulating, protein-bound ^{64}Cu in vivo. This suggests that the retention of the tracers may be significantly influenced by cellular Cu metabolism and processing. Multiple clinical studies demonstrate a clear correlation between high tumour uptake and poor prognosis in a range of tumour sites. However, Cu metabolism itself is altered in cancers, with elevated levels in tissue and serum associated with tumour recurrence and metastasis,[374] and how tumour hypoxia affects Cu metabolism is unknown. Therefore the redox trapping pathway may not fully explain the observed hypoxia selectivity of Cu-ATSM.

1.6.3 Preclinical models

The first report of Cu-ATSM as a hypoxia selective agent was described by Fujibayashi et al in 1997 in myocardial tissue as described above.[361] Lewis et al[375] investigated Cu-ATSM uptake in different canine myocardial ischaemia models, supporting Cu-ATSM as an effective tracer in the detection of global hypoxia. They also demonstrated that Cu-ATSM was not retained in necrotic tissue, and therefore able to distinguish between hypoxic viable and non-functional dead myocardial tissue.

Cu-ATSM uptake in many different tumour models have been studied (Table 1.8). Lewis et al[376] in 1999 showed ^{64}Cu-ATSM to be selectively trapped in vitro in the EMT6 murine mammary carcinoma cell line under hypoxic conditions and in vivo in EMT6 tumour-bearing mice. In vitro kinetics was compared with ^{18}F-MISO after exposure to different concentrations of oxygen. ^{64}Cu-ATSM demonstrated oxygen concentration dependent uptake at 1 hour and ^{18}F-MISO at 2 hours, but the uptake of ^{18}F-MISO was only approximately 10% of the uptake of ^{64}Cu-ATSM. The biodistribution compared with ^{60}Cu-PTSM in mice bearing EMT6 tumours showed that the optimal uptake was after only 10 minutes post injection, suggesting rapid uptake and trapping of ^{64}Cu-ATSM in solid tumours. Ex vivo autoradiography displayed uniform uptake of ^{60}Cu-PTSM compared with heterogeneous uptake of ^{64}Cu-ATSM, consistent with selective trapping into hypoxic cells of the tumour. The same group confirmed in vivo the pO_2 dependent selective uptake of Cu-ATSM in rat 9L gliosarcoma tumours.[359] They demonstrated a good correlation between low tumour pO_2 and high Cu-ATSM accumulation measured using needle oxygen electrodes, PET and autoradiography, and confirmed for the first time that Cu-ATSM uptake in vivo in tumour tissues was related to tissue pO_2. In addition, they compared ^{64}Cu-ATSM uptake with ^{18}F-FDG uptake and found distinctly different uptake regions, which was also observed in rabbits transplanted with VX2 carcinoma[377] and in mice with tumours of different origins.[378] High ^{64}Cu-ATSM uptake regions were found to be hypovascular and consisted of cells arrested in the cell cycle on immunohistochemical (IHC) staining,

whereas high ^{18}F-FDG uptake areas were hypervascular and cells were actively proliferating. This suggests that ^{18}F-FDG regions may respond well to conventional treatments but regions of high ^{64}Cu-ATSM consist of viable but hypoxic and resistant cells, requiring more aggressive treatment.[378] Similarly Oh et al[379] compared ^{64}Cu-ATSM and ^{18}F-FDG distributions using the Lewis lung carcinoma (LLC1) model. They also found ^{64}Cu-ATSM mainly accumulated at the edge of tumours, whilst ^{18}F-FDG distributed inside the tumour and inside the ^{64}Cu-ATSM uptake regions. Pimonidazole staining correlated with high ^{18}F-FDG uptake regions but not ^{64}Cu-ATSM. ^{18}F-FDG can accumulate in normoxic proliferating cells as well as hypoxic non-proliferating cells, as these cells have high demand for energy for anaerobic glycolysis. Ki67 and BrdU IHC suggested that cells in high ^{64}Cu-ATSM regions were quiescent but continued DNA synthesis. The colony forming ability of cells obtained from high ^{64}Cu-ATSM uptake regions was significantly higher compared with cells from intermediate or low accumulation areas. The authors concluded that ^{64}Cu-ATSM regions indicate quiescent but clonogenic tumour cells that continue DNA synthesis, which is induced by mild hypoxia, and these regions may represent areas in extremely reductive conditions rather than in severe hypoxia.

O'Donoghue et al[380] compared the intratumoral distribution of ^{64}Cu-ATSM with ^{18}F-MISO in rats bearing the R3327-AT anaplastic rat prostate tumour and nude rats bearing xenografts from the human SCC cell line FaDu using direct pO_2 measurements, autoradiography and immunofluorescent microscopy. There was poor correlation in R3327-AT tumours at 2 hours post-injection, but when tumours were imaged and sacrificed at 16-20 hours post-injection there was significant correlation in the distribution between the 2 tracers, indicating temporal evolution of the distribution of ^{64}Cu-ATSM. In the FaDu tumour model early and late ^{64}Cu-ATSM images were similar and in concordance with the ^{18}F-MISO scans. This study suggested a tumour specific dependence of Cu-ATSM uptake and retention and raised concerns about the use of Cu-ATSM at early imaging times. This group also studied the uptake in vitro in 4 different human and 2 rodent tumour cell lines and observed ^{64}Cu-ATSM uptake and retention to be rapid during the first 30 to 60 minutes of incubation, but after this initial period the accumulation varied depending on the cell line and oxygenation conditions.[364] A steady state was achieved after approximately 2 hours, with uptake in normoxic cells anywhere between 2 to 9 times lower than hypoxic cells. R3327-AT prostate cancer cells, however, again showed different uptake characteristics. After the initial uptake period in hypoxic/anoxic cells there was rapid efflux of ^{64}Cu and therefore no hypoxia selectivity was demonstrated. ^{64}Cu-ATSM was shown to be metabolised rapidly depending on the oxygenation and cell line, and the ^{64}Cu level was attributable to ^{64}Cu-ATSM uptake only for a limited time. This data suggested hypoxia selectivity is highest at 30 to 60 minutes of incubation, and early imaging may actually provide the most reliable hypoxia

imaging. At late imaging times, cellular levels of ^{64}Cu may reflect the active transport of ^{64}Cu metabolites rather than the uptake of ^{64}Cu-ATSM.

To further assess the difference in uptake seen in prostate cancer cells Vavere et al[381] investigated whether the fatty acid synthesis pathway in these cells may be involved in Cu-ATSM hypoxia selectivity. This pathway is overexpressed and utilised in prostate cancers for improving redox balance, consuming reducing equivalents, such as NADPH, that are required by the Cu-ATSM retention mechanism. They found that inhibition of fatty acid synthase resulted in significantly increased ^{64}Cu-ATSM retention in prostate tumour cells under hypoxia, and this pathway may therefore affect Cu-ATSM metabolism. Yuan et al[382] compared autoradiographic distributions of ^{64}Cu-ATSM with EF5 IHC, as a hypoxia marker, in rodent R3230 mammary adenocarcinoma (R3230Ac), fibrosarcoma (FSA) and 9L glioma tumour models. After 1 hour post-injection close spatial correlation was seen in R3230Ac and 9L glioma, but not in FSA tumours, confirming that ^{64}Cu-ATSM is a valid hypoxia marker only in some tumour types, and may not represent a universal PET hypoxia marker.

Matsumoto et al[383] used mouse SCCVII tumours and different inspired oxygen mixtures to modulate tumour hypoxia to compare the uptake of ^{64}Cu-ATSM and ^{18}F-FMISO. Changes in oxygen levels, assessed by pimonidazole staining, did not result in altered ^{64}Cu-ATSM tumour uptake, whereas ^{18}F-FMISO showed a positive trend towards uptake as a function of changing hypoxia levels, raising concerns regarding the mechanism of hypoxia selectivity of Cu-ATSM. Further tracer comparison studies were carried out by Dence et al.[384] The 9L gliosarcoma rat model was used to compare the distributions of ^{18}F-FMISO 2 hours post-injection, ^{64}Cu-ATSM 10 minutes and 24 hours post-injection, ^{18}F-FDG and ^{18}F-FLT. In contrast to Matsumto et al they found strong correlations between the regional distributions of both early and late ^{64}Cu-ATSM and ^{18}F-FMISO, and with ^{18}F-FLT, but a poor correlation between ^{64}Cu-ATSM and ^{18}F-FDG. ^{64}Cu-ATSM has also been compared with other nitoimidazole-based radiotracers, confirming the cell-dependent distribution and retention kinetics of ^{64}Cu-ATSM.[385,386] The distribution at 2 and 24 hours was compared with ^{18}F-FAZA in EMT6, PC3 and FaDu xenograft tumour models in vivo and ex vivo.[385] The FaDu model demonstrated overlapping radioactivity distributions of the 2 tracers at all time points of ^{64}Cu-ATSM acquisition, which matched CA9 staining, but in the EMT6 and PC3 models there was little similarity between the 2 tracers and between early and late in ^{64}Cu-ATSM imaging. Carlin et al[386] compared ^{18}F-MISO, ^{18}F-HX4, ^{18}F-FAZA and ^{64}Cu-ATSM in SQ20b human HCSCC cell line xenograft 80-90 minutes after tracer administration. Autoradiographic distribution was compared with the exogenous hypoxia marker pimonidazole and the endogenous hypoxia marker CA9, as well as the vascular perfusion marker Hoechst 33342. The nitroimidazoles showed uptake increasing with

pimonidazole and CA9 staining, but ^{64}Cu-ATSM showed the opposite pattern with the highest uptake in regions with lowest pimonidazole and CA9 staining. An inverse pattern of staining was observed with Hoechst 33342, suggesting correlation between tracer uptake and vascular delivery.

Dynamic PET imaging and kinetic analysis were performed in the FaDu head and neck tumour model in rats to further investigate the extent to which ^{64}Cu-ATSM distribution is determined by vascular delivery and perfusion or pO_2.[387] Cu-ATSM was rapidly taken up by tumours, resulting in a 4-fold higher ^{64}Cu-ATSM uptake than muscle. Tumour to muscle ratios (TMRs) continued to increase over the course of imaging of 18 hours. At 1 hour post-injection ^{64}Cu-ATSM showed no correlation with pimonidazole staining but strong correlation with Hoechst-33342, indicating highly perfused regions, and at 18 hours there was no correlation with Hoechst-33342 nor with pimonidazole, suggesting Cu-ATSM is related to perfusion rather than pO_2.

There have also been a number of studies in cats and dogs. Hansen et al[388] compared ^{64}Cu-ATSM and ^{18}F-FDG uptake in 9 dogs with spontaneous soft tissue sarcomas or carcinomas. ^{64}Cu-ATSM imaging at 3 and 24 hours demonstrated moderate correlation but temporal changes were observed, especially in hypoperfused regions, attributed to cycling hypoxic changes, regional differences in uptake kinetics, or reversibility of ^{64}Cu-ATSM. The hypoperfused regions displayed delayed uptake, possibly limited by perfusion, and slower washout. Cu-ATSM scans at 3 hours after injection showed a strong positive correlation with pimonidazole uptake in the most heterogeneous tumour regions.[389] In a further study 22 dogs with sinonasal carcinomas and sarcomas imaged with ^{61}Cu-ATSM before and mid-treatment with radiotherapy showed stable spatiotemporal distribution, with carcinomas demonstrating significant decreased uptake mid-treatment.[390,391] Canine tumours have also been used to demonstrate the feasibility of dose escalating radiotherapy dose to ^{64}Cu-ATSM or ^{18}F-FDG or overlapping uptake regions.[392,393]

Table 1.8 Summary of in vitro and in vivo preclinical studies in tumour models.

Radiotracer	Cell line/Tumour	Technique	Result	Ref
^{64}Cu-ATSM ^{18}F-MISO	EMT6 cell line	Incubation with tracer and different concentrations of dissolved oxygen; ^{64}Cu activity assessed using γ counter	^{64}Cu-ATSM more efficient uptake and washout kinetics.	376
^{64}Cu-ATSM ^{60}Cu-PTSM	EMT6 in mice	Autoradiography	^{64}Cu-ATSM heterogeneous uptake distribution, ^{60}Cu-PTSM homogeneous distribution.	376
^{67}Cu-ATSM	9L gliosarcoma in rats	Hydralazine administration; 100% oxygen administration; needle oxygen electrode; dynamic PET imaging over 25 minutes; autoradiography	Hydralazine decreased tumour pO_2, increased relative uptake of ^{67}Cu-ATSM by 37% compared with control animals. 100% oxygen increased tumour pO_2, decreased relative ^{67}Cu-ATSM uptake by 48% compared with control.	359
^{64}Cu-ATSM ^{18}F-FDG	9L gliosarcoma in rats	Autoradiography to compare distribution	Regions of uptake at 60 minutes post 18F-FDG administration and 10 minutes post ^{64}Cu-ATSM administration distinctly different.	359
^{64}Cu-ATSM ^{18}F-FDG	VX2 in white rabbits	Autoradiography	^{64}Cu-ATSM uptake around outer rim of tumour, ^{18}F-FDG uptake widely distributed with highest levels in inner regions of tumour.	377
^{64}Cu-ATSM ^{18}F-FDG	LLC1, Meth-A, B16, colon26 in mice	Autoradiography; Ki67, CD34 (blood vessel marker) IHC	^{64}Cu-ATSM accumulation at edge of tumours, not in centre where cells necrotic. ^{18}F-FDG accumulation inner adjacent to ^{64}Cu-ATSM. High ^{64}Cu-ATSM regions hypovascular, less proliferating compared with ^{18}F-FDG.	378
^{64}Cu-ATSM ^{18}F-MISO	R3327-AT prostate and human FaDu xenografts in rats	PET imaging at 0.5 to 2 hours (early) and 16 to 20 hours (late) post-injection; oxygen probe measurements; autoradiography; pimonidazole IHC	R3327-AT tumours – correlation of tracers at late PET imaging but not early. Oxygen probe measurements consistent with late ^{64}Cu-ATSM and ^{18}F-MISO images. Pimonidazole IHC correlated with late ^{64}Cu-ATSM distribution only. FaDu tumours – correlation of tracers on PET imaging at early and late time points.	380
^{64}Cu-ATSM	Human MDA468, MCF7, DU145, FaDu and rodent R3327-AT, FSaII cell lines	Incubation with ^{64}Cu-ATSM for different times under normoxic, hypoxic or anoxic conditions; ^{64}Cu activity assessed using γ counter	Most cell lines – accumulation rapid during first 0.5-1 hour of incubation followed by steady state level after 2 hours. Uptake in normoxic cells 2-9 times lower, depending on cell line and incubation time. R3327-AT cell line – no hypoxia selectivity demonstrated after 1 hour.	364

^{64}Cu-ATSM	R3230Ac, FSA, 9L glioma in rats	Dynamic PET imaging over 60 minutes; EF5, pimonidazole, CA9, Hoechst 33342 IHC; carbogen breathing (95% pO_2) in FSA	Significantly higher TMR and SUV in FSA compared with R3230Ac and 9L. R3230Ac and 9L - correlation between ^{64}Cu-ATSM uptake and EF5 IHC. FSA – no correlation between ^{64}Cu-ATSM and EF5, pimonidazole, CA9. Carbogen in FSA – reduced EF5 but no change in ^{64}Cu-ATSM uptake.	382
^{64}Cu-ATSM ^{18}F-FMISO	SCCVII in mice	Dynamic PET imaging after inspired air, 10% oxygen or carbogen; pimonidazole IHC	Significant changes in pimonidazole staining but no change in ^{64}Cu-ATSM uptake, ^{18}F-FMISO uptake showed non-significant trend corresponding to pimonidazole.	383
^{64}Cu-ATSM ^{18}F-FMISO ^{18}F-FDG ^{18}F-FLT	9L gliosarcoma in rats	PET imaging at 10 minutes (early) and 24 hours (late); autoradiography	Distribution of ^{64}Cu-ATSM at early and late time points correlated with ^{18}F-FMISO. Poor correlation between ^{64}Cu-ATSM and ^{18}F-FDG. Good correlation between ^{64}Cu-ATSM and ^{18}F-FLT.	384
^{64}Cu-ATSM ^{18}F-FDG	LLC1 in mice	Autoradiography; Ki67, BrdU, pimonidazole IHC; colony formation	^{64}Cu-ATSM accumulation at edge of tumours, none in necrotic tumour centre. ^{18}F-FDG accumulation inside ^{64}Cu-ATSM region. ^{64}Cu-ATSM negative correlation with Ki67, positive with BrdU. Cells from high ^{64}Cu-ATSM regions greater colony forming ability.	379
^{64}Cu-ATSM	FaDu in rats	Dynamic PET imaging for min 1 hour (early) and at 18 hours (late); autoradiography; pimonidazole, Hoechst 33342 IHC	Rapid tumour uptake and retention, uptake continued to rise at 18 hours. Early – no correlation with pimonidazole, positive correlation with Hoechst 33342. Late – no correlation with pimonidazole or Hoechst 33342.	387
^{64}Cu-ATSM ^{18}F-FAZA	Human PC3, FaDu and EMT6 in mice	PET imaging at 2 hours (early) and 24 hours (late); autoradiography; CA9, CTR1 and ATP7B IHC	Higher TMR with ^{64}Cu-ATSM in all 3 models. FaDu – early and late ^{64}Cu-ATSM distribution matched ^{18}F-FAZA and CA9. EMT6 and PC3 – no correlation. No correlation between CTR1/ATP7B and radioactivity distribution.	385
^{64}Cu-ATSM ^{18}F-FMISO ^{18}F-FAZA ^{18}F-HX4	Human SQ20b in mice	PET imaging after 80-90 minutes; autoradiography; pimonidazole, CA9, Hoechst 33342 IHC	TMR significantly greater with Cu compared with nitoimidazole tracers. ^{64}Cu-ATSM uptake corresponded to low pimonidazole, low CA9 staining, high Hoechst 33342 staining. Nitroimidazole tracers - uptake corresponded to pimonidazole, CA9 staining.	386
^{64}Cu-ATSM ^{64}Cu-acetate ^{18}F-MISO	EMT6, CaNT in mice	Dynamic PET imaging early and late; autoradiography; EF5 IHC; 60% and 100% inspired oxygen	^{64}Cu-ATSM and ^{64}Cu-acetate uptake and biodistribution similar at 2 & 16 hrs. EF5 correlated with imaging at 16 hrs and with ^{18}F-MISO at 2 hrs. ^{64}Cu-ATSM and ^{64}Cu-acetate uptake decrease with increasing inspired O_2.	373

1.6.4 Clinical studies

The first published study using Cu-ATSM in patients was in 2000. Takahashi et al[394] used ^{62}Cu-ATSM in 4 normal subjects and 6 patients with lung cancer and to evaluate the characteristics in humans. ^{62}Cu-ATSM was rapidly cleared from the blood with little lung uptake in normal subjects and intense uptake in the liver. Patients with lung cancer had intense tumour uptake, which did not correlate with ^{18}F-FDG uptake. ^{15}O-water PET scans were performed in 4 patients to compare blood flow and ^{62}Cu-ATSM uptake, and a negative correlation was found suggesting that ^{62}Cu-ATSM is retained in poorly perfused regions. Takahashi also investigated ^{62}Cu-ATSM in 7 patients with coronary heart disease and found increased myocardial uptake in one patient with unstable angina, whereas clinically stable patients had no increased uptake.[395]

Lung cancer

Further work in lung cancer was carried out by Dehdashti et al[396] to compare the pretreatment uptake of ^{60}Cu-ATSM in non-small cell lung cancers with tumour response to therapy. The primary lesion and bilateral back muscle groups were defined by delineating regions of interest (ROIs) in multiple planes, guided by CT and ^{18}F-FDG PET. The overall tumour uptake was assessed semi-quantitatively on the 30-60 minute summed images by determining the TMR using the maximum pixel value for the tumour and average value for the muscle. In 14 out of 19 patients with response evaluation the mean TMR of non-responders was significantly higher that responders. An arbitrarily selected TMR threshold of < 3.0 was a cut-off value for distinguishing responders and non-responders. The maximum standardised uptake value (SUV_{max}) of either ^{60}Cu-ATSM or ^{18}F-FDG were not significantly different between the 2 groups. Cu-ATSM has been investigated as a diagnostic imaging biomarker in lung tumours. Two patients with lung nodules suspicious for malignancy received ^{62}Cu-ATSM, ^{62}Cu-PTSM and ^{18}F-FDG PET imaging prior to surgery, one lesion was subsequently identified on histology as adenocarcinoma and the other granuloma.[397] SUVs were compared and ^{62}Cu-ATSM was the only radiotracer that could potentially distinguish benign from malignant disease. Lolith et al[398] compared ^{62}Cu-ATSM and ^{18}F-FDG uptake in patients with histologically different types of lung cancer and found differences in the intratumoural distributions between SCC and adenocarcinoma.

Cervix cancer

Dehdashti et al have also investigated the use of ^{60}CuATSM in cervix cancer. ^{60}Cu-ATSM scans were carried out initially in a group of 14 patients,[399] followed by a larger series of 38.[400] A dynamic scan over 60 minutes was performed and ROIs were drawn in multiple planes on the summed images obtained at 30-60 minutes, guided by CT or FDG-PET.

Volumes of interest (VOIs) were then created of the primary cancers and bilateral gluteal muscles and the TMR calculated. They found that a TMR threshold of 3.5 distinguished patients who did and did not develop recurrent disease, with a significantly improved progression-free and cause-specific survival in patients with a TMR of ≤ 3.5. There was no difference between the 2 groups in frequency of lymph node involvement, total radiation dose or overall treatment time, and there was no correlation between disease stage and ^{60}Cu-ATSM uptake. The patients also received an ^{18}F-FDG PET in this study and again no correlation was seen between ^{18}F-FDG SUV_{max} and ^{60}Cu-ATSM uptake. Paraffin blocks from the initial diagnostic biopsy of 15 patients were analysed for hypoxia-related molecular markers. ^{60}Cu-ATSM hypoxia correlated with overexpression of VEGF, COX-2, CA9 and EGFR by immunohistochemistry and an increase in apoptosis.[401] Lewis et al[402] compared PET image quality and tumour uptake of ^{60}CuATSM and ^{64}CuATSM in 10 patients with cervix cancer. ^{64}CuATSM provided better image quality, allowing clearer delineation of tumours. The uptake pattern and TMRs of the 2 tracers were similar in studies carried out on different days, indicating that the distribution of hypoxia did not change during this period.

Rectal cancer

Similar analysis has been performed on 19 patients with cancer of the rectum who received a dynamic ^{60}Cu-ATSM PET scan prior to treatment with neoadjuvant chemoradiation followed by surgery.[403] ROIs were drawn around the primary rectal cancer and bilateral gluteal muscle groups in multiple planes to calculate the TMR. The median TMR value of 2.6 was used to define hypoxia. The mean TMR for downstaged tumours was significantly lower than tumours not downstaged, and after a median follow up of 4.1 years none of the patients with TMR < 2.6 had developed recurrent disease or died from their cancer, compared with a progression-free survival and overall survival at 3 years of 50% and 63% respectively in the hypoxic group. There was no correlation between tumour size or stage and ^{60}Cu-ATSM uptake, and no correlation with ^{18}F-FDG uptake.

Glioma

More recently ^{62}Cu-ATSM PET has been used in 22 newly diagnosed and recurrent glioma patients to investigate the ability to predict tumour grade and HIF1α expression.[404] ROIs were outlined within areas of increased tracer uptake on each section. SUV_{max}, SUV_{mean} and tumour to background ratio (TBR; tumour uptake relative to uptake in contralateral normal brain) were significantly higher in grade 4 compared with grade 3 tumours, and at a TBR cut off threshold of 1.8 ^{62}Cu-ATSM uptake predicted HIF1α positivity on immunohistochemical staining of the tumour specimens. MRI correlation revealed ^{62}Cu-ATSM uptake only within MRI enhanced regions and not in necrotic tissue identified on

MRI. The same group studied a further 23 patients and compared the uptake to ^{18}F-FDG and L-methyl-^{11}C-methionine (^{11}C-MET) uptake.[405] The mean ^{62}Cu-ATSM TBR and SUV_{max} were significantly higher in glioblastomas (GBM) compared with non-glioblastomas. Receiver operating characteristic analysis showed a TBR cut off of 1.9 was most predictive of GBM, which had better sensitivity than ^{11}C-MET, whilst ^{18}F-FDG had no predictive value.

Head and neck cancer

In 2001 Chao et al[406] used ^{60}Cu-ATSM in a radiotherapy planning study to demonstrate the feasibility of Cu-ATSM-guided IMRT to overcome hypoxia tumour resistance. TMR ≥ 2 was defined as hypoxia as at this threshold no normal tissue in the contralateral neck displayed ^{60}Cu-ATSM activity. The region of ^{60}Cu-ATSM uptake within the gross tumour volume (GTV) was targeted to deliver 85 Gy in 35 fractions, with the remaining GTV receiving 70 Gy in 35 fractions, and a plan without compromising normal tissue sparing was achieved. Minagawa et al[407] assessed ^{62}Cu-ATSM as a predictor of response in 17 patients. ROIs were manually drawn around the primary tumour, with the tumour volume defined as the sum of ROIs on CT. Tumour uptake was assessed semi-quantitatively by determining the SUV_{max} and TMR. The muscle uptake was determined by drawing 2 muscular ROIs on the bilateral posterior cervical muscles and the uptake determined by the mean of each SUV_{mean}. After 2 years of follow up SUV_{max} but not TMR was significantly different in patients with or without residual/recurrent tumour, and a $SUV_{max} > 5$ was a possible cut off threshold for poor outcome. There was no significant difference in ^{18}F-FDG between patients with and without residual/recurrence tumour. Sato et al[408] also evaluated the prognostic potential of ^{62}Cu-ATSM in 25 patients with head and neck cancer. Time activity curves from dynamic PET acquisition over 20 minutes showed that all tumours had stable tracer retention at approximately 10 minutes, and therefore an average image of the last 10-minute frame was used to evaluate hypoxia. VOIs were drawn on the primary tumour and bilateral sternocleidomastoid muscles and the overall uptake assessed semi-quantitatively by determining SUV_{max} and TMR, using the SUV_{max} for the tumour and mean SUV_{max} for the muscles. ^{62}Cu-ATSM $SUV_{max} > 3.6$ was associated significantly worse progression free survival (PFS), and a TMR > 3.2 was associated with significantly worse progression free survival and cause specific survival (CSS). ^{18}F-FDG uptake parameters did not distinguish patients with good and poor outcome.

Studies comparing different tracers have been conducted. The distribution of ^{62}Cu-ATSM and ^{18}F-FDG uptake was compared in 30 patients with any subtype of head and neck cancer, including paranasal sinus and parotid carcinomas.[409] The scans were analysed by drawing multiple small circular ROIs of 8mm in diameter on each tumour lesion, with at least 10 in total placed on the soft tissue density area inside the tumour, excluding necrotic

areas. The SUV_{mean} of each ROI was calculated to determine the intratumoural distribution. Similar to the comparison in lung cancer, a negative correlation between ^{62}Cu-ATSM and ^{18}F-FDG uptake was found in squamous cell carcinomas, suggesting these 2 tracers detect different tumour characteristics. However, in the 3 adenocarcinoma cases investigated they showed similar and homogeneous tracer accumulation. Nyflot et al[410] compared ^{18}F-FDG, ^{18}F-FLT, and ^{61}Cu-ATSM uptake in 13 patients with locally advanced oropharyngeal cancer. CT images were coregistered to corresponding PET images, and GTV and clinical target volumes (CTV) were defined on contrast-enhanced CT and ^{18}F-FDG PET/CT images. The volumes were used to calculate the SUV_{mean} and SUV_{max}. There was high voxel-based correlation between ^{18}F-FDG and ^{18}F-FLT uptake, but hypoxia was less clearly associated with metabolic or proliferative status. Nyflot et al[411] recently reported a phase I study to assess the use of ^{18}F-FLT and ^{61}Cu-ATSM to monitor early tumour response when bevacizumab was combined with radiation and cisplatin in locally advanced HNSCC. Ten patients received scans before and after bevacizumab, and during combined therapy, which showed measurable decreases in tumour proliferation and hypoxia at each time point.

^{64}Cu-ATSM has been used in head and neck cancers to compare early and late ^{64}Cu-ATSM PET scans in 11 patients, and with ^{18}F-FDG .[412] Cu-ATSM PET scans were carried out at 1 hour and 16 hours after injection. The SUV_{max} of the primary tumour was measured and a cut off of 42% of the lesion SUV_{max} was used to delineate a volume defined as the biological target volume (BTV). There was no difference in the SUV_{max} between early and late scans, and SUV_{max} and BTV had high sensitivity but low specificity in predicting complete response to therapy.

Table 1.9 summaries the Cu-ATSM PET imaging clinical studies conducted in cancer patient.

1.6.5 Summary

There have been a large number of studies attempting to validate Cu-ATSM as a hypoxic tracer and elucidate the exact mechanisms, with conflicting results. Preclinical studies have not been able to consistently demonstrate the hypoxia selectivity, but they have used a range of different cell lines, animal models and techniques. It is clear that Cu-ATSM accumulation is dependent on the cell or tumour type and would not be suitable as a universal tracer of hypoxia, but this is the true for all PET radiopharmaceutical agents. Despite the uncertainties regarding the precise mechanism, small clinical studies have suggested the potential as an imaging biomarker that warrants further investigation, with clear advantages over the nitroimidazole-based hypoxia tracers.

Table 1.9 Summary of Cu-ATSM clinical studies in cancer.

Radiotracer	Tumour	Patient no.	PET scan acquisition	PET analysis	Outcome	Ref
^{62}Cu-ATSM ^{18}F-FDG ^{15}O-water	Lung	6 patients 4 normal subjects	Dynamic PET imaging over 20 minutes	^{62}Cu-ATSM TBR ^{18}F-FDG SUV	High ^{62}Cu-ATSM uptake in tumours. No correlation between ^{62}Cu-ATSM and ^{18}F-FDG. Negative correlation between ^{62}Cu-ATSM and ^{15}O-water in 3 out of 4 tumours.	394
^{60}Cu-ATSM ^{18}F-FDG	Lung	19 (response evaluation in 14)	Dynamic PET over 60 minutes	^{60}Cu-ATSM TMR, SUV_{max} ^{18}F-FDG SUV_{max}	Response at 3 months: mean TMR non-responders greater than responders. SUV_{max} no difference. TMR and SUV_{max} no significant correlation. TMR 3.0 cut-off distinguished responders and non-responders.	396
^{62}Cu-ATSM ^{18}F-FDG	Lung	8 SCC, 5 adenocarcinoma	Dynamic PET over 20 minutes	SUV_{mean} SUV_{roi}	Intratumoural distribution in SCC – high ^{62}Cu-ATSM uptake in periphery of tumour, high ^{18}F-FDG in centre. Adenocarcinoma – similar pattern of uptake.	398
^{62}Cu-ATSM ^{62}Cu-PTSM ^{18}F-FDG	Lung nodules	2 (1 malignant, 1 benign)	Dynamic PET over 20 minutes	SUV_{max}	Malignant lesion high SUV_{max}. Benign lesion high ^{62}Cu-PTSM and ^{18}F-FDG SUV_{max}, low ^{62}Cu-ATSM SUV_{max}.	397
^{62}Cu-ATSM ^{62}Cu-PTSM	Lung nodules	6 (5 malignant, 1 benign)	Dynamic PET over 20 minutes	^{62}Cu-ATSM to ^{62}Cu-PTSM SUV ratio	Ratio did not distinguish malignant from benign.	413
^{60}Cu-ATSM ^{18}F-FDG	Cervix	14[399], 38[400]	Dynamic PET over 60 minutes	^{60}Cu-ATSM TMR ^{18}F-FDG SUV_{max}	^{60}Cu-ATSM uptake inversely related to PFS and OS. TMR 3.5 cut-off distinguished likely recurrence and no recurrence. No correlation between ^{60}Cu-ATSM and ^{18}F-FDG uptake.	399,400
^{60}Cu-ATSM ^{64}Cu-ATSM	Cervix	10	Dynamic PET over 60 minutes	TMR	^{64}Cu-ATSM better image quality. Distribution and TMR of tracers carried out on different days similar.	402
^{60}Cu-ATSM ^{18}F-FDG	Rectum	19 (response evaluation in 17)	Dynamic PET over 60 minutes	^{60}Cu-ATSM TMR ^{18}F-FDG SUV_{max}	Median TMR 2.6 cut-off distinguished worse and better prognosis. Mean TMR significantly lower for downstaged tumours. No correlation between ^{60}Cu-ATSM and ^{18}F-FDG uptake.	403
^{62}Cu-ATSM	Glioma	22	Dynamic PET over 40 minutes	TBR	TBR significantly higher in grade 4 compared with grade 3 tumours. TBR 1.8 cut-off distinguished HIF1α positivity on IHC. ^{62}Cu-ATSM uptake within MRI enhanced regions, not in necrotic.	404

^{62}Cu-ATSM ^{18}F-FDG ^{11}C-MET	Glioma	23	Dynamic PET over 40 minutes	TBR SUV_{max}	^{62}Cu-ATSM uptake significantly higher in GBM. TBR 1.9 cut off predictive off GBM with better sensitivity than ^{11}C-MET. ^{18}F-FDG had no predictive value.	**405**
^{62}Cu-ATSM	Glioma	40	Dynamic PET over 30 minutes	TBR SUV_{max}	TBR and SUV_{max} high in primary CNS lymphoma and GBM, low in low grade glioma. Inverse correlation with apparent diffusion coefficient on diffusion-weighted MRI.	414
^{60}Cu-ATSM	Head and neck	1	Dynamic PET over 60 minutes	RT planning study	Feasible to deliver increased dose to ^{60}Cu-ATSM avid tumour subvolume with IMRT.	406
^{62}Cu-ATSM ^{18}F-FDG	Head and neck	17 (15 in analysis)	Static PET	TMR SUV_{max}	SUV_{max} significantly different in patients with and without recurrence. SUV_{max} 5.0 cut off distinguished patients with and without recurrence. No correlation between ^{18}F-FDG and outcome.	407
^{62}Cu-ATSM ^{18}F-FDG	Head and neck	27 SCC, 3 adeno-carcinoma	Dynamic PET over 20 minutes	SUV_{mean}	Intratumoural distribution in SCC - ^{62}Cu-ATSM uptake higher in periphery of tumour, high ^{18}F-FDG in centre. Adenocarcinoma – similar homogeneous accumulation.	409
^{61}Cu-ATSM ^{18}F-FLT ^{18}F-FDG	Oropharynx	13 (11 analysed)	Static PET	SUV_{max} SUV_{mean}	High voxel-based correlation values between ^{18}F-FLT and ^{18}F-FDG uptake. ^{61}Cu-ATSM more heterogeneous.	410
^{64}Cu-ATSM ^{18}F-FDG	Head and neck	11	Static PET at 1 and 16 hrs	SUV_{max}	No significant difference in SUV_{max} between early and late scans. No difference in BTV calculated with ^{64}Cu-ATSM and ^{18}F-FDG. SUV_{max} and BTV high sensitivity in predicting treatment response.	412
^{62}Cu-ATSM ^{18}F-FDG	Head and neck	25	Dynamic PET over 20 minutes	TMR SUV_{max}	Optimal cut off for TMR 3.2, SUV_{max} 3.6. TMR > 3.2 worse PFS and CSS, SUV_{max} > 3.6 worse PFS. ^{18}F-FDG parameters not prognostic.	408
^{61}Cu-ATSM ^{18}F-FLT	Head and neck	10	Static PET	SUV_{mean} SUV_{peak}	^{61}Cu-ATSM – significant decrease in SUV_{mean} after bevacizumab and combined therapy. ^{18}F-FLT – significant decrease in SUV_{mean} and SUV_{peak}.	411

1.7 Thesis aims

The development of individualised treatments in oncology requires understanding of the molecular biology of cancer and the ability to translate this into therapy. Due to the heterogeneity of HNSCCs biomarkers are needed to identify the mechanisms of tumourigenesis and treatment resistance to improve outcome. Radioresistance is a major cause of treatment failure, and identification of biomarkers at the diagnostic step in the patient pathway that can predict the response of tumours to radiotherapy would open up the potential to incorporate different strategies to overcome radioresistance.

MicroRNAs represent novel biomarkers. The first part of this thesis aims to investigate the characteristics a potential novel biomarker of intrinsic radioresistance, miR-196a, which was identified from miRNA expression profiling of a small number of patients with differential outcomes after radical treatment. The oncogenic effects and response to radiotherapy after alteration of this single miRNA is explored in HNSCC cell lines.

The second part focuses on hypoxia, a well-established biomarker of radioresistance. The use of an imaging biomarker, ^{64}Cu-ATSM, in conjunction with gene expression from diagnostic FFPE biopsy samples is explored as a method to identify hypoxia as well as assess its distribution. A 15 patient pilot study has been conducted as part of a larger study, which aims to define a gene signature that can enable the selection of patients who would benefit from hypoxia imaging.

Chapter 2

The Oncogenic Role of MicroRNA-196a in Head and Neck Squamous Cell Carcinoma

2.1 Introduction

2.1.1 MicroRNA-196a as a biomarker in HNSCC

Previous work carried out in our lab identified miR-196a as a potential biomarker for poor outcome in HNSCC. Briefly, 16 patients with HNSCC were selected based on their long-term outcome to anti-cancer treatment. All patients were treated with surgery and post-operative radiotherapy and classified as 'good' responders of therapy if they had no evidence of recurrent disease within 5 years of follow up, or 'bad' responders if they had relapsed. Cases were selected as representative stages and sites in each group to include the range of oral carcinoma presentations. All carcinomas were from oral sites with surface origin; those from posterior tongue or soft palate were not of human papillomavirus type. Tissue samples were collected prior to treatment, immediately snap-frozen in liquid nitrogen and stored at -80°C until RNA extraction. Ethics approval was covered by an existing project (REC reference 04/02/10). The samples were profiled for miRNA gene expression using Illumina v2 miRNA Beadchip (Illumina, San Diego, USA) according to manufacturer instructions. Differential expression of miRNAs between the two patient groups ('good' and 'bad' responders) was estimated by fitting a linear model and empirical Bayes moderated t-tests using the limma package, and $\log_2$ fold-change and P-values were inspected to define the top-ranked miRNAs for differential expression (Figure 2.1). MiR-196a was the highest overexpressed miRNA in the 'bad' outcome group and therefore selected for further investigation.

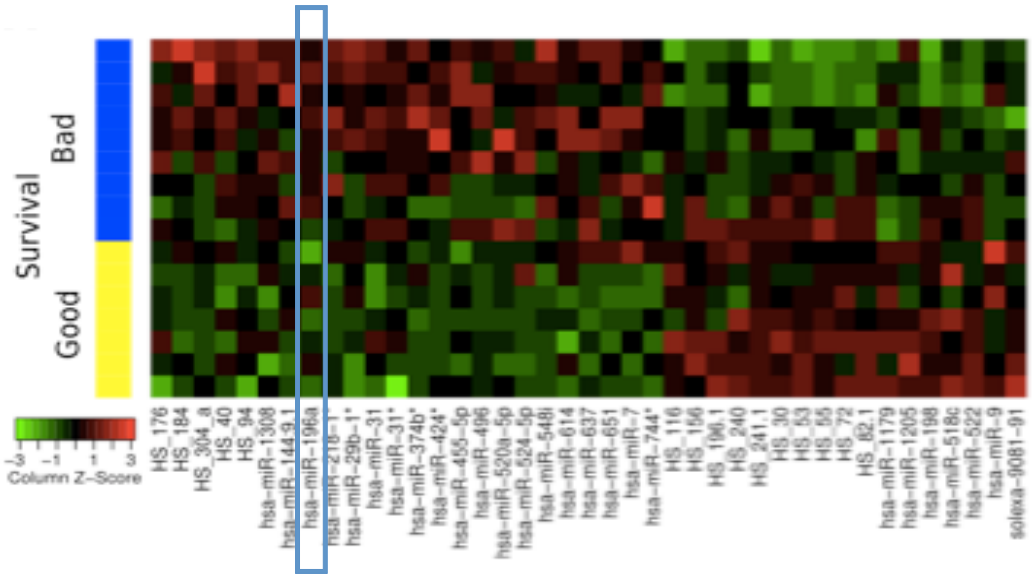

Figure 2.1 Heatmap displaying miRNA expression in tissue samples with differing outcomes.
Sixteen fresh frozen HNSCC samples from patients with 'good' (yellow) and 'bad' (blue) outcome were profiled for miRNA expression. The 41 top-ranked miRNAs for differential expression between the two groups are shown. Rows (samples) are ordered by expression score. Columns (miRNAs) are ordered by the direction of fold-change then alphabetically.

Eight HNSCC cell lines were then profiled for the endogenous expression level of miR-196a (Figure 2.2).

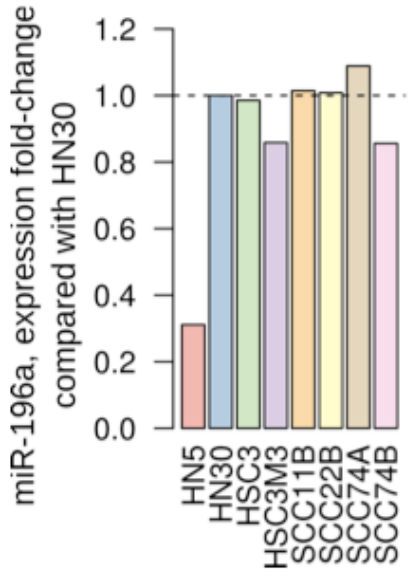

Figure 2.2 MiR-196a gene expression levels in eight HNSCC cell lines.
Eight HNSCC cell lines were profiled for the expression of miR-196a and displayed as expression fold-change compared with HN30. Cell line expression values are shown as the mean of two duplicate samples. The cell lines HN5 and HN30, with low and high endogenous levels of miR-196a respectively, were selected for further investigation.

2.1.2 MicroRNA-196a

The miRNA-196 gene family is encoded at three locations in the mammalian homeobox (HOX) clusters, A, B and C. It has extensive evolutionarily conserved complementarity to the mRNA of HOXB8, HOXC8, and HOXD8, with full complementarity to the 3' UTR of HOXB8 mRNA, resulting in cleavage and rapid degradation.[415] HOX genes encode transcription factors essential for embryonic patterning during embryogenesis, and for controlling cell growth, differentiation, identity, and cell-to-cell interaction in adult eukaryotic organisms.[416] There are two miR-196a genes, miR-196a-1 and miR-196a-2, located on different chromosomes but transcribing the same functional mature miRNA sequence. The miR-196a-1 gene is located on chromosome 17q21 between HOXB9 and HOXB10 genes, and the miR-196a-2 gene is on chromosome 12q13 between HOXC10 and HOXC9. The third gene in the miR-196 family is miR-196b, located on chromosome 7p15 between HOXA9 and HOXA10 genes, and differs from miR-196a sequence by one nucleotide (Table 2.1).[417]

Table 2.1 MiR-196 gene location and mature sequance.

miRNA	Location	Sequence
miR-196a-1	Chromosome 17q21.32	3'-GGGUUGUUGUACUUUGAUGGAU-5'
miR-196a-2	Chromosome 12q13.13	3'-GGGUUGUUGUACUUUGAUGGAU-5'
miR-196b	Chromosome 7p.15.2	3'-GGGUUGUUGUCCUUUGAUGGAU-5'

MiRNA-196a is overexpressed in several tumours and increasing evidence indicates that abnormal expression contributes to tumourigenesis and tumour progression. Epigenetic changes and single nucleotide polymorohisms have been identified in this miRNA, which are associated with altered susceptibility to some cancers. For example, a single nucleotide polymorphism with a specific homozygous CC genotype in the pre-miRNA-196a, affecting the mature miRNA expression and the binding efficiency to target mRNA, has been associated with reduced survival in lung cancer in the Chinese population.[418] This genotype is also associated with increased susceptibility to lung,[419] gastric[420] and breast cancers[421] in the same population, but a decreased risk of glioma.[422] MiR-196a has been shown to act both as an oncogenic and TSG miRNA depending on the target and tumour type.

2.1.2.1 MiR-196a as oncogenes

MiR-196a is significantly upregulated in a variety of cancers compared to normal controls, such as pancreas,[423] oesophagus,[424] gastric,[425,426] lung,[427] colorectal,[428] cervix,[429] larynx[430] and oral cancer[431], and high levels are associated with worse outcome. MiR-196a has been shown to promote cell proliferation, anchorage dependent growth and suppression of apoptosis, and act as a potential marker of progression to invasive adenocarcinoma in oesophageal cancer.[424,432] Annexin A1 (ANXA1), keratin 5 (KT5), S100 calcium-binding protein A9 (S100A9) and small proline-rich protein 2C (SPRR2C) were identified as potential targets through which miR-196a exerted its effects. Similar studies have been carried out in oral SCC and non-small cell lung cancer cell lines, tissues and mouse models. MiR-196a overexpression is associated with tumour recurrence, nodal metastasis and mortality in oral cancers,[431] and, acting through HOXA5, resulted in increased cell proliferation, migration and invasion in lung cancer cell lines.[427] HOX genes have also been found to be associated with miR-196a in colorectal cancer, where high levels of miR-196a promoted the AKT signaling pathway, cell detachment, migration, invasion and increased lung metastases in mice. HOXA7, HOXB8, HOXC8 and HOXD8 were all inhibited by miR-196a.[433]

More recently IκBα, an inhibitor of NF-κB, has been identified as a direct target of miR-196a. In glioblastoma multiforme miR-196a, which is upregulated and associated with poor outcome, directly interacted with IκBα 3'-UTR to suppress IκBα expression and

subsequently promote NF-κB activation. This resulted in enhanced proliferation and apoptosis suppression.[434] Similarly in pancreatic cancer miR-196a downregulation in cell lines suppressed proliferation and migration, while silencing of IκBα enhanced cell proliferation and migration.[435] MiR-196a has also been associated with abnormal apoptosis and proliferation in pancreatic cancer cells through downregulation of inhibitor of growth 5 (ING5).[436] In gastric cancer miR-196a overexpression enhanced cellular proliferation and $p27^{kip1}$, a cyclin-dependent kinase inhibitor known to prevent cell cycle progression, was identified as a direct target,[425] as was radixin, a cytoskeletal protein, in both cells and tissue samples where both miR-196a and miR-196b promoted metastases.[426] $p27^{kip1}$ along with FOXO1, two important regulators of the PI3K/AKT signaling pathway, were also found to be regulated by miR-196a in cervix cancer.[429] A further study in cervix cancer confirmed the oncogenic potential of miR-196a, this time through netrin-4, which is involved in axon guidance and angiogenesis.[437]

2.1.2.2 MiR-196a as TSGs

The majority of studies on miR-196a suggest it has an oncogenic role. However a few studies have demonstrated that miR-196a can act as a TSG. MiR-196a has been found to be downregulated in melanoma[438] and breast cancer,[439] with overexpression resulting in the inhibition of invasion and metastasis by targeting HOXC8, and the suppression of miR-196a causing increased migration through HOXB7.[440] The role of miR-196a is clearly cell and tissue specific and the downstream effect dependent on the target gene/or genes through which it is acting.

2.1.2.3 Summary of targets of miRNA-196a

Identification of the mRNA targets of miRNAs is essential in understanding the function of each miRNA. Due to the potential multiple targets of a single miRNA and a single mRNA being targeted by multiple miRNA, as well as imperfect base pairing to the 3'-UTR of the mRNA, this is a huge challenge. Table 2.2 summarises the gene targets of miR-196a involved in cancer pathways that have been experimentally verified by functional analysis and luciferase reporter assays.

Table 2.2 Published targets of miR-196a.

Gene	Cell type	Reference
HOXB8	Colon cancer cell line SW480 Leukaemic cell line HL60	415,433,441
HOXC8	Colon cancer cell line SW480 Melanoma cell line Mel Im Breast cancer cell line MDA-MB-231	415,433,438,439
HOXD8	Colon cancer cell line SW480	415,433
HOXA7	Colon cancer cell line SW480	415,433
HOXB7	Melanoma cell line Mel Im	440
HOXA5	Lung cancer cell lines A549, SPC-A1	427
ANXA1	Human umbilical vein endothelial cells Oesophageal cancer cell lines BIC-1, OE33, SEG-1 Breast cancer cell lines MDA-453, MDA-231 Endometrial cancer cell HEC-1B	424,442
S100A9	Oesophageal cancer cell line BIC-1	432
SPRR2C	Oesophageal cancer cell line BIC-1	432
KRT5	Oesophageal cancer cell line BIC-1	432
ERG	Leukaemia cell lines KG1a and MOLT-4	443
HMGA2	Mouse embryonic fibroblast cell line NIH313	444
IκBα	Glioblastoma cell lines U87MG, T98G Pancreatic cancer cell line PANC-1, BxPC-3	434,435
$p27^{kip1}$	Gastric cancer cell line SGC-7901 Cervix cancer cell lines CaSki, C33A	425,429
ING5	Pancreatic cancer cell line PANC-1	436
Radixin	Gastric cancer cell line GC	426
FOXO1	Cervix cancer cell lines CaSki, C33A	429
Netrin-4	Cervix cancer cell lines CaSki, Hela	437

2.1.2.4 Annexin A1

Annexin A1 (ANXA1) is a member of the annexin family of calcium-dependent phospholipid-binding proteins and has been shown to exhibit anti-inflammatory and anti-proliferative effects.[445] However, the molecular mechanisms by which ANXA1 modulates these cellular responses have not been fully determined. Due to its anti-proliferative effects and role in cellular adhesion and motility,[446] ANXA1 protein has been studied in several types of cancers, but in vivo studies have demonstrated that the expression pattern of ANXA1 in human cancers is not well defined. While ANXA1 has been reported to be upregulated in glioma[447] and lung adenocarcinoma,[448] its expression is reduced or lost in other cancer tissues including head and neck,[449-451] oesophageal and prostate.[452] In addition ANXA1 has been found to behave as both an oncogene and TSG in different types of cancer. In HNSCC the expression of ANXA1 has been shown to correlate with higher grades of differentiation, or less aggressive tumours, suggesting a tumour suppressor role.[449,453] ANXA1 has been shown to be a target of miR-196a in oesophageal and breast

cancer cells,[424] but the association with miR-196a has not been established in HNSCC and warrants further investigation.

2.2 Aims

The microarray data demonstrated that miR-196a may have a role in the outcome of HNSCC. Single miRNAs have been shown to be able to impact on the behaviour of cancer cell lines and therefore may represent potential biomarkers of tumour phenotype and response to treatment.

This in vitro study aimed to investigate whether miR-196a has a role as a prognostic and/or predictive marker in HNSCC by:

- Characterising the behaviour of miR-196a overexpressing cells through functional analysis.
- Assessing whether the opposite behaviour can be induced in miR-196a knockdown cells.
- Determining the effect of miR-196a on the response to irradiation.
- Elucidating underlying mechanisms for any differential response.
- Investigating annexin A1 as putative target of miR-196a in HNSCC cell lines.
- Validating the effect of miRNA-196a in patient samples.

2.3 Materials

Plasticware used in tissue culture were purchased from Grenier Bio-One, Scientific Laboratory Supplies or Thermo Scientific.

2.3.1 Chemicals, reagents and solutions

All chemicals were purchased from Sigma-Aldrich, unless otherwise stated. Solutions were stored at room temperature unless otherwise specified.

10% Ammonium persulphate (APS)

The solution was made up in dH_2O and store at 4°C for up to 2 weeks.

Antibiotics

Carbenicillin was purchased from Bioline, stored at -20°C and used at a working concentration of 100 µg/ml.

Puromycin was purchased from Source Bioscience and stored at -20°C. The required working concentration was determined before use.

BD BioCoat Matrigel Invasion Chamber

Stored at -20°C and purchased from BD Biosciences with corresponding Control Inserts.

Blocking buffer

For immunofluorescence: 3% (w/v) bovine serum albumin (BSA, Scientific Laboratory Supplies) in PBS.

For Western blot analysis: 5% (w/v) dry milk powder or 5% BSA in 1x TBS-T.

Calcium chloride ($CaCl_2$)

0.5 M $CaCl_2$ solution

Made up in dH_2O and sterilised by filtering through a 0.2 µm filter (Fisher Scientific).

Cell lysis buffer

2 mM $MgCl_2$

25 mM HEPES KOH pH 7.4

2 mM EGTA

Diluted 1:1 in 2% Trition X-100. Protease inhibitors aprotinin and leupeptin at a final concentration of 1µg/ml and PMSF at a concentration of 100 µg/ml added before use.

Coumaric acid

90 mM p-coumaric acid made up in dimethyl sulfoxide (DMSO) and stored at -20°C.

Dual-Glo Luciferase Assay System

Purchased from Promega and stored at -20°

Dubecco's modified eagle media (DMEM) high glucose

Purchased from Life Technologies and supplemented with 10% foetal bovine serum (FBS), 1 ml 100x penicillin/streptomycin to a final concentration of 20 µg/ml penicillin and 10 µg/ml streptomycin (PAA Laboratories), and 1mM sodium pyruvate. Media was stored at 4°C.

Enhanced chemiluminescence (ECL) buffer

100 mM Tris-HCl pH 8.5, stored at 4°C.

Prior to use 10 ml of ECL buffer mixed with 3 µl hydrogen peroxide, 25 µl 90 mM coumaric acid and 50 µl 250 mM luminol.

EDTA solution (pH 8.0)

0.5 M EDTA solution

Made up in dH_2O, pH adjusted to 8.0 with NaOH and autoclaved before use.

100% Ethanol

Fermentas PageRuler Prestained Protein Ladder

Purchased from Thermo Fisher Scientific and stored at -20°C.

Freezing medium

10% DMSO

40% FBS

50% culture medium

2x HEPES-buffered saline (HEBS)

50 mM HEPES

1.5 mM Na_2HPO_4

280 mM NaCl

Made up in dH_2O, pH adjusted to 7.05 with NaOH and sterilised by filtering through a 0.2 µm filter.

Isopropanol

3x Lamelli sample buffer (LSB)

62 mM Tris-base pH 6.8

10% glycerol

2% SDS

5% β-mercaptoethanol

Prepared in dH_2O and stored at -20°C. Protease inhibitors aprotinin and leupeptin both at a final concentration of 1 µg/ml, PMSF at a final concentration of 100 µg/ml and 5 µl saturated bromophenol blue added to 1 ml of LSB prior to use.

Luminol

250 mM luminol in DMSO, stored at -20°C.

Luria-Bertani (LB) medium

1% NaCl

0.5% Bacto-yeast extract

1% Bacto-tryptone

Made up in dH_2O, pH adjusted to 7.0 with NaOH and sterilised by autoclaving.

LB agar plates

1.5% (w/v) agar dissolved in LB medium, autoclaved and cooled to 50°C. Plates were poured after adding carbenicillin, allowed to set and stored for several months at 4°C.

100% methanol

1% methylene blue

1% (w/v) made up in dH_2O.

3-(4,5-Dimethylthiazol-2-yl)-2,5-diphenyltetrazolium bromide (MTT)

5 mg/ml MTT (Calbiochem)

Prepared in 1x PBS, sterilised by filtering through a 0.2 µm filter and stored at -20°C protected from light.

MTT solubilisation solution

50% dimethylformamide

0.2% glacial acetic acid

20 mM HCl

20% SDS

Prepared in dH_2O.

OptiMEM reduced serum medium

Purchased from Life Technologies and stored at 4°C.

4% Paraformaldehyde (PFA)

8 g PFA powder dissolved in 100 ml dH_2O and heated to 60°C in fume hood. 3 M NaOH added drop-wise until solution turned clear, followed by 20 ml of 10x PBS and dH_2O to a final volume of 200 ml. Aliquots stored at -20°C.

Phenylmethylsulfonyl fluoride (PMSF)

10 mM PMSF made up in isopropanol and stored at -20°C.

10x Phosphate-buffered saline (PBS)

140 mM NaCl

2.7 mM KCl

8.0 mM Na_2HPO_4

1.5 mM KH_2PO_4

Made up in dH_2O and sterilised by autoclaving.

Plasmid Midi Kit

Purchased from Qiagen.

Polybrene

10 mg/ml, purchased from Santa Cruz Biotechnology and stored at -20°C. Working concentration 5 µl/ml.

QRT-PCR reagents

TaqMan MicroRNA Reverse Transcription Kit

TaqMan Universal PCR Master Mix II (No UNG)

TaqMan microRNA assay primers:

hsa-miR-196a-5p (mature miRNA sequence UAGGUAGUUUCAUGUUGUUGGG)

RNU48 control miRNA assay

Purchased from Life Technologies and stored at -20°C.

ReBlot Plus stripping buffer

Reblot Plus 10x stripping buffer (Millipore) was diluted 1:10 in dH_2O and stored at 4°C.

RNeasy formalin fixed paraffin embedded (FFPE) Kit

Purchased from Qiagen.

10x Running/Transfer buffer

250 mM Tris-base

2.5 M glycine

1% SDS

Made up in dH_2O.

1x Running buffer for SDS-PAGE

10% 10x running/transfer buffer

90% dH_2O

10% Sodium dodecyl sulphate (SDS)

Made up in dH_2O, heated to 68°C to dissolve and pH adjusted to 7.2 using concentrated HCl.

SDS polyacrylamide gels

Protogel 30% Acrylamide Mix (37.5:1 acrylamide to bisacrylamide stabilised solution) was purchased from National diagnostics.

Table 2.3 SDS-PAGE gel components for two gels.
The smaller the size of the protein of interest, the higher the percentage resolving gel used.

Resolving gel	10%	12%	15%
1.5 mM Tris pH 8.8	5.0 ml	5.0 ml	5.0 ml
30% Acrylamide	6.7 ml	8.0 ml	10.0 ml
ddH_2O	7.9 ml	6.6 ml	4.6 ml
10% SDS	200 µl	200 µl	200 µl
10% APS	200 µl	200 µl	200 µl
TEMED	8 µl	8 µl	8 µl

Stacking gel	4%
1.0 mM Tris pH 6.8	750 µl
30% Acrylamide	1.0 ml
ddH_2O	4.1 ml
10% SDS	60 µl
10% APS	60 µl
TEMED	6 µl

10x Tris-buffered saline (TBS)

250 mM Tris-base

1.5M NaCl

Made up in dH_2O, pH adjusted to 7.4 with concentrated HCl.

1x TBS-Tween (TBS-T)

0.1% Tween 20 in 1x TBS

Tris-EDTA (TE) buffer

10 mM Tris-HCl pH 8.0

1 mM EDTA pH 8.0

Made up in dH_2O.

1% toluidine blue in 1% borax

1% (w/v) toluidine blue, 1% (w/v) borax

Made up in dH_2O.

Transfection reagents

X-tremeGENE HP DNA transfection reagent, purchased from Roche.

FuGENE HD transfection reagent, purchased from Promega.

1x Transfer buffer for Western blot

10% 10x running/transfer buffer

20% methanol

70% dH_2O

0.2% Triton X-100

Triton X-100 0.1 ml dissolved in 49.9 ml of 1x PBS.

TRIzol (guanidinium thiocyanate-phenol-chloroform)

Purchased from Life Technologies.

1x Trypsin

10% 10x trypsin

90% versene

VECTASHIELD mounting medium with DAPI

Purchased from Vector Laboratories and stored at 4°C.

Versene

0.270 mM EDTA pH 8.0

Made up in PBS and sterilised by autoclaving.

2.3.2 Antibodies

2.3.2.1 Primary antibodies

Annexin A1

Rabbit monoclonal antibody to annexin A1, MW 38 kDa.

Dilution: 1:1000 in 5% BSA for Western blotting.

Purchased from Cell Signaling.

β-Actin

Mouse monoclonal antibody to β-Actin, molecular weight (MW) 42 kDa.

Dilution: 1:5000 in 5% milk for Western blotting.

Purchased form Sigma-Aldrich.

Caspase-3

Rabbit polyclonal antibody to caspase-3 (full length and cleaved), MW 17, 19, 35 kDa.

Dilution: 1:1000 in 5% milk for Western blotting.

Purchased from Cell Signaling.

Cleaved PARP

Mouse monoclonal antibody to cleaved PARP, MW 89 kDa.

Dilution: 1:1000 in 5% milk for Western blotting.

Purchased from Cell Signaling.

E-cadherin

Rabbit monoclonal antibody to E-cadherin, MW 135 kDa.

Dilution: 1:1000 in 5% BSA for Western blotting, 1:100 in 3% BSA for immunofluorescence.

Purchased from Cell Signaling.

Phospho-Histone H2AX (gamma H2AX)

Rabbit polyclonal antibody to gamma H2AX.

Dilution: 1:100 in 3% BSA for immunofluorescence.

Purchased from Cell Signaling.

Tubulin

Mouse monoclonal antibody to tubulin, MW 55 kDa.

Dilution: 1:2000 in 5% milk for Western blotting.

Purchased from Sigma-Aldrich.

Vimentin

Rabbit monoclonal antibody to vimentin, MW 57 kDa.

Dilution: 1:1000 in 5% BSA for Western blotting, 1:100 in 3% BSA for immunofluorescence.

Purchased from Cell Signaling.

2.3.2.2 Secondary antibodies

Mouse-HRP

Goat anti-mouse IgG conjugated to horseradish peroxidase (HRP).

Dilution: 1:2000 in 5% milk for Western blotting.

Purchased from Sigma-Aldrich.

Rabbit-HRP

Donkey anti-rabbit IgG conjugated to HRP.

Dilution: 1:2000 in 5% milk for Western blotting.

Purchased from GE Healthcare.

Mouse-FITC

Goat anti-mouse IgG conjugated to fluorescein isothiocyanate (FITC).

Dilution 1:100 in 3% BSA for immunofluorescence.

Purchased from Sigma-Aldrich.

Rabbit-FITC

Goat anti-rabbit IgG conjugated to FITC.

Dilution 1:100 in 3% BSA for immunofluorescence.

Purchased from Sigma-Aldrich.

2.3.3 Plasmids/viral constructs

pBabe-puro plasmid

Provided by Dr Joop Gäken, Department of Haemato-Oncology, King's College London.

miR-196a expression plasmid

MiR-196a expression plasmid was prepared by Dr Joop Gäken, Department of Haemato-Oncology, King's College London, by PCR amplification of a 630 bp genomic DNA fragment containing miR-196a using the following forward and reverse primers: CAGGCTTGTGCCTGTGTCTA and GTGCCTCGGGAGAGTTGAC. The PCR product was sequenced, verified and cloned into the retroviral expression vector pBabe-puro.

Retroviral miR-196a sponge and corresponding empty vector control

Expresses red fluorescent protein (RFP) and contains puromycin resistance gene.

Provided by Dr Sebastian Herzog, Division of Developmental Immunology, Medical University of Innsbruck, Austria.

Retroviral ANXA1 shRNA and corresponding empty vector control

Contains puromycin resistance gene.

Provided by Dr Stéphane Gobeil, CHUL Research Centre, Laval University, Canada.

Retrovirus plasmids

VSV-G envelope plasmid, HIT60 Gag and Pol expressing plasmid

Provided by Dr Ulrich Maurer, University of Freiburg, Germany.

ANXA1 dual luciferase reporter plasmid

Expresses green fluorescent protein (GFP).

Provided by Prof Jacques Huot, Laval University Cancer Research Centre, Canada.

2.3.4 Cell lines

HEK293T

Cell line derived from Human Embryonic Kidney 293 cells

Constitutively express simian virus 40 (SV40) large T antigen involved in viral genome replication.

Provided by Dr Lucas Chan, Rayne Institute, King's College London.

HN5

Human tongue SCC cell line

Provided by Dr Barry Gusterson, Department of Pathology, University of Glasgow.

HN30

Human pharynx SCC cell line

Provided by Dr Andrew Yeudall, Department of Craniofacial Development and Stem Cell Biology, King's College London.

MDA-MB-231

Human metastatic (pleural fluid) breast adenocarcinoma cell line

Provided by Prof Joy Burchell, Breast Cancer Biology Group, King's College London.

SCC11B

Human hypopharynx cell line

Provided by Dr Thomas Carey, University of Michigan.

SCC22B

Human metastatic (cervical lymph node) hypopharyngeal cell line

Provided by Dr Thomas Carey, University of Michigan.

HT-1080

Human fibrosarcoma cell line

Purchased from American Type Culture Collection (ATCC).

2.4 Methods

2.4.1 Cell culture

2.4.1.1 Cell maintenance

All cell lines were maintained in DMEM high glucose, supplemented with 10% FBS, 20 µl/ml penicillin, 10 µl/ml streptomycin, and 1 mM sodium pyruvate. HN5 miR-196a overexpressing cells and HN5 pBabe-puro empty vector control cells were also supplemented with 2 µl/ml puromycin.

Cells were grown in 75 cm^2 flasks, incubated in a humidified tissue culture incubator at 37ºC and 5% CO_2, and passaged every 3 to 4 days once 80-90% confluent. The old medium was removed, cells were washed with 5 ml versene and incubated with 1 ml trypsin at 37ºC. Once the cells had detached they were resuspended in fresh medium to neutralise the trypsin and diluted as necessary for further use.

2.4.1.2 Counting cells

Cells were trypsinised, collected in 5 ml of media and centrifuged at 1000 x g for 5 minutes. The resultant pellet was resuspended in 10 ml of media. Ten microlitres of cell suspension was pipetted into a haemocytometer and cells in the outer 4 large squares were counted. Cell number was calculated as follows:
Cells/ml = (number of cells in 4 squares/4) x 10^4.

2.4.1.3 Freezing and thawing of cell

Cells were collected by trypsinisation and centrifuged for at 1000 x g for 5 minutes. The cell pellet was resuspended in 1 ml of freezing medium, transferred into a cryovial and stored at -80°C in a container filled with isopropanol to control the freezing speed. The cells were transferred to a liquid nitrogen tank for long term storage. For thawing cells, the cryovial was placed in a 37°C waterbath, diluted in 10 ml of medium and centrifuged for 5 minutes at 1000 x g. The resulting cell pellet was resuspended in fresh medium and placed into a flask.

2.4.2 Preparation of plasmid DNA

2.4.2.1 Transformation of plasmid DNA into competent bacteria and bacteria culture

Chemically competent E.Coli (One Shot Mach1-T1, Invitrogen) were used for plasmid amplification. One microlitre of plasmid DNA was added to 100 µl of bacteria, incubated on ice for 30 minutes, heat shocked at 42°C for 45 seconds in a waterbath, then transferred back on ice for 2 minutes. LB medium (250 µl) was added and the bacteria cultured in a shaker at 37°C for 1 hour, after which they were spread on a pre-warmed agar plate supplemented with the appropriate antibiotic and incubated at 37°C overnight. A single colony was selected, placed in 5 ml LB medium supplemented with carbenicillin and cultured in a shaker at 37°C for 6-8 hours at 250 rpm. This was transferred into 50 ml LB medium with carbenicillin and cultured overnight under the same conditions.

2.4.2.2 Plasmid purification and extraction

This was carried out using the Plasmid Midi Kit according to the manufacturer's instructions. Briefly, the bacterial cells were harvested by centrifugation at 6000 x g for 15 minutes at 4°C and the pellet mixed with 4 ml resuspension buffer. Four millilitres of lysis buffer was added, incubated at room temperature for 5 minutes followed by the addition of 4 ml of neutralisation buffer and incubation for 15 minutes on ice. The cells were then centrifuged for at 20000 x g for 1 hour at 4°C, during which 4 ml of equilibrium buffer was passed through the purification columns. After centrifugation, the supernatant was applied to the column and allowed to empty by gravity. The column was washed twice and the plasmid DNA eluted using 5 ml of elution buffer, then precipitated by adding 3.5 ml isopropanol and centrifuging at 5000 x g for 1 hour at 4°C. The supernatant was removed and the pellet air-dried, before dissolving in 150 µl TE buffer. The DNA was stored overnight at 4°C and the concentration determined using a NanoDrop^{TM} 1000 Spectrophotometer (Thermo Scientific). DNA was placed in -20°C for long term storage.

2.4.3 Transfection methods

2.4.3.1 Transfection of HN5 cells to overexpress miR-196a using transfection reagent

For transfection of HN5 cell with miR-196a or pBabe-puro plasmids, cells were seeded in 6 well-plates to achieve 80% confluency the following day. A transfection mix of 200 µl OptiMEM, 2 µg DNA and 4 µl X-tremGENE HP DNA transfection reagent (2:1 transfection reagent to DNA ratio), which acts by complexing with and transporting DNA into cells, was

prepared and incubated at room temperature for 20 minutes for complex formation. This mix was added drop by drop to different areas of the well and the plate was gently rocked back and forth and side-to-side for even distribution. The cells were incubated at 37°C and 5% CO_2 for 48 hours, at which point cells were placed under selection or harvested for transient transfection experiments.

2.4.3.2 Generation of stable HN5 miR-196a overexpressing cell lines

The optimum concentration of puromycin was first determined for each cell line by incubating cells with medium containing increasing concentrations from 1 to 10 µg/ml. The lowest dose to completely kill the parental cell line at 48 hours was 2 µg/ml. Forty eight hours after transfection with the plasmid DNA, the medium of the cells was replaced with medium supplemented with 2 µg/ml of puromycin alongside untransfected controls. The majority of the cells died after 24 to 48 hours, with the remaining single cells and small colonies successfully transfected. One hundred percent of the control cells died. The medium with puromycin was changed every 3 to 4 days and cells were grown over 6 weeks. Cells originating from single colonies were selected when they had reached a diameter of approximately 5 mm and not coalescing with adjacent colonies. Hole-punched pieces of circular filter paper were autoclaved, soaked in trypsin and placed over the colonies using autoclaved forceps. After 10 minutes the filter paper was removed and placed in conditioned medium supplemented with puromycin in 24-well plates. Conditioned medium was prepared by collecting medium from confluent parental cells, passing this medium through a 0.45 µm filter (Fisher Scientific) and diluting 1:10 with fresh medium. Of the ten colonies suitable for this procedure two colonies survived and were expanded. The remainder of the cells after single colony selection were pooled together to form a mixed population of cells. The cells were tested for successful modulation by qRT-PCR.

2.4.3.3 Virus production

HEK293T cells were seeded in 10 cm dishes and grown to 70-80% confluence. A vector mix of 10 µg retroviral vector, 3.5 µg VSV-G envelope plasmid and 6.5 µg HIT60 Gag and Pol expressing plasmid were prepared in 250 µl sterile dH_2O and 250 µl $CaCl_2$ solution for transfection by calcium phosphate precipitation. This was added dropwise to 500 µl 2x HEBS buffer while vortexing and incubated for 30 minutes at room temperature. This mix was adding to the HEK293T cells. The virus-containing supernatant was harvested at 8, 16 and 24 hours post-transfection, filtered through a 0.45 µm filter and stored at -80°C. Prior to use polybrene was added to the supernatant to a final concentration of 5 µg/ml.

2.4.3.4 Generation of stable virus infected knockdown cell lines

The optimum concentration of puromycin was determined as above. Cells were seeded in 6-well plated to achieve 80% confluency the following day and infected by adding 1 ml of virus supernatant supplemented with 5 µg/ml polybrene. Two millilitres of fresh medium was added 8 hours after infection. After 48 hours the medium was replaced with medium containing puromycin. For the miR-196a sponge or control infected cells successful transduction could be confirmed by the expression of RFP. A high proportion of cells survived the selection process after virus infection; these cells were expanded and knockdown confirmed by qRT-PCR or Western blot analysis.

2.4.4 RNA methods

2.4.4.1 RNA extraction form cells

RNA was extracted using the following 3 steps:

a) Phase separation: Cells were plated in 10 cm dishes and grown until confluent. One millilitre of TRIzol was added directly to the dish and the lysate collected in an eppendorf tube. After 5 minutes incubation at room temperature, 0.2 ml chloroform was added and the tube shaken vigorously. Samples were incubated at room temperature for 3 minutes and centrifuged at 12000 x g for 15 minutes at 4°C to separate the mixture into three phases.
b) RNA precipitation: The top aqueous phase was transferred into a new eppendorf tube, without disturbing the interphase. RNA was then precipitated by adding 0.5 ml isopropanol per 1 ml TRIzol and incubated at room temperature for 10 minutes. The samples were centrifuged again at 12000 x g for 10 minutes at 4°C.
c) RNA wash and resuspension: The supernatant was removed and the RNA pellet washed with 1 ml 75% ethanol per 1 ml TRIzol. The samples were vortexed and centrifuged at 7500 x g for 5 minutes at 4°C. The supernatant was removed and the any remaining ethanol allowed to air dry. The resultant pellet was dissolved in 30 µl of RNAse free water, stored at -20°C overnight and quantified the following day using the NanoDrop Spectrophotometer. RNA was placed in -80°C for long term storage.

2.4.4.2 RNA extraction from FFPE samples

Forty cases of radiosensitive and radioresistant patient tumour samples were selected using the Head and Neck clinical database. Patients had stage III or IV primary oropharyngeal cancer and were treated radically with concomitant chemoradiation. Radioresistance was defined as residual tumour or progressive disease in the radiation field after completion of treatment, and radiosensitivity was defined as having a complete

response to treatment and remaining disease free for a minimum of 3 years. Tumour slides were reviewed by a consultant pathologist and samples containing a minimum tumour percentage of 60% were selected for RNA extraction. Ethics approval was covered by an existing project (REC reference 10/H0701/27).

Extraction was carried out using the miRNeasy FFPE kit following manufacturer instructions. Two 20 µm sections were cut from each selected FFPE block and placed into an eppendorf tube. The microtome was cleaned with ethanol and a new blade used for each sample. One millilitre of xylene was added for deparaffinisation and the samples vortexed and centrifuged at full speed (16000 x g) for 2 minutes. The supernatant was removed, 1 ml of 100% ethanol added to the pellet, and the tubes were vortexed and centrifuged at full speed again for 2 minutes. The supernatant and residual ethanol were removed and the samples incubated at room temperature for 10 minutes. The samples were lysed with 150 µl buffer PKD (proteinase K digestion) and 10 µl proteinase K (concentration not specified), followed by heat treatment at 56°C for 15 minutes, then 80°C for 15 minutes. They were then incubated on ice for 3 minutes, centrifuged for 15 minutes at 16000 x g and the supernatant transferred into a new eppendorf. The supernatant was treated with 16 µl of DNase booster buffer and 10 µl DNase I and incubated at room temperature for 15 minutes. Three hundred and twenty microlitres of Buffer RBC (exact composition proprietary) and 720 µl of ethanol were added, the mixture transferred into RNeasy MiniElute spin columns placed in collection tubes, and centrifuged at ≥ 8000 x g for 15 seconds. Buffer RPE (500 µl) was added to the spin columns to wash the samples. The columns were centrifuged and the flow-through discarded. This step was repeated. The spin columns were placed in new collection tubes, centrifuged with the lid open for 5 minutes and the flow-through discarded. The spin columns were placed in new eppendorfs and 20 µl of RNase free water was added directly to the spin column membranes. The spin columns were centrifuged for 1 minute at full speed to elute the RNA. RNA was stored at -20°C overnight and quantified the following day using the NanoDrop Spectrophotometer. RNA was placed in -80°C for long term storage.

2.4.4.3 Reverse Transcription Polymerase Chain Reaction (RT-PCR)

This technique is used to create complementary DNA (cDNA) transcripts from RNA using reverse transcriptase enzymes. The cDNA can then be amplified and quantified by quantitative real time PCR (qRT-PCR).

Complementary DNA was created using Taqman miRNA reverse transcription kit. Each reaction had a volume of 15 µl and RNA samples were diluted to a concentration of 10 ng/5

µl for each reaction. A master mix was prepared containing 0.15 µl of 100 mM dNTP (deoxynucleoside triphosphate) building blocks, 1 µl of 50 U/µl MultiScribe reverse transcriptase, 1.5 µl reverse transcription buffer, 0.19 µl of 20 U/µl RNase inhibitor, which protects RNA during the reverse transcription, and 4.16 µl nuclease-free water for each reaction. The reverse transcription reaction was prepared by combing 7 µl of mastermix, 5 µl (10 ng) total RNA and 3 µl of miR-196a or RNU48 reverse transcription primer. RT primers were diluted to a 5x working stock solution using 0.1x TE buffer. The primer is the starting point for the reaction and is complementary to the miR-196a or RNU48 sequence. The samples were loaded into a thermal cycler (G-Storm) with the following program:

Table 2.4 RT-PCR thermal cycler parameters.

Step	Time	Temperature
Hold	30 minutes	16ºC
Hold	30 minutes	42ºC
Hold	5 minutes	85ºC
Hold	∞	4ºC

2.4.4.4 Quantitative Real Time Polymerase Chain Reaction (qRT-PCR)

QRT-PCR simultaneously amplifies and quantifies targeted DNA sequences. During amplification, a fluorescent dye binds via a labelled hybridising probe (TaqMan Small RNA Assay) to the accumulated DNA molecules. The fluorescence signal is directly proportional to the DNA concentration and linear correlation used to calculate the amount of template present at the beginning of the reaction. The relative standard curve method was used to quantitate the miRNA expression levels, with RNU48 used as the housekeeping or reference gene expressed in all cells. The standard curve was optimised for each sample set.

Each reaction volume was 10 µl. A master mix was prepared containing 0.5 µl TaqMan Small RNA Assay (miR-196a or RNU48), 5 µl TaqMan Universal PCR Master Mix II (No UNG) and 3 µl nuclease-free water. The qRT-PCR reaction was prepared by combining 8.5 µl of master mix and 1.5 µl of cDNA. Samples were run in triplicate with a standard curve, in a Rotor-Gene (Corbett) real time PCR machine. The following settings were used:

Table 2.5 qRT-PCR thermal cycling conditions.

Step	Enzyme activation	PCR	
	HOLD	Cycle (40 cycles)	
		Denature	Anneal/Extend
Temperature	95ºC	95ºC	60ºC
Time	10 minutes	15 seconds	60 seconds

2.4.5 Protein methods

2.4.5.1 Protein extraction

Cells were trypsinised and collected in cold 1x PBS, centrifuged at 1000 x g for 5 minutes and resuspended in 1 ml PBS. This was centrifuged at 4°C and 5000 x g for 5 minutes and the resultant cell pellet was stored at -20° until further use. To prepare total cell lysates the cell pellet was resuspended in 30-60 µl of cell lysis buffer containing protease inhibitors (PMSF, aprotinin/leupeptin), incubated on ice for 10 minutes and centrifuged at 4°C and 16000 x g for 5 minutes. The solubilised proteins contained within the supernatant were transferred into a new eppendorf tube.

2.4.5.2 Bradford assay

This colorimetric protein assay used to determine protein concentrations and is based on the binding of Coomassie blue dye to proteins. When the dye binds to protein, it is converted from a doubly pronated red cationic form to a stable unpronated blue form, and the increase of absorbance at 595 nm is proportional to the amount of bound dye, and therefore the concentration of protein.

Bovine serum albumin (BSA) was serially diluted from 20 µg/ml to 0 for a standard curve, and samples diluted between 1:500 to 1:1000. In a 96-well plate 100 µl of Bradford reagent was added to 100 µl of sample or standard, and the absorbance of each well was measured at 595 nm on a LT-4000 microplate reader (Labtech, Manta software). The protein concentration of each sample was calculated via the standard curve.

2.4.5.3 Sodium Dodecyl sulphate Polyacrylamide Gel Electrophoresis (SDS-PAGE)

This technique is used to separate proteins according to their molecular weight on a polyacrylamide gel. The SDS in the LSB is anionic and both denatures the protein and confers a negative charge to them, allowing migration through the gel by molecular weight, not intrinsic electric charge. The separation is determined by the relative size of the pores

in the gel, which is determined by the amount of acrylamide in the gel. The smaller the size of protein of interest, the higher the percentage of acrylamide.

Gels were cast according to the manufacturer's instructions (BioRad, Mini-PROTEAN system) with the stacking gel cast over the resolving gel. The stacking gel has a lower concentration of acrylamide, lower pH and ionic content, allowing proteins in a loaded sample to be concentrated into a tight band during the start of electropheresis before entering the resolving gel. Equal concentrations of protein was resuspended in LSB and heated at 95°C for 5 minutes to denature the protein. Gels were placed in an electrophoresis tank filled with 1x running buffer and protein samples loaded into the lanes in the gel. The first lane was loaded with 4 µl of prestained protein ladder as a molecular weight marker. Electrophoresis was carried out at 80 V for protein migration through the stacking gel, then the voltage was increased to 100 V for approximately 2 hours.

2.4.5.4 Western Blot analysis

This method is based on inducing the proteins, which have an electrical charge, to travel in an electrical field from the gel onto a nitrocellulose or polyvinylidene membrane, where they can be detected by specific antibodies.

Once the proteins were separated by SDS-PAGE, the gel and nitrocellulose membrane (Sigma-Aldrich) were sandwiched between sponges and three layers of filter paper on each side and clamped together. The sandwich was submerged into a transfer tank (BioRad Criterion Blotter) filled with 1x transfer buffer, to which an electrical field was applied with the gel closer to the cathode. Negatively-charged proteins travelling towards the anode are stopped and bound by the membrane. The transfer was carried out at 400 mA for 90 minutes.

After the transfer, the membrane was blocked for one hour in 5% milk solution prepared in TBS-T, to prevent non-specific background binding of the antibodies to the membrane. The membrane was then incubated with the primary antibody of interest overnight at 4°C. After incubation the membrane was washed three times for 10 minutes with TBS-T and incubated for one hour at room temperature with the corresponding secondary antibody. The primary antibody binds directly to the protein of interest on the membrane and the secondary antibody, which is linked to an enzyme horseradish peroxidase, detects the primary antibody. The membrane was washed again three times for 10 minutes with TBS-T and incubated with an enhanced chemoluminescence (ECL) solution for one minute. The enzyme in the secondary antibody catalyses oxidation of luminol in the ECL solution, resulting in emission of light. This emission can be captured on photographic films which

creates an image of the bound antibodies on the membrane. The intensity of the signal is proportional to the amount of antibody, which is in turn related to the concentration of protein on the membrane. The membranes were exposed to X-ray films (Fujifilm) for seconds to 15 minutes depending on the strength of the signal and developed in a JB-33 X-ray film processor (JPI). Before re-probing with another primary antibody, the membrane was stripped with Reblot Plus Strong Buffer for 10 minutes and incubated with blocking buffer twice for 5 minutes.

Each western blot was also incubated with tubulin or β-actin as a loading control to check the concentration of the protein loaded. The intensity of the bands was compared using ImageJ software (National Institutes of Health, USA).

2.4.6 Radiation assays

2.4.6.1 Clonogenic assay

This cell survival assay determines the ability of a cell to proliferate and form a colony, and is commonly used after an exposure to an insult such as ionising radiation.

Cells were grown in 25 cm^2 flasks until 70-80% confluent. They were then irradiated at 0 (control), 2, 4 and 6 Gy using a Nordion GC-1000S v2.9 cell irradiator, which uses a caesium source at a dose rate of 250 +/- 0.59% Gy/hr, and incubated at 37°C overnight. The cells were trypsinised and counted and, depending on the behaviour of the cell line, 600-1000 cells were seeded into 6 cm dishes in triplicate. The optimal seeding density was determined using the parental cell lines. The dishes were placed in the incubator, reviewed daily and the medium changed every 4 days. They were left for 14-20 days until the cells in the control dishes had formed individual colonies that could be counted. At this point the cells were washed with versene, fixed with buffered formalin and stained with 1% methylene blue. Colonies of greater than 50 cells were counted in triplicate in each dish and the plating efficiency (PE) calculated:
PE = Number of colonies/number of cells plated x 100.
This was used to calculate the surviving fraction (SF):
SF = PE of treated sample/PE of control x 100.

2.4.6.2 MTT assay

The MTT assay is a colorimetric assay, which determines the viable number of cells in proliferation and cytotoxicity studies. It measures the reduction of soluble yellow MTT salts by mitochondrial enzymes to an insoluble purple formazan product. The cells are then solubilised and the intensity of the colour is measured spectrophotometrically. As reduction

of MTT can only occur in metabolically active cells the intensity of the colour is proportional to cell viability.

Cells were grown and irradiated as in the clonogenic assay. Three thousand cells for each cell line and dose were seeded into a 96-well plate, with 6 wells for each dose. In parallel cells were seeded in 6 well plates and counted on alternate days. The MTT assay was carried out when the control cells became confluent on visualisation under a microscope or when the growth plateaued (5-7 days). At this point 20 µl of MTT solution was added to each well and incubated for 2 hours at 37°C and 5% CO_2, after which 150 µl of MTT solubilisation solution was added. After 24 hours of further incubation the optical density was measured at 595 nm using an LT-4000 Microplate reader.

2.4.6.3 Gamma H2AX immunofluorescence

Radiation acts by creating double strand DNA breaks (DSB). Cells react by recruiting a number of proteins to the site of damage. One of the earliest events, which occurs within minutes, is the phosphorylation of histone H2AX, which becomes gamma H2AX. This is necessary for the recruitment of the other proteins involved in the DNA damage response pathway. Gamma H2AX foci can be visualised by using a primary antibody against gamma H2AX, followed by a secondary antibody labelled with fluorescence. These foci represent an accumulation of gamma H2AX, along with the other proteins that have localised to the site of damage. Gamma H2AX foci rapidly accumulate and peak 30 minutes after irradiation, with foci remaining at 24 hours representing persistent damage and therefore increased radiosensitivity.

Forty thousand cells were seeded in duplicate into 8-chamber slides (BD Biosciences) and incubated overnight to attach. They were irradiated at 0 (control), 0.5, 1 and 2 Gy and incubated for 30 minutes or 24 hours, after which they were processed in the following 3 steps:

a) Fixation and permabilisation: Cells were washed three times with PBS and fixed with 200 µl 4% paraformaldehyade for 15 minutes at 37°C. After further washing with PBS cells were permeabilised with 200 µl 0.2% Triron X-100 for 15 minutes and washed again.
b) Antibody staining: Cells were blocked for 30 minutes in 200 µl 3% bovine serum albumin in TBS-T (BSA/TBS-T) and then incubated overnight at 4°C with 100 µl of rabbit phospho-histone H2AX antibody diluted 1:100 in 3% BSA/TBS-T. Cells were washed with PBS and incubated with 100 µl of 1:100 goat anti-rabbit fluorescein isothiocyanate (FITC) antibody for 90 minutes.

c) Preparation for imaging: The chamber was removed from the slide and 8 µl of Vectashield mounting medium was added. The mounting medium contains 4',6-diamidino-2-phenylindole (DAPI) which is a fluorescent stain that binds to DNA and therefore allows visualisation of the nucleus of the cell. The slide was covered with a coverslip and stored at 4°C for at least 10 minutes before imaging or -20°C for long term storage.

Images were acquired at 60x magnification using an Olympus BX61 automated fluorescence microscope and Cell^F software. BlobFinder image analysis software (Centre for Image Analysis, Sweden) was used for automated reproducible foci detection.

2.4.7 Functional assays

2.4.7.1 Cell proliferation

This was assessed using 2 methods: daily cell counting and MTT assay. For each cell line 100000 cells were seeded in triplicate in 6-well plates (day 0). Cells were trypsinised and counted from days 1 to 7. For the MTT assay 3000 were seeded in 96 well plates, with 6 wells per time point and left overnight (day 0). MTT was added and cells processed as previously described in section 2.4.6.2 on days 1 to 5.

2.4.7.2 Cell migration (Scratch assay)

This assay was performed to investigate the migratory ability of the cell lines. Perpendicular lines were marked on the bottom surface of 6-well plates as reference points for imaging. Four to five hundred thousand cells were seeded in triplicate and grown until confluent. Confluent cells were serum starved for 24 hours by replacing the media with media without FBS, to synchronise the cells in G_0 of the cell cycle. A p200 pipette tip was used to create a straight scratch along the diameter of the well, with a minimum of three scratched per well. Floating cells were removed by washing the well twice with media and the plates were imaged at 4x magnification using an Olympus CKX41 microscope and Cell^F software. Cells were incubated at 37ºC and imaged again at various time points from 16 to 24 hours. The assay was performed in triplicate and the area between the scratch was imaged, analysed using ImageJ, and the percentage of the scratch area closed between the two time points calculated.

2.4.7.3 Matrigel invasion assay

The invasive property of the cell lines was assessed using BD BioCoat Matrigel Invasion Chambers. The chambers, or inserts, fit in the wells of a 24-well plate and contain a

membrane coated with Matrigel, a protein mixture that resembles extracellular matrix, through which cells can invade.

Invasion chambers were placed into the wells of a 24-well plate and warm medium added to the chamber and well and incubated for 2 hours to allow rehydration. An equal number of control chambers, which do not have Matrigel coating on their membrane, were also prepared. The optimal seeding density of the parental cell lines was determined alongside the HT-1080 cell line, which is known to be highly invasive, as a control. Between $2x10^5$ to $4x10^5$ cells/ml in serum free medium were prepared in duplicate and placed in the invasion chambers, with chemoattractant (medium containing 5% FBS) added to the wells. Cells were incubated for 22 hours, after which the non-invading cells on the upper surface of the chamber were scrubbed off with a cotton swab, and the invading cells on the lower surface were fixed with 100% methanol and stained with 1% toluidine blue in 1% borax and counted. The membrane was then removed using a scalpel, placed gently onto a microscope slide and covered with a coverslip. Images of the invasion and control cells were taken at 40x magnification using a Zeiss Axioplan microscope with a ColorView Soft Imaging System camera. The assay was carried out in duplicate and five random images were taken of each membrane. Invasion was expressed as the percent invasion through the Matrigel membrane relative to the migration through the control membrane:
% invasion = Mean number of cells invading through Matrigel insert membrane/mean number of cells migrating through control insert membrane x 100.

2.4.8 Other methods

2.4.8.1 E-cadherin and vimentin immunofluorescence

Forty thousand cells were seeded in duplicate into 8-chamber slides and allowed to attach overnight. Cells were processed as described in section 2.4.6.3 and incubated overnight at 4°C with rabbit E-cadherin or vimentin antibody (1:100 dilution), followed by secondary FITC-conjugated antibody for 90 minutes. Images were acquired at 60x magnification as above.

2.4.8.2 Luciferase reporter assay

Cells were seeded in 96-well plates at a density of 10000 cells per well in triplicate and incubated overnight. A transfection mix of 10 µl OptiMEM, 0.1 µg of luciferase plasmid DNA and 0.2 µl X-tremeGENE HP DNA transfection reagent or 0.4 µl FuGENE HD transfection reagent was prepared and incubated at room temperature for 20 minutes. Ten microlitres of this mix was added to each well and incubated for 24 to 48 hours before the luciferase assay was performed using the Dual-Glo Luciferase Assay System. Dual-Glo Reagent was

added to each well and incubated for 15 minutes to allow cell lysis to occur. The Firefly luminescence was then measured in a Veritas Luminometer (Turner Biosystems). Dual-Glo Stop & Glo Reagent was then added and left for 15 minutes, after which the Renilla luminescence was read in the same order as the Firefly luminescence. Measurements from untransfected cells were used as negative controls and the data was normalised by dividing the Firefly activity by the Renilla activity.

2.4.9 Statistical analysis

Data is presented as the mean of independent experiments and the error bars indicate the standard deviation unless otherwise stated. Data was assessed for normality using the D'Agostino-Pearson normality test. The difference between two groups was compared using the unpaired, two-tailed Student's t-tests if the data was normally distributed, or the Mann-Whitney U test if the data was not normally distributed. Data was analysed using Microsoft Excel and statistical analysis was performed using GraphPad Prism version 6.0 (Graphpad Software Inc, La Jolla, CA, USA). P values less than 0.05, indicated by * in the figures, were considered statistically significant.

2.5 Results

2.5.1 MiR-196a expression level in HN5 and HN30 cell lines

Expression profiling of eight head and neck cell lines showed only the HN5 cell line to have low endogenous levels of miR-196a (Figure 2.2). This cell line and HN30, with high endogenous levels, were initially selected for further investigation. The expression levels of miR-196a were confirmed by qRT-PCR; miR-196a expression was significantly higher in HN30 compared with HN5, relative to the housekeeping gene RNU48 ($P < 0.01$, Figure 2.3).

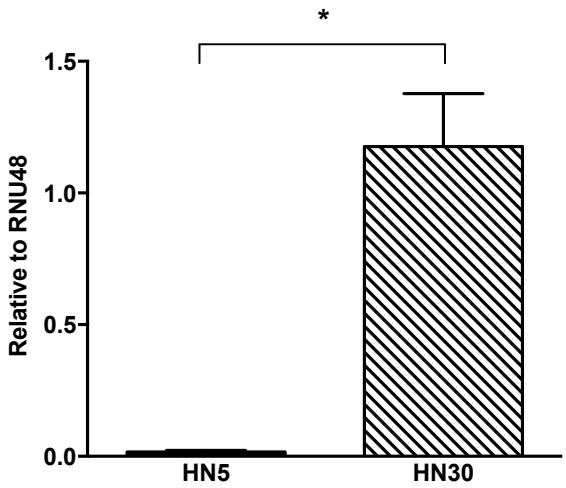

Figure 2.3 QRT-PCR of endogenous miR-196a levels in HN5 and HN30 cell lines. RNA was extracted from HN5 and HN30 cell lines at 80-90% confluence and miR-196a levels compared using qRT-PCR. Data is expressed relative to the housekeeping gene RNU48, and is the mean of three independent RNA extractions. Error bars indicate standard deviation of the independent experiments. Statistical analysis was performed using Student's t-test, $P < 0.01$.

To characterise and compare the behaviour of these two cell lines, the cell proliferation was compared by daily counting over 7 days. HN30 demonstrated significantly faster proliferation from day 4 (Figure 2.4).

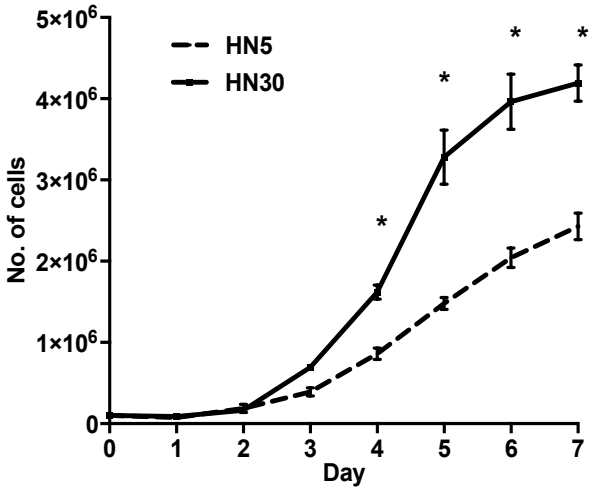

Figure 2.4 Cell proliferation in HN5 versus HN30 cell lines.
Equal numbers of cells were plated in 6 well plates on day 0. Cells were trypsinised and counted every 24 hours for 7 consecutive days. The experiment was performed in triplicate and error bars indicate standard deviation. * Student's t-test P values days 4 to 7 < 0.01.

2.5.2 MiR-196a overexpression in HN5 cells

To investigate how miR-196a affects cell behaviour, the miR-196a gene was inserted into the retroviral pBabe-puro vector and transfected into HN5 cells. HN5 cells were also transfected with empty vector pBabe-puro, as the control cell line, and stable populations were selected using puromycin. Two cell populations grown from single colonies survived the selection process and were expanded over 6 weeks. The remaining cells were pooled together to form a mixed population of miR-196a overexpressing cells, and the levels of miR-196a expression were compared (Figure 2.5). The mixed population showed the highest level of overexpression of approximately 50-fold and was therefore selected for further investigation, whilst the second highest (colony 2 cells) was used for validation.

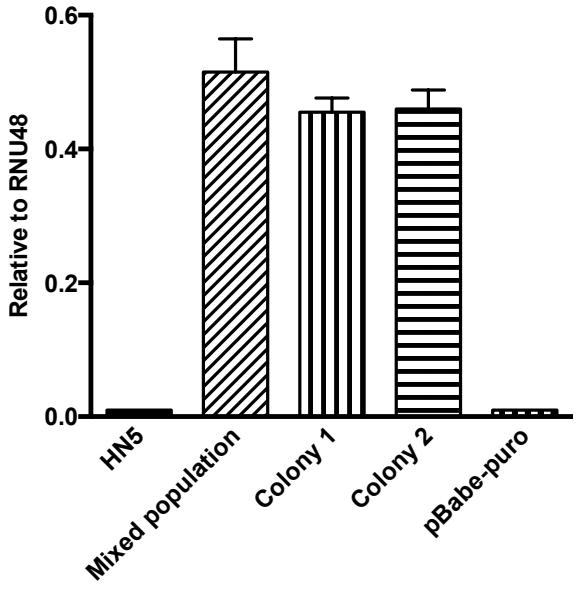

Figure 2.5 MiR-196a expression in HN5 cells after transfection with miR-196a plasmid.
MiR-196a was transfected into HN5 and stable populations selected using puromycin. Two cell populations grown from single colonies, colony 1 and colony 2, and a mixed population of overexpressing cells were grown. RNA was extracted once and miR-196a levels assessed using qRT-PCR. The levels were compared with HN5 cells and HN5 cells stably transfected with empty vector pBabe-puro as the control. Data is expressed relative to RNU48 and represents the mean of three independent RNA extractions.

2.5.2.1 Exogenous miR-196a overexpression promotes cell proliferation, migration and invasion

The functional consequences of increased expression of miR-196a were investigated. The effect on cell proliferation was assessed using two methods: daily cell counting over 7 days and the MTT cell viability assay over 5 days. Both assays demonstrated significantly increased rate of growth in the miR-196a overexpressing cells compared with the control empty vector cells (Figure 2.6).

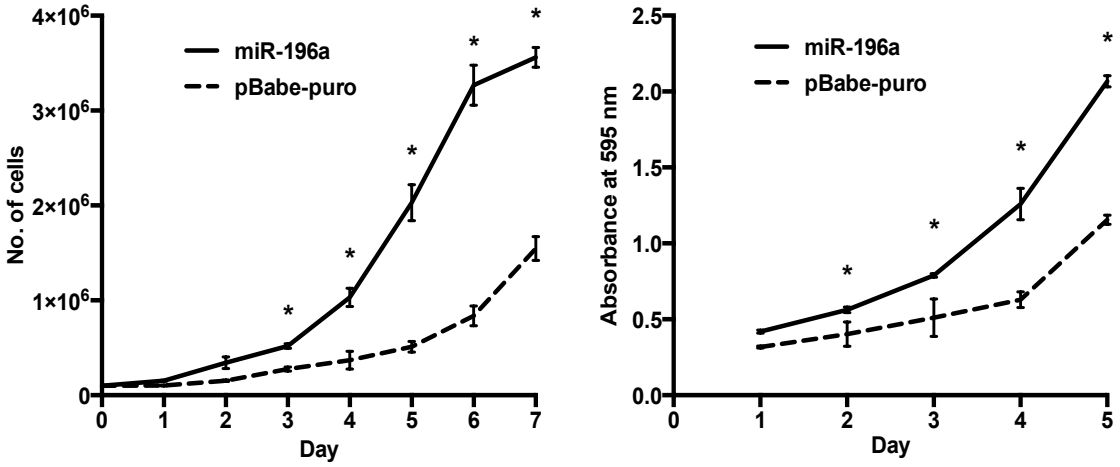

Figure 2.6 Cell proliferation of miR-196a overexpressing cells compared with pBabe-puro empty vector control.
Left graph: equal numbers of cells were plated in triplicate on day 0 and counted every 24 hours for 7 consecutive days. Data is the mean of 2 independent experiment and error bars indicate standard deviation. Statistical significance determined by Student's t-test. Days 3 to 7, $P < 0.01$. Right graph: cells were plated in 6 wells of a 96-well plate and the MTT assay was performed daily over 5 days (right). Data is the mean of 2 independent experiments. Days 2 and 3, $P = 0.01$, days 4 and 5 , $P < 0.01$.

The effect of miR-196a on migration was investigated using the scratch assay. MiR-196a significantly enhanced migration after 16 hours, with an average of 78% of the scratch area closed in the miR-196a cells versus 28% in the control cells ($P < 0.01$, Figure 2.7). The invasive potential of the cells was tested using the Matrigel invasion assay, which demonstrated a clear difference in the behavior of the cells. The mean percentage invasion relative to the control membrane was 53% in miR-196a cells compared with 16% in the control cells ($P = 0.01$, Figure 2.8).

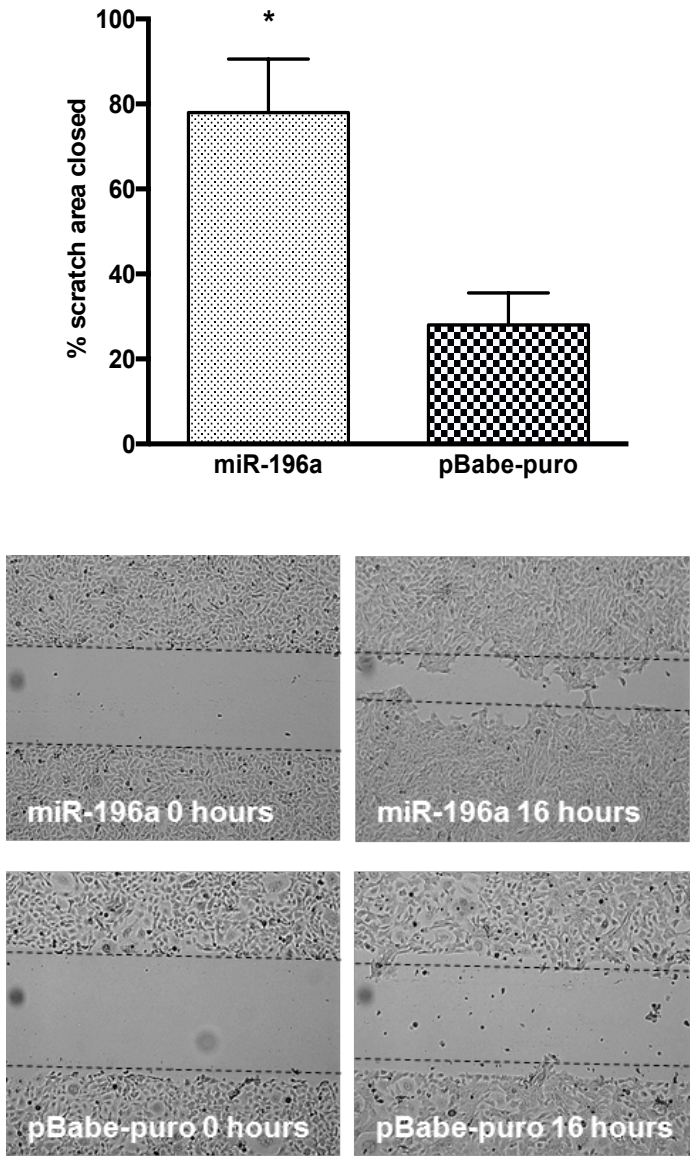

Figure 2.7 Scratch assay to assess the cell migration of miR-196a ovrexpressing cells compared with pBabe-puro control.
Cells were grown in 6 well plates in triplicate until confluent and a pipette tip used to create 3 scratches in each well. Bar graph shows the mean percentage scratch area closed after 16 hours from 2 independent experiments. Student's t-test was used to assess statistical significance ($P < 0.01$). Images show representative examples at 0 and 16 hours at 4x magnification.

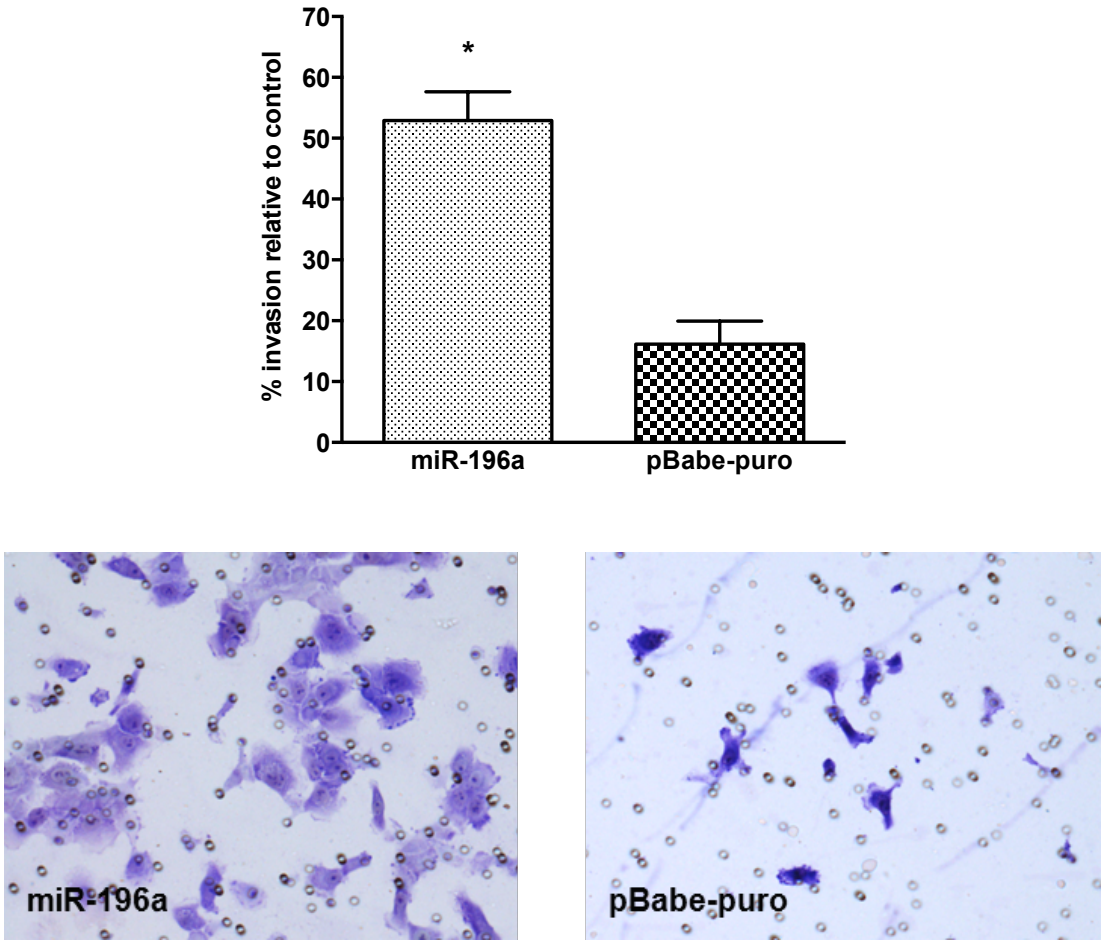

Figure 2.8 Invasion assay of miR-196a overexpressing cells compared with pBabe-puro control.
The Matrigel invasion chamber was used to assess the invasive ability of the cells. Equal number of cells were seeded into the chamber and incubated for 22 hours, before counting the number of cells that have invaded through the Matrigel membrane. Cells were also seeded into a control chamber without Matrigel on the membrane. Bar graph represents the mean number of cells that have invaded through the membrane, relative to the mean number of cells that have migration through the control membrane (P = 0.01). The assay was carried out in repeated duplicates. Images are representative of cells fixed and stained on the invasion membrane at 10x magnification.

2.5.2.2 MiR-196a overexpression affects vimentin expression

The behaviour of the miR-196a overexpressing cells suggested a role for miR-196a in the process of epithelial-mesenchymal transition (EMT). EMT is characterised by the loss of various cell surface proteins and reorganisation of cytoskeletal proteins. Loss of E-cadherin and gain of vimentin are two of the main protein expression alterations associated with EMT.[454] Western blot analysis was performed to detect changes in expression of E-cadherin and vimentin. There was no difference in the expression of E-cadherin. Vimentin expression was very low in the control cells and further reduced in the miR-196a upregulated cells (Figure 2.9).

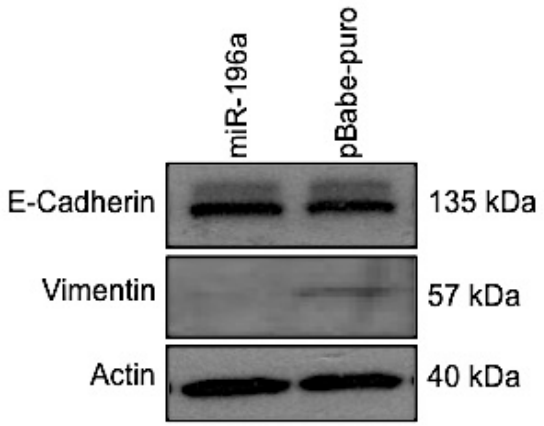

Figure 2.9 E-cadherin and vimentin protein expression levels in miR-196a overexpressing and pBabe-puro control cells.
Western blot analysis of the EMT markers E-cadherin and vimentin in miR-196a overexpressing cells compared with pBabe-puro control cells. Actin was used as loading control.

To further assess the changes in expression of E-cadherin and vimentin, immunofluorescence was performed. Consistent with the Western blot data there was no clear difference in the staining pattern of E-cadherin between the miR-196a and control cells (Figure 2.10). However the pattern of vimentin expression was significantly altered after overexpressing miR-196a (Figure 2.11, upper panel). Vimentin immunofluorescence was also carried out using MDA-MB-231 breast cancer cells, a well-established mesenchymal cell line, for comparison and the appearances of the miR-196a cells were similar (Figure 2.11, lower panel). This suggests miR-196a may contribute to a change in the configuration of vimentin in preparation for transition into the mesenchymal phenotype.

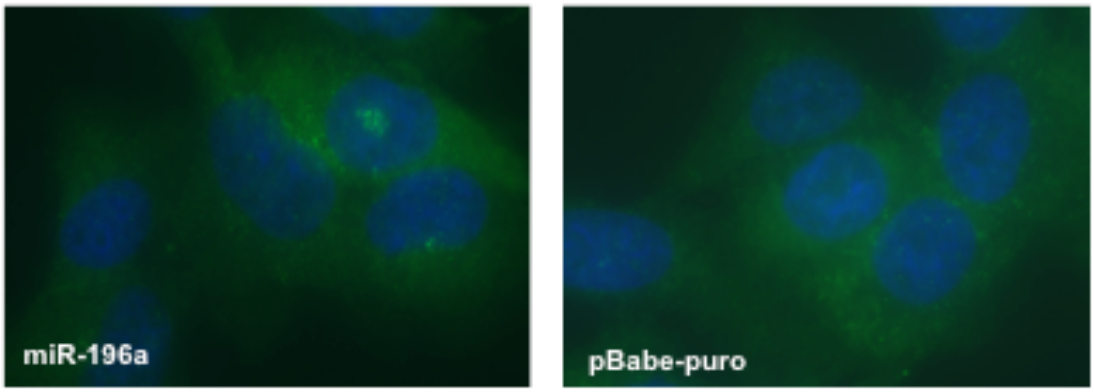

Figure 2.10 E-cadherin immunofluorescence of miR-196a overexpressing HN5 cells compared with pBabe-puro empty vector control.
Cells were fixed and stained with primary rabbit anti-E-cadherin and secondary FITC-conjugated anti-rabbit antibody (green). Nuclei were detected by counterstaining with DAPI (blue). Representative images were taken at 60x magnification.

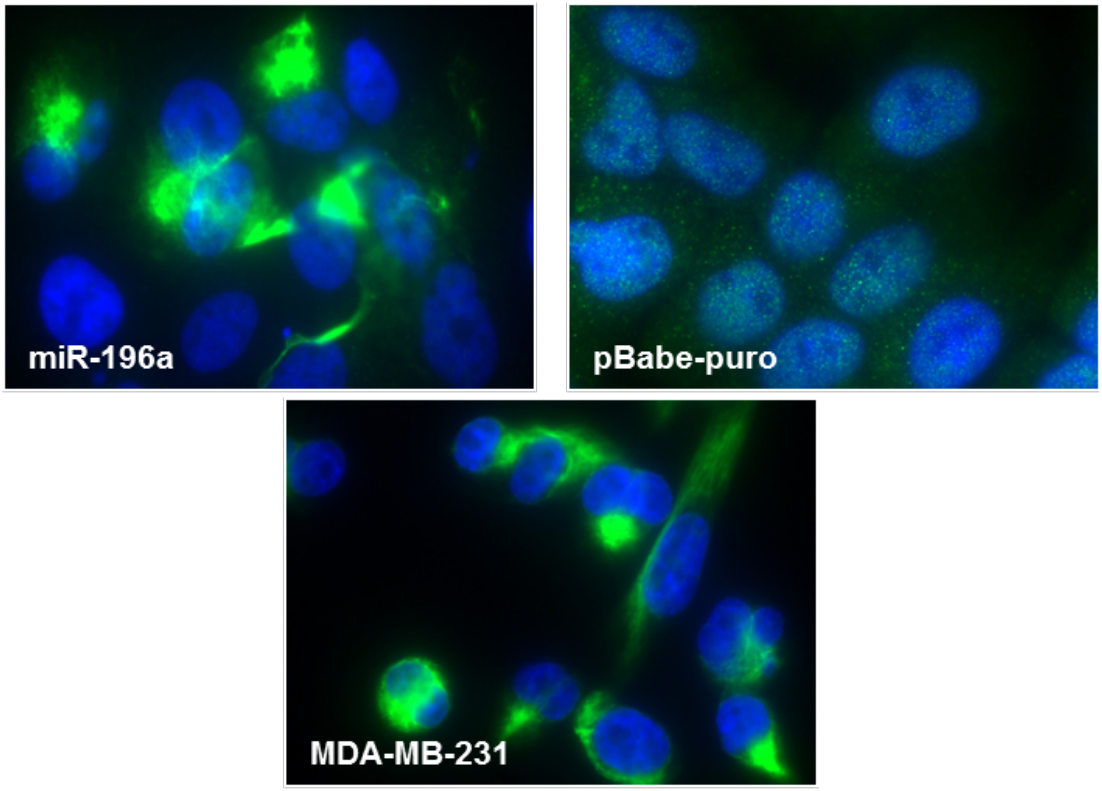

Figure 2.11 Vimentin immunofluoresence of miR-196a cells compared with empty vector control and the mesenchymal breast cancer cell line MDA-MB-231.
Cells were fixed and stained with primary rabbit anti-vimentin and secondary FITC-conjugated anti-rabbit antibody (green). Nuclei were stained with DAPI (blue) and images taken at 60x magnification.

2.5.2.3 MiR-196a alters the radiosensitivity of head and neck cancer cells

The sixteen patients with and without disease recurrence selected for the initial miRNA expression profiling received surgery and postoperative radiotherapy. Patients who developed disease recurrence had higher levels of pretreatment miR-196a in their tumour compared with patients who remained disease free. This observation prompted further investigation into whether overexpression of this miRNA had an effect on the sensitivity to radiation.

HN5 miR-196a overexpressing cells and empty vector control cells were irradiated at 0, 2, 4 and 6 Gy and the clonogenic assay performed. After 14 days, miR-196a overexpressing cells demonstrated a higher surviving fraction at 2 and 4 Gy compared with the control cells (Figure 2.12 and Figure 2.13). Radiosensitivity was further investigated using the MTT cell survival assay. This also showed significantly enhanced cell viability 5 days after irradiation at 2 and 4 Gy, and also at 6 Gy (Figure 2.14).

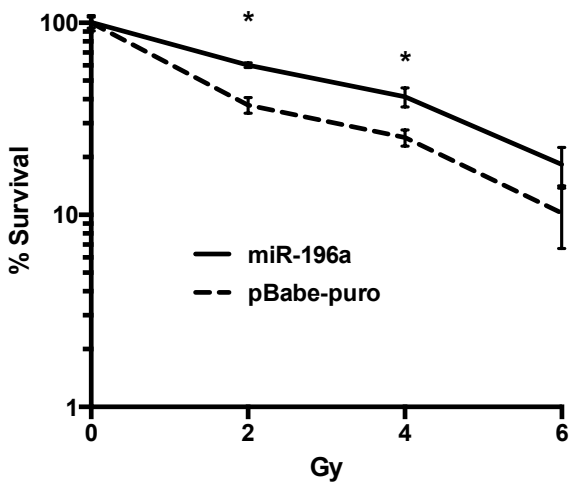

Figure 2.12 Clonogenicity of miR-196a overexpressing cells compared with control post-irradiation.
Cells were irradiated at 0 (control), 2, 4 and 6 Gy and 1000 cells plated in 6 well dishes in triplicate the following day. Cell medium was changed every 4 days. Colony formation after 14 days was assessed by counting colonies of greater than 50 cells in triplicate. The plating efficiency and surviving fraction was calculated and the graph represents data from two independent clonogenic assays. Student's t-test at 2 Gy and 4 Gy $P < 0.01$, and $P = 0.07$ at 6 Gy.

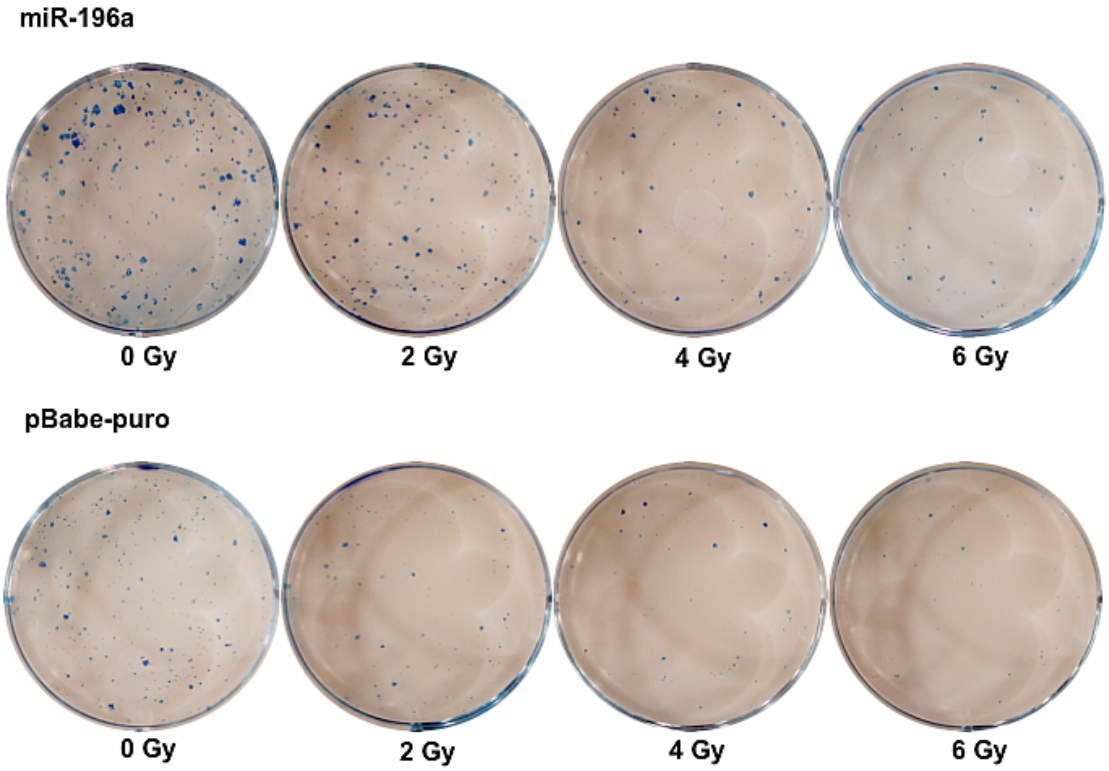

Figure 2.13 Colony formation of miR-196a overexpressing cells compared with control.
Representative images of colony formation 14 days after irradiation with 0, 2, 4 and 6 Gy in miR-196a overexpressing (upper panel) and pBabe-puro empty vector control cells (lower panel) are shown.

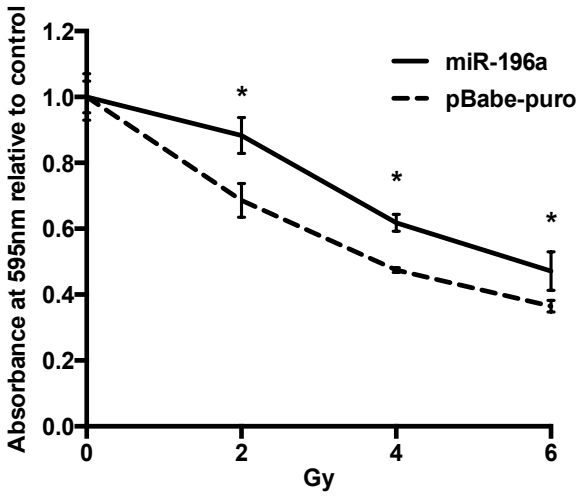

Figure 2.14 MTT cell viability assay of miR-196a and pBabe-puro control cells post-irradiation.
Cells were seeded in 96 well plates 24 hours after irradiation and the absorbance at wavelength 595nm was measured after 5 days. Data is presented relative to the absorbance of the 0 Gy (unirradiated control) cells and represents two independent experiments. Error bars indicate standard deviation, Student's t-test was used to determine significance, P = 0.01 at 2 Gy, P < 0.01 at 4 Gy and P = 0.04 at 6 Gy.

The cells were also irradiated at lower doses and stained for the presence of gamma H2AX foci within the nucleus at 30 minutes and 24 hours, as a biomarker for double-stranded DNA breaks. Gamma H2AX foci rapidly accumulate and peak 30 minutes after irradiation, with foci remaining at 24 hours representing persistent damage and therefore increased radiosensitivity.[455,456] At 30 minutes post-irradiation, miR-196a overexpressing cells demonstrated similar numbers of gamma H2AX foci per nucleus compared with the control cells. However, after 24 hours significantly fewer foci were detected in the miR-196a cells, indicating more efficient repair (Figure 2.15).

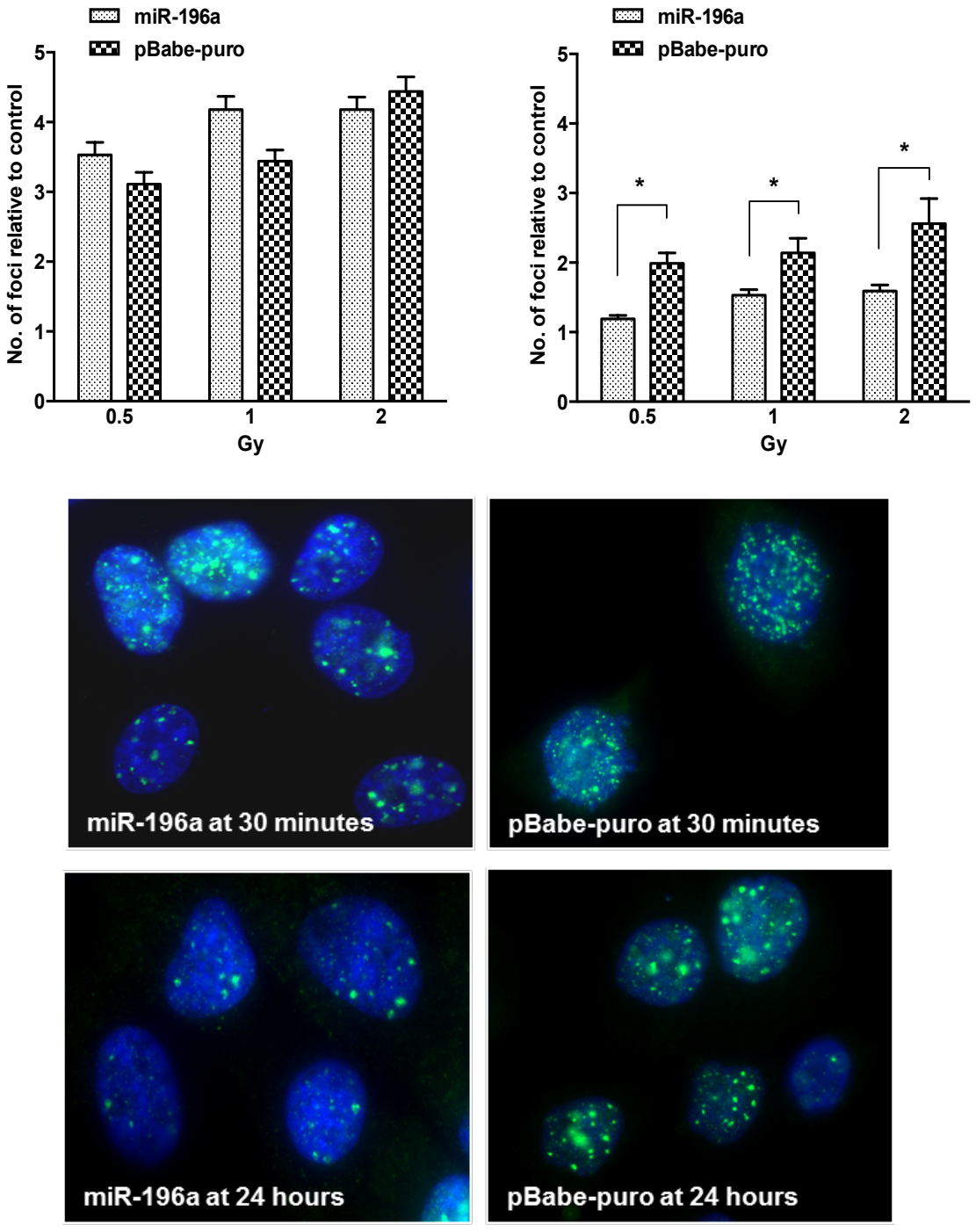

Figure 2.15 Gamma H2Ax staining for double stranded DNA damage in miR-196a and pBabe-puro control cells post-irradiation.
Cells were irradiated with 0 (control), 0.5, 1 and 2 Gy after 30 minutes (upper left graph) and 24 hours (upper right graph) post-irradiation. The number of foci was analysed in a minimum of 100 cells at each dose point and data is presented as the mean number of foci relative to the unirradiated 0 Gy cells. Error bars represent standard error. Differences between the mean number of foci in miR-196a and pBabe-puro cells were not significant using the Student's t-test after 30 minutes. After 24 hours at 0.5 Gy $P < 0.01$, at 1 Gy $P = 0.04$, at 2 Gy $P = 0.02$. Images are representative of cells irradiated at 0.5 Gy at 60x magnification.

2.5.3 MiR-196a knockdown in HN30 cells

The cell line HN30, with high endogenous levels of miR-196 (Figure 2.3), was selected for miR-196a knockdown experiments. MiRNA sponges are transcripts that contain multiple target sites that are complementary to the miRNA under investigation and sequester endogenous miRNAs, resulting in functional inhibition of the mature miRNA.[457] Red fluorescent protein (RFP) expression pre- and post-transduction was checked (Figure 2.16) and qRT-PCR demonstrated an approximate 60% reduction in the expression level of miR-196a in HN30 cells infected with miR-196a sponge plasmid compared with cells infected with sponge control (Figure 2.17).

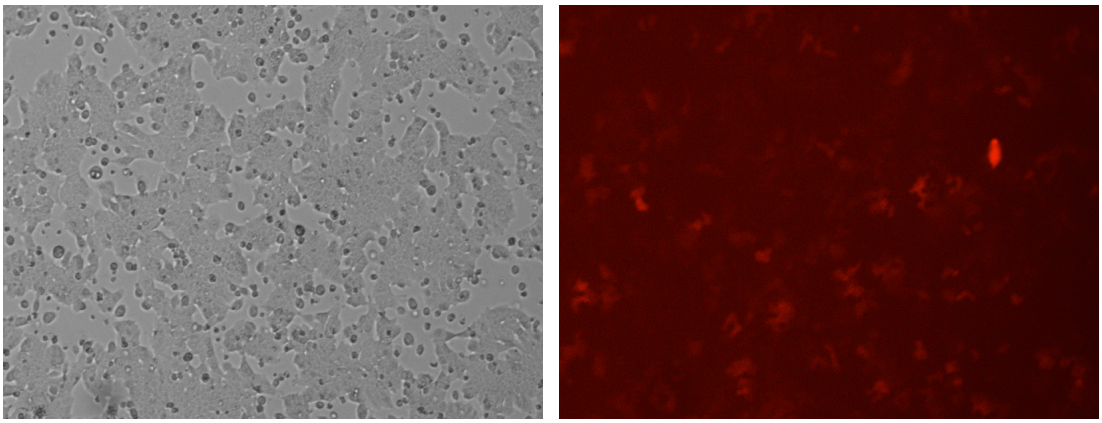

Figure 2.16 HN30 miR-196a sponge cells after puromycin selection.
Example of RFP expression in miR-196a sponge cells after puromycin selection.

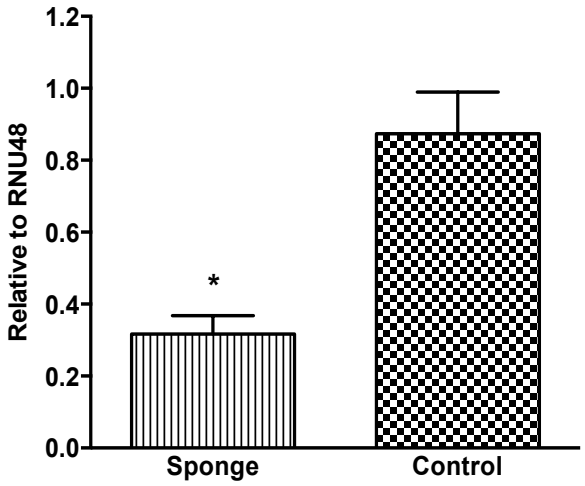

Figure 2.17 QRT-PCR of miR-196a knockdown in HN30 cells compared with control.
HN30 cells were stably infected with miR-196a sponge or control and the expression relative to the housekeeping gene RNU48 was measured by qRT-PCR. Data shown is the mean of three independents RNA extractions, $P < 0.01$.

2.5.3.1 MiR-196a knockdown results in decreased cell proliferation, migration and invasion, and increased radiosensitivity

Downregulation of miR-196a in HN30 cells resulted in the opposite functional effects seen with overexpressing miR-196a in HN5 cells. Cell proliferation was significantly inhibited (Figure 2.18). Cell migration was also inhibited, with a mean percent of scratch area closed at 24 hours in miR-196a sponge cells of 39% compared with 76% in the sponge control cells ($P < 0.01$, Figure 2.19). The mean percentage invasion relative to the control membrane was 18% and 46% in the sponge and control cells respectively ($P = 0.02$, Figure 2.20).

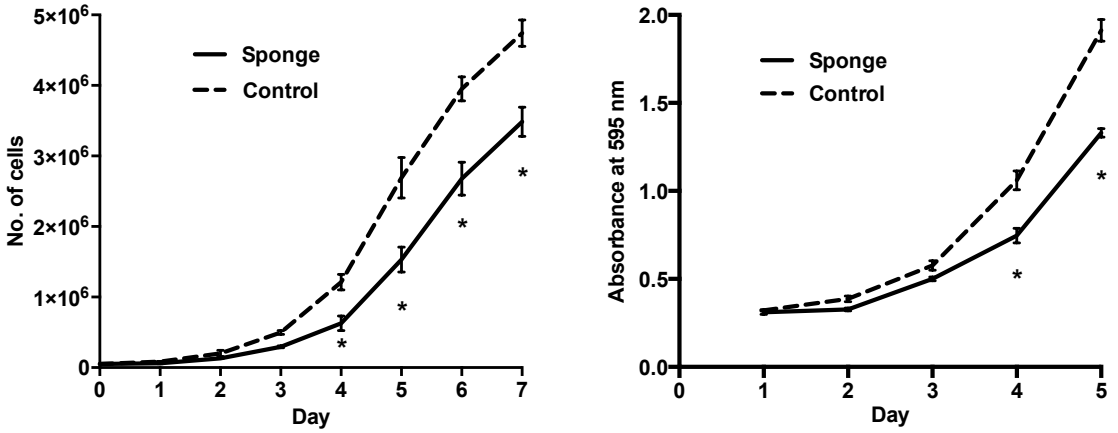

Figure 2.18 Cell proliferation of miR-196a sponge cells compared with control. Left graph: equal numbers of cells were plated in triplicate on day 0 and counted every 24 hours for 7 consecutive days. Data is the mean of 2 independent experiments and error bars indicate standard deviation. Statistical significance determined by Student's t-test. Days 4 to 7, $P < 0.01$. Right graph: cells were plated in 6 wells of a 96-well plate and the MTT assay was performed daily over 5 days (right). Data is the mean of 2 independent experiments. Days 4 and 5, $P < 0.01$.

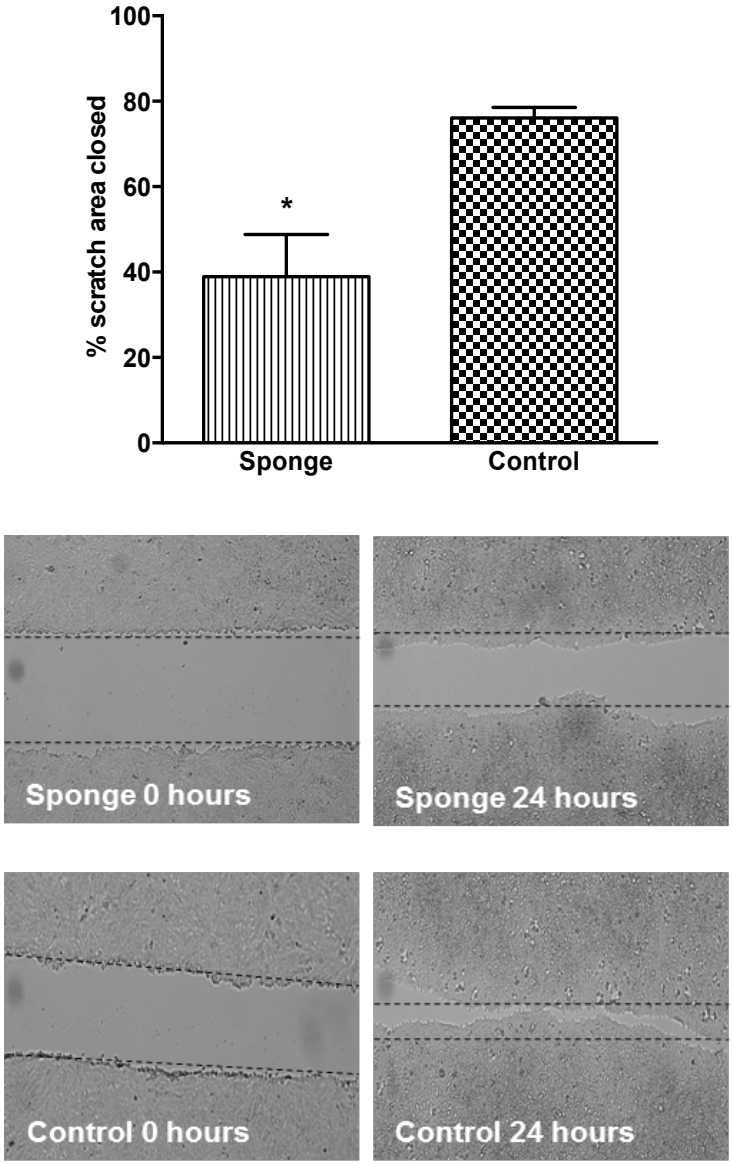

Figure 2.19 Cell migration assessed by scratch assay of miR-196a knockdown sponge cells compared with control cells.
Cells were grown in 6 well plates in triplicate until confluent and a pipette tip used to create 3 scratches in each well. Bar graph shows the mean percentage scratch area closed after 24 hours from 2 independent experiments. Student's t-test was used to assess statistical significance ($P < 0.01$). Images show representative examples at 0 and 24 hours at 4x magnification.

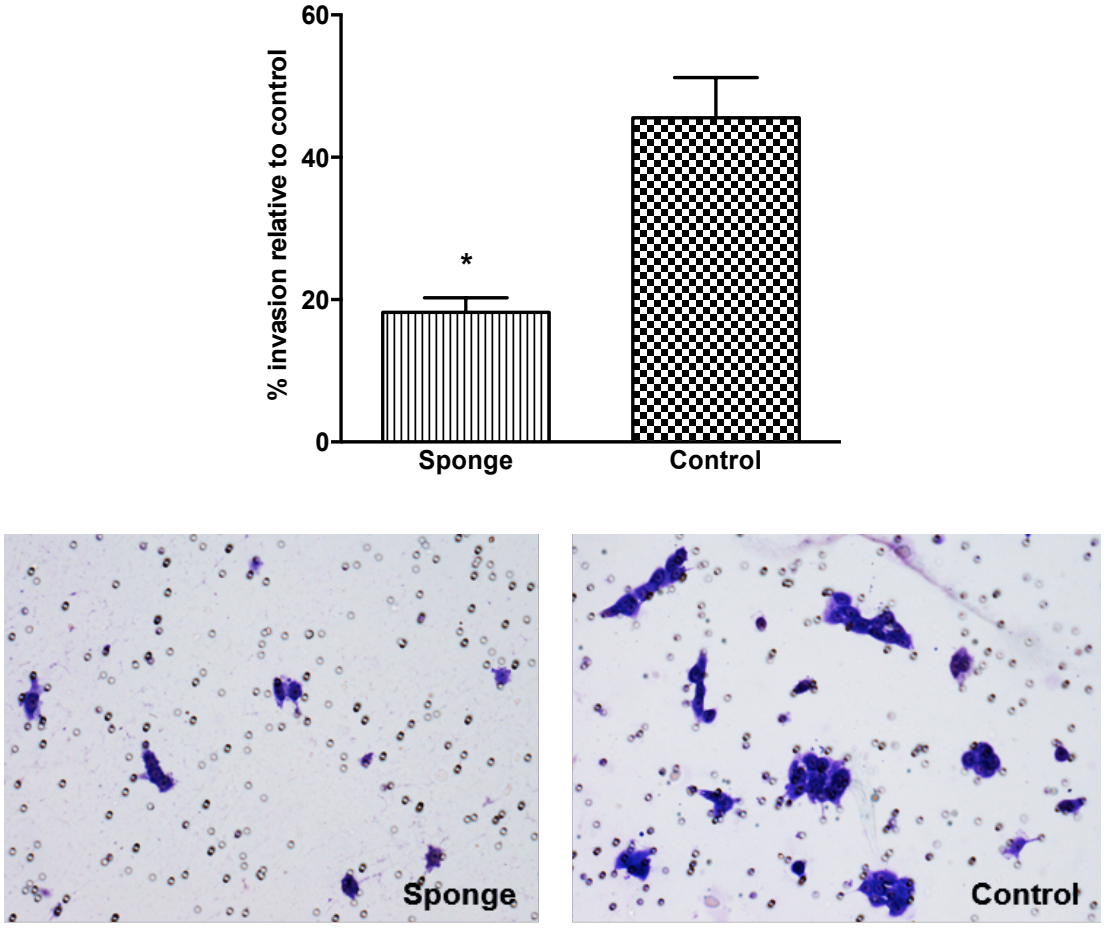

Figure 2.20 Invasion through Matrigel membrane by miR-196a knockdown cells compared with control.
Equal number of cells were seeded into the Matrigel chamber and incubated for 22 hours, before counting the number of cells that have invaded through the Matrigel membrane. Cells were also seeded into a control chamber without Matrigel on the membrane. Bar graph represents the mean number of cells that have invaded through the membrane, relative to the mean number of cells that have migration through the control membrane (P = 0.02). The assay was carried out in repeated duplicates. Images are representative of cells fixed and stained on the invasion membrane at 10x magnification.

The radiosensitivity of miR-196a knockdown cells was planned to be assessed using the clonogenic assay. However when the optimal seeding density was being determined using a range of cell numbers and incubation times, it became clear that the colonies formed by this cell line were small and compact and too difficult to count (Figure 2.21). Similar colonies were formed by the modulated HN30 cells.

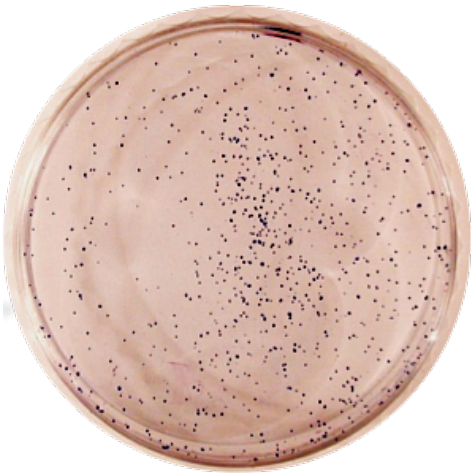

Figure 2.21 Colony formation of HN30 cells.
Six hundred cells were seeded in a 6 well plate and incubated for 20 days.

The MTT cell viability assay was performed after irradiating the miR-196a knockdown and control cells with 0 (unirradiated control), 2, 4 and 6 Gy. This clearly demonstrated reduced cell survival in the miR-196a knockdown cells at all doses (Figure 2.22), suggesting increased radiosensitivity.

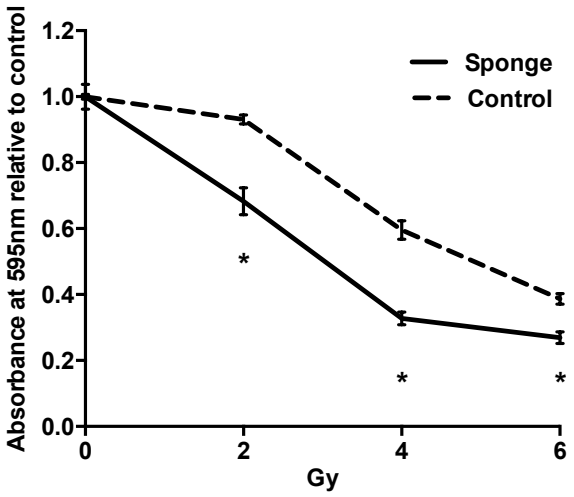

Figure 2.22 MTT cell viability assay of miR-196a sponge and control cells.
Cells were seeded in 96 well plates 24 hours after irradiation and the absorbance at wavelength 595nm measured after 5 days. Data is presented relative to the absorbance of the 0 Gy (unirradiated control) cells, from two independent experiments. Student's t-test was used to determine statistical significance. P = 0.02 at 2 Gy, P = 0.01 at 4 Gy and P = 0.04 at 6 Gy.

To investigate whether the inhibition in growth and cellular migration was due to the induction of apoptosis, HN30 cells were transiently transduced with miR-196a sponge and control, and the cell lysates were analysed for apoptotic markers at 48 and 72 hours. Cleaved PARP and cleaved caspase-3 protein levels were measured by Western blot analysis. There were no clear differences between the miR-196a sponge and control cells (Figure 2.23), suggesting that the observed effects of miR-196a downregulation of suppressing proliferation and migration are unlikely to be due to increased apoptosis.

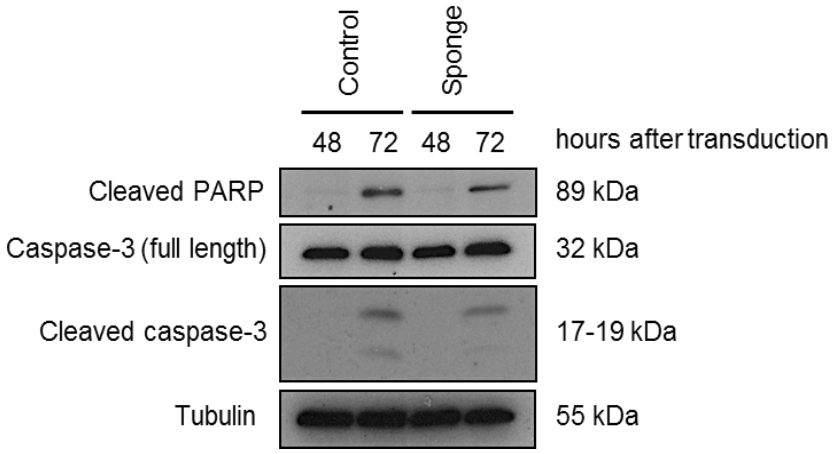

Figure 2.23 Western blot of the pro-apoptotic markers cleaved PARP and cleaved caspase-3 in HN30 sponge and control cells.
HN30 cells were harvested 48 and 72 hours after transient miR-196a knockdown using miR-196a sponge and empty vector control. Tubulin was used as loading control.

2.5.3.2 MiR-196a inhibition in HN30 cells do not affect markers of EMT

E-cadherin and vimentin expression was assessed by Western blot analysis. There was no clear difference in the expression of these EMT-associated proteins between the miR-196a sponge and control cells (Figure 2.24). There was also no change detected using E-cadherin and vimentin immunofluorescence (Figure 2.25 and Figure 2.26).

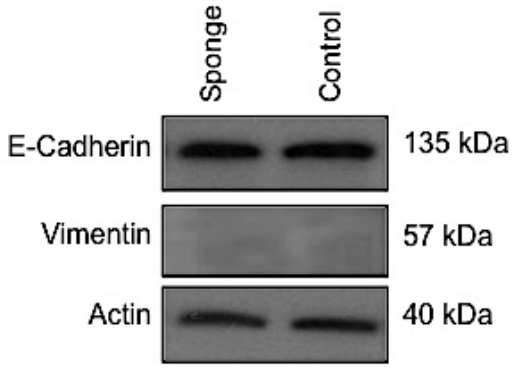

Figure 2.24 E-cadherin and vimentin protein expression levels in miR-196a knockdown cells compared with control cells.
Western blot analysis of EMT markers E-cadherin and vimentin was performed, with actin as loading control.

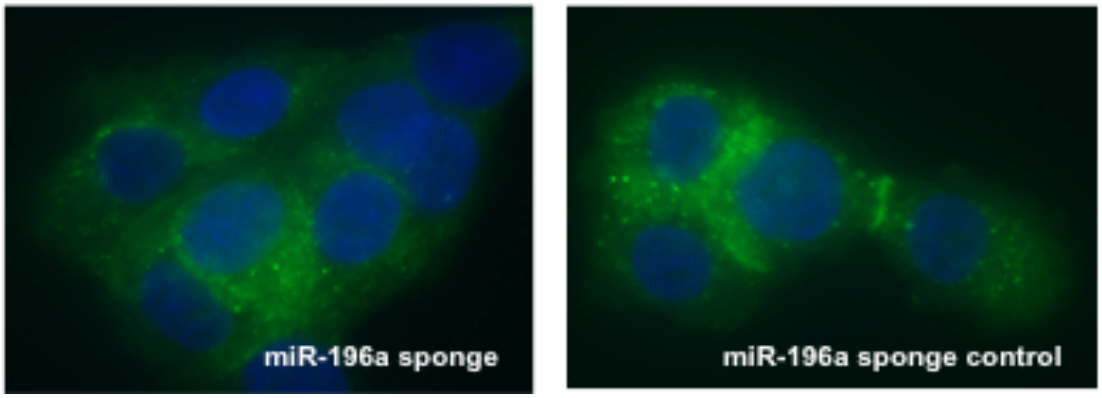

Figure 2.25 E-cadherin immunofluorescence in miR-196a sponge cells compared with control.
Cells were fixed and stained with primary rabbit anti-E-cadherin and secondary FITC-conjugated anti-rabbit antibody (green). Nuclei were detected by counterstaining with DAPI (blue). Representative images were taken at 60x magnification.

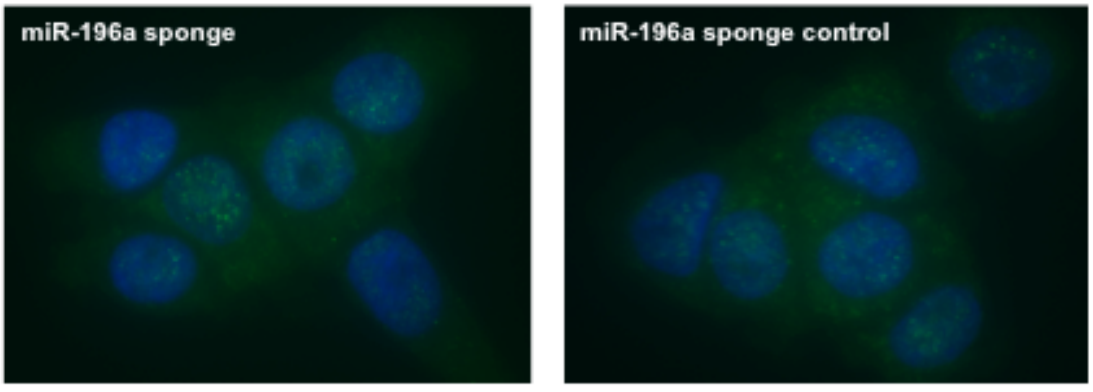

Figure 2.26 Vimentin immunofluorescence in miR-196a sponge and control cells.
Cells were fixed stained with primary rabbit anti-vimentin and secondary FITC-conjugated anti-rabbit antibody (green). Nuclei were stained with DAPI (blue) and images taken at 60x magnification.

2.5.4 Confirmation in other modulated cells

2.5.4.1 MiR-196a overexpressing HN5 cells from single colony

There were no other head and neck cell lines with low endogenous levels of miR-196a to confirm the effect of overexpressing this miRNA. The HN5 miR-196a overexpressing cell line developed from a single colony with the second highest level of miR-196a (single colony 2, Figure 2.5) was therefore used to validate some of the results. This colony had an approximate 45-fold increase in the level of miR-196a compared with the pBabe-puro control cells.

The MTT assay was used as measure of cell proliferation over 5 days. This demonstrated significantly increased cell proliferation in the miR-196a overexpression cells compared with empty vector control (Figure 2.27).

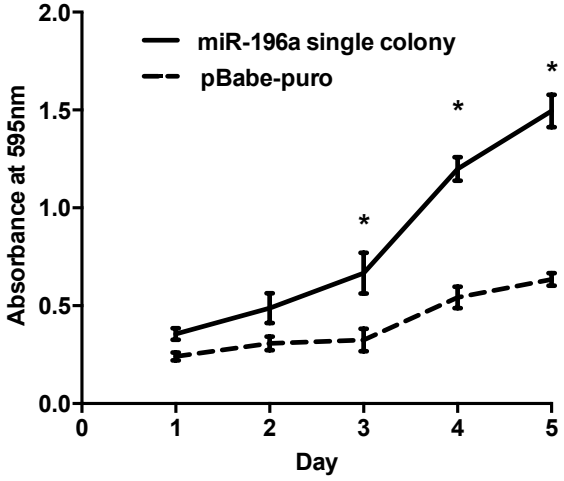

Figure 2.27 MTT assay over 5 days comparing the cell proliferation of miR-196a overexpressing cells grown from a single conlony compared with control.
MTT assay was performed daily over 5 days, 6 wells per day, and repeated in an independent experiment. $P < 0.01$ days 3 to 5, determined by Student's t-test.

The scratch assay was also performed, which confirmed that miR-196a overexpression promoted migration, with an average of 52% of the scratch area closed after 20 hours compared with 22% in the control cells ($P < 0.01$, Figure 2.28).

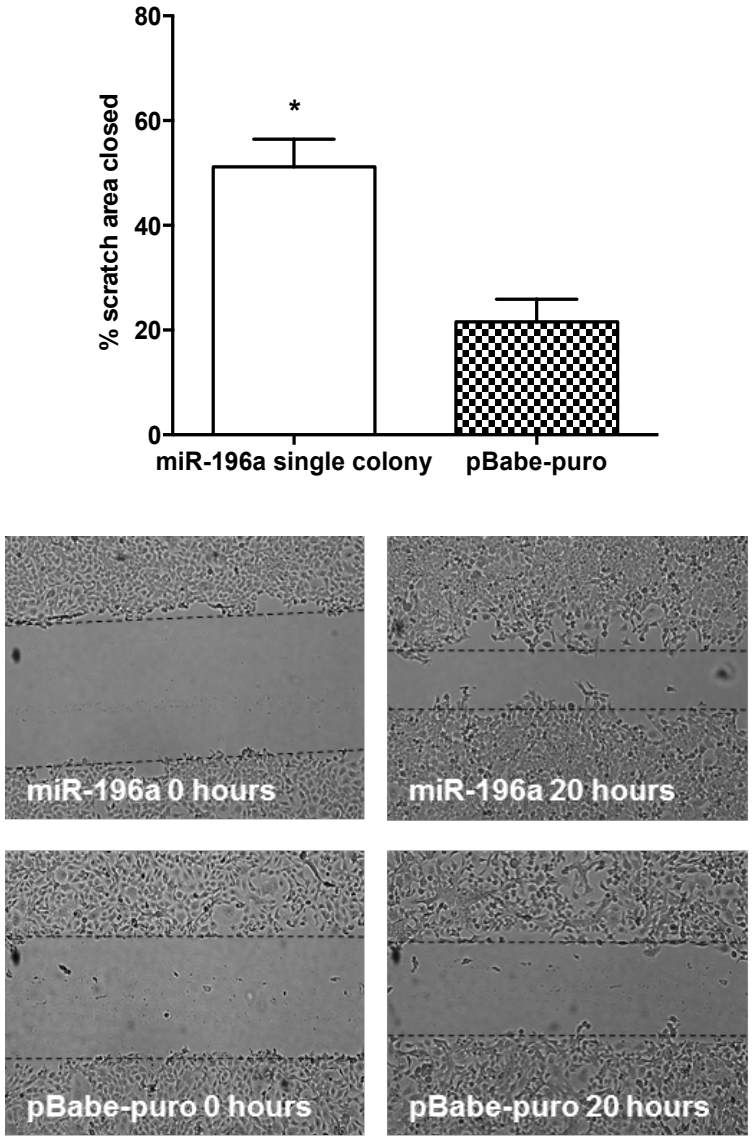

Figure 2.28 Cell migration assessed by scratch assay of miR-196a overexpressing cells (single colony) compared with pBabe-puro control cells. Bar graph shows the mean percentage scratch area closed after 20 hours of three scratches in triplicate wells in repeated experiments, $P < 0.01$. The images show representative examples at 0 and 20 hours at 4x magnification.

2.5.4.2 MiR-196a knockdown in SCC11B and SCC22B head and neck cancer cells lines

MiR-196a sponge was used to knockdown the expression of miR-196a in SCC11B and SCC22B cell lines, which both have high endogenous levels of the miRNA. Figure 2.29 shows the level of knockdown achieved in these two cell lines, compared with the cell lines transduced with the empty vector control. In the SCC11B cell line a 42% knockdown was achieved and in SCC22B there was a 50% reduction in miR-196a expression. The effect of this knockdown on cell proliferation was assessed using the MTT assay. This confirmed the

results seen using HN30 cells, with inhibition of cell proliferation in the knockdown cells (Figure 2.30).

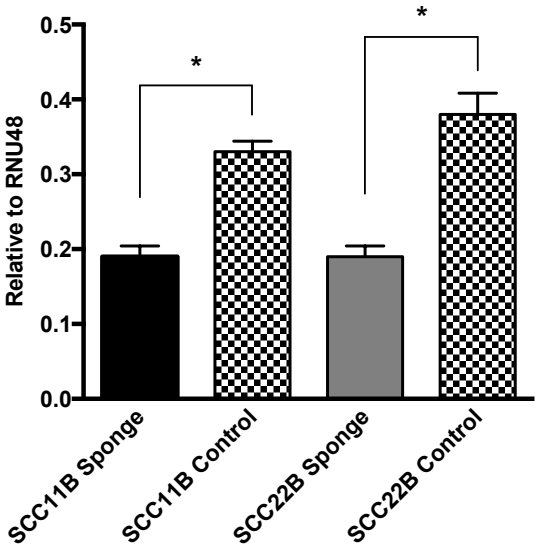

Figure 2.29 QRT-PCR of miR-196a knockdown with miR-196a sponge compared with control in SCC11B and SCC22B.
Expression is expressed relative to the housekeeping gene RNU48 and represents the mean of two RNA extractions. Student's t-test was used to assess statistical significance. SCC11B P = 0.01 and SCC22B P = 0.01.

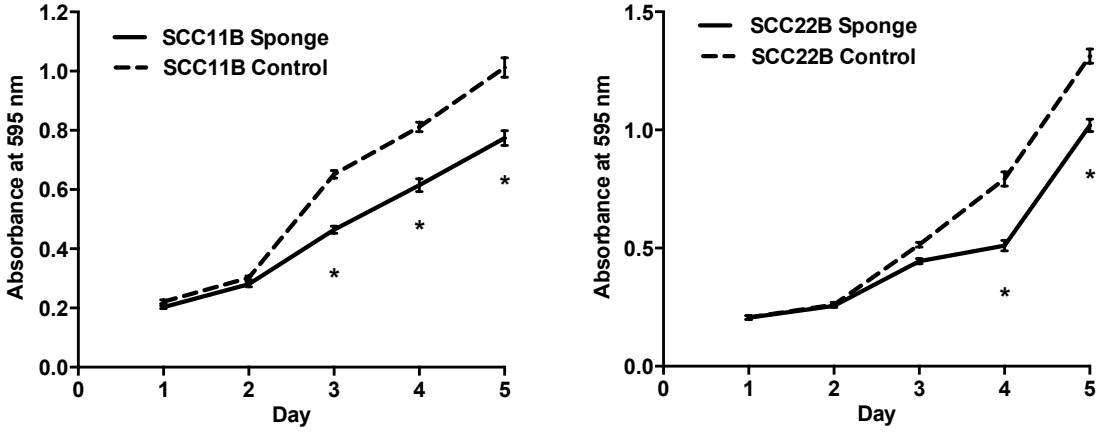

Figure 2.30 MTT assay comparing the effect of miR-196a knockdown in SCC11B cells (left) and SCC22B cells (right) on cell proliferation.
Cells were seeded in 6 wells of a 96-well plate per time point and the MTT assay performed daily over 5 days in two independent experiments. SCC11B days 3 to 5 and SCC22B days 4 and 5. P < 0.01, Student's t-test.

MiR-196a knockdown also had a similar effect to HN30 on migration demonstrated by the scratch assay. In SCC11B the mean scratch area closed at 14 hours was 14% versus 41% in the sponge and control cells respectively ($P < 0.01$, Figure 2.31). Similarly in SCC22B the mean scratch area closed after 12hours was 29% versus 56% in the sponge cells compared with control ($P < 0.01$, Figure 2.32).

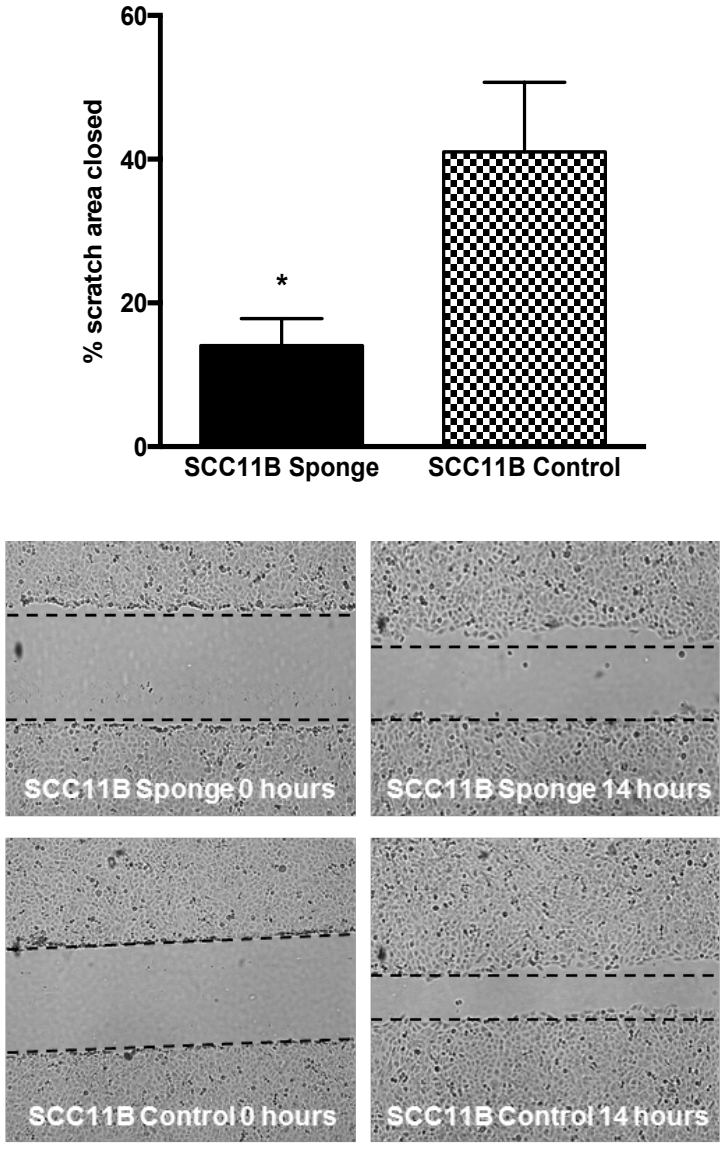

Figure 2.31 Cell migration assessed by scratch assay of SCC11B miR-196a sponge and control cells.
Cells were grown in 6 well plates in triplicate until confluent and a pipette tip used to create 3 scratches in each well. Bar graph shows the mean percentage scratch area closed after 14 hours from 2 independent experiments. Student's t-test was used to assess statistical significance ($P < 0.01$). Images show representative examples at 0 and 14 hours at 4x magnification.

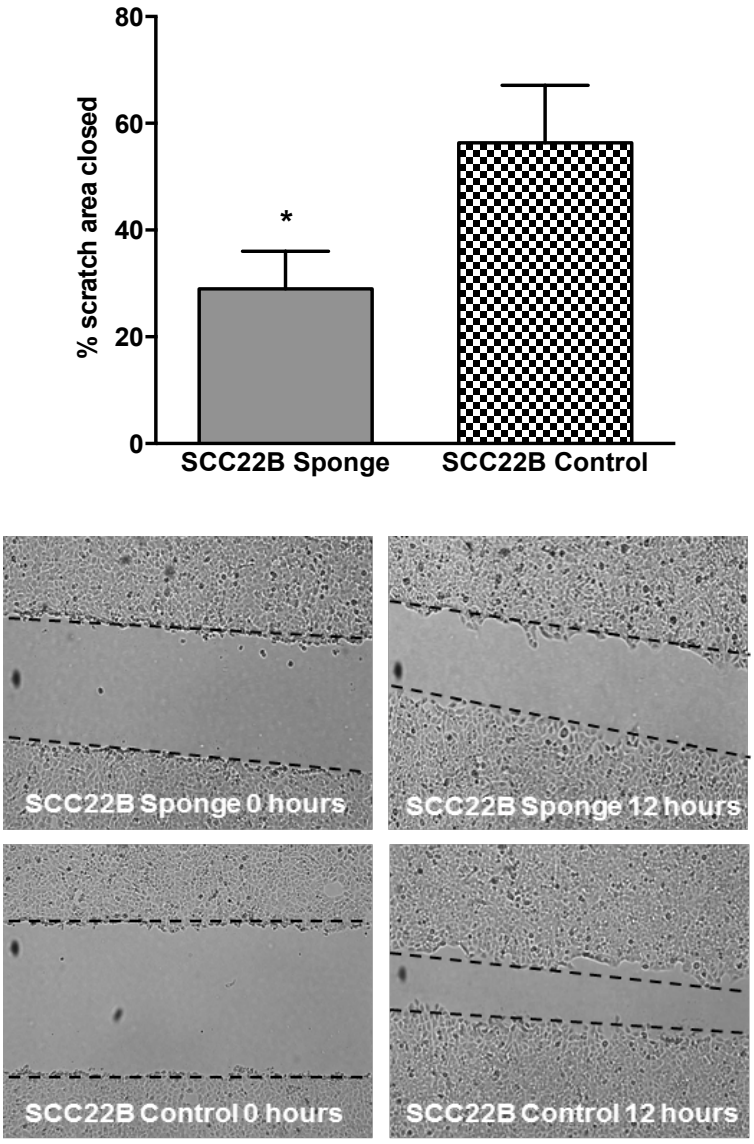

Figure 2.32 Cell migration assessed by scratch assay of SCC22B miR-196a knockdown cells versus control.
Bar graph represents the average percentage scratch area closed after 12 hours of three scratches in triplicate wells in repeated independent experiments. P < 0.01. Images are examples at 0 and 12 hours at 4x magnification.

2.5.5 Annexin A1 is a direct target of miR-196a

Several cellular genes have been identified as targets of miR-196a. ANXA1 was further investigated as a putative target in of miR-196a in head and neck cell lines due to its role as a tumour suppressor and potential prognostic marker in this tumour group. MiR-196a overexpression in HN5 cells resulted in suppression of ANXA1 protein expression (Figure 2.33), whereas miR-196a knockdown induced increased ANXA1 protein levels in HN30 cells, compared with their respective empty control vectors (Figure 2.34).

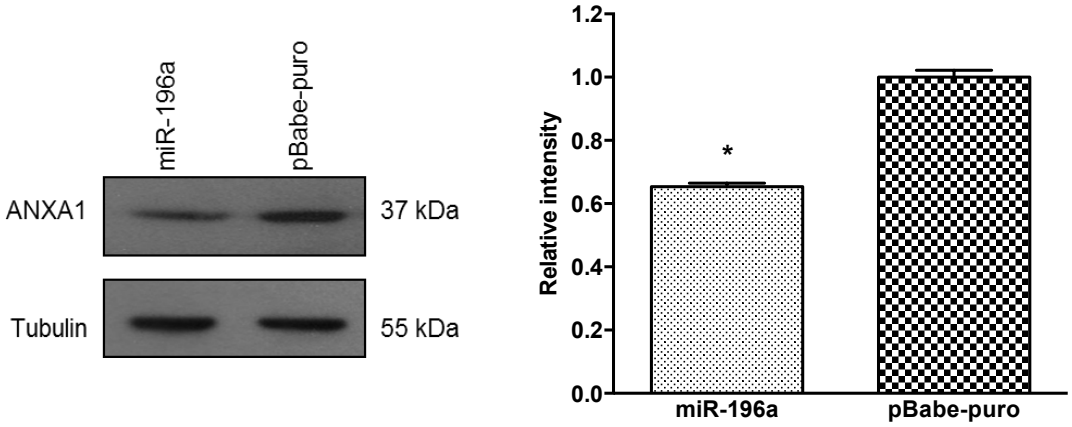

Figure 2.33 ANXA1 protein levels in miR-196a overexpressing and control cells. Western blot analysis was carried out in miR-196a overexpressing HN5 cells to detect ANXA1 protein expression. Bar graph shows the mean quantification of the intensity of bands, normalised to tubulin, from two separate experiments using ImageJ. Statistical difference between miR-196a and control cells were assessed using Student's t-test, $P < 0.01$.

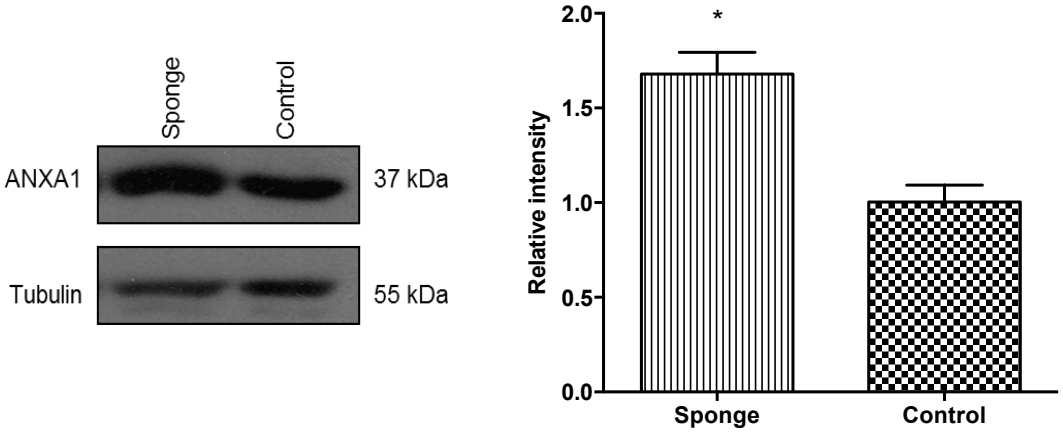

Figure 2.34 ANXA1 protein levels in miR-196a knockdown and control cells. Western blot of miR-196a knockdown HN30 cells to measure ANXA1 protein expression levels. Bar graph shows the mean quantification of the intensity of bands using ImageJ of western blots performed on two separate experiments, normalised to tubulin. $P < 0.01$.

A dual luciferase reporter plasmid containing the 3'-UTR of the ANXA1 gene was transiently transfected into miR-196a overexpressing and control cells, and miR-196a knockdown and control cells. The plasmid contains both Firefly and Renilla (control) luciferase activity. Binding of miR-196a to the 3'UTR of ANXA1 leads to a reduction in Firefly luciferase protein production resulting in reduced light emission detected by a luminometer, whereas the Renilla activity is constitutively expressed at a different wavelength. The Firefly activity is then expressed relative to the expression of the Renilla control. The assay was initially carried out using X-tremeGENE transfection reagent, which showed a small but statistically significant reduction in the relative luciferase activity in the miR-196a overexpressing cells compared with controls (P = 0.01) and increased relative luciferase activity in the miR-196a knockdown cells compared to their control (P = 0.02, Figure 2.35). The luciferase plasmid also contained a GFP marker, which showed that there was a high proportion of cell death. This may be due to toxicity to the cell caused by successful transfection or directly by the transfection reagent (Figure 2.36).

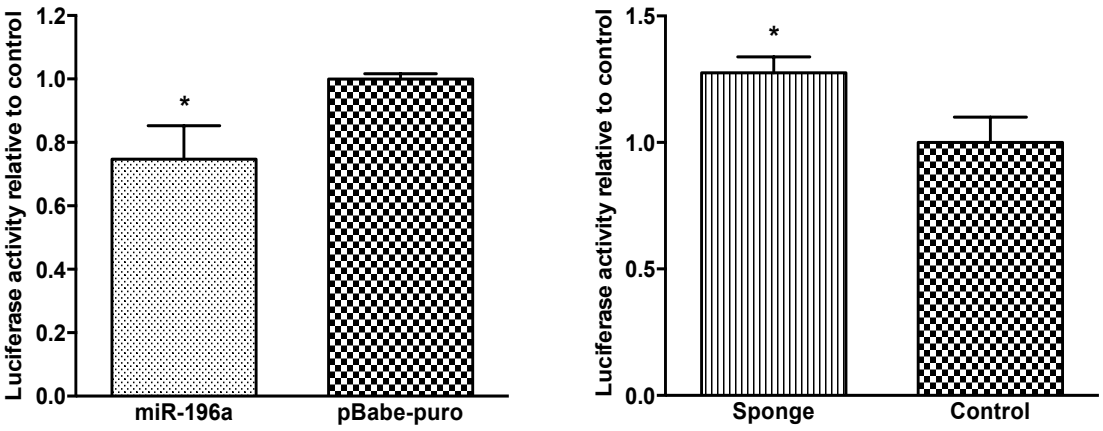

Figure 2.35 ANXA1 luciferase assay using X-tremeGENE transfection of miR-196a modulated cells and their respective controls.
Luciferase reporter plasmid containing ANXA1 3'UTR was transiently transfected into miR-196a overexpressing HN5 cells and pBabe-puro control cells, and the relative luciferase activity measured using the dual luciferase assay, P = 0.01 (left graph). The same experiment was carried out on miR-196a knockdown HN30 cells and control cells, P = 0.02 (right graph). Graphs represent transfection in triplicate carried out in three independent experiments.

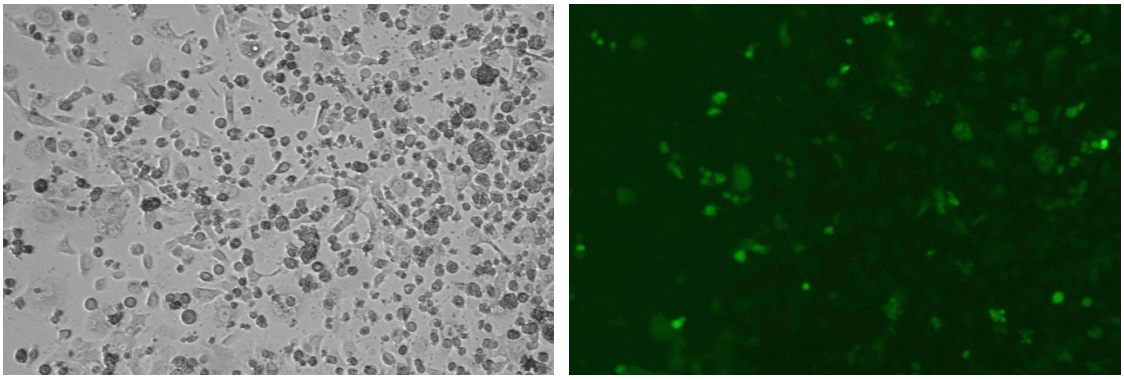

Figure 2.36 HN5 miR-196a overexpressing cells after transfection with ANXA1 luciferase plasmid using X-tremeGENE transfection reagent.
An example of the appearance of cells 24 hours after transient transfection using X-tremeGENE. Left panel shows appearance of cells at 4x magnification. Right panel shows GFP transfection efficiency.

The experiment was repeated using FuGENE transfection reagent. There were a higher proportion of cells surviving after 24 hours and high transfection efficiency (Figure 2.37). This resulted in a greater difference in the luciferase activity between the modulated cells and their respective controls ($P < 0.01$, Figure 2.38).

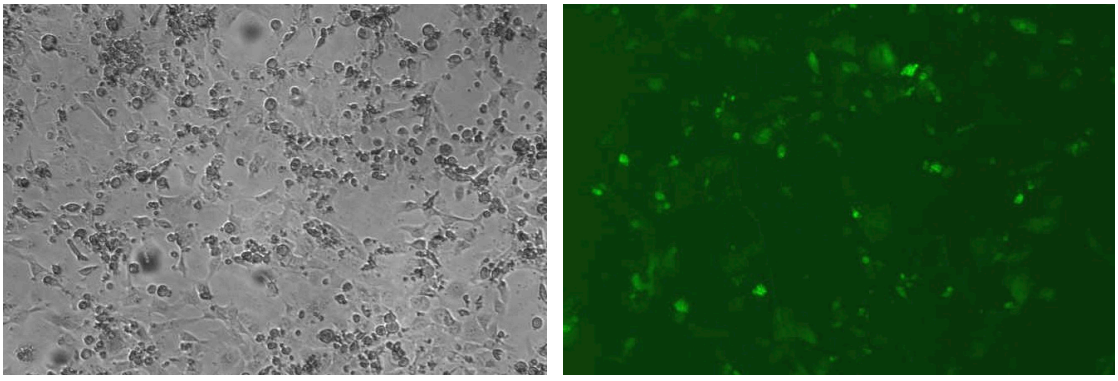

Figure 2.37 HN5 miR-196a overexpressing cells post-transfection with ANXA1 luciferase plasmid isung FuGENE transfection reagent.
Example of the appearance of cells 24 hours after transient transfection using FuGENE. Left panel shows higher proportion of surviving cells at 4x magnification. Right panel shows GFP transfection efficiency.

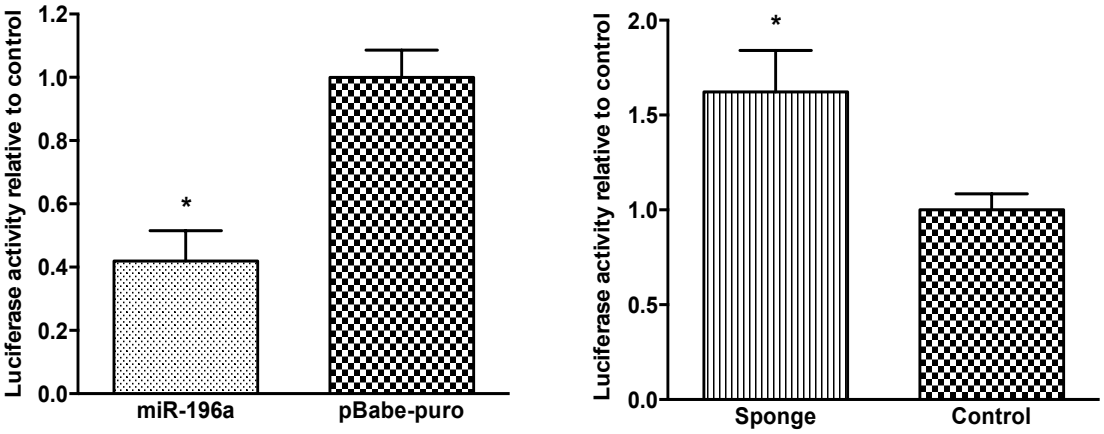

Figure 2.38 ANXA1 luciferase assay of miR-196a modulated cells and their respective controls using FuGENE transfection reagent.
Luciferase reporter plasmid containing ANXA1 3'UTR was transiently transfected into miR-196a overexpressing (left) and knockdown (right) cells with their corresponding control cells. Transfection was carried out in triplicate and repeated in an independent experiment. Statistical difference was determined by Student's t-test, $P < 0.01$.

In addition the baseline endogenous levels of ANXA1 in the cell lines investigated demonstrate a reverse association with the endogenous levels of miR-196a (Figure 2.39).

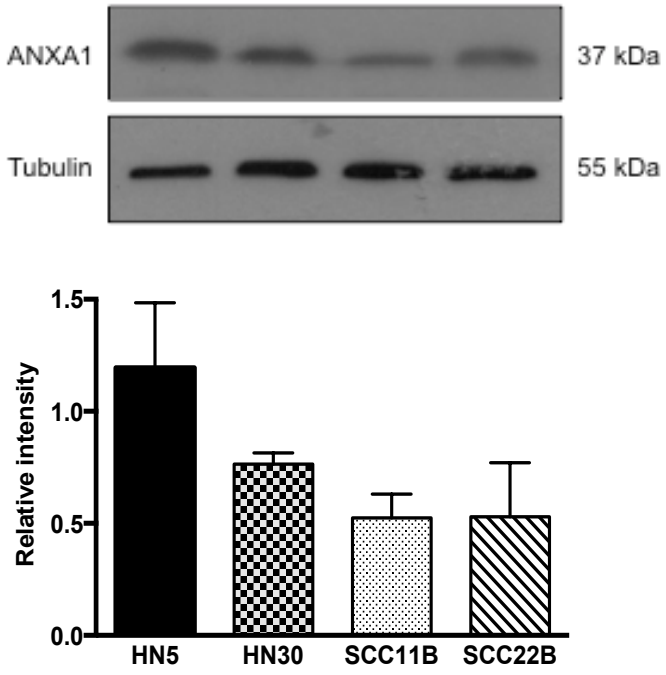

Figure 2.39 Endogenous ANXA1 protein expression levels of ANXA1 in the head and neck cancer cell lines tested.
Western blot was carried out to assess the baseline levels of ANXA1. Tubulin was used as loading control and the graph represents the mean intensity assessed by ImageJ relative to the loading control from two independent blots.

2.5.6 Annexin A1 silencing reproduces the oncogenic phenotype of miR-196a overexpression

To investigate whether the effects seen after modulating miR-196a levels were due to its target ANXA1, HN5 cells were stably transfected with ANXA1 shRNA. Western blot confirmed successful knockdown (Figure 2.40).

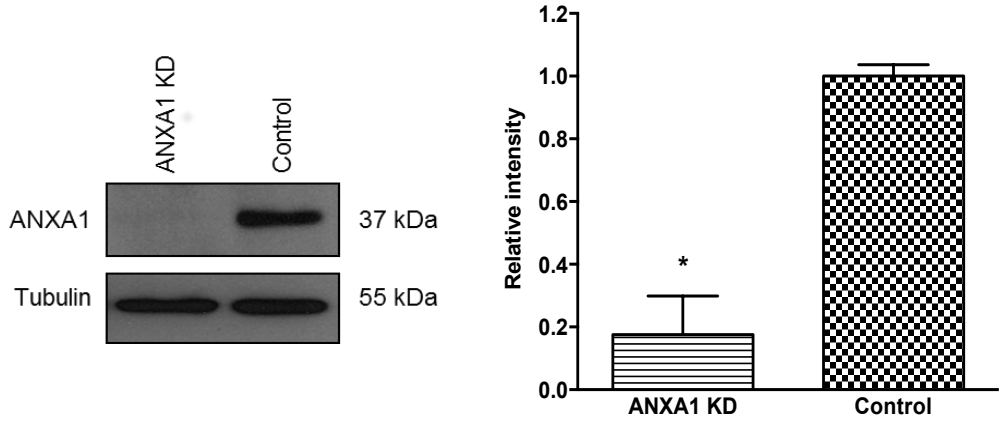

Figure 2.40 Western blot of ANXA1 knockdown in HN5 cells.
HN5 cells were transduced with ANXA1 shRNA or empty vector control and the knockdown efficiency was assessed by Western blot. Graph shows the mean intensity of the bands using ImageJ, relative to tubulin, from two independent blots.

The effect of this knockdown on cell proliferation, migration and invasion were investigated. Similar to the behaviour of miR-196a overexpressing HN5 cells, ANXA1 knockdown (KD) resulted in increased cell proliferation assessed growth rate over seven days, as well as cell survival measured by MTT assay over 5 days (Figure 2.41).

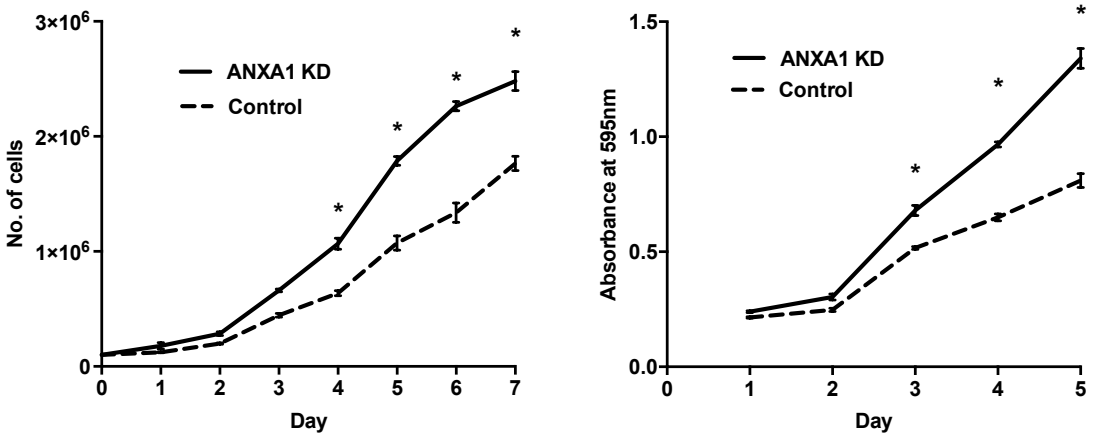

Figure 2.41 Cell proliferation in ANXA1 KD and control cells.
Left graph: equal numbers of cells were plated in triplicate on day 0 and counted every 24 hours for 7 consecutive days. Data is the mean of 2 independent experiment and error bars indicate standard deviation. Statistical significance determined by Student's t-test. Days 4 to 7, $P < 0.01$. Right graph: cells were plated in 6 wells of a 96-well plate and the MTT assay was performed daily over 5 days (right). Data is the mean of 2 independent experiment. Days 3 to 5, $P < 0.01$.

Cell migration was also enhanced after 20 hours, with the mean percentage scratch area closed of 59% and 26% ($P < 0.01$) in the ANXA1 KD cells and the empty vector control cells respectively (Figure 2.42). Invasion was significantly increased, with the mean percentage invasion relative to control of 41% in the ANXA1 KD cells compared with 20% in the control cells ($P < 0.01$, Figure 2.43).

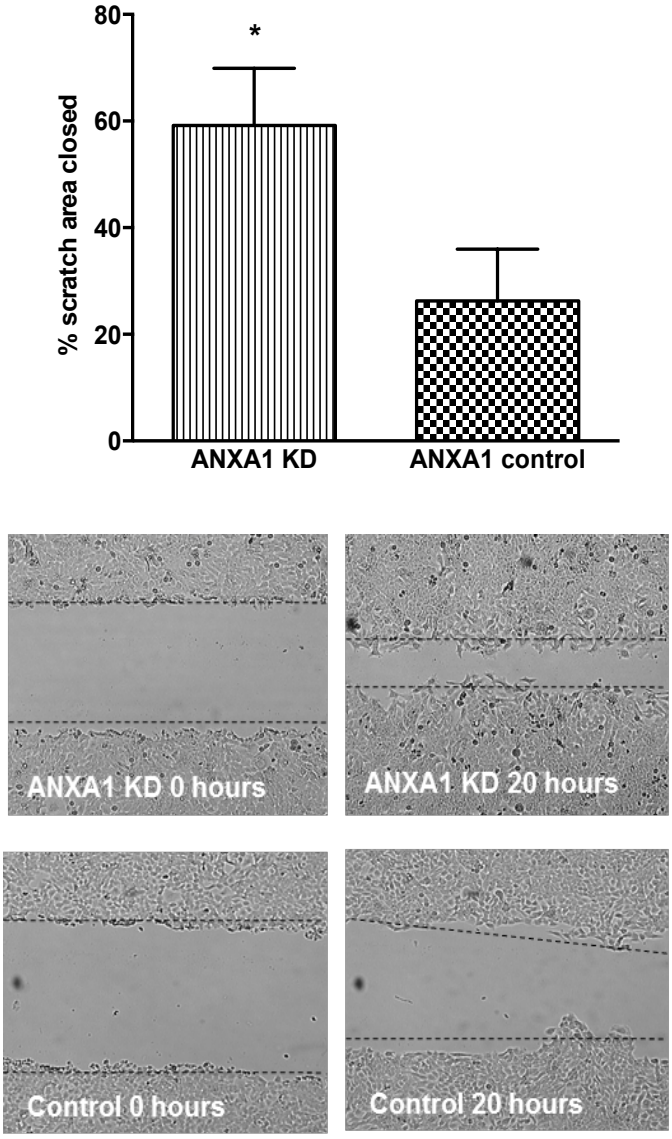

Figure 2.42 Scratch assay to assess migration in ANXA1 KD cells versus control. Data is expressed as mean percentage scratch area closed after 20 hours incubation from repeated triplicate wells, with a minimum of three scratches per well. Student's t-test was used to assess statistical significance ($P < 0.01$). Images are representative from 0 and 20 hours at 4x magnification.

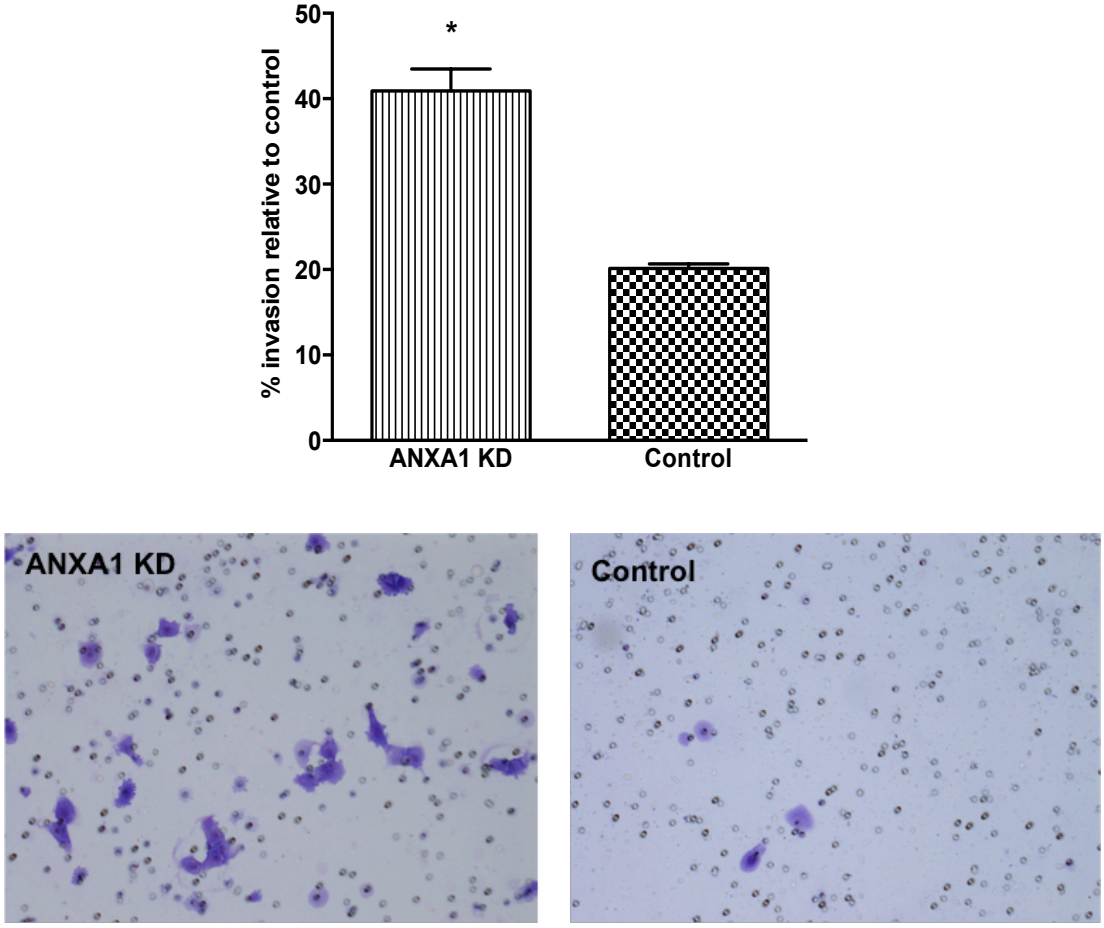

Figure 2.43 Matrigel invasion assay of ANXA1 KD cells versus control.
Equal number of cells were seeded into the Matrigel chamber and incubated for 22 hours, before counting the number of cells that have invaded through the Matrigel membrane. Cells were also seeded into a control chamber without Matrigel on the membrane. Bar graph represents the mean number of cells that have invaded through the membrane, relative to the mean number of cells that have migration through the control membrane ($P < 0.01$). The assay was carried out in repeated duplicates. Images are representative of cells fixed and stained on the invasion membrane at 10x magnification.

Vimentin immunofluorescence of ANXA1 KD cells showed an altered pattern of staining compared with the control cells, similar to the vimentin configuration seen in the miR-196a overexpressing HN5 cells and MDA-MB-231 cells (Figure 2.44).

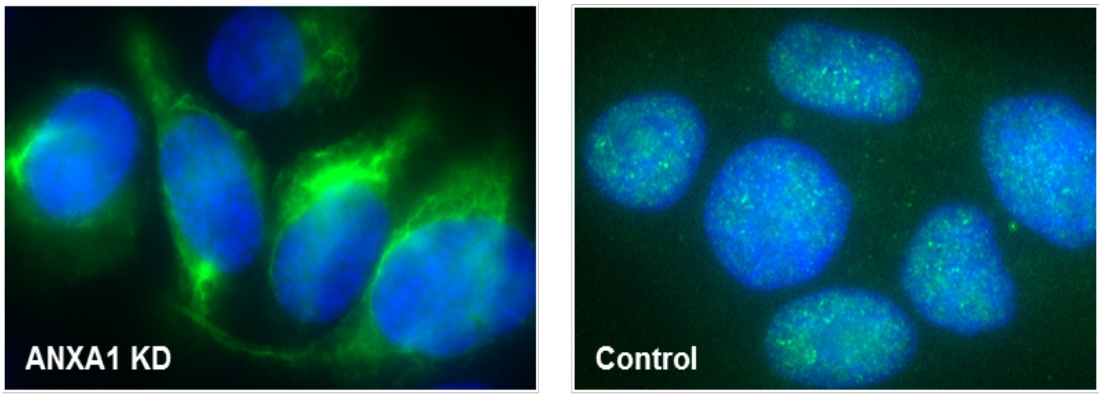

Figure 2.44 Vimentin immunofluorescence staining in ANXA1 KD cells compared with empty vector control.
ANXA1 KD and control cells were fixed and stained with primary rabbit anti-vimentin and secondary FITC-conjugated anti-rabbit antibody (green). Nuclei were stained with DAPI (blue) and images taken at 60x magnification.

ANXA1 KD cells were also irradiated and cell survival assessed using the MTT assay. ANXA1 KD showed some resistance compared to the control cells, but this did not reach significance (Figure 2.45). This suggests that miR-196a-induced radioresistance may not be entirely through ANXA1 suppression, and additional targets are likely to be involved.

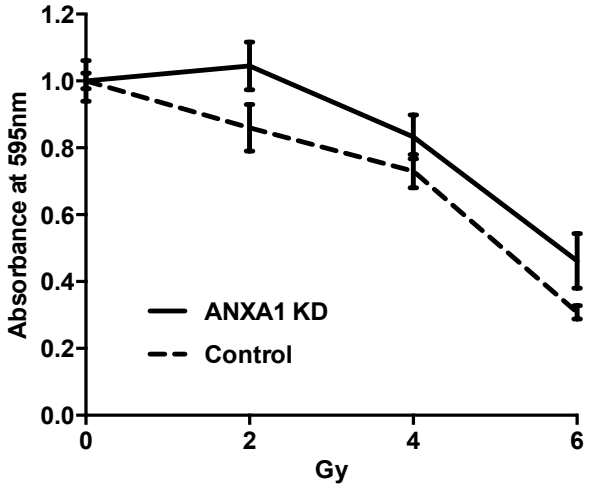

Figure 2.45 MTT assay post-irradiation in ANXA1 KD and control cells.
ANXA1 knockdown cells and their control cells were irradiated at 0 (control), 2, 4 and 6 Gy and cell survival assessed after 5 days. Data is presented relative to the absorbance of the unirradiated control cells (0 Gy) from 2 independent experiments.

2.5.7 MiR-196a expression in an independent panel of radioresistant oropharyngeal FFPE samples

The initial tissue microarray analysis revealed higher levels of miR-196a in patients with disease recurrence after radical treatment a five year follow up period. On review of the patient samples 14 cases were from the oral cavity, 1 from the base of tongue and 1 from the soft palate. Fourteen cases were locally advanced stage III or IV, with one stage I and one stage II. All patients were treated with surgery as the primary modality, followed by post-operative radiotherapy. In all cases RNA was extracted from fresh frozen samples from the primary surgical excision specimen.

Retrospective validation was attempted in tissue samples with selection of a homogeneous group of patients and clearer definition of radioresistance. All patients had received primary chemoradiation and therefore only small diagnostic FFPE samples were available. Out of 40 patients initially selected 10 cases were excluded due to insufficient tumour percentage in the biopsy specimen. A further sample was excluded due to poor RNA quality and the miR-196a level from this sample could not be measured. Therefore a total of 16 radiosensitive and 13 radioresistant cases were analysed for miR-196a expression relative to the housekeeping gene RNU48. The yield of extracted RNA ranged from 57.4 to 1454.6 ng/µl and the ratio of absorbance at 260 nm and 280 nm to assess purity ranged from 1.83 to 2.03. There was no difference in the pattern of expression between the two sample sets (Figure 2.46).

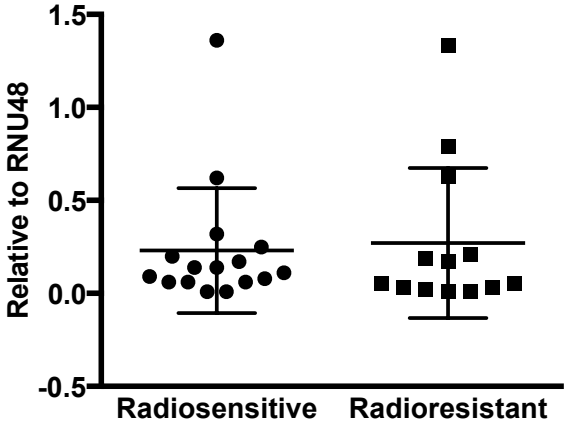

Figure 2.46 MiR-196a expression levels in a panel of radiosensitive and radioresistance FFPE oropharyngeal samples.
Dot plot showing the range of miR-196a expression levels, relative to RNU48, in an independent panel of FFPE oropharyngeal biopsy samples with known response to treatment. Samples with minimum of 60% tumour were selected and the miR-196a expression measured by qRT-PCR. There was no significant difference in the 2 groups (Mann-Whitney U test).

HPV status is an independent prognostic factor in oropharyngeal cancers and therefore the cases were separated into HPV positive and negative cases. However there was still no difference in the pattern of miR-196a expression (Figure 2.47). There was a wider distribution of expression values in the HPV negative samples compared with the HPV positive samples.

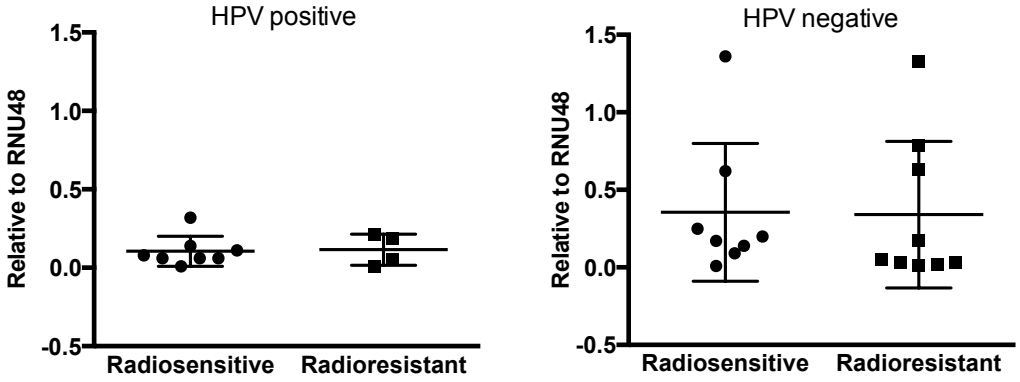

Figure 2.47 MiR-196a expression in HPV positive and negative radiosensitive and radioresistant samples.
Samples were separated into HPV positive and negative groups and the miR-196a levels relative to RNU48 was compared between radiosensitive and radioresistant samples.

2.5.8 Summary

- MiR-196a is upregulated in a group of patients with HNSCC with recurrent disease after radical treatment.
- MiR-196a exerts an oncogenic phenotype in HNSCC cell lines, which may be exerted through targeting ANXA1.
- Suppression of ANAX1 results in an oncogenic phenotype in HNSCC, suggesting a tumour suppressive role.
- MiR-196a overexpression exhibits resistance to irradiation in vitro, and may represent both a prognostic and predictive biomarker, but requires validation in a larger sample of patients.

2.6 Discussion

The deregulation of miRNAs has been reported in nearly all cancers and it has become clear that they play key roles in cancer development and progression, as well as representing potential predictive biomarkers and therapeutic targets. MiRNA expression profiling of a small exploratory cohort of HNSCC biopsy samples identified several miRNAs that were differentially expressed between patients with and without recurrent disease after radical surgery and adjuvant radiotherapy. Amongst these miRNAs, miR-196a was found to be significantly upregulated in patients with recurrence.

2.6.1 Oncogenic role

Functional analysis demonstrated that overexpression of miR-196a in HNSCC cells with low endogenous levels significantly promoted cell proliferation, migration and invasion, whereas knockdown of miR-196a in cells with high endogenous levels led to the opposite effects. Liu et al also reported similar results using the oral SCC cell lines OECM-1 and FaDu.[431] They demonstrated that modulating these cells to overexpress miR-196a enhanced migration and anchorage-dependent colony formation, but without obvious effect on cell growth. Knockdown resulted in decreased migration and growth of FaDu cell xenografts expressing exogenous miR-196a in nude mice compared to controls. Consistent with our initial microarray findings this study also found that high expression of miR-196a was associated with tumour recurrence and mortality. The majority of studies in a variety of different cancers have found miR-196a to have an oncogenic role. Overexpression of miR-196a has been demonstrated in several types of tumours and in general is linked with more aggressive, metastatic, tumor phenotype. There is a growing body of evidence indicating that many reported targets of miR-196a, including Radixin,[426] Netrin 4[437] and ANXA1,[424] regulate cell motility and migration, further supporting a potential role for miR-196a in conferring invasive tumour characteristics.

MiR-196a acts, in part, through ANXA1. However the precise mechanism through which miR-196a modulation of ANXA1 contributes to a more aggressive tumour phenotype requires further investigation. Western blot analysis for apoptotic markers did not show a difference between miR-196a knockdown and control cells, indicating that the anti-proliferative effect of miR-196a knockdown is unlikely to be due to increased apoptosis, further suggesting a role in tumour invasiveness and resistance to therapy. A number of miR-196a studies have investigated the effect on cell cycle progression and apoptosis through flow cytometry or Hoechst staining, with differing results. Huang et al[435] reported transiently silencing miR-196a in Panc-1 cells increased the percentage of cells in the G_0/G_1 phase of the cell cycle at 72 hours with downregulation of cyclin D1 and cyclin-

dependent kinases (CDKs) 4 and 6, suggesting a role in cell cycle arrest. There was no significant difference in apoptosis by flow cytometry after miR-196a knockdown at 24, 48 and 72 hours.[435] In contrast Liu et al,[436] who also used Panc-1 cells and flow cytometry, demonstrated a significant increase in apoptotic fraction after miR-196a inhibitor transfection.[436] In cervix cancer cells lines ectopic expression of miR-196a decreased the percentage of cells in G_0/G_1 and increased the percentage in S phase, whilst miR-196a inhibition had the opposite effects, indicating promotion of G_1/S cell cycle transition by miR-196a. In addition, miR-196a overexpression upregulated cyclin D1 and downregulated the CDK inhibitor $p21^{Cip1}$.[429] Similar effects on cell cycle regulation were found in gastric cancer cells, with no increase in apoptosis as assessed by Hoechst staining and cleaved caspase-3 Western blot analysis.[425] In NSCLC cell lines miR-196a inhibition also had no significant effect on apoptosis.[427] However in glioblastoma cell lines ectopic miR-196a inhibited cell apoptosis[434] and overexpression of miR-196a in SEG-1 oesophageal cancer cell line, in which ANXA1 was found to be a target, inhibited apoptosis induction, suggesting an anti-apoptotic role for miR-196a.[424]

MiR-196a may act through different mechanisms via different targets and cell types. However the contrasting results in the same pancreatic cell line suggests possible alternative pathways in the same cell line. Schimanski et al[433] transiently transfected increasing concentrations of miR-196a into colorectal cancer cell lines and found dose-dependent inhibition of cellular adhesion and dose-dependent differences in restriction of target gene expression. For example only low concentrations of miR-196a were required to suppress HOXB8 as assessed by RT-PCR, whereas higher concentrations were required to completely restrict HOXC7 and partially restrict HOXA7 and HOXD8.[433] MiR-196a may therefore have differing, or even opposing effects, in the same cell type at differing levels of expression, through the regulation of a diverse range of targets.

2.6.2 Epithelial-Mesenchymal Transition

EMT is a process of immotile epithelial cell transition to motile mesenchymal cells, resulting in increased migratory and invasive ability. Cancer cell migration, invasion and metastases involve phenotypic features similar to EMT, such as loss of cell-cell adhesion and increase in cell motility, and is characterised by loss of various cell surface proteins and reorganisation of cytoskeletal proteins, for example loss of E-cadherin and cytokeratin, and gain of vimentin and N-cadherin.[458]

EMT as a mechanism for altered vimentin expression in miR-196a overexpressing cells was therefore investigated. Western blot analysis was initially used to determine the expression levels of E-cadherin and vimentin. The control cell lines had high levels of

baseline E-cadherin, which was not affected by miR-196a modulation. The HN30 cell line did not express vimentin, and the HN5 cell line had very low levels, which was downregulated after miR-196a overexpression. Given that miR-196a overexpression increased migration and invasion, this was not the expected pattern of expression prompting further investigation with immunofluorescence. The change in the pattern of vimentin in both the miR-196a overexpressing and ANXA1 knockdown cells suggested a change in the configuration of the vimentin expression, and resembled that of MDA-MB-231 mesenchymal breast cell lines. This suggests that miR-196a through ANXA1 does have an effect on EMT, but this may not be as straight forward as the typical loss of E-cadherin/gain of vimentin expression.

Three classes of EMT with distinct biological processed have been suggested, with EMT that occurs in cancer cells as a separate class.[454] Cancer cells go through genetic/epigenetic changes affecting oncogenes and TSGs to acquire invasive and metastatic capabilities, but differ in the extent to which they undergo EMT. The expression of the proteins typical for EMT may therefore not be detected. Cancer cells undergoing EMT may retain certain epithelial traits and acquire some mesenchymal ones, whilst others shed all epithelial traits and become fully mesenchymal.[458] EMT markers can identify epithelial or mesenchymal cells and are therefore not necessarily identifying cells that are specifically undergoing EMT, which may only be a proportion of the cells.[459] EMT involves multiple complex signalling pathways, which are regulated by transcription factors such as transforming growth factor-β (TGF-β) and the zinc finger proteins ZEB1 and ZEB2. MiRNAs have been found to be crucial regulators of expression of these factors. For example, the miR-200 family targets ZEB1 and ZEB2, which suppress the transcription of E-cadherin,[177] and miR-155, which is associated with TGF-β-induced EMT.[460] MiR-196a through ANXA1 may have a specific role in vimentin remodelling, contributing to the EMT process, however the nature of this regulation needs further investigation.

2.6.3 Sensitivity to irradiation

MiRNAs are important regulators of the DNA damage response (DDR) pathway and can alter the sensitivity of cancer cells to irradiation. MiR-196a has not previously been linked to radioresistance. The tissue samples initially used for the microarray analysis originated from patients who required post-operative radiotherapy, with those developing recurrent disease demonstrating higher levels of pretreatment miR-196a. The increased cell viability and repair of DNA damage in the miR-196a overexpressing cells compared with the control cells raises the possibility of miR-196a as a biomarker of intrinsic radioresistance, and as a potential predictive marker of radiation response, identifying patients at diagnosis who are

more likely to fail conventional radiation treatments. In addition, the modulation of miR-196a and/or its target genes could have therapeutic potential as a radiation sensitising agent.

Further investigation into the mechanism and pathways through which miR-196a may modify the response to radiation damage is required. Ionising radiation damages cells mainly through double strand DNA breaks, which lead to direct or indirect cell death unless the damage is repaired. The DDR pathway has a key role in determining the sensitivity of cells to radiation, but other cell survival and cell cycle checkpoint pathways are also involved, which influence the expression of genes involved in cell repair or apoptosis and it would therefore be important to examine cell cycle phase and levels of ATM, ATR and cyclin-dependent kinases post-irradiation in miR-196a overexpressing cells. The level of DNA damage and repair after radiation is also known to influence intrinsic cellular radioresistance and miR-196a overexpressing cells showed evidence of fewer gamma H2AX foci 24 hours after irradiation, suggesting miR-196a may be necessary for cell cycle arrest and repair in this situation.

Cell death after irradiation can be immediate via apoptosis, or after a few cell divisions. Improved cell survival 5 days after irradiation suggests the activation of pro-survival signals, such as inhibition of apoptosis, in response to DNA damage. ANXA1 has been shown to be anti-proliferative and pro-apoptotic,[445] and therefore the trend towards radioresistance seen in the ANXA1 knockdown cells may be in part due to inhibition of apoptosis. Downregulation of ANXA1 has been hypothesised to increase radioresistance in nasopharyngeal carcinoma.[461] The trend towards radioresistance in our ANXA1 knockdown cells, compared with the greater effect on radioresistance in our miR-196a modulated cells, suggests that other target proteins of miR-196a also play a role in the response to radiation. For example, the recently reported target of miR-196a IκBα is an inhibitor of NFκB.[434,435] NFκB, in conjunction with ATM, is activated early in response to stresses such as ionising radiation and promotes the upregulation of pro-survival and anti-apoptotic genes.[462] Inhibition of NFκB significantly enhances radiosensitivity,[463,464] and therefore downregulation of IκBα may be an important target in miR-196a-induced radioresistance. FOXO1 and $p27^{kip1}$ have also been identified as targets of miR-196a, and are both negative regulators of the PI3K/AKT signalling pathway.[425,429] This pathway is closely associated with intrinsic radiosensitivity, and inhibition of PI3K and its downstream effector mTOR has been shown to enhance radiation-induced killing in HNSCC cells by persistent DNA damage as evidenced by increase number of gamma H2AX foci, and enhanced G_2 cell cycle delay.[465]

De Jong et al[195] selected 32 HNSCC cell lines with known radiosensitivity and analysed the miRNA expression. They found low expression of miRNAs involved in the inhibition of EMT were important in determining radioresistance, and suggested that the acquisition of an EMT phenotype is associated with less damage, better repair and less cell death after irradiation, resulting in radioresistance. Although miR-196a was not among their miRNA panel of radioresistance, our study did find some evidence that miR-196a contributes to increased EMT, which would be consistent with their results. Therefore miR-196a could represent a new therapeutic target to inhibit multiple pathways involved in both oncogenesis and radioresistance.

2.6.4 ANXA1 as a target of miR-196a

ANXA1 was investigated as a target of miR-196a through luciferase assay, Western blot and ANXA1 knockdown studies. Several genes with important roles in proliferation, adhesion and apoptosis have been shown to be targets of miR-196a. Of these targets there is evidence that ANXA1 expression changes during the development and progression of cancer. It is downregulated in oesophagus,[466] breast[467], prostate,[452] larynx[468] and oropharyngeal cancer[469] compared with normal epithelium suggesting that this protein is an essential component for maintenance of the normal epithelial phenotype. In oral cancer tissues, low ANXA1 expression is associated with poorer differentiation status,[449-451] with forced ANXA1 overexpression significantly reducing cell proliferation in oral SCC cell lines and nude mice, whereas downregulation increased proliferation.[451] In nasopharyngeal cancer (NPC) ANXA1 was decreased in NPC tissue compared with normal adjacent tissue,[470] was only positive in well differentiated SCC areas,[453] and downregulation of ANXA1 in NPC cell lines promoted proliferation, migration and invasion.[471] ANXA1 has also been shown to have a tumour suppressor role in prostate cancer models, where upregulation of ANXA1 blocked EGF-induced proliferation, reduced cell viability, colony formation, and induced apoptosis.[472] In breast cancer ANXA1 knockdown, in conjunction with RAS, induced EMT and metastases in non-metastatic cells.[473] These tumour suppressor effects are consistent with the phenotypic characteristics of the HN5 miR-196a overexpressing cells, prompting further investigation into ANXA1 in HNSCC. An inverse correlation between miR-196a and ANXA1 expression has been shown in oesophageal, breast and endometrial cancer cell lines, and in oesophageal tumour specimens.[424] The use of miR-196a mimics in oesophageal and breast cancer cells resulted in decreased ANXA1 mRNA and protein expression, inhibited ANXA1 luciferase expression, and promoted cell proliferation, anchorage-independent growth and suppressed apoptosis.[424] In agreement with this data ANXA1 is also a direct target of miR-196a in HNSCC, and silencing of ANXA1 results in a more aggressive tumour cell phenotype similar to miR-196a overexpressing cells.

The mechanism of the anti-proliferative effect of ANXA1 is unclear. ANXA1 has been shown to stimulate caspase-mediated apoptosis, mainly in cells of the myelo-monocytic lineage, neutrophils and in broncho-alveolar epithelial cells.[474,475] ANXA1 has been found to bind to NF-κB, suppressing its transcriptional activity by preventing NF-κB binding to DNA, leading to enhancement of apoptotic death and inhibition of cell growth mediated by changes in NF-κB-dependent cell signalling.[476,477] In addition, ANXA1 expression is strongly induced in thyroid carcinoma cells during tumour necrosis factor-related apoptosis inducing ligand (TRAIL)-induced apoptosis.[478] Another possible mechanism for the anti-proliferative action of ANXA1 could be due to its activation of the extracellular signal-regulated kinase (ERK) signalling cascade, as previously demonstrated in a variety of cell types. This results in disruption of the actin cytoskeleton, inhibition of cyclin D1 and subsequent suppression of cell proliferation.[479,480] Furthermore, ANXA1 is a substrate for the tyrosine kinase activity of the epidermal growth factor (EGF) receptor,[481] which is expressed in over 90% of HNSCC,[20] and has been shown to block EGF-induced cell proliferation.[482] Both activation of EGFR signaling and overexpression of cyclin D1 are closely associated with head and neck cancer progression. It would therefore be interesting to explore whether miR-196a through its target ANXA1 influences EGFR signaling and the cell cycle pathway.

ANXA1 has a diverse range of biological functions. It is a steroid-regulated protein and inhibits phospholipase A2 activity, blocking the production of arachidonic acid. It can be found in both subcellular and extracellular locations and has multiple phosphorylation sites.[445] In addition to EGF it is also a substrate for platelet-derived growth factor (PDGR), hepatocyte growth factor and protein kinase C, and can regulate multiple signalling pathways including ERK1/2, p38/MAPK, JAK/STAT3 and TGF-β.[473] It is therefore unsurprising that although ANXA1 appears to have a tumour suppressor role in HNSCC, an oncogenic role has also been reported in other cancers such as breast,[483] lung[448] and stomach.[484] In contrast to the study by Maschler et al where ANXA1 knockdown induced complete EMT and lung metastasis in vivo in breast cancer,[473] ANXA1 knockdown in invasive basal-like breast cancer cell lines reduced migration and impaired TGF-β signalling, as well as decreasing lung metastasis.[485] ANXA1 has also been shown to be a major regulator of endothelial cell migration, and thereby angiogenesis, in response to VEGF.[486,487] Furthermore this pathway is targeted by miR-196a. These opposing functions of ANXA1, and miR-196a, are clearly cell and tissue type specific and complex in nature.

2.6.5 Validation in FFPE samples

To try to validate the correlation between the pretreatment expression of miR-196a and poor outcome, and investigate whether this association is related to radioresistance, an independent panel of tumour samples from patients with homogeneous tumour characteristics was selected. Patients all received radiotherapy as their primary mode of treatment. However this did not reveal a significant difference in the expression levels of miR-196a between tumours with and without recurrence; however many factors could have contributed to this negative finding. The sample size was small and all samples were from the oropharynx, whilst most of the initial samples originated from the oral cavity, as did HN5, the main cell line used in the study. Despite stratifying by HPV status, difference in subsite may have an impact on the expression levels. Although only samples with over 60% tumour were selected, the non-malignant tissue component could influence the miRNA levels.

Fresh frozen samples were not available and therefore FFPE samples had to be used. RNA can undergo degradation during the formalin fixating process, causing a wide variation in the quality of RNA isolated. The purity of RNA extracted was measured using the NanoDrop spectrophotometer, which measures the optical density at 260 nm and 280 nm. A 260/280 ratio greater than 1.8 is considered as suitable for gene expression measurements,[488] which was achieved in all samples used, and the yield of RNA was comparable to other studies.[489] Many expression profiling studies have used FFPE samples to identify a range of gene signatures, as FFPE specimens represent a valuable source of data for investigating biomarkers. MiRNA expression profiles between FFPE and fresh frozen samples have been directly compared with high correlation, in contrast to mRNA expression profiling which shows wider variation.[490,491] In addition miRNA expression from samples stored over a 10-year period remained stable.[490]

The lack of correlation was disappointing but will help to design future validation studies. For further FFPE work we would need to consider macrodissection or microdissection of tumours, depending on the amount of tissue available, and larger numbers of patients will be required.

2.6.6 Conclusions

MiR-196a is an oncogene in head and neck cancer and its overexpression is associated with increased tumorigenic potential and radioresistance. ANXA1 is a direct target of miR-196a and acts as a tumour suppressor in these cells. The association between ANXA1 and cancer suggests that its suppression by miR-196a may be an important step in the oncogenesis of HNSCC. Expression levels of miR-196a may represent a predictive biomarker for selecting patients for individualised therapy, and its target ANXA1 could be an important focus for future targeted therapy in HNSCC. However, it is also clear that miR-196a plays different roles in different tumour types. It is known that most miRNAs can target multiple genes to exert specific effects and that single genes can be targeted by multiple miRNAs, indicating that miRNAs work in a complex network of regulatory pathways.

This study highlights the importance of miR-196a and ANXA1 in HNSCC, but confirmation in a larger number of patient samples and in vivo studies are required in order to establish a clinical application.

2.6.7 Future work

Further work is required to ascertain the mechanism of oncogenesis and radioresistance of miR-196a. This would include:

- Investigating the effect of miR-196a modulation on cell cycle in HNSCC, and further study its role in apoptosis.
- Investigating the role of miR-196a in response to irradiation and identify proteins involved in DNA damage response pathway.
- Identification of new biologically relevant targets using novel functional assays.[492]

ANXA1 is an interesting target for further investigation in HNSCC. Specific areas include:

- Assessing whether ANXA1 knockdown has an anti-apoptotic effect in HNSCC.
- Investigating the association of ANXA1 with EGFR.

Validation of miR-196a as a candidate biomarker in HNSCC is still required by:

- Animal studies to assess the effect of miR-196a on tumour growth and metastases, and response to irradiation.
- Larger cohort of patient tissue samples to assess the potential of miR-196 as a biomarker for prognosis and radiotherapy response.

Chapter 3

Biomarker of Hypoxia Evaluation with Molecular and ^{64}Cu-ATSM PET/CT Imaging Techniques in Head and Neck Squamous Cell Carcinomas (BoHEMIaN study)

3.1 Introduction

Hypoxia has been extensively investigated in HNSCC and the association with radioresistance and poor outcome is well known. There are a number of therapeutic interventions that have been developed which can target global or focal hypoxia in tumours. However hypoxia is difficult to assess as it is heterogeneous and dynamic due to continuing tumour and vessel growth, and constant fluctuations in blood flow. The identification of patients with hypoxic tumours who would benefit from hypoxia-targeted interventions has been the major limiting factor in applying these potential advantages into clinical practice. Accurately detecting and quantifying hypoxic tumours is essential in identifying patients who have aggressive, treatment resistant disease. Various methods have been investigated but with inconsistent and sometimes conflicting results, lacking the sensitivity and specificity needed for clinical utility.

3.1.1 Cu-ATSM PET

There have been a large number of studies attempting to validate Cu-ATSM as a hypoxic tracer and elucidate the exact mechanisms. Preclinical studies have not been able to consistently demonstrate hypoxia selectivity, but they have used a range of different cell lines, animal models and techniques. It is clear that Cu-ATSM accumulation is dependent on the cell or tumour type and would not be suitable as a universal tracer of hypoxia, but this is the true for all PET radiopharmaceutical agents. Despite the uncertainties regarding the precise mechanism, clinical studies have clearly demonstrated its potential as an imaging biomarker that warrants further investigation, with advantages over nitroimidazole-based hypoxia tracers.

3.1.2 Hypoxia gene expression profiling

Hypoxia-specific gene expression profiling has been investigated in HNSCC to identify tumour hypoxia. Signatures developed from microarrays have demonstrated predictive value when applied retrospectively to formalin fixed paraffin embedded (FFPE) samples. These methods require no additional biopsies and have the potential to be directly translated into clinical practice by applying the gene signatures to pretreatment diagnostic biopsy samples to determine hypoxic status. Next generation sequencing has enabled improved the accuracy and speed of sequencing tissue samples, with reduced costs allowing wider accessibility.

RNA-Seq is next generation sequencing of transcripts, qualitatively and quantitatively profiling the gene expression patterns in tissues. RNA is fragmented into millions of short

reads of several hundred base pairs and is converted to a library of complementary DNA with adaptors attached to one or both ends. Each molecule is amplified and sequenced in a high throughput manner to obtain short sequences, which are either aligned to a reference genome, available from whole-genome sequencing projects, or can be assembled de novo. The amount of mapped reads can then be counted and the gene expression level calculated using platform specific algorithms.[493] Compared with hybridisation methods such as microarrays, RNA-Seq captures a wider range of gene expression, allowing a snapshot of the whole transcriptome rather than a predetermined set of genes. It also has a greater dynamic range of expression levels over which transcripts can be detected. It is less affected by the amount of RNA available and by background noise when detecting low expressed genes, and has been shown to be highly reproducible.[494]

Gene expression profiling, however, does not provide information on the spatial distribution of hypoxia within tumours, and therefore there is increasing interest in combining this with hypoxia imaging techniques. A single marker of hypoxia is unlikely to be able to adequately describe the hypoxia response, and by combining molecular and imaging biomarkers of hypoxia a more comprehensive assessment of the pretreatment hypoxic status of tumours could be made. Correlating genomic and imaging data is the expanding field of radiogenomics, and advances in the technology in both areas of research will improve the management and outcome of hypoxic HNSCC.

3.2 Aims

^{64}Cu-ATSM PET is currently a research tool to image hypoxia or hypoxia-related regions, but it is currently only available in specialist centres and would not be suitable for all HNSCC patients. Hypoxia gene signatures from diagnostic biopsies could enable the selection of patient who would benefit from hypoxia imaging, which would provide information on the level and distribution of hypoxia regions. This would in turn inform treatment selection.

In order to achieve this process the aim of the BoHEMIaN study is to investigate whether specific gene signatures can predict for the hypoxic uptake on ^{64}Cu-ATSM PET imaging, by correlating the gene expression profiles from diagnostic FFPE biopsies with the uptake parameters on PET in a homogeneous cohort of patients with locally advanced oropharyngeal squamous cell carcinoma. The combination of genetic and functional imaging biomarker data could potentially lead to a more robust method for hypoxia identification and mapping.

3.2.1 Primary objectives

- To correlate the gene expression profile of oropharyngeal SCC with ^{64}Cu-ATSM PET imaging.
- To investigate whether published hypoxia signatures correlate with ^{64}Cu-ATSM PET imaging parameters.

3.2.2 Secondary objectives

- To investigate whether circulating biomarkers of hypoxia correlates with ^{64}Cu-ATSM PET imaging parameters, specifically miR-196a, following on from our in vitro data, and miR-210, the hypoximiR.
- To evaluate the relationship between gene signatures, ^{64}Cu-ATSM PET uptake and circulating biomarkers with clinical response at 3 months post-treatment.
- To design a validation study of any identified biomarkers for subsequent incorporation into clinical trials.

3.3 Methods

3.3.1 Patients

Research Ethics Committee approval was obtained for the study in November 2012 (reference 12/LO/1123). All patients gave written and voluntary consent to enter the study, which included written consent for the use of a blood sample and their diagnostic biopsy specimen. Fifteen patients were prospectively recruited as part of a pilot phase of the study.

The initial eligibility criteria included patients with newly diagnosed with histologically proven HPV-negative stage III-IV squamous cell carcinoma of the oropharynx to be treated with radical concomitant chemoRT, which was expanded in February 2014 to also include HPV-positive patients. Patients were greater than 18 years of age with performance status 0 – 1 and adequate organ function. Patients with a previous history of cancer other than skin basal cell carcinoma, patients with faecal or urinary incontinence and pregnant or breast feeding women were excluded. Eligible patients were identified from the weekly head and neck multidisciplinary meeting at Guy's and St Thomas' NHS foundation Trust.

3.3.2 Study procedure

All patients were evaluated before treatment with a full history and examination, staging with CT head, neck and chest. Staging MRI head and neck and whole-body (base of brain to mid-thigh) ^{18}F-FDG-PET/CT scans were carried out if clinically indicated. Routine investigations as part of the treatment pathway were performed, and included blood tests, audiology and dental assessment, EDTA kidney and radiotherapy planning CT scans.

Consented patients received a static ^{64}Cu-ATSM PET/CT scan of the head and neck approximately 1 week prior to the start of their treatment and a sample of blood for serum and plasma were obtained at this visit.

Treatment was not affected by the study and was in accordance with institutional protocol. All patients received IMRT, 65 Gy in 30 fractions to gross disease and high-risk regions, and 54 Gy in 30 fractions to low risk prophylactic regions over 6 weeks. Concomitant cisplatin 100 mg/m^2 was delivered on days 1 and 29 of RT. Patients received induction chemotherapy of 2 cycles of cisplatin (80 mg/m^2) and 5-fluorouracil (4000 mg/m^2 over 4 days) prior to chemoRT when indicated. Clinical response to treatment was assessed routinely with clinical assessment at 6 weeks and clinical assessment and ^{18}F-FDG PET/CT scan 3 months after completion of chemoRT.

Fifteen eligible patients were recruited in a pilot study, looking specifically at gene/miRNA association with ^{64}Cu-ATSM derived imaging parameters and the feasibility of evaluating circulating miRNAs. The overall study is planned for 40 patients (Figure 3.1) and also includes immunohistochemical staining for hypoxia-related protein expression from the biopsy samples and assessment of hypoxia-related circulating proteins and cytokines in the serum.

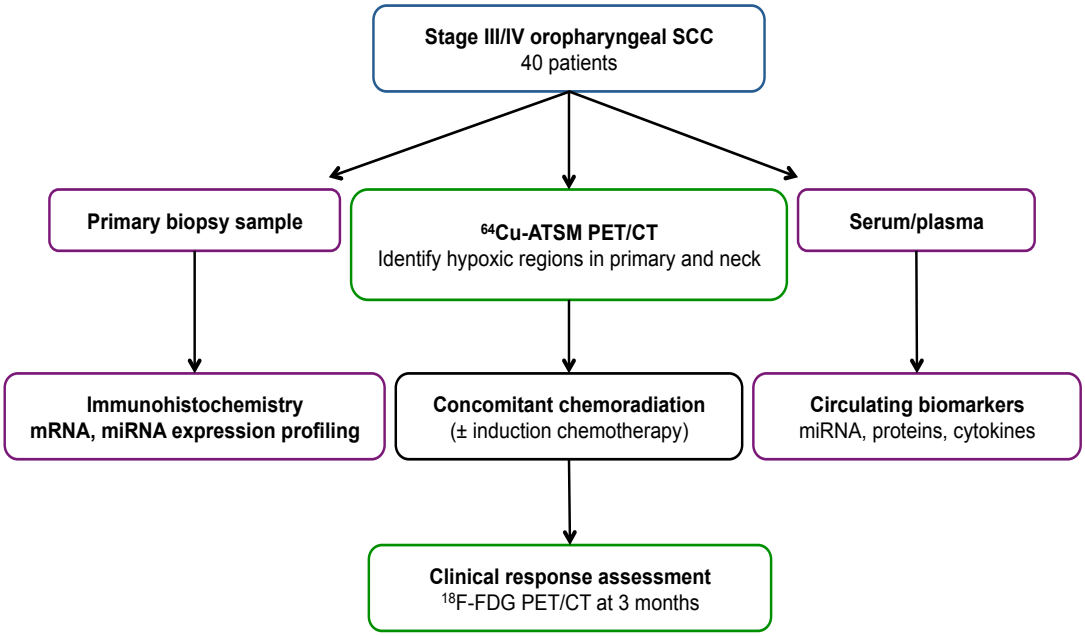

Figure 3.1 Flowchart of overall study plan.

3.3.3 ^{64}Cu-ATSM production

^{64}Cu-ATSM was produced in a CTI RDS-112 cyclotron by the Clinical PET Centre at St Thomas' Hospital, which accelerates protons to 11 MeV. A ^{64}Ni electroplated gold target was bombarded with protons for 5 to 8 hours to produce approximately 1 GBq ^{64}Cu. The ^{64}Cu was separated from the nickel target and other contaminants by dissolving in hydrochloric acid to produce $^{64}CuCl_2$. H_2ATSM was dissolved in dimethyl sulphoxide (DMSO) and added to $^{64}CuCl_2$ to produce ^{64}Cu-ATSM containing solution. This was transferred onto a C18 Sep-Pak Light cartridge, washed with water, and the ^{64}Cu-ATSM eluted from the cartridge with ethanol and diluted with sodium chloride for injection. Quality assurance procedures to check pH, isotope identity and purity were carried out prior to use.

3.3.4 Image acquisition and reconstruction

Patients were injected with 545 ± 27 (range 486 - 577) MBq of ^{64}Cu-ATSM followed by an uptake period of 60 minutes, which was based on in-house data. The first patient

acquisition was performed on a GE Discovery VCT PET/CT scanner (General Electric Medical Systems, Waukesha, Wisconsin, USA). All subsequent patients were imaged on the GE Discovery 710 PET/CT scanner (General Electric Medical Systems, Waukesha, Wisconsin, USA). Patients were positioned supine with their head in a foam head holder and arms down by their sides. First a low dose CT scan was performed from orbits to below the clavicles for attenuation correction and localisation (VCT scanner: 140kVp, 130mA, 0.5s rotation, pitch 1.375:1 and 3.75 mm slice thickness; 710 scanner: 140kVp, 115mA, 0.5s rotation, pitch 1.375:1 and 2.5mm slice thickness). The CT parameters for the new 710 scanner were optimised to improve image quality. A 2 bed position (10 minutes/bed) PET scan of the same region was then acquired in 3-dimentional mode. The PET data was reconstructed using the GE fully 3D OS-EM algorithm (VCT scanner: voxel size 5.47 mm x 5.47 mm x 3.27 mm 1 iteration and 20 subsets, 6 mm full-width-at-half-maximum Gaussian post filter; 710 scanner: 2.73 x 2.73 x 3.27, 2 iterations and 24 subsets, 6.4 mm full-width-at-half-maximum Gaussian post filter. PET data for the 710 scanner incorporated time-of-flight information in the reconstruction.

3.3.4.1 Radiation exposure to patient

The effective dose of radiation was based on a dose of 600 MBq ^{64}Cu-ATSM and was 21.6 mSv for the PET component and 1.1 mSv for the CT component. A total effective dose per scan would expose the patient to 22.7 mSv, with a risk of fatal cancer associated with the additional exposure of approximately 1 in 900. Patients were advised to minimise direct contact or 12 hours and avoid pregnant women for 24 hours as a precaution.

3.3.4.2 Image analysis

The ^{64}Cu-ATSM PET/CT images were interpreted by a nuclear medicine physician and the student using Hermes Hybrid Viewer version 2.2C (Hermes Medical Solutions). PET uptake was assessed semi-quantitatively using standardised uptake values (SUV) normalised to patient body weight determined using the following equation:

SUV_{bw} = ^{64}Cu-ATSM activity concentration measured in the tumour (Bq/cc) x (patient body weight (kg)/injected activity of ^{64}Cu-ATSM (Bq) decay corrected to the time of injection) x 1000 g/cc

Visible lesions on PET with higher than background muscle uptake were considered hypoxic. Background uptake was evaluated by placing fixed 2.5 cm spheres over bilateral posterior neck muscles on the CT images to ensure correct position, transferring the spheres onto the PET images and calculating the average SUV_{mean}. Regions of interest (ROIs) were outlined in multiple planes using a set zoom, SUV scaling and colour scale. An

initial region was drawn using an automatic segmentation seeded region growing tool on each scan slice and manually edited. The seeded region growing technique starts with a seed pixel with the tumour and then adds pixels to the region in all directions. The operator determines the extent of pixel expansion and final region outlined. ROIs were used to create a volume of interest (VOI). For the primary tumour SUV_{max}, tumour to muscle ratio (TMR), SUV_{mean} and hypoxic volume (equal to the VOI) were obtained. For cervical lymph nodes SUV_{max} and TMR were assessed. TMR was determined by the ratio of tumour SUV_{max} to the average SUV_{mean} of the posterior neck muscles.

Abnormal lesions on the CT component were delineated with the aid of diagnostic CT, MRI and ^{18}F-FDG PET/CT, where available, and the number of lesions compared with VOIs outlined on PET.

3.3.5 Blood sample processing

Blood sample collection and serum/plasma separation procedures were adapted from the guidelines from the Early Detection Research Network (edrn.nci.nih.gov). One purple top EDTA Vacutainer for plasma and one red top Vacutainer of blood were taken from each patient and processed immediately in the PET centre. For plasma separation the tube was mixed by inverting gently 8 to 10 times and centrifuged at 1200 x g for 15 minutes. The separated plasma was aliquotted into autoclaved Eppendorf tubes and placed on ice. A further centrifuge step at 3000 x g for 5 minutes was carried out and the plasma transferred into new tubes before storing at -80°C. Serum separation was achieved by mixing the tube gently 5 times and left upright for 30-60 minutes to allow a clot to form. The tube was then centrifuged at 1200 x g for 20 minutes, aliquotted, and placed on ice until transferring to -80°C for long term storage. Between 5 and 6 tubes of 250 µl plasma and serum were obtained.

3.3.6 Biopsy tissue preparation for RNA extraction

OPSCC diagnosis and HPV status were assessed as standard protocol. HPV status was evaluated by both p16 IHC and in-situ hybridisation for high risk subtype DNA. Diagnostic biopsy slides were reviewed by a head and neck pathologist and the tumour outlined on the slide. FFPE tumour blocks were scored with a surgical blade to correspond with the tumour regions on the slide. Ten micrometre thick sections were then cut of the tumour area on a microtome to achieve a minimum of 10 sections with tumour area 100 mm^2 for RNA extraction. All surfaces and equipment were thoroughly decontaminated with RNase AWAY (Thermoscientific) before and in between samples and a new microtome blade was used

for each sample. Samples were placed into autoclaved Eppendorf tubes and sent to BGI TechSolutions, China, for RNA extraction, RNA-Seq and small RNA-Seq.

3.3.7 Bioinformatics

BGI TechSolutions performed RNA-Seq and small RNA-Seq (Illumina HiSeq 2000), filtered the reads to remove adaptors and low quality reads. Bioinformatic analyses were carried out by Dr Katherine Lawler. In brief, RNAseq reads aligned to a reference genome (hg19; BWA v0.7.10-r789) were obtained from BGI and read counts per gene were enumerated using htseq-count (HTSeq v0.6.1p1[495]; union of exons). Read count normalisations and differential expression analyses were performed using DESeq2 v1.6.3.[496] Gene signature activities were estimated from normalised read counts using a weighted sum of *Z*-scores for each gene in the respective gene list, with weights (+1,-1) according to the direction of expression in the original gene signature. Small RNA reads were obtained from BGI and aligned to miRNA mature sequences (MirBase v21 and Rfam v12) using bowtie2 v2.2.5 and read counts per feature were enumerated using reads which were uniquely mapped among reported alignments.

Two published hypoxia signatures were applied to the study samples to assess correlation with ^{64}Cu-ATSM imaging parameters (Table 3.1): the 26-gene signature adapted from Winter et al[112,319] and the 15-gene hypoxia classifier published by Toustrup et al.[321]

Table 3.1 Published hypoxia gene signatures. Adapted from Eustace et al[323] and Toustrup et al.[321]

Winter	Function
ALDOA	Glucose metabolism
ANGPTL4	Lipid and glucose metabolism
ANLN	Cytokinesis
BNC1	Keratinocyte proliferation
C20orf20	Cellular proliferation
CA9	pH regulation
CDKN3	Cellular proliferation
COL4A6	Extracellular matrix metabolism
DCBLD1	Unknown
ENO1	Glucose metabolism
FAM83B	Unknown
FOSL1	Cellular proliferation
GNAI1	Signal transduction
HIG2	Stress response
KCTD11	Apoptosis
KRT17	Keratin production
LDHA	Glucose metabolism
MPRS17	Mitochondrial translation
P4HA1	Extracellular matrix metabolism
PGAM1	Glucose metabolism
PGK1	Glucose metabolism
SDC1	Cellular proliferation
SLC16A1	Glucose metabolism
SCL2A1	Glucose metabolism
TPI1	Glucose metabolism
VEGFA	Angiogenesis

Toustrup	Function
ADM	Stress response
ALDOA	Glucose metabolism
ANKRD37	Protein-protein interaction
BNIP3	Apoptosis
BNIP3L	Apoptosis
C3orf28	Unknown
EGLN3	Regulation of HIF-1 activity
KCTD11	Apoptosis
LOX	Extracellular matrix metabolism
NDRG1	Stress response
P4HA1	Extracellular matrix metabolism
P4HA2	Extracellular matrix metabolism
PDK1	Energy metabolism
PFKFB3	Glucose metabolism
SLC2A1	Glucose metabolism

3.3.8 RNA extraction from plasma and qRT-PCR

RNA extraction from plasma samples was carried out using the Exiquon miRCURY RNA isolation kit for biofluids following the manufacturer's instructions. All surfaces and equipment were decontaminated with RNAse Away before use. After thawing 200 µl of plasma was transferred into a new tube. Five microliters of 5 fmol/µl of synthetic cel-miR-39 spike in (Life Technologies) was added to 60 µl lysis solution BF and then to each sample. The mixture was vortexed and incubated at room temperature for 3 minutes. Twenty microlitres of protein precipitation solution BF was added, the solution vortexes, incubated for 1 minute and centrifuged for 3 minutes at 11000 x g. The clear supernatant was transferred into a new collection tube and 270 µl isopropranol added before loading onto a microRNA mini spin column. This was incubated at room temperature for 2 minutes and then centrifuged for 30 seconds at 11000 x g. The spin column was washed with wash solution containing ethanol and dried by centrifugation 3 times. The RNA was eluted by adding 50 µl of RNA free water onto the membrane of the spin column, incubating for 1 minute and centrifuging for 1 minute at 11000 x g. The RNA was stored overnight and quantified the following day using the NanoDrop Spectrophotometer to provide an indication of the RNA content.

In accordance with the manufacturer's protocol, as determination of yield is not possible or accurate by spectrophotometric reading, the optimum sample input for cDNA production to determine the RNA volume that can be used in the cDNA without inhibiting the RT-PCR reaction, was determined by performing a dilution curve. Five microlitres of RNA was used for assessment of miR-196a and miR-210 (Life Technologies) by qRT-PCR as previously described. All qRT-PCR samples were run in triplicate and the threshold for detection of cycle threshold (Ct) values fixed across all experiments. The level of the housekeeping genes RNU48 and RNU6B were highly variable amongst the plasma samples and therefore the spike in cel-miR-39 was used as the control, and the relative miRNA expression to cel-miR-39 was calculated using the relative standard curve method.

3.3.9 Study statistics

The D'Agostino-Pearson normality test was used to check the normality of the distribution of imaging and circulating miRNA data, before using the Pearson's correlation coefficient (parametric) or Spearman's rank correlation coefficient (non-parametric).

3.4 Results

3.4.1 Patient recruitment and characteristics

Between January 2013 and January 2015, fifteen patients were recruited. Recruitment was severely hampered after the first patient in January 2013 due to a flood in the room housing the cyclotron, followed by the relocation of the PET department at St Thomas' Hospital. When recruitment recommenced in October 2013 there were no HPV-negative OPSCC patients for a number of months and therefore the eligibility criteria was expanded, with relevant permissions, to include HPV-positive locally advanced OPSCC. From March to June 2014 the cyclotron failed to produce ^{64}Cu due to technical issues for 5 consented patients. A further 14 patients were recruited from June 2014 to January 2015 as part of a pilot study. Patient characteristics are summarised Table 3.2.

Table 3.2 Patient characteristics (n = 15).

Study ID	Gender	Age	T stage	N stage	HPV status
1	Female	51	2	2b	Negative
4	Male	60	3	0	Positive
8	Male	71	4	2b	Negative
9	Male	54	2	2b	Positive
10	Male	46	4	0	Positive
11	Female	61	2	2a	Positive
12	Male	64	2	2b	Positive
13	Male	59	3	1	Positive
14	Male	47	3	2b	Positive
15	Male	44	2	2c	Negative
16	Male	66	3	2b	Negative
17	Male	56	2	2a	Positive
18	Male	69	1	2b	Negative
19	Male	64	2	1	Positive
20	Female	60	1	2b	Positive

3.4.2 ^{64}Cu-ATSM uptake

There were no immediate or late adverse reactions after tracer injection. Initial review of the scans demonstrated some tracer remaining in the vessels at the time of the scan, tracking towards the head and neck region on the side of tracer injection in 2 patients (Figure 3.2). This may have resulted in lower tracer delivery to the head and neck region, with reduced availability for uptake by the tumour.

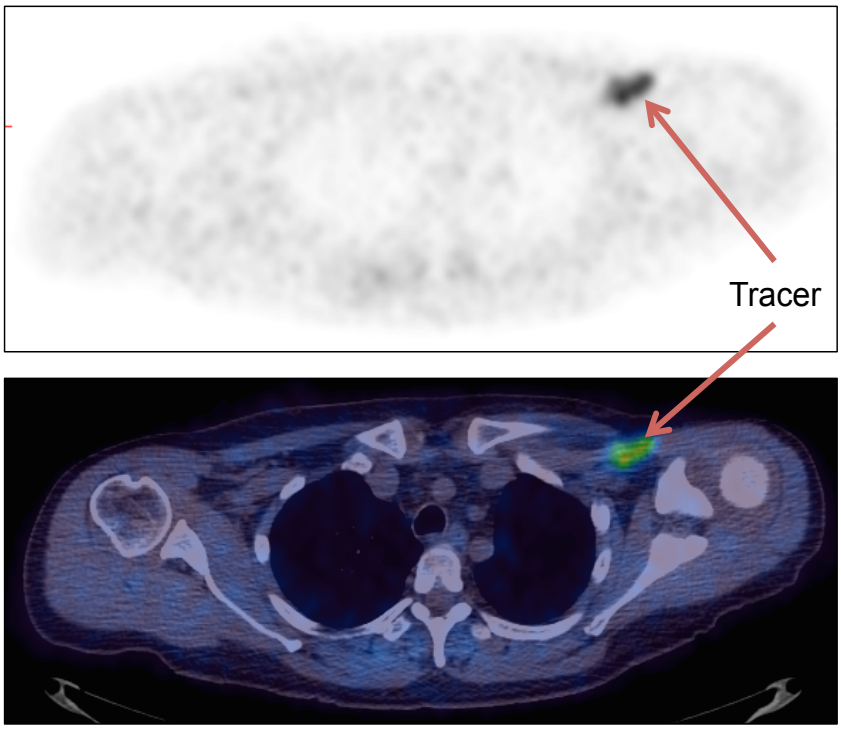

Figure 3.2 Example of ^{64}Cu-ATSM in vein at time of scan.
Viewing axial slices above and below demonstrated the tracer was travelling through the vein on the side of injection at the time of the scan. Top panel is the ^{64}Cu-ATSM PET image and the bottom panel is the coregistered ^{64}Cu-ATSM PET and CT.

Three patients had asymmetrical uptake in their trapezius muscle, making this region unsuitable for background muscle measurements (Figure 3.3).

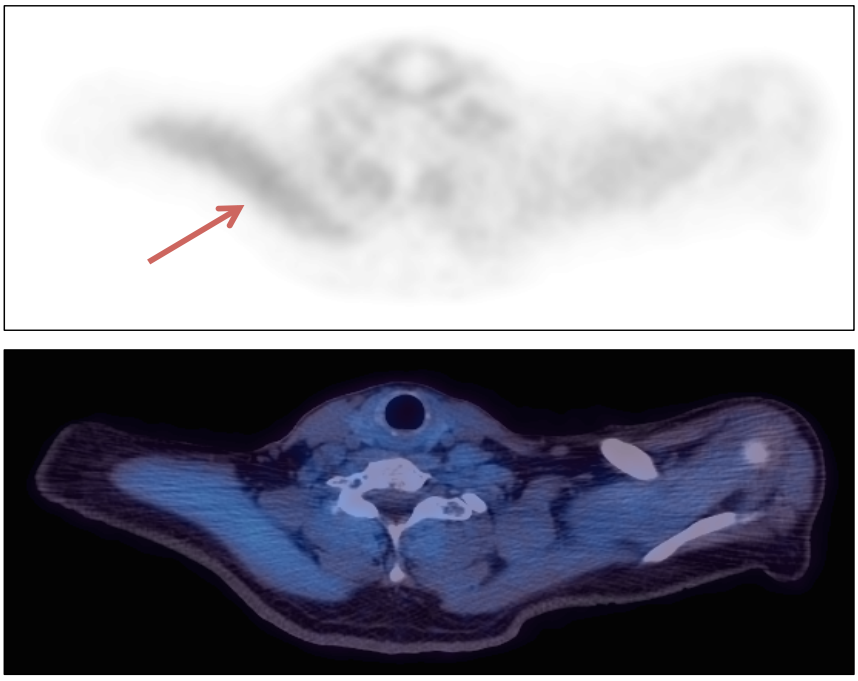

Figure 3.3 Example of increased ^{64}Cu-ATSM in right trapezius muscle.

Eight patients had a staging ^{18}F-FDG-PET/CT scan, which was not part of the study, but visual comparison showed different intensities and patterns of uptake consistent with previous studies (Figure 3.4).[409,410]

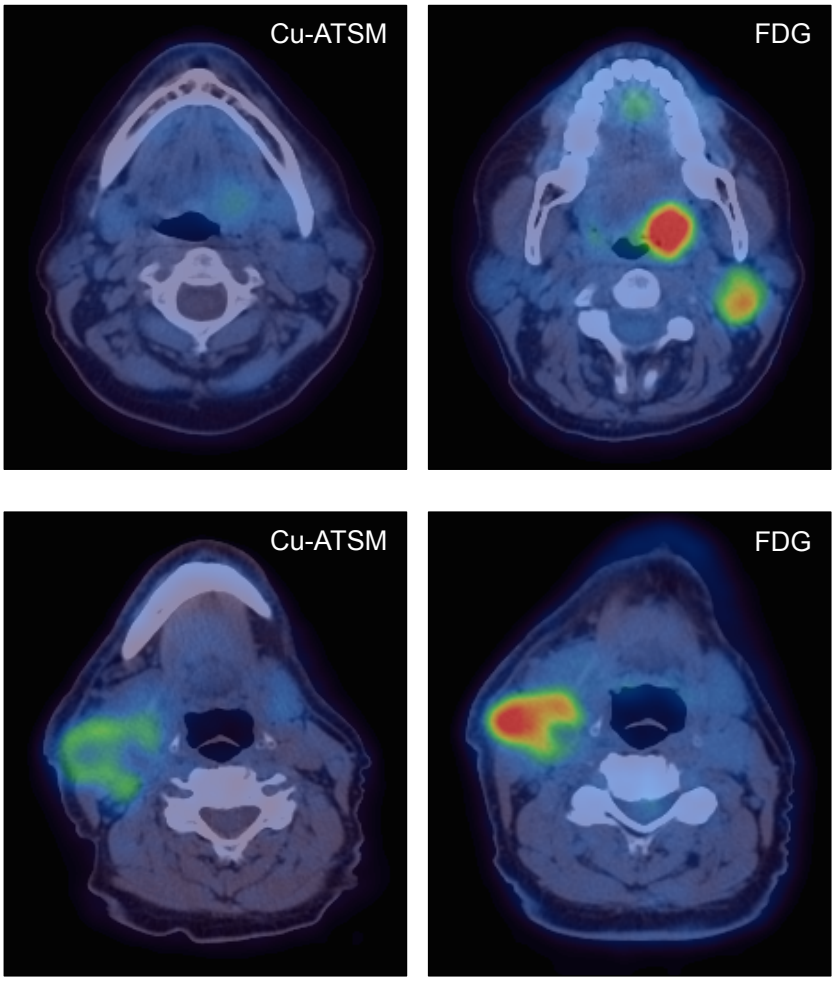

Figure 3.4 Comparison of ^{64}Cu-ATSM PET/CT with ^{18}F-FDG PET/CT.
Top panels demonstrate low ^{64}Cu-ATSM uptake in base on tongue and no uptake in left level 2 lymph node on coregistered PET and CT scans (top left). These regions show high ^{18}F-FDG uptake in same patient (top right). Bottom left image shows a large right lymph node with ^{64}Cu-ATSM uptake in the periphery but more homogeneous ^{18}F-FDG uptake (bottom right). Patients were not scanned in the same position for each scan and image comparisons are centred at the level of the tumour.

3.4.2.1 Uptake in primary tumours and muscle

Uptake was detected in all 15 primary tumours on ^{64}Cu-ATSM PET scans. Regions of interest were outlined around the primary tumour and manually adjusted (Figure 3.5). The mean SUV_{max} for all 15 patients was 3.32 ± 0.85 (median 3.34, range 2.12 – 4.85) (Table 3.3).

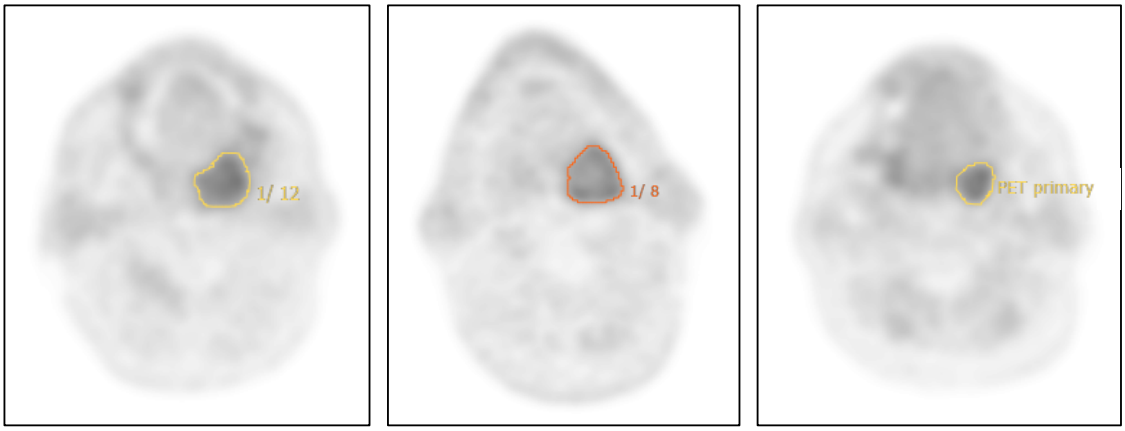

Figure 3.5 Examples of delineation of the primary tumour for 3 patients on axial PET images.

Table 3.3 Summary of uptake parameters for all 15 patients.
The SUV_{max} and tumour to muscle ratio (TMR) were measured. TMR is the ratio of SUV_{max} to average SUV_{mean} of bilateral posterior neck muscle.

Study ID	SUV_{max}	Ipsilateral muscle SUV_{mean}	Contralateral muscle SUV_{mean}	Average muscle SUV_{mean}	TMR
1	2.57	1.04	0.91	0.98	2.64
4	3.61	0.60	0.59	0.60	6.07
8	3.96	0.43	0.45	0.44	9.00
9	2.67	0.75	0.72	0.74	3.63
10	3.14	0.84	0.84	0.84	3.74
11	2.99	0.78	1.07	0.93	3.23
12	4.35	0.80	0.75	0.78	5.61
13	3.83	0.72	0.71	0.72	5.36
14	3.34	0.55	0.58	0.57	5.91
15	4.85	0.99	1.07	1.03	4.71
16	3.75	0.65	0.85	0.75	5.00
17	2.34	0.97	0.64	0.81	2.91
18	2.12	0.80	0.70	0.75	2.83
19	4.21	0.84	0.81	0.83	5.10
20	2.13	1.05	1.26	1.16	1.84

Two patients had diagnostic tonsillectomies at least 4 weeks prior to the ^{64}Cu-ATSM PET scan. The tumour region still showed increased uptake on PET and asymmetry of the tonsillar fossa on CT (Figure 3.6).

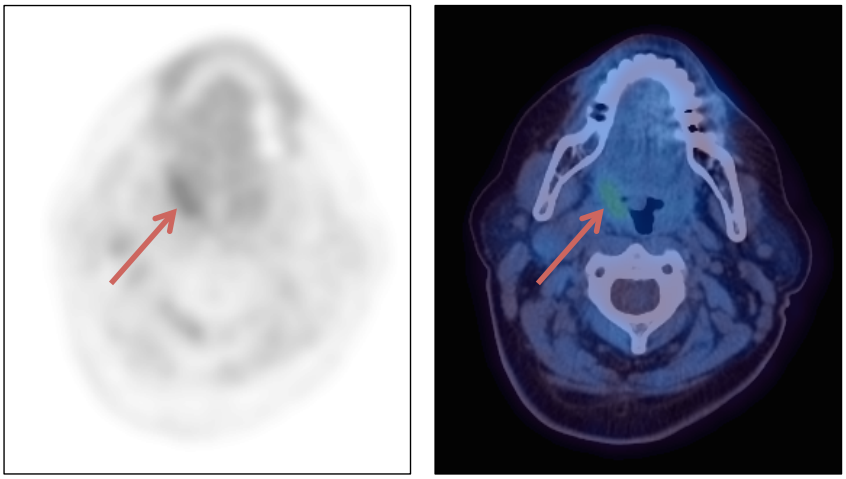

Figure 3.6 Uptake in primary tumour region after diagnostic tonsillectomies.
^{64}Cu-ATSM uptake is seen on PET (left) and asymmetry of the tumour region compared with the opposite side is demonstrated on coregistered PET/CT (right), indicative of residual tumour.

Background uptake was assessed by averaging the SUV_{mean} in fixed spheres placed over bilateral posterior neck muscles (Figure 3.7).

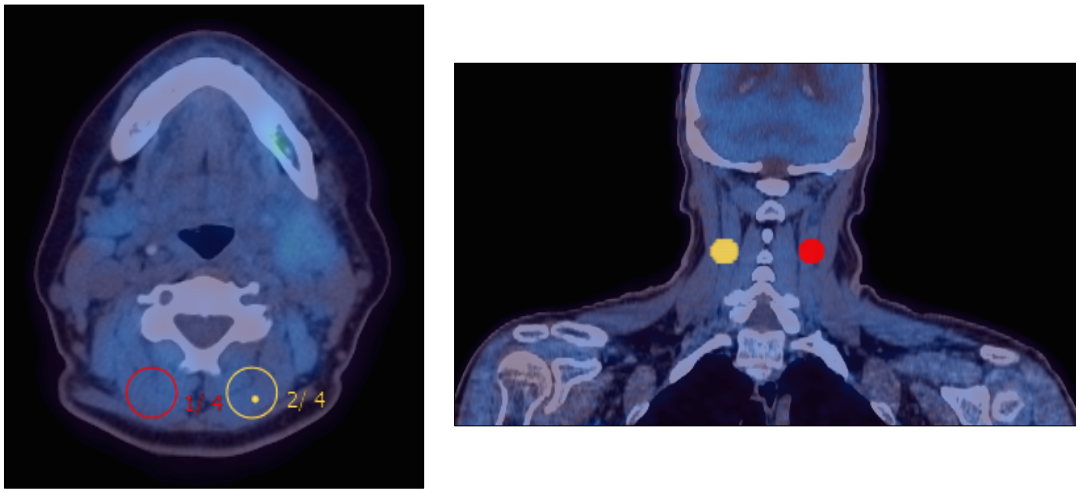

Figure 3.7 Example of spheres placed over posterior neck muscles to measure background uptake.
Spheres were placed on the axial CT images (left), checked on the coronal (right) and sagittal planes, and copied onto the PET images to obtain the SUV_{mean}.

The mean TMR was 4.51 ± 1.82 (median 4.71, range 1.84 – 9.00) (Table 3.3). SUV_{max} and TMR were not significantly different between HPV-positive and HPV-negative patients.

3.4.2.2 Hypoxic volume (HV)

Tonsillectomy patients were excluded from analyses using HV and SUV_{mean}. The mean HV was 12.54 cm^3 ± 11.53 (median 7.55, range 0.68 – 36.89) and the mean SUV_{mean} was 2.34 ± 0.45 (median 2.45, range 1.71 – 3.11) (Table 3.4).

Table 3.4 Hypoxic volume and SUV_{mean}.
Patient in red had tonsillectomies at diagnosis and were excluded from analyses using HV and SUV_{mean}.

Study ID	Hypoxic volume (cm^3)	SUV_{mean}
1	9.78	1.96
4	29.58	2.45
8	5.60	2.46
9	3.28	1.85
10	6.31	2.02
11	5.13	2.29
12	10.76	3.11
13	36.89	2.61
14	7.55	2.27
15	21.66	2.94
16	23.01	2.58
17	2.15	1.90
18	0.68	1.71
19	7.51	2.68
20	1.49	1.77

3.4.2.3 Uptake in cervical lymph nodes

Increased uptake was detected in 22 lymph nodes on ^{64}Cu-ATSM PET scans (Table 3.5). When reviewing the number of abnormal lymph nodes using the CT component of the scan, with guidance from diagnostic imaging, there were 31 lymph nodes in total. Figure 3.8 shows an example on abnormal lymph node visible on CT only. Lymph node uptake was more heterogeneous than uptake in the primary, especially in large nodes which showed uptake in the periphery with central regions of no uptake secondary to necrosis (Figure 3.9).

The mean SUV_{max} of the nodes was 2.43 ± 0.93 (median 2.31, range 1.39 – 5.80) and the mean TMR 3.29 ± 2.41 (median 2.85, range 1.35 – 13.18). In general the uptake in the nodes were lower than the primary. The exception was patient 8, who had a large conglomerate lymph node mass (Figure 3.4 lower panel). This is not consistent with the

data from Eppendorf oxygen electrodes where lymph nodes were used as surrogates for tumour hypoxia.[235]

Table 3.5 Summary of uptake in regional lymph nodes.

Study ID	Lymph node SUV_{max}	Lymph node TMR
1	1.77	1.82
8	5.80	13.18
	2.19	4.98
9	3.55	4.83
	3.05	4.15
11	1.92	2.08
12	2.61	3.37
	2.43	3.14
13	1.62	2.27
14	1.91	3.38
	2.59	2.71
15	3.21	3.12
	2.33	2.26
	1.39	1.35
	1.56	1.51
	1.91	1.85
16	2.22	2.96
17	2.29	2.84
18	2.62	3.49
	1.78	2.37
19	2.36	2.86
20	2.36	2.04

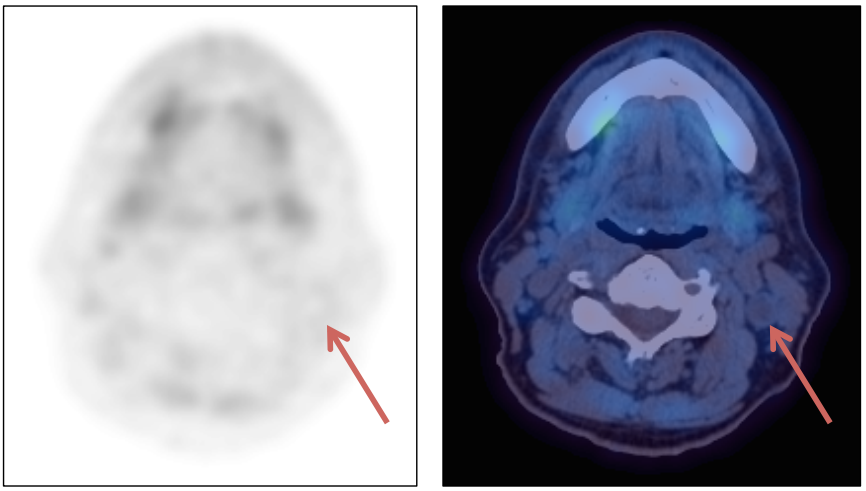

Figure 3.8 Lymph node visible on CT (right) but not on ^{64}Cu-ATSM PET (left).

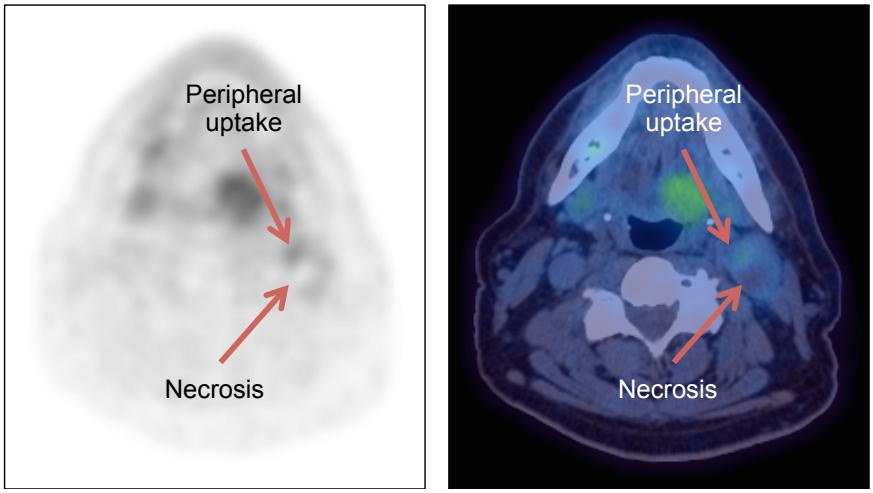

Figure 3.9 Lymph node with peripheral ^{64}Cu-ATSM uptake and central necrosis.

The uptake in the SUV_{max} and TMR in the nodes was compared with the uptake in the primary. For patients with multiple nodes the average uptake was compared, and for the 2 patients with N0 disease the primary uptake was plotted against their background uptake. There was no pattern observed comparing SUV_{max} but there was a positive trend with TMR (Figure 3.10).

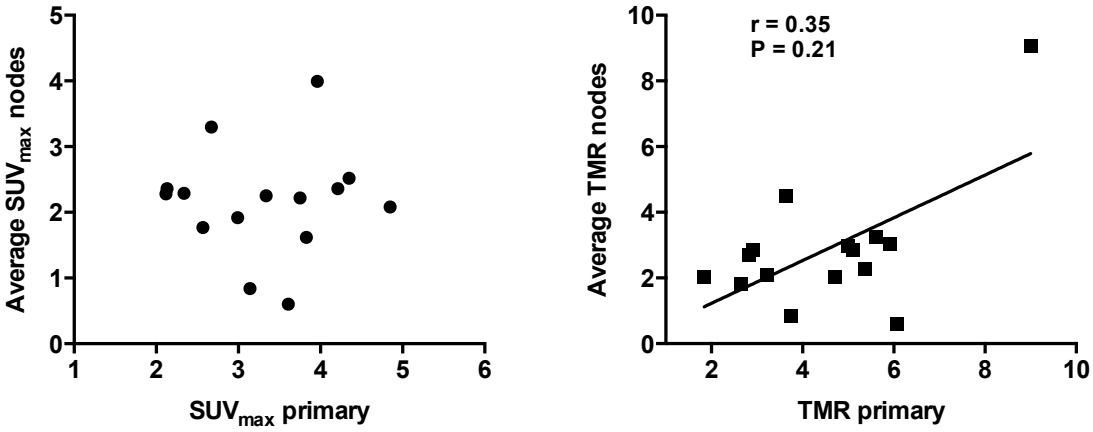

Figure 3.10 SUV_{max} and TMR in primary tumour compared with cervical lymph nodes.
Correlation was assessed using Spearman's correlation coefficient.

3.4.2.4 Other uptake

^{64}Cu-ATSM uptake was seen in the maxilla and mandible, consistent with recent dental extractions (Figure 3.11).

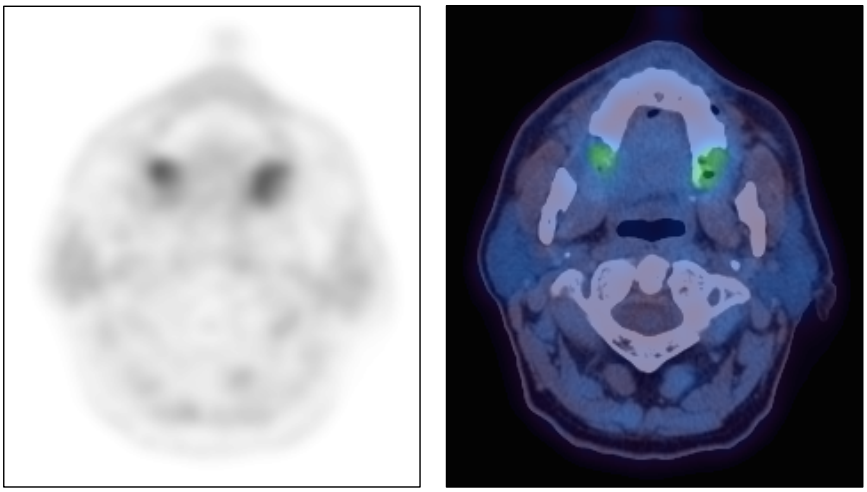

Figure 3.11 Uptake in maxilla after multiple bilateral dental extractions.

All patients had uptake in their salivary glands, in particular in the submandibular glands (Figure 3.12). The average SUV_{max} was 2.20 ± 0.43 (range 1.69 – 3.06) for the submandibular gland ipsilateral to the primary tumour, and 2.08 ± 0.39 (range 1.53 – 2.87) for the contralateral gland. The average SUV_{max} was 1.41 ± 0.22 (range 0.98 – 1.72) and 0.39 ± 0.20 (range 1.07 – 1.64) for the ipsilateral and contralateral parotid glands respectively.

3.4.2.5 Clinical response

One patient died 2 weeks after completion of treatment of bilateral pneumonia but no evidence of cancer. The remaining 14 patients have had a clinical and radiological complete response, assessed by ^{18}F-FDG PET/CT, at 3 months post-treatment and there have been no recurrences to date.

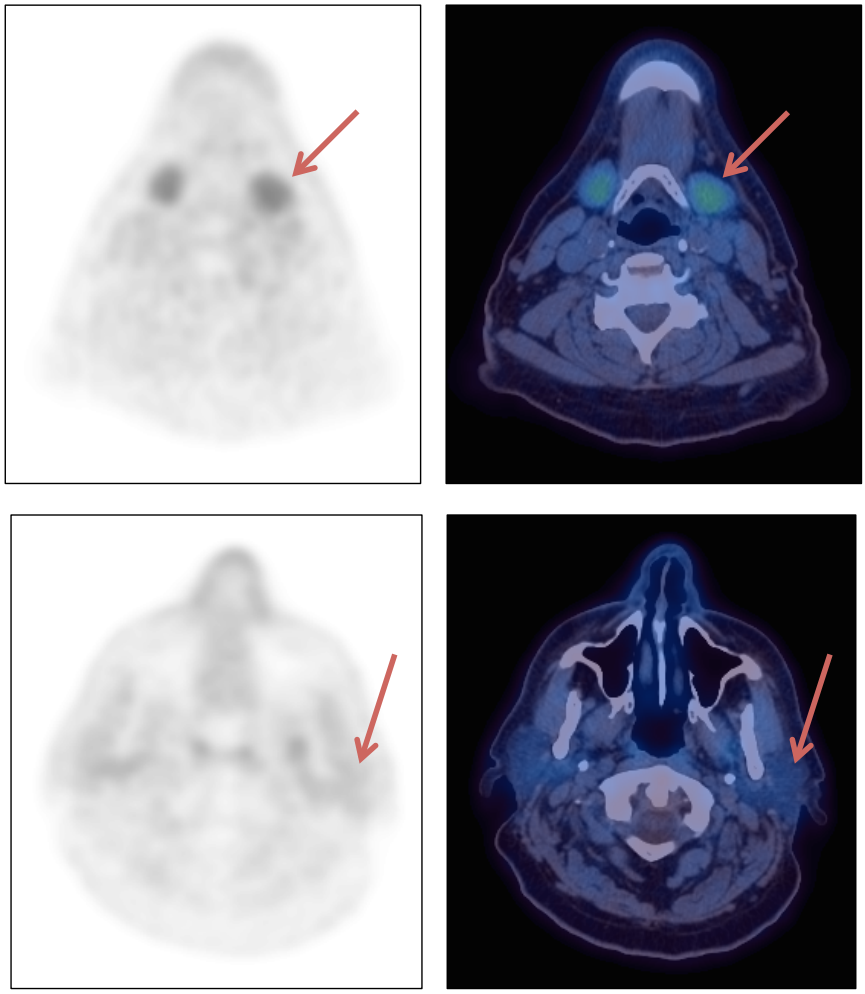

Figure 3.12 Uptake in salivary glands.
All patients showed ^{64}Cu-ATSM uptake in bilateral submandibular glands (top panel) and lower grade uptake in parotid glands (lower panel).

3.4.3 RNA-Seq

RNA extraction by BGI TechSolutions from all 15 samples yielded sufficient RNA concentration with adequate RNA integrity number (RIN) of ≥ 2.3 for both RNA and small RNA sequencing.

As an initial screen to assess gene expression, the differential gene expression between the HPV-positive and HPV-negative samples was compared with previously published HPV-positive and HPV-negative gene expression patterns (Figure 3.13).[497,498] These gene expression patterns were obtained using fresh tumour samples and genome-wide microarrays. Overall the pattern of gene expression profiles of HPV-positive versus HPV-negative of our samples were readily distinguishable and consistent with previous studies. In particular, HPV-positive tumours expressed high levels of *CDKN2A* compared with HPV-negative tumours, whereas HPV-negative samples expressed high *CCND1*.

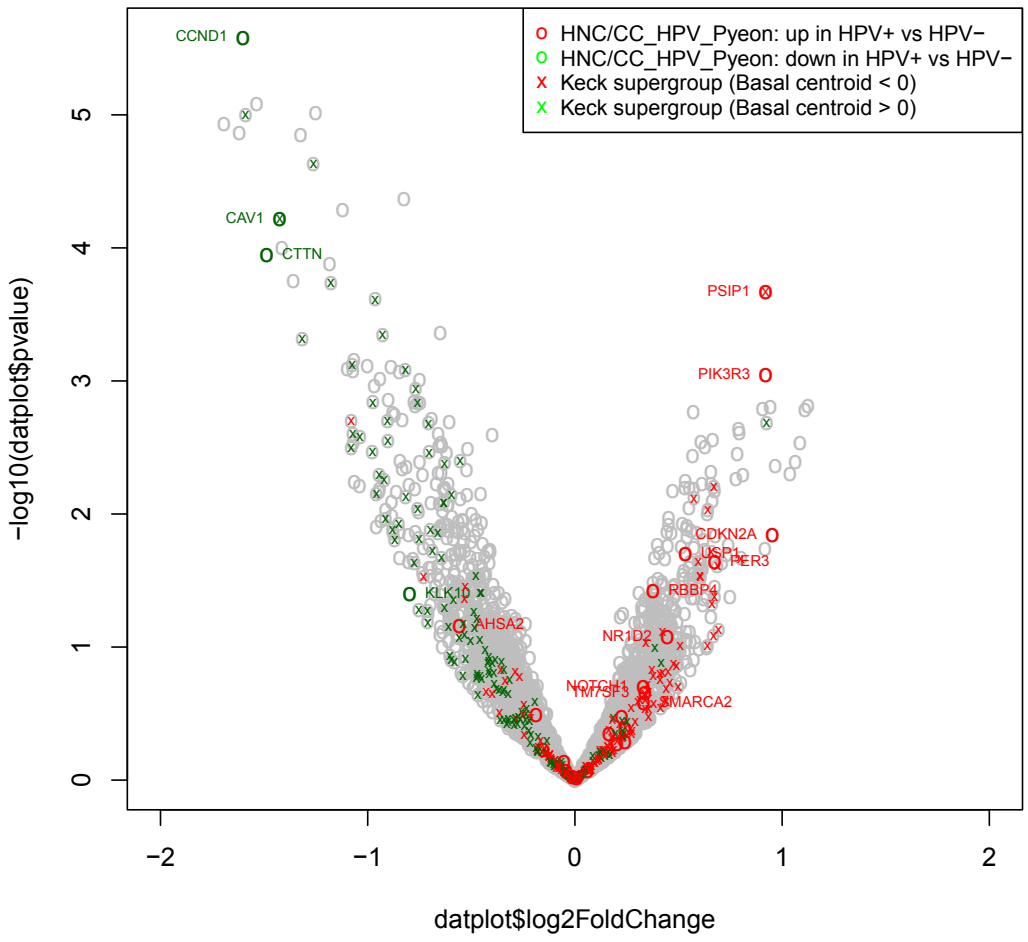

Figure 3.13 Differential expression of genes associated with HPV status.
Volcano plot showing genes differentially expressed between samples from HPV-positive versus HPV-negative tumours, filtered to show genes with more than 200 reads (baseMean > 200). Point labels indicate overlaps with genes previously reported to be differentially expressed in HPV-positive versus HPV-negative tumours.[497,498]

3.4.3.1 Comparison with published hypoxia signatures

Due to the small number of patients recruited, we initially compared the gene expression to the two main published hypoxia signatures used to assess hypoxia, the Winter signature (Winter2007)[112] and the 15-gene hypoxia classifier (Tousrtup2011).[321] The samples were ranked from low to high expression of the signatures and the level of expression compared (Figure 3.14). There was high correlation between the two signatures in our samples.

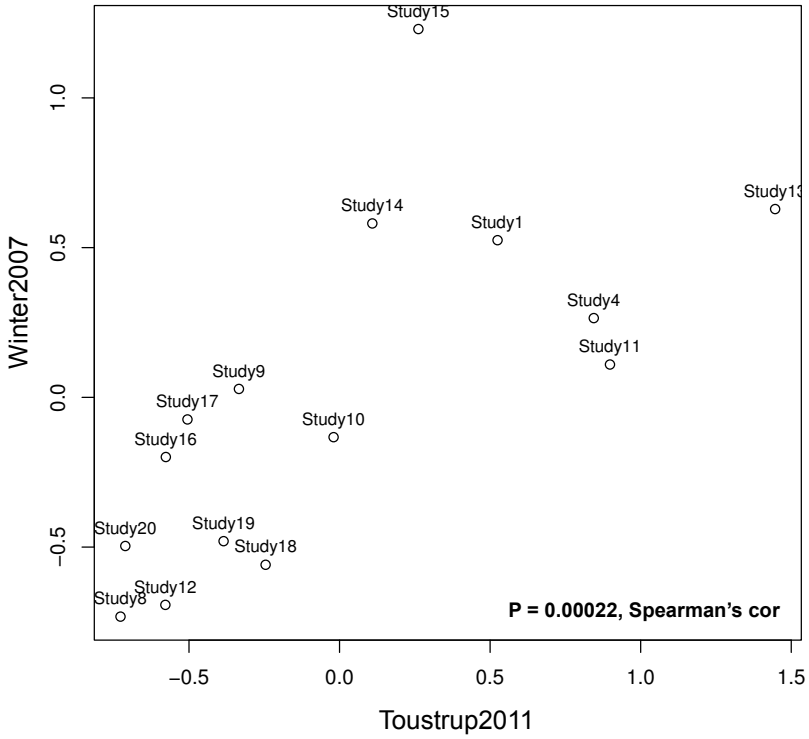

Figure 3.14 Winter and Toustrup hypoxia gene expression signatures correlated in biopsy samples.
The mean weighted score for each gene in the published hypoxia gene expression signatures was assessed in the study samples and ranked from low to high expression. There was strong correlation between the expression of the Winter2007 and Toustrup2011 signatures in the study samples.

The level of expression of the hypoxia gene signatures in our samples was correlated with ^{64}Cu-ATSM imaging parameters (Figure 3.15, Figure 3.16). There was significant correlation between the expression of both signatures and hypoxic volume, but not TMR or SUV_{max}, indicating that hypoxic volume may be a more important imaging parameter of hypoxia.

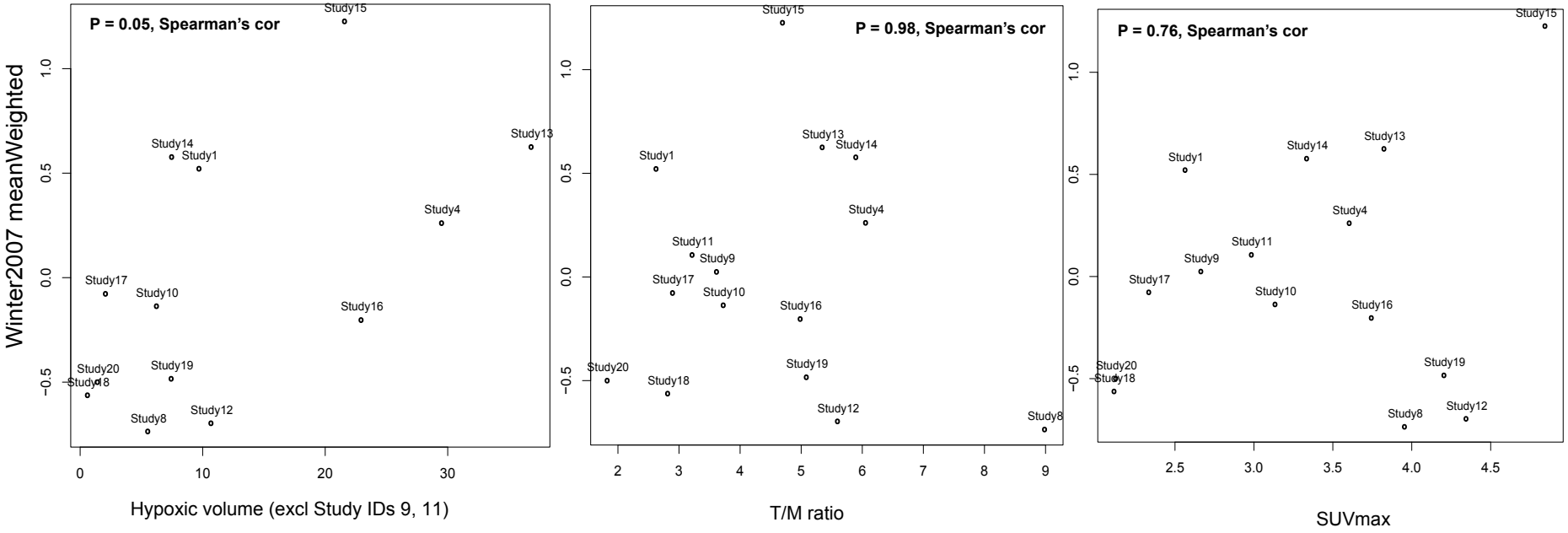

Figure 3.15 Scatterplot of ^{64}Cu-ATSM imaging parameters and Winter hypoxic signature.
Hypoxic volume, TMR and SUV_{max} plotted against the 26-gene hypoxia signature. A significant positive correlation is observed between the hypoxia score and hypoxic volume, but not TMR or SUV_{max}. Samples from patients who had diagnostic tonsillectomies (Study IDs 9 and 11) were excluded as a hypoxic volume could not be determined.

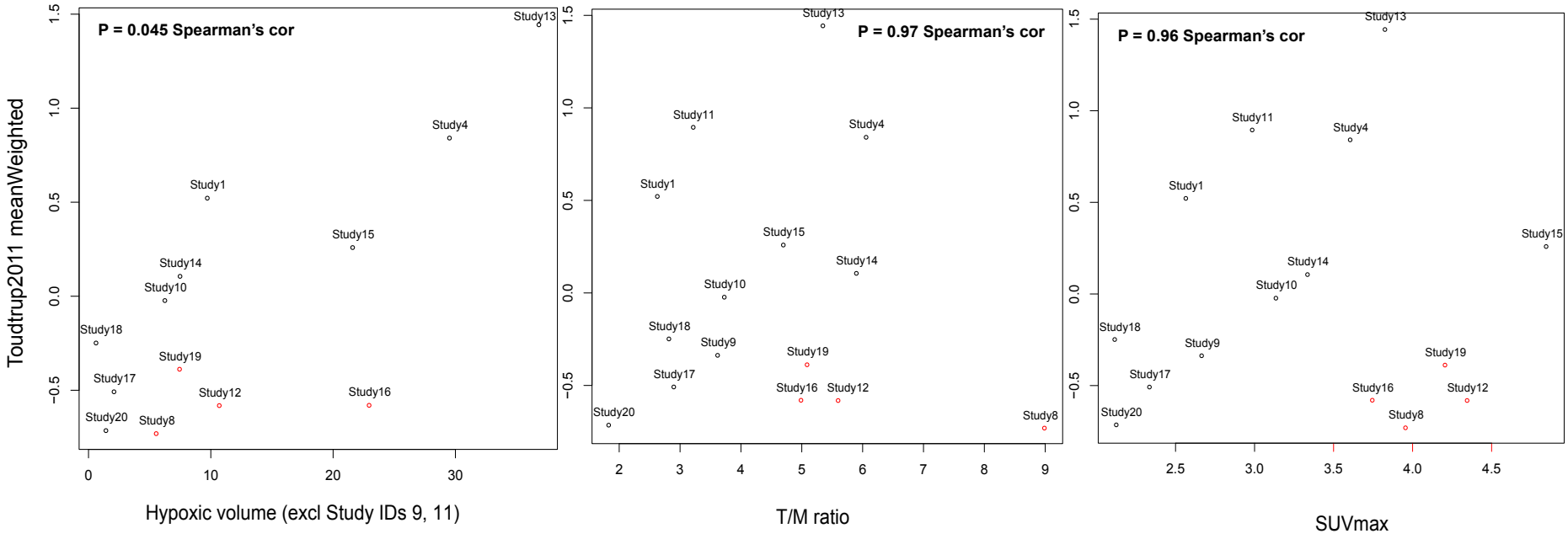

Figure 3.16 Scatterplot of ^{64}Cu-ATSM imaging parameters and Toustrup hypoxia classifier.
Hypoxic volume, TMR and SUV_{max} plotted against the 15-gene hypoxia classifier. A significant positive correlation is observed between the hypoxia score and hypoxic volume, but not TMR or SUV_{max}. Red points indicate samples with low hypoxia score but high SUV_{max}. Samples from patients who had diagnostic tonsillectomies (Study IDs 9 and 11) were excluded as a hypoxic volume could not be determined.

The scatterplots of the hypoxia signatures, particularly the 15-gene classifier, versus SUV_{max} suggest there is a group of samples (n = 4) which have a high SUV_{max} but are low scoring for expression of the hypoxia signatures. A similar effect is seen with TMR in the same samples, suggesting there may be two subpopulations. There were no significant differences in the baseline characteristics between the 'subopulation' and the other samples.

3.4.3.2 De novo gene signature for hypoxic volume

Hypoxic volume was further investigated as it showed a positive correlation with hypoxia signatures. If the hypoxic signatures describe a hypoxic phenotype in the study samples, looking for genes differentially expressed by hypoxic volume could define more accurate ^{64}Cu-ATSM-specific hypoxia signature. The samples were ordered by increasing hypoxic volume and the gene expression analysed. There were two genes which overlapped with the 15-gene hypoxia classifier, *LOX* and *PFKFB3*. In addition when the samples were ranked using the 15-gene hypoxia classifier, in general, there was concordance between the hypoxic volume gene signature and higher hypoxia score (Figure 3.17).

The name and function of the genes in the hypoxic volume gene signature are summarised in Table 3.6. A number of the overexpressed genes encode proteins that are involved in cytoskeletal and extracellular matrix remodelling (*GJB6, LOX, TPM4, CDCP1*) suggesting increased turnover of cells or enhancing the potential for increased cell motility. Other overexpressed genes include those involved in the regulation of inflammatory responses (*IL20RB, S100A7*) and angiogenesis (*S100A7*). Interestingly there are a few genes with specific roles in the glucose metabolism/oxidative phosphorylation pathway (*SOD2, NAMPT, PFKFB3*). There was no clear pattern for the downregulated genes.

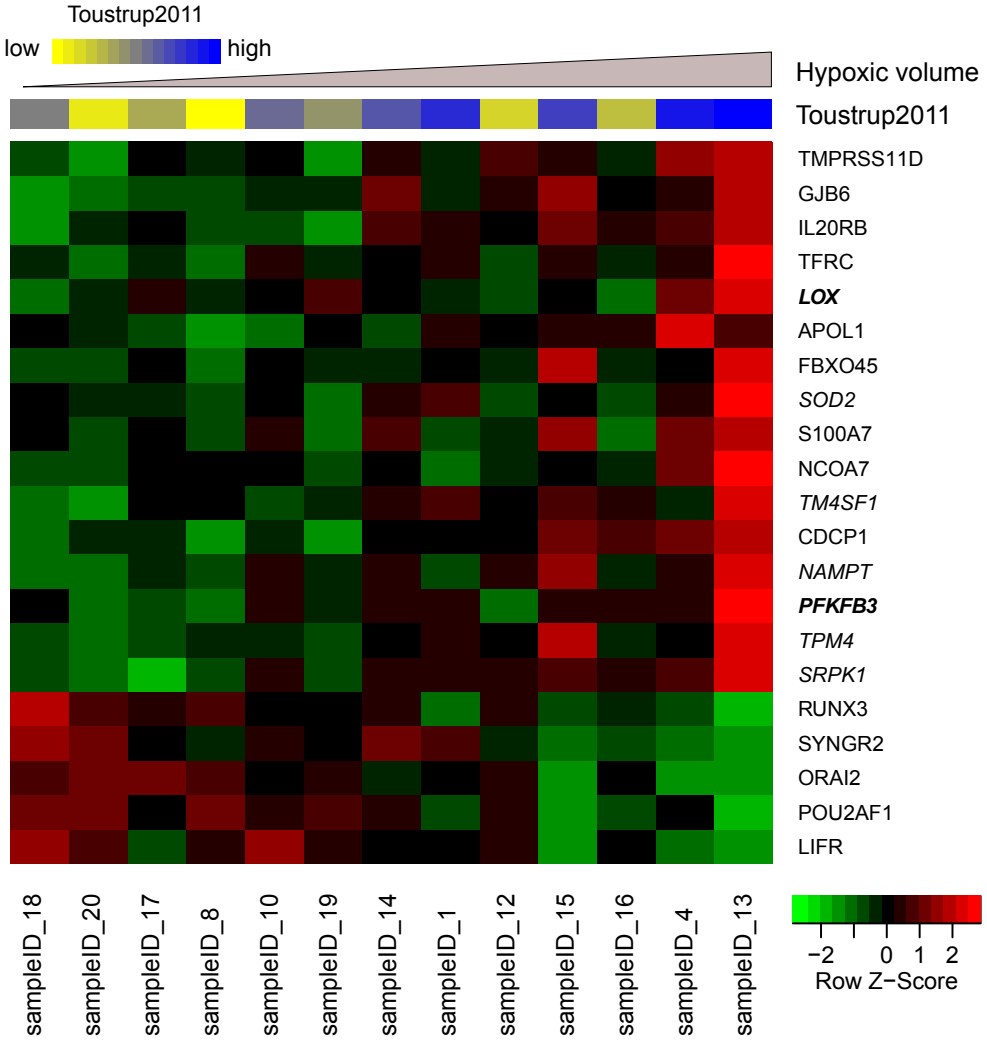

Figure 3.17 Gene expression associated with hypoxic volume.
Samples were ordered by increasing hypoxic volume and the gene expression analysed (reads > 200, adjusted P < 0.05; or *italicised*: adjusted P < 0.1). Two genes which overlapped with the 15-gene hypoxia classifier gene list are shown in bold. Yellow and blue colour bar shows the hypoxia 15-gene classifier score by rank within samples (Toustrup2011).

Table 3.6 Summary of genes associated with hypoxic volume.

Gene	Name	Function of protein
TMPRSS11D	Transmembrane protease, serine 11D	Integral membrane protein, trypsin-like serine protease
GJB6	Gap junction protein beta 6	Connexin protein that is part of gap junctions, cell communication
IL20RB	Interleukin 20 receptor beta	Receptor for interleukin 20, a pro-inflammatory cytokine
TFRC	Transferrin receptor C	Cell surface receptor for cellular iron uptake
LOX	Lysyl oxidase	Copper enzyme that initiates the crosslinking of collagens and elastin in extracellular matrix
APOL1	Apolipoprotien 1	Lipid metabolism
FBXO45	F-box protein 45	Protein-ubiquitin ligase
SOD2	Superoxide dismutase	Mitochondrial protein, binds to the superoxide byproducts of oxidative phosphorylation, antiapoptotic role against oxidative stress
S100A7	S100 calcium-binding protein A7	Mediate inflammation, endothelial proliferation and angiogenesis
NCOA7	Nuclear receptor coactivator 7	Coactivates nuclear receptors, involved in oxidation resistance
TM4SF1	Transmembrane 4 L six family member 1	Mediates signal transduction events in regulation of cell development and growth
CDCP1	CUB domain-containing protein 1	Negative regulation of cell adhesion
NAMPT	Nicotinamide phosphoribosyltransferase	Catalyses step in the biosynthesis of nicotinamide adenine dinucleotide
PFKFB3	6-phosphofructo-2-kinase/fructose-2,6-biphosphate 3	Glucose metabolism, required for cell cycle progression and prevention of apoptosis
TPM4	Tropomyosin 4	Actin-binding proteins involved in the cytoskeleton
SRPK1	SRSF protein kinase 1	Regulation of constitutive and alternative splicing
RUNX3	Runt-related transcription factor 3	Tumour suppressor
SYNGR2	Synaptogyrin 2	Unknown
ORAI2	ORAI calcium release-activated calcium modulator 2	Cellular calcium homeostasis
POU2AF1	POU class 2 associating factor 1	B-cell transcriptional co-activator
LIFR	Leukaemia inhibitory factor receptor alpha	Receptor for cytokine leukaemia inhibitory factor, which affects cell growth

3.4.3.3 SUV_{max} differential gene expression

SUV_{max} is a parameter that is not operator dependent and available for all patients, and has been prognostic in previous clinical studies. To further investigate the lack of association between this parameter and published hypoxia signatures samples were split into less than or greater than the median SUV_{max} and differential gene expression assessed (Figure 3.18).

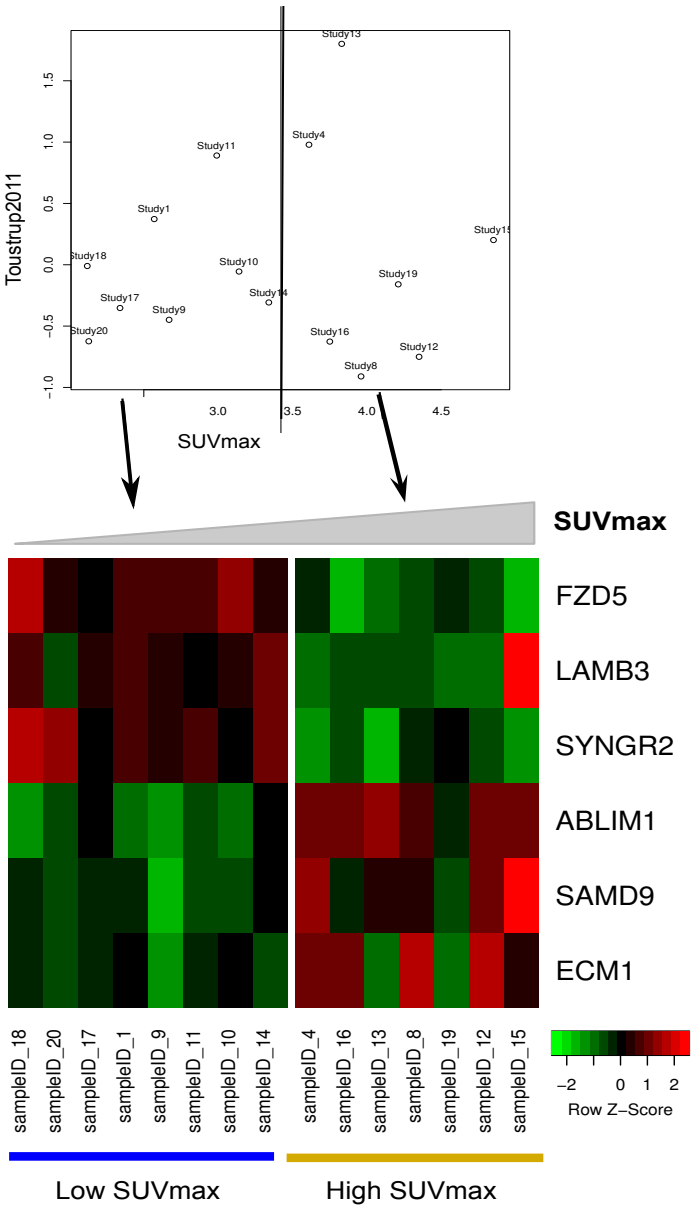

Figure 3.18 Differential gene expression between low and high SUV_{max} samples. The samples were grouped into low and high SUV_{max} using the median SUV_{max} and the differential gene expression compared (adjusted $P < 0.1$).

The function of the proteins encoded by the genes are summarised in Table 3.7. There were no clear links with hypoxia in the genes seen, apart from the overexpression of ECM1 in high SUV_{max} samples, which is important in endothelial cell proliferation and angiogenesis.

Table 3.7 Summary of genes differentially expressed by SUV_{max}.

Gene	Name	Function of protein
FZD5	Frizzled class receptor 5	Receptor for Wnt signalling proteins
LAMB3	Laminin beta 3	Basement membrane protein
SYNGR2	Synaptogyrin 2	Unknown
ABLIM1	Actin-binding LIM protein 1	Cytoskeletal protein, protein binding interface
SAMD9	Sterile alpha motif domain-containing 9	IFN-γ responsive inflammatory response
ECM1	Extracellular matrix protein 1	Promotes endothelial cell proliferation and angiogenesis, inflammatory response

There was no obvious trend with the genes differentially expressed in the high versus low SUV_{max} groups. This may have been affected by the presence of the possible 4 patient subgroup and high SUV_{max} samples may include 2 populations; one with high hypoxic expression according to the 15-gene classifer and one with low hypoxic expression. To look at possible differences in these groups, we compared the gene expression in the 4 high SUV_{max}/low hypoxia score samples with 4 low SUV_{max}/low hypoxia score samples (Figure 3.19).

The function of the proteins encoded by these genes are summarised in Table 3.8. In the high SUV_{max}/low hypoxia score group there is downregulation of genes involved in the inflammatory and immune response.

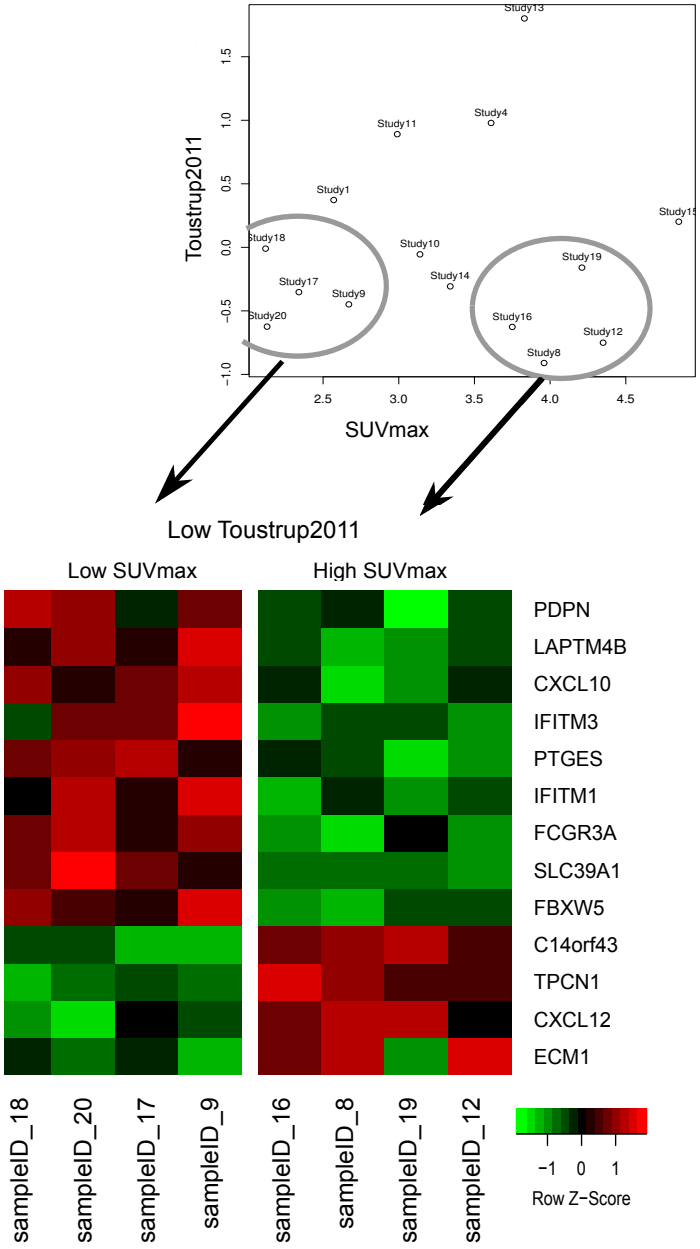

Figure 3.19 Differential gene expression between 4 samples with high SUV_{max}/low hypoxia score and low SUV_{max}/low hypoxia score.
Among biopsy samples with the lowest Tousrup2011 hypoxia score, samples were grouped according to high or low SUV_{max} in the patient's tumour (defined by inspection of scatterplots). The heatmap shows top-ranked genes by evidence of differential expression between the two sample groups (adjusted P < 0.1).

Table 3.8 Summary of differentially expressed genes in low and high SUV_{max} groups.

Gene	Name	Function of protein
PDPN	Popoplanin	Transmembrane glycoprotein, roles in development, cell motility and immune response
LAPTM4B	Lysosomal protein transmembrane 4 beta	Lysosome homeostasis
CXCL10	Chemokine ligand 10	Chemoattracts monocytes, natural killer and T cells, inhibition of angiogenesis
IFITM3	Interferon-induced transmembrane protein 3	Immune response signalling
PTGES	Prostagladin E synthase	Inflammation response
IFITM1	Interferon-induced transmembrane protein 1	Immune response signalling
FCGR3A	Fc fragment of IgG, low affinity IIIa, receptor	Immune response
SLC39A1	Solute carrier family 39, member 1	Zinc uptake transporter on cell membrane
FBXW5	F-box and WD repeat domain-containing 5	Proteosome-mediated ubiquitin-dependent protein, promotes degradation of TSC2
C14orf43	ELM2 and Myb/SANT-like domain-containing 1 (ELMSAN1)	Unknown
TPCN1	Two pore segment-containing channel 1	Calcium transmembrane transport
CXCL12	Chemokine ligand 12	Immune surveillance, inflammation response, angiogenesis
ECM1	Extracellular matrix protein 1	Promotes endothelial cell proliferation and angiogenesis, inflammatory response

3.4.3.4 MicroRNAs associated with hypoxic volume

As the hypoxic volume correlated with the hypoxic signatures, the top ranked miRNAs by association with increasing hypoxic volume were assessed (Figure 3.20). There was no overlap between the miRNAs in our samples and published HIF-1-associated hypoxia response miRNAs.[230] MiR-210 was not found to be upregulated in samples with increasing hypoxic volume defined by ^{64}Cu-ATSM. Samples were also ranked by increasing hypoxia score, as defined by the 15-gene classifier, and miR-31-5p and miR-21-5p were top ranked in samples with increasing hypoxia score (Figure 3.20).

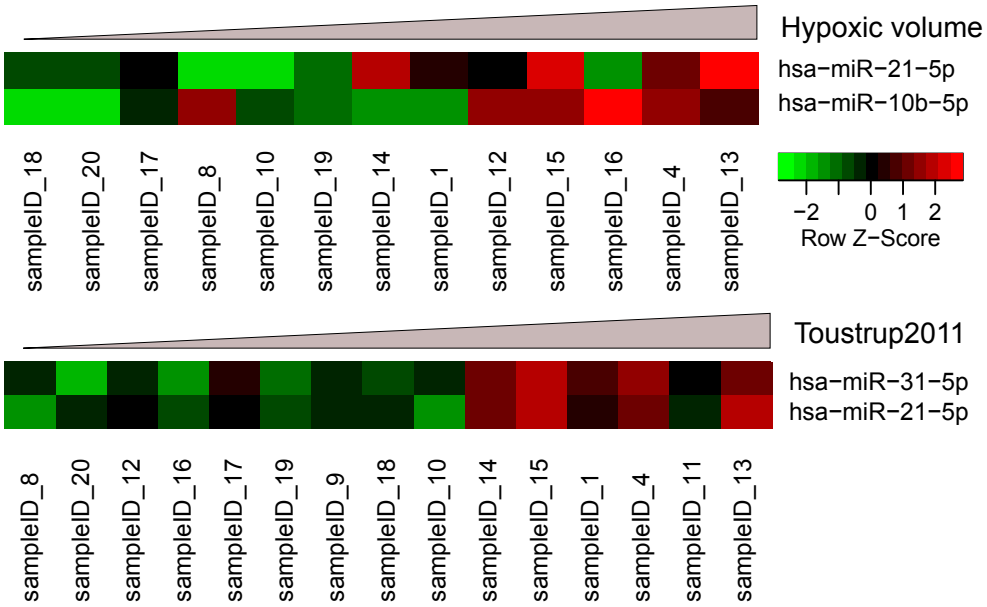

Figure 3.20 MiRNAs associated with increasing hypoxic volume and increasing 15-gene classifier hypoxia score.
Samples were ordered by increasing hypoxic volume and the top ranked miRNAs by association with hypoxic volume are shown (top panel, P < 0.006, adjusted P = 0.99). The top ranked miRNAs by association with the 15-gene classifier Toustrup2011 are shown in the lower panel (P < 0.002, adjusted P < 0.08).

3.4.4 Plasma analysis

RNA extraction from plasma samples was performed in triplicate once 15 patient samples were collected. NanoDrop measurements were taken for each extraction as a broad indication of the presence and quantity of RNA. The concentration ranged from 11.2 – 22.7 ng/µl and the absorbance at 260/280 ranged from 1.29 – 1.79. The expression of the commonly used housekeeping genes RNU48 and RNU6B were measured by qRT-PCR but the Ct values obtained were high, inconsistent and non-reproducible. The Ct values for cel-miR-39 were consistent and reproducible. Two samples were visibly haemolysed and not included in further analyses.

MiR-196a showed no correlation with SUV_{max} and TMR (Figure 3.21). However there was a significant correlation between increasing hypoxic volume and increasing miR-196a levels, assessed by Spearman's rank correlation coefficient (Figure 3.22, left). The tumour volume delineated on the CT images also correlated with miR-196a levels (Figure 3.22, right).

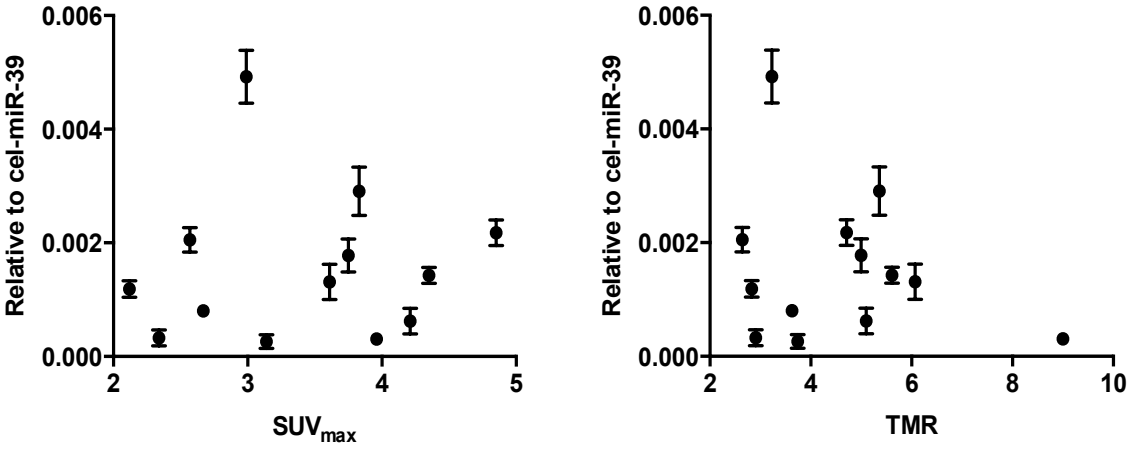

Figure 3.21 Correlation between SUV_{max} (left) or TMR (right) and plasma miR-196a expression relative to cel-miR-39.
MiR-196a expression levels in plasma were measured in triplicate from 3 separate RNA extractions and expressed relative to the expression of an exogenous spike in, cel-miR-39. The levels were plotted against the imaging parameters obtained from ^{64}Cu-ATSM PET/CT scans.

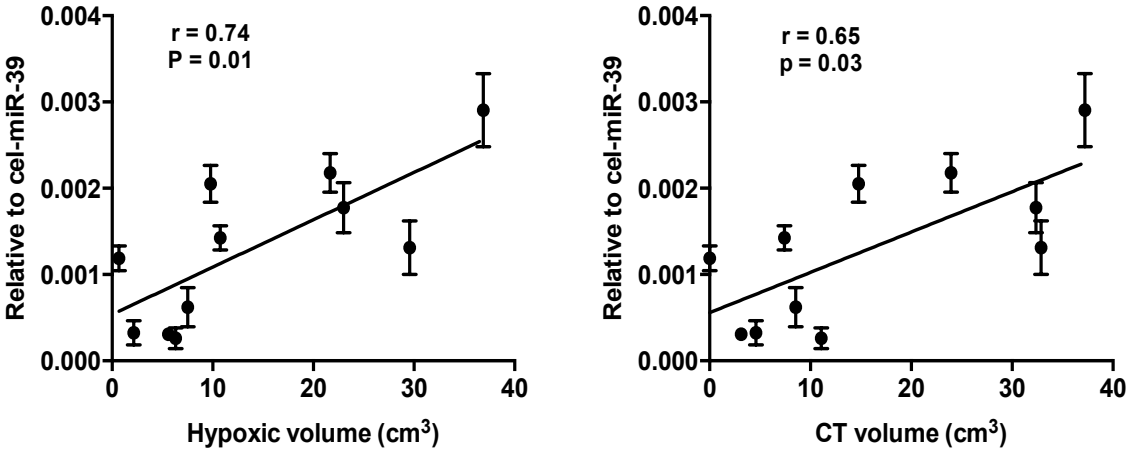

Figure 3.22 Correlation between hypoxic volume (left) or CT volume and plasma miR-196a expression relative to cel-miR-39.
MiR-196a levels were correlated with tumour volumes. The hypoxic volume was delineated on PET images, whereas the CT volume was based on outlining the gross tumour volume seen on the CT component of the ^{64}Cu-ATSM PET/CT scan.

Similarly miR-210 was compared with the imaging parameters. There was a non-significant positive correlation between increasing SUV_{max} or TMR with increasing miR-210 levels in the plasma (Figure 3.23), but no correlation with hypoxic volume (Figure 3.24, left). There was also a positive trend between SUV_{mean} and miR-210 (Figure 3.24, right).

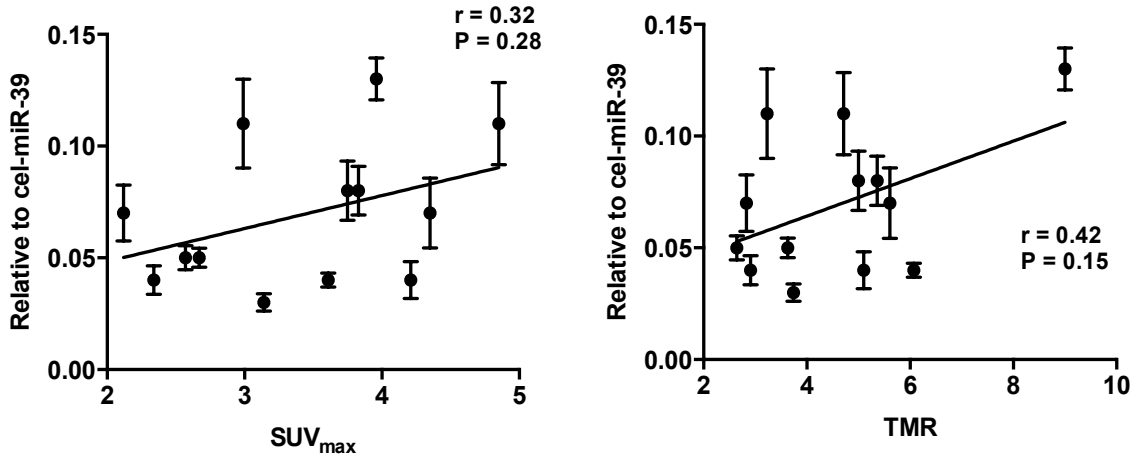

Figure 3.23 Relationship between SUV_{max} (left) or TMR (right) with plasma miR-210 expression relative to cel-miR-39.
MiR-210 expression levels were measured in triplicate from 3 separate RNA extractions and expressed relative to the expression of an exogenous spike in, cel-miR-39. The levels were correlated with the imaging parameters obtained from ^{64}Cu-ATSM PET/CT scans.

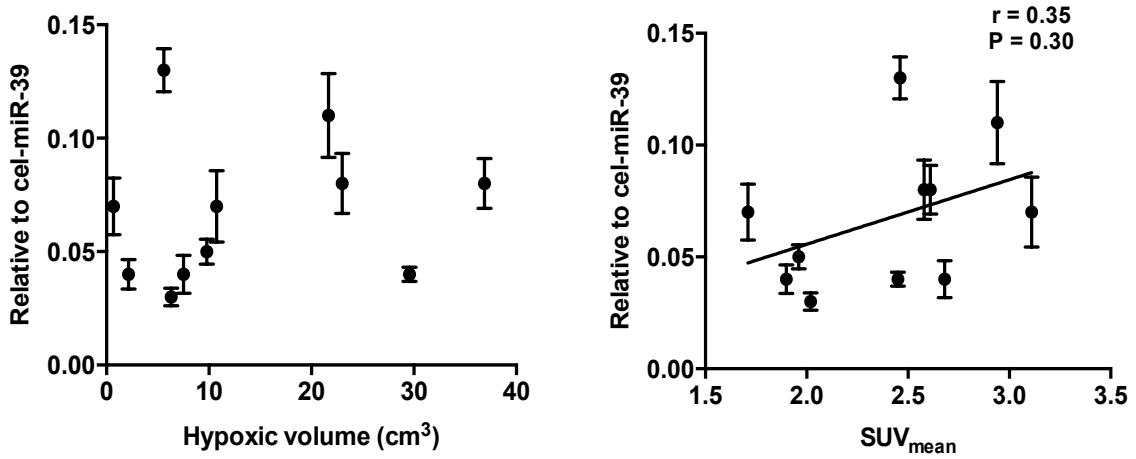

Figure 3.24 Relationship between hypoxic volume (left) or SUV_{mean} (right) with plasma miR-210 expression relative to cel-miR-39.
MiR-210 levels were correlated with hypoxic volume, delineated on PET images, and the SUV_{mean}.

3.5 Discussion

3.5.1 Patient recruitment

The recruitment rate was initially slow due to problems with the production of the tracer and relocation of the PET centre. A second site for recruitment was set up at University College Hospital London, but as ^{64}Cu-ATSM production could not be guaranteed we were unable to recruit from this site during the pilot phase of the study. Locally advanced HPV-negative OPSCC was initially selected for study eligibility as a homogeneous population that would potentially benefit the most from hypoxia-targeted intensification strategies. However, there were few eligible HPV-negative OPSCC patients, reflecting the change in aetiology and incidence of this group in the Western world. Hypoxia has been demonstrated in both HPV-positive and negative OPSCC at the same frequency by pO_2 measurement, CA9[499] and HIF-1α IHC,[500] hypoxia gene expression signature,[324] ^{18}F-FMISO[501] and ^{18}F-FAZA PET imaging.[352] HPV-positive oropharyngeal cell lines in vitro have been shown to upregulate the same hypoxia-related genes as HPV negative cell lines when exposed to hypoxic conditions.[502] However HPV-positive OPSCC demonstrates good outcomes after RT irrespective of hypoxia or hypoxic modification, despite in vitro data suggesting HPV oncoproteins stabilise HIF-1α and contribute to downstream biological effects of hypoxia.[503] Not all HPV-positive tumours have the same good outcome and a subset of these patients may benefit from hypoxia-targeted treatment. Cell line data has shown that although HPV-positive HNSCC have increased intrinsic radiosensitivity compared to HPV-negative cells, they also demonstrate a sensitiser effect with nimorazole similar in magnitude to HPV-negative cell lines.[502] Investigation into the role of hypoxia in HPV-positive OPSCC and the potential for radiotherapy dose reduction in the presence of a hypoxic modifier is therefore warranted as a strategy in these patients.

3.5.2 Cu-ATSM PET as a hypoxia imaging agent

Preclinical studies of Cu-ATSM have shown the tracer to be selective for hypoxic cancers, ischaemic myocardium, and other states of impaired mitochondrial ETC activity, and small clinical studies have demonstrated prognostic potential and response prediction to radiotherapy. Despite many studies investigating the chemical and biochemical properties of Cu-ATSM in vitro an in vivo, the precise mechanism of the pO_2 dependence and factors that can affect cellular uptake and retention in both normoxic and hypoxic tissues is unclear. Emerging evidence suggests that Cu-ATSM may be an indirect marker for hypoxia. Hypoxia results in the accumulation of cellular NADH, which is the primary source of electrons for the mitochondrial electron transport chain (ETC). Hypoxia reduces the availability of oxygen as the terminal electron acceptor in the ETC resulting in the

accumulation of NADH, which is then able to reduce Cu(II) to Cu(I) with subsequent dissociation from ATSM and cellular trapping. However, this mechanism still provides support for Cu-ATSM as a radiotracer to detect hypoxia, although possible other sources of uptake need to be taken into consideration when interpreting the images.

Other uncertainties include the optimal time for hypoxia imaging after injection. One clinical study in 11 HNSCC patients demonstrated that scans at 1 and 16 hours showed no significant difference in the mean SUV_{max} of the primary lesions between the two time points. However they did not report on whether there was any change in the spatial distribution of uptake. Canine studies have suggested temporal changes between early and late scans, whereas rodent studies demonstrate conflicting results when comparing with nitroimidazole-based markers for validation. However, it has been shown that anaesthetic and carrier gases influence the uptake of ^{64}Cu-ATSM and ^{18}F-FMISO by murine adenocarcinoma bearing mice, with different regimes having varied effects, which may have affected animal studies.[504]

Cu-ATSM has also been criticised for variation in uptake with different cell lines, especially prostate cancer cell lines, which may be explained by differences in the extent of trapping and retention of Cu-ATSM, and more specifically due to fatty acid synthase in prostate cell lines.[381] Unreliable uptake is also true for other tracers including ^{18}F-FMISO, which has been shown to be a poor tracer in soft tissue sarcomas,[505,506] and ^{18}F-FDG PET, which is not good for differentiating benign and malignant prostate disease.[507] In general Cu-ATSM shows consistent uptake kinetics in squamous cell carcinomas, but with variable spatial correlation with nitroimidazole-based IHC staining, especially when compared with ^{18}F-FMISO. However it is not surprising that ^{18}F-FMISO correlates well in these situations as the retention mechanism is the same. Unless the differences in uptake and retention of both tracers are known, direct comparisons are likely to result in inconsistent results as they have different underlying mechanisms. Bowen et al,[508] through electrochemical modelling, observed that dual tracer imaging which has been used in preclinical studies, where both Cu-ATSM and ^{18}F-FMISO are injected at the same time, may lead to competition for the cytochrome reductases required for Cu-ATSM reduction by ^{18}F-FMISO, as FMISO is reduced by a larger family of nitroreductases that includes the cytochrome reductases. This may result in higher ^{18}F-FMISO retention compared with Cu-ATSM when imaging at early time points and more equal retention at late time points, which has been seen in some preclinical studies.[380] They also suggested that cell line dependent uptake of Cu-ATSM may be related to variations in enzymatic activity and intracellular pH, and that Cu-ATSM uptake may be more sensitive to changes in low pO_2, whereas FMISO is more

discriminating over larger ranges of oxygen tension. The 2 tracers may therefore both provide information on hypoxia and may be complementary to each other.

3.5.3 ^{64}Cu-ATSM uptake measurements

^{64}Cu-ATSM uptake was mainly assessed using SUVs, which is a semi-quantitative measure of regional tracer uptake commonly used in ^{18}F-FDG PET interpretation. In a region of interest it is the decay corrected tumour activity concentration normalised to injected activity per unit body weight at fixed time point.[509] In this study it provided a simplified surrogate measure of tracer uptake that allowed intra- and inter-patient quantification and comparison, as well as correlation with other molecular markers. Full quantitative measures require arterial blood sampling, dynamic scanning and kinetic modelling, limiting patient recruitment and direct clinical applicability. This has already been carried out in a previous in-house study, which showed stable tracer uptake from approximately 15 minutes post-injection, and guided the protocol used for static imaging at 60 minutes post-injection in the current study.

3.5.3.1 SUV

The SUV_{max} reflects the highest voxel value within a ROI or VOI, and is the most widely used parameter. It is independent of ROI definition, less observer dependent and more reproducible.[509] The SUV_{max} ranged from 1.39 to 5.80 in lesions with uptake seen on PET images. A study using ^{64}Cu-ATSM in 11 HNSCC reported a higher mean SUV_{max} in tumour (various subsites) and nodes of 16.2 ± 7.9.[412] The reported mean SUV_{max} in the primary tumour only in HNSCC studies using ^{62}Cu-ATSM was 5.48 ± 1.69 (range 1.75 – 7.55 in 15 patients)[407] and using ^{61}Cu-ATSM was 4.6 ± 2.3 (range 2.2 – 9.3 in 11 patients),[410] which again are higher than the mean SUV_{max} of 3.32 ± 0.85 (range 2.12 – 4.85) in our patient population.

Other SUV measurements reported in previous studies include SUV_{mean} and SUV_{peak} using ^{61}Cu-ATSM in OPSCC.[410] The SUV_{mean} incorporates uptake from multiple voxels but changes depending on the definition of the VOI, resulting in intra- and interobserver variability.[510] The reported SUV_{mean} ranged from 0.7 to 2.8 (average 1.5 ± 0.6), which is lower than that seen in our study. However this group defined the gross tumour volume (GTV) on CT images, expanded the volume by 2 mm after coregistering the CT and PET images. This is not likely to reflect the hypoxic volume of the tumour, which may be a subvolume within the GTV, resulting in lower SUV_{mean} values. SUV_{peak} is the average SUV in 8 voxels surrounding the voxel with highest activity and has been suggested to be more representative of the tumour uptake than SUV_{max}, whilst maintaining high reproducibility.[511]

However this parameter requires a minimum size of tumour and was not available in 4 out of our 15 patients.

The main limitation of utilising SUV parameters to quantify hypoxia is that a single value is used to describe a heterogeneous tumour mass, which does not take into account the complex mixture of hypoxic, necrotic and inflammatory cells, blood vessels and metabolism. Many factors affect SUV including technical errors, such as inaccurate estimation of residual tracer activity in administration system, resulting in lower net administered dose and lower SUV.[509] This usually refers to the syringe and tubes used, which is measured post-injection, but may have also affected the SUV of the 2 patients who had uptake in their vascular system at the time of the scan. It is unclear why this occurred; no discomfort or signs suggestive of extravasation were apparent during or after injection but the tracer may have caused irritation and inflammation of the vein during delivery.

The PET image acquisition and reconstruction procedures can have an impact on the SUV, as well as interscanner variability.[512] After the first patient was scanned there was a delay of over a year, and the remaining patients were scanned on a more advanced PET scanner with improved image acquisition parameters. Although reconstruction procedures were performed to ensure similar interpretation the images from the new scanner were of higher resolution (Figure 3.25), which may affect tumour volume outlining.

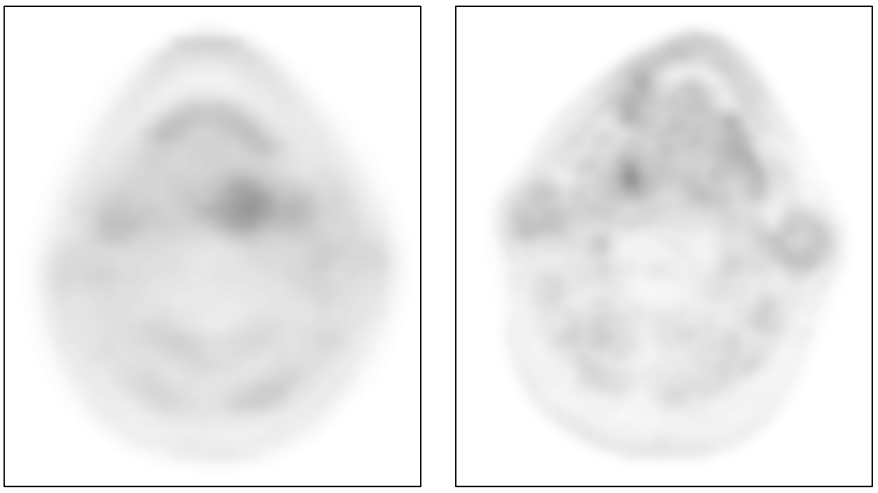

Figure 3.25 Different image quality between PET scanners.
The first patient recruited to the study was scanned in a different PET scanner to the remaining 14 patients. The images from the old scanner (left) is of slightly lower quality than images from the new scanner (right).

Other general limitations of PET can affect SUV. The 2 coincident photons travelling in opposite directions from the positron decay of ^{64}Cu are detected by scintillation crystals in a ring around the patient. They record photon pairs that interact at approximately the same time with a pair of detectors, and an image reconstruction algorithm is used to compute the image of the tracer distribution from the collected coincidence count data. Corrections are required for tissue attenuation, non-uniform detector activity, scattered and random coincidence events when photons are deviated from their true path, and dead time when the scintillation crystal is unable to record photon counts until the detection process is complete. These factors and the finite number of photon detection lead to noise, to which SUV_{max} is more susceptible, due to loss of precision.[510] There is limited spatial resolution of approximately 4 mm due to factors such as positron range, non-colinearity of the photon pair and the detector size, resulting in the spill in or out of activity into adjacent voxels, known as partial volume effects.[509] The partial volume effect means that a small source of radioactivity may show up as a larger less intense source, underestimating SUVs. Two patients had T1 tumours, of which one did not have a tumour visible on CT imaging but detected on PET imaging and histology, and 2 patients had tonsillectomies, which may have significantly reduced the tumour size. Newer scanners have better sensitivity with better corrections and image reconstruction, including time of flight data, which records the precise time that each of the coincident photons is detected and calculates the difference to accurately locate the site of the annihilation reaction along the line of the 2 detectors, and therefore imaging analysis and interpretation are constantly improving.

3.5.3.2 TMR

Kinetic analysis demonstrated that muscle activity is essentially stable after the first 10 minutes post-^{60}Cu-ATSM injection and parallels the time course of the tracer in blood. The muscle activity has therefore been used as an estimation of blood activity, as it avoids blood sampling, to estimate the net trapping of radiotracer in a tumour under blood activity of constant value.[396] TMR performed better as a prognostic indicator in lung and cervix cancers in Cu-ATSM PET studies.[396,399] In HNSCC one group found a TMR cut off of 3.2 to be associated with better outcome,[408] whereas another group found no difference in TMR between responders and non-responders to treatment.[407] Both studies used SUV_{max} to calculate the TMR, but one study used bilateral sternocleidomastoid muscles as the background uptake, whilst the other used posterior cervical muscle groups. We investigated the sternocleidomastoid muscles as a measure of background uptake, but these were in close proximity to metastatic cervical lymph nodes and salivary glands with increased uptake. We also looked at using 3 cm fixed spheres over the trapezius muscles as they are larger and further away from the primary tumour and lymph nodes, but found asymmetrical uptake in some patients. The range of TMRs in the primary tumours and

nodes was greater than SUV_{max} (1.39 – 13.18), which may result in better discrimination when determining cut off values for prognostic groups.

3.5.3.3 Hypoxic volume delineation

The hypoxic primary tumour volume and corresponding SUV_{mean} were also used as parameters for assessing ^{64}Cu-ATSM uptake, as it estimates tumour volume based on the distribution of hypoxic activity and quantifies the overall tumour volume. The volume was determined by visual delineation of the tumour edge, as there is no validated automated segmentation method for Cu-ATSM, but this method is highly operator dependent. Chao et al used a TMR ≥ 2, or uptake twice that of the contralateral normal neck, to define ^{60}Cu-ATSM hypoxic volume as no normal tissue in the neck displayed activity at this threshold. This was defined to demonstrate RT dose escalation to the hypoxic volume in 1 patient, and it is not clear how many patients they assessed overall to determine the threshold. We did attempt to use this threshold but, depending on the individual background uptake and size of tumour, this resulted in large volumes that required extensive manual editing in a large proportion of patients (Figure 3.26). Although the aim was not to determine the optimal method for hypoxic volume outlining, we tried applying higher TMR thresholds, which resulted in smaller volumes, but there was no single threshold that could be applied to all cases.

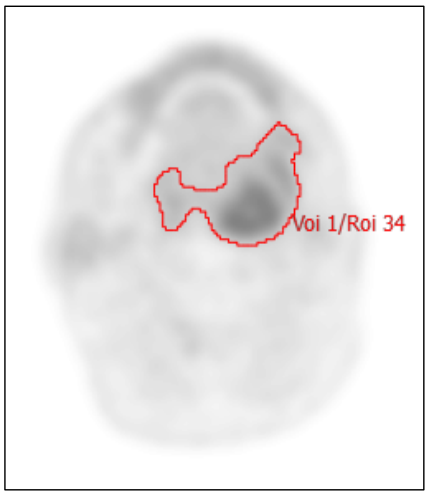

Figure 3.26 Example of tumour delineation using TMR > 2 automated segmentation.
Tumour delineation using this threshold resulted in overestimation of tumour size without extensive manual editing.

Grassi et al[412] used a cut off of 42% of the lesion SUV_{max} to delineate a biological target volume in 11 HNSCC patients to compare the volumes obtained from ^{64}Cu-ATSM and ^{18}F-FDG PET images. European guidelines in ^{18}F-FDG PET recommend using a 3D isocontour

at 41% of the maximum pixel value in metabolic tumour volume reporting where indicated, unless the tumour to background ratio is low or the tumour has heterogeneous uptake. For these cases 50% of the maximum uptake should be used consistently when assessing response to therapy.[513] These cut offs are not validated in Cu-ATSM PET but were also attempted in our dataset. However this again resulted in large volumes due the lower tumour to background contrast (Figure 3.27).

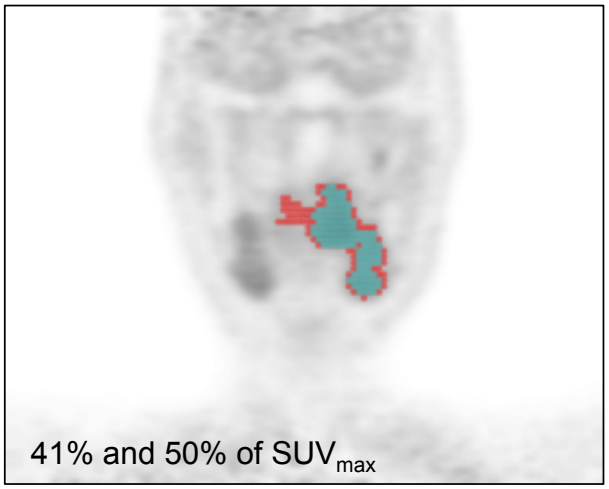

Figure 3.27 Example of delineation using 41% (red) and 50% (blue) of SUV_{max}. Automated segmentation of primary tumour in this case resulted in extension across midline and into submandibular gland seen on coronal imaging.

As there is no standard to which these various volumes from different thresholds could be compared, we could not conclude if any were superior or more accurate. One difficulty is whether the whole visible tumour volume with uptake above background or whether a threshold defined hypoxic subvolume represents clinically relevant radioresistant regions. TMR or SUV_{max} cut offs identified by previous studies associated with residual or recurrent disease or poorer long-term outcome, may be the thresholds that should be applied to define biologically significant hypoxic volumes within tumours. However these cut offs are variable between studies. The limited spatial resolution of PET makes defining the edge of tumour uptake difficult, but also means that PET imaging does not necessarily show the microregional, true heterogeneity of hypoxia within the tumour.[330] Clinically relevant cellular hypoxia may be present in smaller areas that are not detected by PET, making any of the PET parameters used to quantify hypoxia inaccurate. Further studies with larger numbers of patients are required be able to investigate a more robust method for defining hypoxic volume.

A further volumetric measure that has been explored using ^{18}F-FAZA in HNSCC is the fractional hypoxic volume, or the percentage of hypoxic volume within the whole primary

tumour, using a fixed TMR threshold to define hypoxic volume and manually delineated tumour volume on CT.[352] This was also performed using our data but the volumes were similar or larger on PET in over half the cases. PET manual delineation may have overestimated the hypoxic volume and the CT delineation was performed on images without contrast, making tumour edges more difficult to identify. Two patients had tonsillectomies, which were not included in hypoxic volume or SUV_{mean} correlations. For future recruitment we would need to consider whether these patients, and possibly T1 tumours, should be excluded.

Lymph node Cu-ATSM uptake in HNSCC has only been reported in one study.[412] The uptake or distribution has not been associated with outcome or correlated with primary tumour uptake in Cu-ATSM studies. ^{18}F-FAZA uptake has been assessed in HNSCC lymph nodes, where the TMR of the lymph node with the highest uptake was compared with the TMR of the primary tumour.[352] Similar to our results a positive correlation was seen between the TMR of the primary and lymph nodes. Although in general the uptake was lower in lymph nodes compared with primary tumours, this positive correlation and the peripheral pattern of hypoxia in lymph nodes may explain why Eppendorf pO_2 electrode measurements from neck nodes were similar to measurements from primary tumours.[235,239] In addition HPV-positive patients have more cystic nodal metastases,[514] which may be why the lymph node uptake was lower in our dataset.

3.5.3.4 Other uptake

The asymmetric uptake seen muscle may be related to sustained muscle contraction just prior to injection, during the uptake period or due to patient position during the 20 minute scan. This may result in reduced intracellular oxygen levels, which occurs during muscle contractile activity, leading to irreversible tracer trapping which is seen on the scan. ^{64}Cu-ATSM imaging immediately and 1 hour after 10 minutes of calf muscle contractions in rats showed a 1.5-fold increase in uptake in the muscles compared with resting conditions.[515] The SUV in muscles correlated with HIF-1α and CA9 mRNA expression. Patients should be advised to avoid exercise before the scan, rest once the tracer has been injected, and set up on the scanner couch with sufficient time prior to the start of the scan to ensure comfortable positioning.

The salivary glands had ^{64}Cu-ATSM uptake above background, which has not been reported in previous clinical HNSCC studies. Cu(II) is present in salivary secretions, with the majority of saliva in the oral cavity produced by the submandibular glands. The copper transporting ATPase ATP7A (Menkes protein) has been localised in the acinar cells in parotid glands and is involved in Cu secretion into saliva.[516] The uptake may also be due to

histatins, which are histidine-rich antimicrobial peptides present in the saliva and secreted by the salivary glands. Histatin 5 has Cu(II) binding motif, as well as a Zn(II) binding motif which is characteristic of metalloproteases.[517] This supports the suggestion that ^{64}Cu-ATSM may become incorporated into the intracellular copper pool and used in the normal Cu metabolism of the salivary glands. The normal parotid gland has been shown to be a site of misonidazole binding in mice under conditions of normoxia, which may be due to high local nitroreductase activity.[518] This may also be a cause of high ^{64}Cu-ATSM retention in the salivary glands.

Recent dental extractions were associated with uptake. In feline studies uptake was also seen in other inflammatory conditions such as tooth abscess and otitis media. Cu is an essential trace element that is involved in the expression and control of inflammation. It is transported in the blood mainly by the acute phase protein ceruloplasmin and intracellular metallothioneins, which are a family of metalloprotiens with high affinity for Cu and Zn, and modulate the binding, exchange and transport of copper.[519,520] Both ceruloplasmin and metallothioneins are induced by inflammatory stress and increase the transport of copper to sites of inflammation. In addition superoxide radicals are released from activated neutrophils and macrophages, which stimulate superoxide dismutase, a copper/zinc utilising antioxidant enzyme. Therefore ^{64}Cu may be transported and localised to the site of active inflammation.

Other physiological or non-malignant uptake does not prevent the use of a tracer, as long as this is known. ^{18}F-FDG is well documented to be taken up by inflammatory conditions due to increased glycolysis and by physiological mechanisms in various organs.[521] For example, in the salivary glands ^{18}F-FDG is taken up physiologically and secreted into the saliva, and uptake is usually seen bilaterally. Muscle uptake due to straining or contractions increases ^{18}F-FDG uptake, generally a linear pattern. Brown adipose fat uptake due to increased metabolic activity secondary to sympathetic stimulation is often seen in the lower neck, and can lead to misinterpretation in HNSCC, as can physiological uptake in Waldeyer's ring.[522] In addition there are malignant lesions that are known to not take up ^{18}F-FDG significantly, such as certain histological types of gastric cancer.[523] A high SUV is associated with a higher suspicion of cancer, but the reported cut offs are variable. Similarly with ^{64}Cu-ATSM it will be difficult to establish a cut off for clinically significant hypoxia that can be applied to all tumours. Further experience in imaging is required to confirm physiological and benign causes of ^{64}Cu-ATSM uptake.

3.5.4 Gene expression analysis

The study was initially designed to use microarrays to analyse and quantify gene expression. However in the 3 years from set up to recruiting 15 patients, due to the development, availability and affordability of next generation sequencing, RNA-Seq has become the new standard for transcriptome analysis. The major advantage of using this technology, although outsourcing the majority of the work, was that only a limited amount of tissue was available from each sample. Each patient only had one or two diagnostic biopsy blocks, from which only the tumour region was macrodissected. Microdissection of the tumour would have been technically challenging and may not have yielded sufficient RNA quantities. Inclusion of stromal cells in macrodissection has been shown to have a minimal effect on tumour gene expression, and extra amplification after microdissection to obtain sufficient RNA for sequencing actually had a high impact on gene expression profiles.[524] During the development and response of tumours to hypoxia the tumour microenvironment has a crucial role and therefore the exclusion of stromal cells may miss important information. In addition, for potential future clinical use, macrodissection is a technique that can be applied more directly.

FFPE samples were used in this study to increase the potential for clinical translation. Formalin fixation can lead to significant fragmentation and cross-linking and chemical modification of nucleic acids, potentially creating artificial sequence alterations. Many factors can affect the quality of the RNA including specimen size, time and duration of fixation and storage time RNA.[525] As RNA-Seq can analyse large numbers of short sequences, it is potentially the ideal technique to apply to FFPE samples. More studies are applying NGS to FFPE samples and high correlation of expression profiles between fresh frozen and FFPE tumour sample pairs has been demonstrated using RNA-Seq,[526] and RNA-Seq provides data of sufficient quality to enable biomarker discovery.[527]

3.5.4.1 Correlation between hypoxic signatures and hypoxic volume

The overall study aims to recruit 40 patients to allow an interim sample size calculation. At this analysis point if there is supporting evidence for potential discovery of gene-imaging or gene-outcome associations the recruitment would extend to 60 patients, as in a previous study this sample size was sufficient to identify 4 de novo intrinsic subtypes in HNSCC tumours.[115] Due to the small number of patients in the pilot study we chose to initially investigate whether validated hypoxia signatures were relevant in our study population. The Winter hypoxia signature was developed initially from fresh frozen HNSCC samples followed by in silico generation of hypoxia co-expression networks, to form a hyopxia metagene. This was subsequently applied retrospectively to laryngeal FFPE samples, where tumours were scored and categorised into high and low hypoxia groups, and found

to be predictive of benefit from ARCON. The 15-gene classifier used ^{18}F-FAZA as an endogenous hypoxia radiotracer in xenografts and validated in FFPE HNSCC samples with known oxygen electrode measurements. This classifier was used to retrospectively categorise HNSCC FFPE samples to more or less hypoxic groups and similarly was found to be predictive of benefit from nimorazole. Despite the differences in the way these 2 signatures were developed, when our samples were ranked according to the expression the Winter hypoxia signature and the 15-gene hypoxia classifier, a strong correlation was found between the 2 signatures, suggesting both these signatures are able to detect a similar tumour phenotype.

When samples were ranked according to each Cu-ATSM imaging parameter, hypoxic volume was the only feature to correlate with both hypoxic signatures. A recent publication by Lopci et al[528] investigated a number of ^{64}Cu-ATSM PET parameters including hypoxic tumour volume and hypoxic burden (hypoxic tumour volume x SUV_{mean}), $SUV_{max,}$ SUV_{mean} and SUV ratio to muscle, in 18 patients with lung cancer or HNSCC. After a median follow-up period of 14.6 months they found that the hypoxic tumour volume and hypoxic burden were more robust prognostic parameters for progression free survival. Similarly in ^{18}F-FDG PET many studies have demonstrated that metabolic tumour volume and metabolic tumour burden may represent better measures for prognosis, but is limited by the difficulties in defining this volume.[529]

Assuming the hypoxia signatures can be used to describe a hypoxic phenotype in our samples, as there was a positive correlation with hypoxic volume, we looked at the genes differentially expressed by hypoxic volume. There were a number of upregulated genes relating to the hypoxia response pathways. S100A7 is expressed in many malignancies and is a poor prognostic marker in HNSCC.[530] It has been shown to enhance cell growth by activating pro-inflammatory pathways, upregulate VEGF and induce endothelial cell proliferation.[531] SOD2 is an antioxidant enzyme, which prevents redox-mediated damage of mitochondrial proteins, and is associated with aggressive cancers with enhanced cell migration and metastases. Stress such as hypoxia leads to increased reactive oxygen species (ROS) and tumours may increase their expression of *SOD2* to prevent ROS-mediated DNA damage.[532] NAMPT tissue expression has also been found to be upregulated in tumours and shown to induce cell proliferation and angiogenesis.[533] It is the rate-limiting enzyme for the biosynthesis of NAD essential for metabolism and energy production. Tumour cells have high metabolic rate and NAD consumption and therefore depend on the production of NAD, and hypoxia has been shown to result in *NAMPT* induction.[534] NAMPT small molecule inhibitors are under investigation as a novel therapeutic, which reduce NAD levels resulting in ATP loss and inhibition of tumour cell

proliferation.[535] PFKFB3, which is also included in the 15-gene classifier, is a key enzyme in glycolysis, and activated in cancer cells to increase glycolysis to meet metabolic demands. It promotes cell cycle progression, suppressed apoptosis[536] and is involved in angiogenesis.[537] TM4SF1 is expressed on cancer cells and endothelial cells and is a potential new vascular therapeutic target in cancer,[538] and SRPK1 expression is elevated in hypoxic cells, with inhibition suppressing angiogenesis and tumour growth in animal models.[539]

RUNX3 is downregulated in our samples with increasing hypoxic volume. RUNX3 has been shown to inhibit HIF-1α stability through enhancing the interaction between HIF-1α and PHD2, promoting HIF-1α degradation in gastric cancer cells,[540] with resulting inhibition of angiogenesis. Its expression has been shown to be downregulated in response to hypoxia and is frequently inactivated in gastric cancer, resulting in stimulation of proliferation and suppression of apoptosis.[541]

3.5.4.2 Correlation with SUV_{max}

SUV_{max} and TMR are the main parameters in previous studies reported to have association with outcomes. However we did not find a correlation between these parameters and the hypoxia signatures, and therefore using these signatures to define low to high hypoxic phenotypes in our samples, then looking for genes differentially expressed by SUV_{max} or TMR would not be expected to define a hypoxia-related gene list. We also did not find a clear pattern of hypoxia related gene expression in the high versus low SUV_{max} groups, when comparing all samples or just the 4 patient outlying group. However *ECM1* was consistently upregulated in the high SUV_{max} groups, which has been reported to induce the expression of genes that promote the Warburg effect, such as GLUT1, LDHA and HIF-1α.[542] In the high SUV_{max} outlying group there were a number of downregulated genes that have roles in the immune response, such as *IFITM1, IFITM3* and *CXCL10.* Immune cells, especially tumour-associated macrophages, are recruited to the tumour site and can stabilise HIF-1α when deprived of oxygen. They stimulate angiogenesis, tumour cell growth, motility and invasion,[543] and are also immunosuppressive by depressing adaptive T-cell responses.[544] The pattern of downregulated genes may reflect modulation of the immune system in tumours with high Cu-ATSM uptake.

One explanation for the lack of association could be sampling bias. A snapshot of gene expression is captured through sequencing and may be highly variable from one region of the same tumour to another. The published hypoxia signatures were validated by retrospectively applying them to FFPE needle biopsy samples taken from any region of tumours and they demonstrated predictive value, suggesting that the specific location from

which a sample is not essential in determining the overall hypoxic status of the tumour. The signatures may consist of key genes that are expressed throughout hypoxic tumours. However when trying to correlate gene expression with an imaging parameter such as SUV_{max} which is measured from a small region of the tumour, the area from which the biopsy is taken may be more relevant. This may also be the case with TMR, as it is obtained from the SUV_{max}. In contrast hypoxic volume may be a better marker as it may take into account more of the overall behaviour of the tumour. Long-term follow data could help to assess which parameters have the potential to provide prognostic information.

3.5.4.3 MicroRNA

MiRNAs are better able to withstand the formalin fixation process and demonstrate stability win both FFPE and plasma.[156] However small RNA-Seq did not lead to a hypoxia-specific signature and disappointingly miR-210 and miR-196a we not found to be upregulated. When our samples were ranked by the 15-gene classifier, miR-21 and miR-31 were the top upregulated genes in more hypoxic samples. MiR-21 is the most frequently dysregulated miRNA in HNSCC. Upregulation promotes cell proliferation migration and inhibition of apoptosis, and is associated with poor prognosis.[166] MiR-31 is also known to be oncogenic and upregulated in HNSCC, where it targets factor-inhibiting hypoxia-inducible factor (FIH) resulting in increased HIF activity.[167] Ranking by hypoxic volume demonstrated miR-21 to be consistently upregulated in samples with greater hypoxic volume, along with miR-10b. There are conflicting studies regarding the role of miR-10b in HNSCC, and no reported associations with hypoxia. However in breast cancer, miR-10b is highly expressed in metastatic breast cancer cells and is induced by *TWIST*, which is involved in EMT, which in turn is regulated by HIF-1α.[545]

3.5.5 Circulating miRNAs

Reports on circulating miRNAs were first published in 2008. Lawrie et al[546] demonstrated that miR-155, miR-21 and miR-210 were higher in the serum of patients with diffuse large B cell lymphoma compared with healthy controls, and miR-21 levels are associated with relapse free survival. Mitchell et al[547] found that plasma miR-141 was able to distinguish patients with prostate cancer from healthy controls, and Chen et al[155] systematically characterised miRNAs in serum of healthy subjects and patients with lung cancer, colorectal cancer and diabetes, identifying a unique expression profile for each. In addition they demonstrated that circulating miRNAs are stable and reproducible, and are resistance to pH extremes, extended storage, boiling temperatures and multiple freeze thaw cycles. MiRNAs are released into the circulation as a result of cell damage, death and active secretion. They are released in microvesicles such as exosomes and apoptotic bodies, and

can also form complexes with RNA-binding proteins such as argonaute 2 (AGO2). These mechanisms protect them from RNAse degradation and make them highly stable in a variety of conditions.[548] Circulating miRNAs act as a mode of cell-cell communication. They are taken up by recipient cells by endocytosis or fusion with the plasma membrane and function in signalling events that can trigger tumourigenesis and metastasis in recipient cells.[549,550] In addition they can trigger a paracrine effect on tumour growth by binding to Toll-like receptor 8 (TLR8) on surrounding immune cells, resulting in the release of cytokines that promote cell proliferation and metastases.[551] Circulating miRNAs have been matched to the miRNAs expression in tumour tissue, and may therefore be representative of the primary tumour expression, providing a less invasive way to measure miRNAs.[552]

The sample size in our study was too small to make any conclusions about the clinical significance of circulating miR-196a and miR-210, but a few hypothesis-generating observations can potentially be made. MiR-196a correlated with increasing primary tumour size measured by both hypoxic volume and gross tumour volume, but not with ^{64}Cu-ATSM SUV_{max} or TMR. Our in vitro data demonstrated increased cell proliferation in miR-196a overexpressing HNSCC cell lines and the increased circulating miR-196a expression may reflect the proliferative characteristics of the primary tumour, representing tumours with faster growth. Clinical stage and change in tumour volume has been linked to the quantity of circulating miRNAs in other cancers. Larger, more advanced tumours were associated with higher levels of miR-21 in gastric cancers.[553] Pre-operative serum miR-21 was increased in HNSCC patients compared with normal volunteers, which significantly decreased 1 month after surgery. This remained low in patients with good prognosis, potentially representing a biomarker that could be used to monitor for recurrence.[552] Lu et al[554] recently found both miR-196a and miR-196b to be upregulated in plasma samples of patients with pre-cancerous oral lesions and oral squamous cell carcinoma compared with healthy controls, with higher fold increases in carcinoma, suggesting that they could serve as biomarkers for the early detection of oral cancer.

There was a trend towards increasing miR-210 expression and the hypoxia uptake parameters SUV_{max}, TMR and SUV_{mean}, suggesting a link between tumour hypoxia and circulating miR-210 levels. Circulating miR-210 has been investigated in various tumour types as a biomarker as high tissue expression correlates with hypoxia and poor prognosis. However it has not previously been correlated with other markers of hypoxia, such as hypoxia imaging measures. Hale et al[555] demonstrated that miR-210 is released from cells in culture during hypoxia, using human pulmonary arterial endothelial cells and HT-29 adenocarcinoma cells, under the control of AGO2 to facilitate hypoxic communication between cells. Higher levels of plasma miR-210 under conditions of hypoxia or ischaemia

were also demonstrated in vivo in pregnant Andean women living at high altitude and humans with intermittent claudication secondary to peripheral artery disease compared with their respective controls.[555] This suggests that circulating miR-210 could reflect the level of hypoxia of the primary tumour and may represent a potential screening tool for patients who would benefit from hypoxia imaging. However as other non-malignant conditions, such as peripheral vascular disease and aortic stenosis, can elevate circulating miR-210 release, further investigation into whether the level can distinguish between malignant and benign disease is required.[556]

Since the initial discovery there have been numerous studies investigating the diagnostic, prognostic and predictive potential of circulating miRNAs in cancer, including HNSCC.[557,558] However there has been a lack of consistent expression in the same malignancies due the many different methods in sample collection, isolation and analysis. Some studies have used serum samples, whilst others used plasma samples, and direct comparisons have resulted in conflicting results. No differences have been reported, with strong correlation of miRNA measurements between plasma and serum, indicating both would be suitable for investigation as blood-based biomarkers.[547] However others have shown that using serum samples result in higher RNA concentrations and have suggested that additional RNA could be released from cell lysis or platelets during the coagulation process.[559] We therefore opted to use plasma samples for miRNA analysis. Different methods for obtaining serum and plasma have been reported and may groups recommend a second centrifugation step with plasma samples to reduce platelet contamination, although a variety of different speeds and times have been used.[560,561] We used guidance from the NCI protocol and performed a second centrifugation step in accordance with the recommendation of the RNA extraction kit used.

Haemolysis of the blood during collection may release miRNAs from white and red blood cells, which contaminates the overall miRNA population.[562] Unfortunately 2 of our samples had obvious haemolysis and were excluded from analysis. Future improvements to the study could include a different time point for blood collection. Blood was collected through a vacutainer when patients were cannulated for tracer injection, to prevent further unnecessary discomfort. However blood could be collected at the pretreatment stage when routine bloods are checked and collected through a larger needle. Methods to identify haemolysis have been investigated such as spectrophotometric measurements of oxyhaemoglobin, but other factors such as lipaemia interferes with haemoglobin absorbance.[562] More recently, a lipaemia-independent NanoDrop-based method using a small volume of sample has been reported, which could be tested in future samples.[563]

Commercially available RNA extraction kits have been compared with differing RNA yields. Commercial column-based kits have shown better yield than TRIzol extraction and the biofluid-specific miRCURY kit from Exiquon outperformed other kits for isolation of miRNAs from plasma.[564,565] In addition it was easier to use, with shorter processing time, and therefore the Exiquon kit was used in our study. Quantification of extracted RNA is not accurate using measures such as NanoDrop.[566] RNA was normalised for concentration and technical variation by using fixed volume of starting plasma rather than mass and the same volume of eluted RNA was used for the RT-PCR reaction. Internal controls used to normalise miRNA expression in cells or tissue, such as RNU6B, are not stably expressed in blood.[567] MiR-16 has been shown to be stable and used as an internal control in certain cancers, but has also been shown to be dysregulated in others and sensitive to haemolysis.[547,562] As miR-16 has not been investigated as a control in HNSCC we used an exogenous miRNA, cel-miR-39, of known concentration which has no effect on human miRNA detection to normalise our data.

Further work is required to ascertain the optimal method to process and interpret circulating miRNA data and there is a need to standardise protocols. However, despite the very small sample size, the potential correlations seen with miR-196a and miR-210 are worth investigating. It is tempting to speculate that miR-196a is a potential biomarker of tumour proliferation and aggressiveness, whereas increasing miR-210 is a potential indicator of hypoxia in the primary tumour.

3.5.6 Conclusions

Although the sample size was small this exploratory pilot study has generated hypotheses to guide future recruitment and data analyses. Static ^{64}Cu-ATSM PET is well tolerated and demonstrates a spectrum of hypoxic imaging phenotypes in oropharyngeal squamous cell carcinomas. ^{64}Cu-ATSM as a radiotracer provides hypoxic-to-normoxic contrast of sufficient quality to define a hypoxic volume, but the optimal method for hypoxic volume delineation requires further investigation. RNA-Seq can assess the expression of published hypoxia gene signatures in FFPE biopsy samples. These signatures are significantly associated with increasing hypoxic volume as defined by ^{64}Cu-ATSM PET, and a hypoxic volume-specific gene expression signature has been derived. Using SUV parameters to quantify hypoxia may not be the optimal method for reporting Cu-ATSM PET scans as this does not take into account tumour heterogeneity. Circulating miR-196a may be associated with increasing tumour volume and warrants further investigation.

Combing molecular and imaging biomarkers of hypoxia is a feasible strategy to identify HNSCC patients with hypoxia and subsequently alter their management to improve outcome.

3.5.7 Future work

The BoHEMIaN study is currently open for ongoing recruitment. Given the finding that hypoxic volume is an important parameter, patients who have received diagnostic tonsillectomies will be excluded. Further analysis would include:

- Immunohistochemical staining with a panel of hypoxia-related antibodies, including HIF-1, CA9, VEGF, GLUT1, FIH and PHD, and correlation with imaging parameters and gene expression. Sections have already been prepared from the 15 patients recruited.
- Applying the Cu-ATSM hypoxic volume gene signature to further samples and comparing with imaging parameters.
- Hypoxia-induced serum protein measurements, such as osteopontin and VEGF, using multiplex Luminex assays.
- Correlation with long term outcome data.
- Validation of the hypoxic volume gene signature in an independent publically available dataset to assess the potential as a prognostic biomarker.

Continuing on from this study, future studies could look at comparing the gene expression from tumour samples from high Cu-ASTM uptake regions and low uptake regions to provide more information on tumour heterogenity. A recently completed study at our centre has mapped and compared preoperative Cu-ATSM scans with postoperative laryngectomy specimens. Patients received pimonidazole infusion before surgery and aim of this study was to validate Cu-ATSM as a hypoxic tracer by correlating pimonidazole staining with Cu-ATSM uptake. Using this data, regions of tumours with different SUVs could be sampled and differential gene expression assessed.

Chapter 4

Summary and discussion

Forty percent of patients cured of their cancer receive radiotherapy as part of their curative treatment and 16% of all cures can be attributed to radiotherapy alone.[3] Despite advances in tumour voluming, radiation dose coverage and delivery techniques, the majority of recurrences occur within the high dose irradiated volume.[568] Radioresistance is a major cause of treatment failure in HNSCC and biomarkers to identify and geographically map these regions could direct strategies to overcome radioresistance and improve outcome.

Locally advanced HNSCC represents tumours with multiple genetic aberrations and is characterised by tumour heterogeneity. A wide range of biomarkers are under investigation with the aim of improving the identification and stratification of this heterogeneity. This would enable the tailoring of treatments based on prognosis and prediction of response to radiation, optimising the therapeutic ratio. Established biomarkers in HNSCC, such as HPV and ^{18}F-FDG, currently have a clear prognostic role and this is now translating into the development of studies which use these biomarkers to alter management. A current phase I study recruiting at our centre utilises both these biomarkers to overcome radioresistance; ^{18}F-FDG avid regions of HPV-negative OPSCC primary tumours are selectively dose-escalated using intensity modulated radiotherapy. If radioresistance can be reliably and easily identified, standard treatment techniques can be modified to target resistance, as well as guiding the direction of the development of newer therapeutics. However the lack of robust biomarkers for early detection and response prediction represents one of the current challenges in the management of HNSCC.

Genome-wide sequencing studies have improved the understanding of the molecular mechanisms of tumourigenesis and treatment resistance in HNSCC, and identified the major mutations involved. In addition gene expression profiling has improved the categorisation of HNSCC into different phenotypes, identifying specific characteristics associated with differing outcomes. Advances in molecular biology has led to the discovery of miRNAs, which are now known to be major players in the pathogenesis of cancer and treatment resistance. They represent a huge bank for novel biomarker discovery, not just from tissues but also blood and saliva.[548] Developments in imaging have led to the investigation of new radiotracers and scanning techniques to identify established and new biomarkers of radioresistance and to achieve non-invasive patient stratification. All these research strategies have allowed the discovery of potential new biomarkers as well as the advancement of investigation of known biomarkers of radioresistance, creating opportunities for personalised medicine.

4.1 MiR-196a

MiRNAs are involved in the response to ionising radiation and many studies have demonstrated that their expression significantly changes in response to radiation. However to investigate miRNAs that underlie the mechanisms of intrinsic radioresistance, pretreatment alterations need to be identified. Our study identified miR-196a and the alteration of this single miRNA resulted in significant changes in the proliferation, migration, invasion and radiosensitivity of head and neck cell lines. This suggests that miR-196a potentially represents a novel prognostic and predictive biomarker.

However, the path from biomarker discovery in in vitro exploratory studies to use in clinical trials requires rigorous preclinical and clinical validation. The behaviour of miR-196a overexpressing cells was confirmed in head and neck cancer cell lines from different subsite origins, and the opposite effects demonstrated in miR-196a knockdown studies. However, the negative correlation of miR-196a in a small independent group of radioresistant patient samples suggests that further in vitro or animal work is required to establish patterns of behaviour and mechanisms before planning a clinical validation study. The number of samples, sample handling and preparation, number of replicates and methods for analyses need careful consideration before limited patient samples are used.

MiRNAs work in a complex interactive network, utilising the imperfect matching between the seed region of the miRNA with the 3'-UTR of the target mRNA to potentially interact with multiple mRNA target sites.[127] Although ANXA1 was identified as a direct target of miR-196a this did not fully explain the effects of miR-196a modulation, in particular the effects on radiosensitivity, suggesting that other targets of miR-196a may be involved. When investigating miRNA function, multiple downstream targets should be considered rather than focusing on one gene target or pathway to gain an accurate insight into the biological effects.

MiRNAs have been shown to be stable in plasma and serum,[155] and the ease of collection of blood makes it an attractive source for identifying biomarkers. The level of miRNA-196a measured in the plasma samples of patients in the BoHEMIaN pilot study was significantly associated with the tumour volumes of the primary tumour, correlating with the in vitro behaviour of increased cell proliferation. However there are many uncertainties in the processing and analysis of circulating miRNAs, especially in relation to quantification and internal normalisation methods. Unlike cells and tissues where normalisation with housekeeping genes is generally reliable, these controls in serum or plasma are easily degraded and not reliably detected.[567] Levels of the commonly used housekeeping genes RNU48 and RNU6B were measured in our samples but with wide variations and lack of

reproducibility. MiR-196a was not found to be a miRNA of interest on small RNA sequencing of the RNA extracted from the tissue samples, but it would be interesting to separately measure the level of miR-196a using the RNA extracted from the tissue samples. Combined miR-196a assessment from the tumour and blood to identify more aggressive radioresistant tumours could increase the sensitivity and specificity of diagnosis.

Although thousands of miRNAs have been discovered, targeting a single miRNA could be an effective strategy as they affect the expression of multiple genes and their pathways. Further knowledge of the critical pathways involved in radioresistance and the interplay with miRNAs is required, but encouragingly early phase studies are currently underway using miRNA inhibitors or mimics, confirming their potential as treatment targets. MiRNA-targeting therapeutics could have a future role in combination with conventional and other targeted treatments, enhancing their effects as well as inhibiting specific pathways via more that one mechanism to reduce resistance.

4.2 Hypoxia

Hypoxia has been extensively investigated, both at a molecular and clinical levels, and it is clear that it is a major cause of radioresistance and recurrence in HNSCC. Much of the research has focused on therapeutic approaches to overcome hypoxia-associated radioresistance, but this has not led to changes in routine management. Due to the heterogeneity of hypoxia in HNSCC the identification, and therefore stratification, of patients who would benefit from these modifications in treatment has been a major issue. Investigations into the detection of hypoxia using molecular and imaging biomarkers have shown some promise, each having their own advantages and disadvantages. However results have been inconsistent, which may reflect the heterogeneous nature of both HNSCC and hypoxia, and have not led to the translation of these methods into clinical practice.

Hypoxia imaging is a challenging area of research, as hypoxia is spatially and temporally heterogeneous. It has the potential to identify and quantify hypoxia, which can be used as a prognostic or predictive biomarker, as well as provide information on the distribution of hypoxia within primary tumours and metastatic lesions. The distribution of hypoxia would then inform decisions on possible localised targeted versus systemic treatment strategies. ^{64}Cu-ATSM is the hypoxia radiotracer under investigation at our centre and separate studies are being carried out to further analyse the mechanism and to validate its use in cancer. Previous clinical studies have shown associations between different Cu-ATSM

imaging parameters and outcomes.[399,408] However there have been no consistency in the results, as studies have used different cohorts of patients, a range of Cu-ATSM uptake times and PET image acquisition and analysis methods, and all have only a limited number of patients. We used the main reported parameters of SUV_{max} and TMR, but also included hypoxic volume as an alternative measure. Hypoxia is not well defined, with no threshold, and can have variable consequences in different situations. All of our patients showed some uptake in their primary tumours, but not in all metastatic lymph nodes. It is unclear whether any level of uptake or above a certain threshold represents clinically relevant hypoxia. Radioresistance has been reported to start at pO_2 levels < 25-30 mmHg.[197] There have not been any clinical studies comparing Eppendorf electrode measurements and Cu-ATSM uptake, but studies using FMISO and pimonidazole show retention at O_2 levels lower than 25 mmHg.[569] In head and neck cancer patients FMISO TMR correlated with pO_2 readings of ≤ 5 mmHg,[338] suggesting that a large fraction of radioresistant cells are not hypoxic enough to take up the tracer. Many large lymph nodes and primary tumours showed reduced uptake centrally, which may be secondary to tumour necrosis. However an alternative explanation could be due to disordered tumour vasculature affecting tracer uptake and retention, which would result in inaccuracies in image interpretation.

A lot more work needs to be carried out before Cu-ATSM can be used in the clinical setting to assess the optimal tracer uptake time, reproducibility and repeatability, and spatiotemporal stability of the tracer. Test-retest repeatability studies are limited by the radiation dose associated with ^{64}Cu-ATSM and therefore ^{62}Cu can be used as an alternative, especially as it is not reliant on a cyclotron for production. Repeated FMISO data suggests that there are significant intratumoural changes in hypoxia distribution between scans carried out a few days apart,[335] and hypoxia imaging during RT may be a better method to identify clinically relevant radioresistance within tumours, as this may be indicative of incomplete reoxygenation with increased hypoxic fraction. Validation of Cu-ATSM as a reliable hypoxic tracer is also a major area of research that is required, which may be difficult, as the gold standard for measuring hypoxia remains the Eppendorf polargraphic needle electrode with its sampling limitations. Other methods would be to compare uptake with FMISO or pimonidazole, but as the mechanism of uptake is different lack of correlation does not necessarily exclude Cu-ATSM as a clinically useful tracer to detect hypoxia. Due to the dynamic nature of hypoxia in different situations, it is unlikely that one hypoxia tracer could have universal application. The cost and availability of Cu-ATSM PET scans will also be a factor in the clinical setting and further investigation into which group of patients whose management could potentially be changed through the knowledge of hypoxia distribution needs to be determined.

Hypoxia gene expression signatures have shown encouraging results as a biomarker for identifying hypoxia, using multiple genes rather than a single marker to detect hypoxia. Advancements in gene sequencing have enabled more accurate gene expression analysis using smaller RNA samples and FFPE samples that have been archived for a number of years. FFPE samples represent a huge bank of data and retrospective analyses have enabled the validation of gene expression signatures, as well as demonstrate predictive potential.[324,570] When two published hypoxia signatures were applied to our samples, there was a significant correlation with increasing Cu-ATSM defined hypoxic volume, but not SUV_{max} or TMR, suggesting that hypoxic volume may be an important marker for hypoxia. A larger hypoxic volume could represent a more aggressive, rapidly growing tumour or represent of sampling bias, as there is a greater chance of sampling a region of hypoxia from a tumour with a larger hypoxic volume. It is unclear whether the gene signature from a small part of a tumour could be representative of the phenotype of the whole tumour. Although retrospective stratification of FFPE biopsy samples into low or high hypoxia groups using hypoxia gene signatures could identify subgroups of patients with poorer outcome and predict benefit from hypoxic modification,[324,570] comparison of gene signatures from multiple biopsies from the same tumour would be required to further clarify the issue of sampling bias.

The aim of the BoHEMIaN study is to identify a gene signature that would predict for a ^{64}Cu-ATSM hypoxic phenotype, to enable the selection of patients who would benefit from ^{64}Cu-ATSM imaging, which would in turn inform treatment. The use of two methods to identify hypoxia before altering management would enhance the accuracy of hypoxia diagnosis and assessment. The combined use of imaging and molecular biomarkers to improve tumour characterisation is a relatively new field of radiogenomics.[571] Studies such as the Cancer Genome Atlas have described distinct molecular gene expression profiles within tumours originating from the same site, leading to the development of radiogenomic maps that associate imaging features with underlying molecular data. Gene expression data only allows analysis of small regions of tumour tissue, whereas imaging can provide a more comprehensive view of the entire tumour and then be used on an ongoing basis to monitor disease response or progression. This pilot study has suggested that hypoxic volume is important and a novel gene signature associated with hypoxic volume has been developed which will need further investigation with the recruitment of more patients and correlation with long term outcome data. However this has raised the question of how the hypoxic volume should be defined. PET-based tumour volume delineation for dose escalation has been investigated in ^{18}F-FDG PET, without a consensus on the optimal method, despite higher tumour to background contrast compared with hypoxia tracers. Methods include manual delineation, fixed percentage of SUV_{max} thresholds, gradient

based methods and fully automated segmentation algorithms.[529] The edge of the tumour is difficult to determine due to the limited spatial resolution of PET. Cellular hypoxia in the edges of tumours may not be detected on the scan but clinically relevant at the microscopic level. We used manual delineation with supervision from an experienced nuclear medicine physician, but the level of accuracy required to define the overall hypoxic volume requires further clarification.

4.3 Conclusions

The aim of this thesis was to further explore biomarkers of radioresistance in HNSCC, from initial discovery and experimentation at the molecular level, and the early process for translation of an established biomarker into clinical practice. MiRNA-196a and tumour hypoxia in HNSCC promote aggressive, radioresistant tumour phenotypes associated with poorer outcomes. We have found that:

- MiR-196a promotes an oncogenic phenotype in head and neck cancer cells in vitro and confers radioresistance, partly through targeting ANXA1.
- Circulating miR-196a is associated with increasing tumour volume in patients from a limited cohort.
- ^{64}Cu-ATSM PET defined tumour volume correlates with hypoxia gene signatures and may be an important parameter to report on scan analysis.
- A gene signature associated with ^{64}Cu-ATSM PET defined tumour volume has been developed for future application.

Studies are continuing to further investigate both miR-196a and the combination of ^{64}Cu-ATSM PET and gene expression signatures as biomarkers of radioresistance.

References

1. Pai SI, Westra WH. Molecular pathology of head and neck cancer: implications for diagnosis, prognosis, and treatment. Annual review of pathology 2009;4:49-70.
2. Ferlay J, Soerjomataram I, Dikshit R, et al. Cancer incidence and mortality worldwide: sources, methods and major patterns in GLOBOCAN 2012. International journal of cancer Journal international du cancer 2015;136:E359-86.
3. cancerresearchuk.org.
4. Hashibe M, Brennan P, Benhamou S, et al. Alcohol drinking in never users of tobacco, cigarette smoking in never drinkers, and the risk of head and neck cancer: pooled analysis in the International Head and Neck Cancer Epidemiology Consortium. Journal of the National Cancer Institute 2007;99:777-89.
5. Hashibe M, Brennan P, Chuang SC, et al. Interaction between tobacco and alcohol use and the risk of head and neck cancer: pooled analysis in the International Head and Neck Cancer Epidemiology Consortium. Cancer epidemiology, biomarkers & prevention : a publication of the American Association for Cancer Research, cosponsored by the American Society of Preventive Oncology 2009;18:541-50.
6. Chaturvedi AK, Anderson WF, Lortet-Tieulent J, et al. Worldwide Trends in Incidence Rates for Oral Cavity and Oropharyngeal Cancers. Journal of clinical oncology : official journal of the American Society of Clinical Oncology 2013.
7. Chaturvedi AK, Engels EA, Anderson WF, Gillison ML. Incidence trends for human papillomavirus-related and -unrelated oral squamous cell carcinomas in the United States. Journal of clinical oncology : official journal of the American Society of Clinical Oncology 2008;26:612-9.
8. Gillison ML, Koch WM, Capone RB, et al. Evidence for a causal association between human papillomavirus and a subset of head and neck cancers. Journal of the National Cancer Institute 2000;92:709-20.
9. Goldenberg D, Lee J, Koch WM, et al. Habitual risk factors for head and neck cancer. Otolaryngology--head and neck surgery : official journal of American Academy of Otolaryngology-Head and Neck Surgery 2004;131:986-93.
10. Kutler DI, Auerbach AD, Satagopan J, et al. High incidence of head and neck squamous cell carcinoma in patients with Fanconi anemia. Archives of otolaryngology--head & neck surgery 2003;129:106-12.
11. Argiris A, Karamouzis MV, Raben D, Ferris RL. Head and neck cancer. Lancet 2008;371:1695-709.
12. Pignon JP, le Maitre A, Maillard E, Bourhis J, Group M-NC. Meta-analysis of chemotherapy in head and neck cancer (MACH-NC): an update on 93 randomised trials and 17,346 patients. Radiotherapy and oncology : journal of the European Society for Therapeutic Radiology and Oncology 2009;92:4-14.
13. Bernier J, Cooper JS, Pajak TF, et al. Defining risk levels in locally advanced head and neck cancers: a comparative analysis of concurrent postoperative radiation plus chemotherapy trials of the EORTC (#22931) and RTOG (# 9501). Head & neck 2005;27:843-50.
14. Tupchong L, Scott CB, Blitzer PH, et al. Randomized study of preoperative versus postoperative radiation therapy in advanced head and neck carcinoma: long-term follow-up of RTOG study 73-03. International journal of radiation oncology, biology, physics 1991;20:21-8.
15. Cooper JS, Pajak TF, Forastiere AA, et al. Postoperative concurrent radiotherapy and chemotherapy for high-risk squamous-cell carcinoma of the head and neck. The New England journal of medicine 2004;350:1937-44.
16. Fletcher GH. Regaud lecture perspectives on the history of radiotherapy. Radiotherapy and oncology : journal of the European Society for Therapeutic Radiology and Oncology 1988;12:iii-v, 253-71.
17. Pignon JP, Bourhis J, Domenge C, Designe L. Chemotherapy added to locoregional treatment for head and neck squamous-cell carcinoma: three meta-analyses of updated individual data. MACH-NC Collaborative Group. Meta-Analysis of Chemotherapy on Head and Neck Cancer. Lancet 2000;355:949-55.
18. Trotti A, Bellm LA, Epstein JB, et al. Mucositis incidence, severity and associated outcomes in patients with head and neck cancer receiving radiotherapy with or without chemotherapy: a systematic literature review. Radiotherapy and oncology : journal of the European Society for Therapeutic Radiology and Oncology 2003;66:253-62.
19. Machtay M, Moughan J, Trotti A, et al. Factors associated with severe late toxicity after concurrent chemoradiation for locally advanced head and neck cancer: an RTOG analysis. Journal of clinical oncology : official journal of the American Society of Clinical Oncology 2008;26:3582-9.
20. Ang KK, Berkey BA, Tu X, et al. Impact of epidermal growth factor receptor expression on survival and pattern of relapse in patients with advanced head and neck carcinoma. Cancer research 2002;62:7350-6.
21. Huang SM, Harari PM. Modulation of radiation response after epidermal growth factor receptor blockade in squamous cell carcinomas: inhibition of damage repair, cell cycle kinetics, and tumor angiogenesis. Clinical cancer research : an official journal of the American Association for Cancer Research 2000;6:2166-74.

22. Bonner JA, Harari PM, Giralt J, et al. Radiotherapy plus cetuximab for squamous-cell carcinoma of the head and neck. The New England journal of medicine 2006;354:567-78.
23. Withers HR, Taylor JM, Maciejewski B. The hazard of accelerated tumor clonogen repopulation during radiotherapy. Acta Oncol 1988;27:131-46.
24. Fu KK, Pajak TF, Trotti A, et al. A Radiation Therapy Oncology Group (RTOG) phase III randomized study to compare hyperfractionation and two variants of accelerated fractionation to standard fractionation radiotherapy for head and neck squamous cell carcinomas: first report of RTOG 9003. International journal of radiation oncology, biology, physics 2000;48:7-16.
25. Overgaard J, Hansen HS, Specht L, et al. Five compared with six fractions per week of conventional radiotherapy of squamous-cell carcinoma of head and neck: DAHANCA 6 and 7 randomised controlled trial. Lancet 2003;362:933-40.
26. Bourhis J, Overgaard J, Audry H, et al. Hyperfractionated or accelerated radiotherapy in head and neck cancer: a meta-analysis. Lancet 2006;368:843-54.
27. Bensadoun RJ, Benezery K, Dassonville O, et al. French multicenter phase III randomized study testing concurrent twice-a-day radiotherapy and cisplatin/5-fluorouracil chemotherapy (BiRCF) in unresectable pharyngeal carcinoma: Results at 2 years (FNCLCC-GORTEC). International journal of radiation oncology, biology, physics 2006;64:983-94.
28. Bourhis J, Sire C, Graff P, et al. Concomitant chemoradiotherapy versus acceleration of radiotherapy with or without concomitant chemotherapy in locally advanced head and neck carcinoma (GORTEC 99-02): an open-label phase 3 randomised trial. The Lancet Oncology 2012;13:145-53.
29. Brockstein BE. Management of recurrent head and neck cancer: recent progress and future directions. Drugs 2011;71:1551-9.
30. Forastiere AA, Metch B, Schuller DE, et al. Randomized comparison of cisplatin plus fluorouracil and carboplatin plus fluorouracil versus methotrexate in advanced squamous-cell carcinoma of the head and neck: a Southwest Oncology Group study. Journal of clinical oncology : official journal of the American Society of Clinical Oncology 1992;10:1245-51.
31. Vermorken JB, Trigo J, Hitt R, et al. Open-label, uncontrolled, multicenter phase II study to evaluate the efficacy and toxicity of cetuximab as a single agent in patients with recurrent and/or metastatic squamous cell carcinoma of the head and neck who failed to respond to platinum-based therapy. Journal of clinical oncology : official journal of the American Society of Clinical Oncology 2007;25:2171-7.
32. Burtness B, Goldwasser MA, Flood W, Mattar B, Forastiere AA, Eastern Cooperative Oncology G. Phase III randomized trial of cisplatin plus placebo compared with cisplatin plus cetuximab in metastatic/recurrent head and neck cancer: an Eastern Cooperative Oncology Group study. Journal of clinical oncology : official journal of the American Society of Clinical Oncology 2005;23:8646-54.
33. Vermorken JB, Mesia R, Rivera F, et al. Platinum-based chemotherapy plus cetuximab in head and neck cancer. The New England journal of medicine 2008;359:1116-27.
34. Rosell R, Perez-Roca L, Sanchez JJ, et al. Customized treatment in non-small-cell lung cancer based on EGFR mutations and BRCA1 mRNA expression. PLoS One 2009;4:e5133.
35. Chapman PB, Hauschild A, Robert C, et al. Improved survival with vemurafenib in melanoma with BRAF V600E mutation. The New England journal of medicine 2011;364:2507-16.
36. Isayeva T, Li Y, Maswahu D, Brandwein-Gensler M. Human papillomavirus in non-oropharyngeal head and neck cancers: a systematic literature review. Head and neck pathology 2012;6 Suppl 1:S104-20.
37. Giroglou T, Florin L, Schafer F, Streeck RE, Sapp M. Human papillomavirus infection requires cell surface heparan sulfate. Journal of virology 2001;75:1565-70.
38. Scheffner M, Werness BA, Huibregtse JM, Levine AJ, Howley PM. The E6 oncoprotein encoded by human papillomavirus types 16 and 18 promotes the degradation of p53. Cell 1990;63:1129-36.
39. Dyson N, Howley PM, Munger K, Harlow E. The human papilloma virus-16 E7 oncoprotein is able to bind to the retinoblastoma gene product. Science 1989;243:934-7.
40. Weinberger PM, Yu Z, Haffty BG, et al. Prognostic significance of p16 protein levels in oropharyngeal squamous cell cancer. Clinical cancer research : an official journal of the American Association for Cancer Research 2004;10:5684-91.
41. Ang KK, Harris J, Wheeler R, et al. Human papillomavirus and survival of patients with oropharyngeal cancer. The New England journal of medicine 2010;363:24-35.
42. Weinberger PM, Yu Z, Haffty BG, et al. Molecular classification identifies a subset of human papillomavirus--associated oropharyngeal cancers with favorable prognosis. Journal of clinical oncology : official journal of the American Society of Clinical Oncology 2006;24:736-47.
43. Masterson L, Moualed D, Liu ZW, et al. De-escalation treatment protocols for human papillomavirus-associated oropharyngeal squamous cell carcinoma: a systematic review and meta-analysis of current clinical trials. Eur J Cancer 2014;50:2636-48.
44. Herrero R. Human Papillomavirus and Oral Cancer: The International Agency for Research on Cancer Multicenter Study. CancerSpectrum Knowledge Environment 2003;95:1772-83.
45. Voskens CJ, Sewell D, Hertzano R, et al. Induction of MAGE-A3 and HPV-16 immunity by Trojan vaccines in patients with head and neck carcinoma. Head & neck 2012;34:1734-46.
46. Lyford-Pike S, Peng S, Young GD, et al. Evidence for a role of the PD-1:PD-L1 pathway in immune resistance of HPV-associated head and neck squamous cell carcinoma. Cancer research 2013;73:1733-41.

47. Parsa AT, Waldron JS, Panner A, et al. Loss of tumor suppressor PTEN function increases B7-H1 expression and immunoresistance in glioma. Nature medicine 2007;13:84-8.
48. Agrawal N, Frederick MJ, Pickering CR, et al. Exome sequencing of head and neck squamous cell carcinoma reveals inactivating mutations in NOTCH1. Science 2011;333:1154-7.
49. Stransky N, Egloff AM, Tward AD, et al. The mutational landscape of head and neck squamous cell carcinoma. Science 2011;333:1157-60.
50. Brahmer JR, Tykodi SS, Chow LQ, et al. Safety and activity of anti-PD-L1 antibody in patients with advanced cancer. The New England journal of medicine 2012;366:2455-65.
51. Topalian SL, Hodi FS, Brahmer JR, et al. Safety, activity, and immune correlates of anti-PD-1 antibody in cancer. The New England journal of medicine 2012;366:2443-54.
52. Liao CT, Chang JT, Wang HM, et al. Pretreatment primary tumor SUVmax measured by FDG-PET and pathologic tumor depth predict for poor outcomes in patients with oral cavity squamous cell carcinoma and pathologically positive lymph nodes. International journal of radiation oncology, biology, physics 2009;73:764-71.
53. Xie P, Li M, Zhao H, Sun X, Fu Z, Yu J. 18F-FDG PET or PET-CT to evaluate prognosis for head and neck cancer: a meta-analysis. Journal of cancer research and clinical oncology 2011;137:1085-93.
54. Zhang B, Li X, Lu X. Standardized uptake value is of prognostic value for outcome in head and neck squamous cell carcinoma. Acta oto-laryngologica 2010;130:756-62.
55. Paidpally V, Tahari AK, Lam S, et al. Addition of 18F-FDG PET/CT to clinical assessment predicts overall survival in HNSCC: a retrospective analysis with follow-up for 12 years. Journal of nuclear medicine : official publication, Society of Nuclear Medicine 2013;54:2039-45.
56. Gupta T, Master Z, Kannan S, et al. Diagnostic performance of post-treatment FDG PET or FDG PET/CT imaging in head and neck cancer: a systematic review and meta-analysis. European journal of nuclear medicine and molecular imaging 2011;38:2083-95.
57. Ong SC, Schoder H, Lee NY, et al. Clinical utility of 18F-FDG PET/CT in assessing the neck after concurrent chemoradiotherapy for Locoregional advanced head and neck cancer. Journal of nuclear medicine : official publication, Society of Nuclear Medicine 2008;49:532-40.
58. Abgral R, Le Roux PY, Keromnes N, et al. Early prediction of survival following induction chemotherapy with DCF (docetaxel, cisplatin, 5-fluorouracil) using FDG PET/CT imaging in patients with locally advanced head and neck squamous cell carcinoma. European journal of nuclear medicine and molecular imaging 2012;39:1839-47.
59. Hentschel M, Appold S, Schreiber A, et al. Early FDG PET at 10 or 20 Gy under chemoradiotherapy is prognostic for locoregional control and overall survival in patients with head and neck cancer. European journal of nuclear medicine and molecular imaging 2011;38:1203-11.
60. Daisne JF, Duprez T, Weynand B, et al. Tumor volume in pharyngolaryngeal squamous cell carcinoma: comparison at CT, MR imaging, and FDG PET and validation with surgical specimen. Radiology 2004;233:93-100.
61. Schinagl DA, Vogel WV, Hoffmann AL, van Dalen JA, Oyen WJ, Kaanders JH. Comparison of five segmentation tools for 18F-fluoro-deoxy-glucose-positron emission tomography-based target volume definition in head and neck cancer. International journal of radiation oncology, biology, physics 2007;69:1282-9.
62. Due AK, Vogelius IR, Aznar MC, et al. Recurrences after intensity modulated radiotherapy for head and neck squamous cell carcinoma more likely to originate from regions with high baseline [18F]-FDG uptake. Radiotherapy and oncology : journal of the European Society for Therapeutic Radiology and Oncology 2014;111:360-5.
63. Christian N, Lee JA, Bol A, De Bast M, Jordan B, Gregoire V. The limitation of PET imaging for biological adaptive-IMRT assessed in animal models. Radiotherapy and oncology : journal of the European Society for Therapeutic Radiology and Oncology 2009;91:101-6.
64. Cancer Genome Atlas N. Comprehensive genomic characterization of head and neck squamous cell carcinomas. Nature 2015;517:576-82.
65. Sun W, Califano JA. Sequencing the head and neck cancer genome: implications for therapy. Annals of the New York Academy of Sciences 2014;1333:33-42.
66. Vogelstein B, Lane D, Levine AJ. Surfing the p53 network. Nature 2000;408:307-10.
67. Sherr CJ, McCormick F. The RB and p53 pathways in cancer. Cancer cell 2002;2:103-12.
68. Poeta ML, Manola J, Goldwasser MA, et al. TP53 mutations and survival in squamous-cell carcinoma of the head and neck. The New England journal of medicine 2007;357:2552-61.
69. Pickering CR, Zhang J, Yoo SY, et al. Integrative genomic characterization of oral squamous cell carcinoma identifies frequent somatic drivers. Cancer discovery 2013;3:770-81.
70. Koch WM, Brennan JA, Zahurak M, et al. p53 mutation and locoregional treatment failure in head and neck squamous cell carcinoma. Journal of the National Cancer Institute 1996;88:1580-6.
71. Kalish LH, Kwong RA, Cole IE, Gallagher RM, Sutherland RL, Musgrove EA. Deregulated cyclin D1 expression is associated with decreased efficacy of the selective epidermal growth factor receptor tyrosine kinase inhibitor gefitinib in head and neck squamous cell carcinoma cell lines. Clinical cancer research : an official journal of the American Association for Cancer Research 2004;10:7764-74.
72. Schuler PJ, Harasymczuk M, Visus C, et al. Phase I dendritic cell p53 peptide vaccine for head and neck cancer. Clinical cancer research : an official journal of the American Association for Cancer Research 2014;20:2433-44.

73. Roh JL, Kang SK, Minn I, Califano JA, Sidransky D, Koch WM. p53-Reactivating small molecules induce apoptosis and enhance chemotherapeutic cytotoxicity in head and neck squamous cell carcinoma. Oral oncology 2011;47:8-15.
74. Hynes NE, Lane HA. ERBB receptors and cancer: the complexity of targeted inhibitors. Nature reviews Cancer 2005;5:341-54.
75. Lin SY, Makino K, Xia W, et al. Nuclear localization of EGF receptor and its potential new role as a transcription factor. Nature cell biology 2001;3:802-8.
76. Grandis JR, Tweardy DJ. Elevated levels of transforming growth factor alpha and epidermal growth factor receptor messenger RNA are early markers of carcinogenesis in head and neck cancer. Cancer research 1993;53:3579-84.
77. Bohlius J, Schmidlin K, Brillant C, et al. Recombinant human erythropoiesis-stimulating agents and mortality in patients with cancer: a meta-analysis of randomised trials. Lancet 2009;373:1532-42.
78. Chung CH, Ely K, McGavran L, et al. Increased epidermal growth factor receptor gene copy number is associated with poor prognosis in head and neck squamous cell carcinomas. Journal of clinical oncology : official journal of the American Society of Clinical Oncology 2006;24:4170-6.
79. Licitra L, Mesia R, Rivera F, et al. Evaluation of EGFR gene copy number as a predictive biomarker for the efficacy of cetuximab in combination with chemotherapy in the first-line treatment of recurrent and/or metastatic squamous cell carcinoma of the head and neck: EXTREME study. Annals of oncology : official journal of the European Society for Medical Oncology / ESMO 2011;22:1078-87.
80. Stewart JS, Cohen EE, Licitra L, et al. Phase III study of gefitinib compared with intravenous methotrexate for recurrent squamous cell carcinoma of the head and neck [corrected]. Journal of clinical oncology : official journal of the American Society of Clinical Oncology 2009;27:1864-71.
81. Soulieres D, Senzer NN, Vokes EE, Hidalgo M, Agarwala SS, Siu LL. Multicenter phase II study of erlotinib, an oral epidermal growth factor receptor tyrosine kinase inhibitor, in patients with recurrent or metastatic squamous cell cancer of the head and neck. Journal of clinical oncology : official journal of the American Society of Clinical Oncology 2004;22:77-85.
82. Egloff AM, Grandis JR. Molecular pathways: context-dependent approaches to Notch targeting as cancer therapy. Clinical cancer research : an official journal of the American Association for Cancer Research 2012;18:5188-95.
83. Song X, Xia R, Li J, et al. Common and complex Notch1 mutations in Chinese oral squamous cell carcinoma. Clinical cancer research : an official journal of the American Association for Cancer Research 2014;20:701-10.
84. Sun W, Gaykalova DA, Ochs MF, et al. Activation of the NOTCH pathway in head and neck cancer. Cancer research 2014;74:1091-104.
85. Tolcher AW, Messersmith WA, Mikulski SM, et al. Phase I study of RO4929097, a gamma secretase inhibitor of Notch signaling, in patients with refractory metastatic or locally advanced solid tumors. Journal of clinical oncology : official journal of the American Society of Clinical Oncology 2012;30:2348-53.
86. Engelman JA. Targeting PI3K signalling in cancer: opportunities, challenges and limitations. Nature reviews Cancer 2009;9:550-62.
87. Lui VW, Hedberg ML, Li H, et al. Frequent mutation of the PI3K pathway in head and neck cancer defines predictive biomarkers. Cancer discovery 2013;3:761-9.
88. Janku F, Wheler JJ, Naing A, et al. PIK3CA mutation H1047R is associated with response to PI3K/AKT/mTOR signaling pathway inhibitors in early-phase clinical trials. Cancer research 2013;73:276-84.
89. Molinolo AA, Hewitt SM, Amornphimoltham P, et al. Dissecting the Akt/mammalian target of rapamycin signaling network: emerging results from the head and neck cancer tissue array initiative. Clinical cancer research : an official journal of the American Association for Cancer Research 2007;13:4964-73.
90. Molinolo AA, Marsh C, El Dinali M, et al. mTOR as a molecular target in HPV-associated oral and cervical squamous carcinomas. Clinical cancer research : an official journal of the American Association for Cancer Research 2012;18:2558-68.
91. Bussink J, van der Kogel AJ, Kaanders JH. Activation of the PI3-K/AKT pathway and implications for radioresistance mechanisms in head and neck cancer. The Lancet Oncology 2008;9:288-96.
92. Sewell A, Brown B, Biktasova A, et al. Reverse-phase protein array profiling of oropharyngeal cancer and significance of PIK3CA mutations in HPV-associated head and neck cancer. Clinical cancer research : an official journal of the American Association for Cancer Research 2014;20:2300-11.
93. Bauman JE, Arias-Pulido H, Lee SJ, et al. A phase II study of temsirolimus and erlotinib in patients with recurrent and/or metastatic, platinum-refractory head and neck squamous cell carcinoma. Oral oncology 2013;49:461-7.
94. Kubicek GJ, Axelrod RS, Machtay M, et al. Phase I trial using the proteasome inhibitor bortezomib and concurrent chemoradiotherapy for head-and-neck malignancies. International journal of radiation oncology, biology, physics 2012;83:1192-7.
95. Bos JL. ras oncogenes in human cancer: a review. Cancer research 1989;49:4682-9.
96. Bardelli A, Siena S. Molecular mechanisms of resistance to cetuximab and panitumumab in colorectal cancer. Journal of clinical oncology : official journal of the American Society of Clinical Oncology 2010;28:1254-61.

97. Blumenschein GR, Jr., Glisson BS, C. L, et al. Final results of a phase II study of sorafenib in combination with carboplatin and paclitaxel in patients with metastatic or recurrent SCCHN. Journal of clinical oncology : official journal of the American Society of Clinical Oncology 2012;30:Abstract 5592.
98. Knowles LM, Stabile LP, Egloff AM, et al. HGF and c-Met participate in paracrine tumorigenic pathways in head and neck squamous cell cancer. Clinical cancer research : an official journal of the American Association for Cancer Research 2009;15:3740-50.
99. Seiwert TY, Jagadeeswaran R, Faoro L, et al. The MET receptor tyrosine kinase is a potential novel therapeutic target for head and neck squamous cell carcinoma. Cancer research 2009;69:3021-31.
100. Lo Muzio L, Farina A, Rubini C, et al. Effect of c-Met expression on survival in head and neck squamous cell carcinoma. Tumour biology : the journal of the International Society for Oncodevelopmental Biology and Medicine 2006;27:115-21.
101. De Bacco F, Luraghi P, Medico E, et al. Induction of MET by ionizing radiation and its role in radioresistance and invasive growth of cancer. Journal of the National Cancer Institute 2011;103:645-61.
102. Sun S, Wang Z. Head neck squamous cell carcinoma c-Met(+) cells display cancer stem cell properties and are responsible for cisplatin-resistance and metastasis. International journal of cancer Journal international du cancer 2011;129:2337-48.
103. Krumbach R, Schuler J, Hofmann M, Giesemann T, Fiebig HH, Beckers T. Primary resistance to cetuximab in a panel of patient-derived tumour xenograft models: activation of MET as one mechanism for drug resistance. Eur J Cancer 2011;47:1231-43.
104. Seiwert T, Sarantopoulos J, Kallender H, McCallum S, Keer HN, Blumenschein G, Jr. Phase II trial of single-agent foretinib (GSK1363089) in patients with recurrent or metastatic squamous cell carcinoma of the head and neck. Investigational new drugs 2013;31:417-24.
105. Aaronson DS, Horvath CM. A road map for those who don't know JAK-STAT. Science 2002;296:1653-5.
106. Grandis JR, Drenning SD, Zeng Q, et al. Constitutive activation of Stat3 signaling abrogates apoptosis in squamous cell carcinogenesis in vivo. Proceedings of the National Academy of Sciences of the United States of America 2000;97:4227-32.
107. Bonner JA, Yang ES, Trummell HQ, Nowsheen S, Willey CD, Raisch KP. Inhibition of STAT-3 results in greater cetuximab sensitivity in head and neck squamous cell carcinoma. Radiotherapy and oncology : journal of the European Society for Therapeutic Radiology and Oncology 2011;99:339-43.
108. Jarnicki A, Putoczki T, Ernst M. Stat3: linking inflammation to epithelial cancer - more than a "gut" feeling? Cell division 2010;5:14.
109. Sen M, Thomas SM, Kim S, et al. First-in-human trial of a STAT3 decoy oligonucleotide in head and neck tumors: implications for cancer therapy. Cancer discovery 2012;2:694-705.
110. Chung CH, Parker JS, Ely K, et al. Gene expression profiles identify epithelial-to-mesenchymal transition and activation of nuclear factor-kappaB signaling as characteristics of a high-risk head and neck squamous cell carcinoma. Cancer research 2006;66:8210-8.
111. Roepman P, Kemmeren P, Wessels LF, Slootweg PJ, Holstege FC. Multiple robust signatures for detecting lymph node metastasis in head and neck cancer. Cancer research 2006;66:2361-6.
112. Winter SC, Buffa FM, Silva P, et al. Relation of a hypoxia metagene derived from head and neck cancer to prognosis of multiple cancers. Cancer research 2007;67:3441-9.
113. Pramana J, Van den Brekel MW, van Velthuysen ML, et al. Gene expression profiling to predict outcome after chemoradiation in head and neck cancer. International journal of radiation oncology, biology, physics 2007;69:1544-52.
114. De Cecco L, Bossi P, Locati L, Canevari S, Licitra L. Comprehensive gene expression meta-analysis of head and neck squamous cell carcinoma microarray data defines a robust survival predictor. Annals of oncology : official journal of the European Society for Medical Oncology / ESMO 2014;25:1628-35.
115. Chung CH, Parker JS, Karaca G, et al. Molecular classification of head and neck squamous cell carcinomas using patterns of gene expression. Cancer cell 2004;5:489-500.
116. Walter V, Yin X, Wilkerson MD, et al. Molecular subtypes in head and neck cancer exhibit distinct patterns of chromosomal gain and loss of canonical cancer genes. PLoS One 2013;8:e56823.
117. Lechner M, Frampton GM, Fenton T, et al. Targeted next-generation sequencing of head and neck squamous cell carcinoma identifies novel genetic alterations in HPV+ and HPV- tumors. Genome medicine 2013;5:49.
118. Kim JJ, Tannock IF. Repopulation of cancer cells during therapy: an important cause of treatment failure. Nature reviews Cancer 2005;5:516-25.
119. Shields AF, Grierson JR, Dohmen BM, et al. Imaging proliferation in vivo with [F-18]FLT and positron emission tomography. Nature medicine 1998;4:1334-6.
120. Hoeben BA, Troost EG, Span PN, et al. 18F-FLT PET during radiotherapy or chemoradiotherapy in head and neck squamous cell carcinoma is an early predictor of outcome. Journal of nuclear medicine : official publication, Society of Nuclear Medicine 2013;54:532-40.
121. Troost EG, Bussink J, Hoffmann AL, Boerman OC, Oyen WJ, Kaanders JH. 18F-FLT PET/CT for early response monitoring and dose escalation in oropharyngeal tumors. Journal of nuclear medicine : official publication, Society of Nuclear Medicine 2010;51:866-74.

122. Kishino T, Hoshikawa H, Nishiyama Y, Yamamoto Y, Mori N. Usefulness of 3'-deoxy-3'-18F-fluorothymidine PET for predicting early response to chemoradiotherapy in head and neck cancer. Journal of nuclear medicine : official publication, Society of Nuclear Medicine 2012;53:1521-7.
123. Perk LR, Visser GW, Vosjan MJ, et al. (89)Zr as a PET surrogate radioisotope for scouting biodistribution of the therapeutic radiometals (90)Y and (177)Lu in tumor-bearing nude mice after coupling to the internalizing antibody cetuximab. Journal of nuclear medicine : official publication, Society of Nuclear Medicine 2005;46:1898-906.
124. Cai W, Chen K, He L, Cao Q, Koong A, Chen X. Quantitative PET of EGFR expression in xenograft-bearing mice using 64Cu-labeled cetuximab, a chimeric anti-EGFR monoclonal antibody. European journal of nuclear medicine and molecular imaging 2007;34:850-8.
125. van Dijk LK, Boerman OC, Franssen GM, Lok J, Kaanders JH, Bussink J. Early response monitoring with 18F-FDG PET and cetuximab-F(ab')2-SPECT after radiotherapy of human head and neck squamous cell carcinomas in a mouse model. Journal of nuclear medicine : official publication, Society of Nuclear Medicine 2014;55:1665-70.
126. Bartel DP. MicroRNAs: genomics, biogenesis, mechanism, and function. Cell 2004;116:281-97.
127. Lewis BP, Burge CB, Bartel DP. Conserved seed pairing, often flanked by adenosines, indicates that thousands of human genes are microRNA targets. Cell 2005;120:15-20.
128. Ambros V. The functions of animal microRNAs. Nature 2004;431:350-5.
129. Bartel DP, Chen CZ. Micromanagers of gene expression: the potentially widespread influence of metazoan microRNAs. Nature reviews Genetics 2004;5:396-400.
130. Lee RC, Feinbaum RL, Ambros V. The C. elegans heterochronic gene lin-4 encodes small RNAs with antisense complementarity to lin-14. Cell 1993;75:843-54.
131. Reinhart BJ, Slack FJ, Basson M, et al. The 21-nucleotide let-7 RNA regulates developmental timing in Caenorhabditis elegans. Nature 2000;403:901-6.
132. Lagos-Quintana M, Rauhut R, Lendeckel W, Tuschl T. Identification of novel genes coding for small expressed RNAs. Science 2001;294:853-8.
133. Rodriguez A, Griffiths-Jones S, Ashurst JL, Bradley A. Identification of mammalian microRNA host genes and transcription units. Genome research 2004;14:1902-10.
134. Baskerville S, Bartel DP. Microarray profiling of microRNAs reveals frequent coexpression with neighboring miRNAs and host genes. RNA 2005;11:241-7.
135. Altuvia Y, Landgraf P, Lithwick G, et al. Clustering and conservation patterns of human microRNAs. Nucleic acids research 2005;33:2697-706.
136. Bohnsack MT. Exportin 5 is a RanGTP-dependent dsRNA-binding protein that mediates nuclear export of pre-miRNAs. Rna 2004;10:185-91.
137. Garzon R, Calin GA, Croce CM. MicroRNAs in Cancer. Annual review of medicine 2009;60:167-79.
138. Bartel DP. MicroRNAs: target recognition and regulatory functions. Cell 2009;136:215-33.
139. Jones-Rhoades MW, Bartel DP, Bartel B. MicroRNAS and their regulatory roles in plants. Annual review of plant biology 2006;57:19-53.
140. Brennecke J, Stark A, Russell RB, Cohen SM. Principles of microRNA-target recognition. PLoS biology 2005;3:e85.
141. Vasudevan S, Tong Y, Steitz JA. Switching from repression to activation: microRNAs can up-regulate translation. Science 2007;318:1931-4.
142. Berezikov E, Chung WJ, Willis J, Cuppen E, Lai EC. Mammalian mirtron genes. Molecular cell 2007;28:328-36.
143. Eiring AM, Harb JG, Neviani P, et al. miR-328 functions as an RNA decoy to modulate hnRNP E2 regulation of mRNA translation in leukemic blasts. Cell 2010;140:652-65.
144. Calin GA, Dumitru CD, Shimizu M, et al. Frequent deletions and down-regulation of micro- RNA genes miR15 and miR16 at 13q14 in chronic lymphocytic leukemia. Proceedings of the National Academy of Sciences of the United States of America 2002;99:15524-9.
145. Lu J, Getz G, Miska EA, et al. MicroRNA expression profiles classify human cancers. Nature 2005;435:834-8.
146. Huppi K, Volfovsky N, Mackiewicz M, et al. MicroRNAs and genomic instability. Seminars in cancer biology 2007;17:65-73.
147. Ryan BM, Robles AI, Harris CC. Genetic variation in microRNA networks: the implications for cancer research. Nature reviews Cancer 2010;10:389-402.
148. Chuang JC, Jones PA. Epigenetics and microRNAs. Pediatric research 2007;61:24R-9R.
149. Aguda BD, Kim Y, Piper-Hunter MG, Friedman A, Marsh CB. MicroRNA regulation of a cancer network: consequences of the feedback loops involving miR-17-92, E2F, and Myc. Proceedings of the National Academy of Sciences of the United States of America 2008;105:19678-83.
150. Ma H, Yuan H, Yuan Z, et al. Genetic variations in key microRNA processing genes and risk of head and neck cancer: a case-control study in Chinese population. PLoS One 2012;7:e47544.
151. le Sage C, Nagel R, Egan DA, et al. Regulation of the p27(Kip1) tumor suppressor by miR-221 and miR-222 promotes cancer cell proliferation. The EMBO journal 2007;26:3699-708.
152. Hua Z, Lv Q, Ye W, et al. MiRNA-directed regulation of VEGF and other angiogenic factors under hypoxia. PLoS One 2006;1:e116.

153. Takebe N, Harris PJ, Warren RQ, Ivy SP. Targeting cancer stem cells by inhibiting Wnt, Notch, and Hedgehog pathways. Nature reviews Clinical oncology 2011;8:97-106.
154. Jung HM, Phillips BL, Patel RS, et al. Keratinization-associated miR-7 and miR-21 regulate tumor suppressor reversion-inducing cysteine-rich protein with kazal motifs (RECK) in oral cancer. The Journal of biological chemistry 2012;287:29261-72.
155. Chen X, Ba Y, Ma L, et al. Characterization of microRNAs in serum: a novel class of biomarkers for diagnosis of cancer and other diseases. Cell research 2008;18:997-1006.
156. Hall JS, Taylor J, Valentine HR, et al. Enhanced stability of microRNA expression facilitates classification of FFPE tumour samples exhibiting near total mRNA degradation. British journal of cancer 2012;107:684-94.
157. Sempere LF, Christensen M, Silahtaroglu A, et al. Altered MicroRNA expression confined to specific epithelial cell subpopulations in breast cancer. Cancer research 2007;67:11612-20.
158. Yanaihara N, Caplen N, Bowman E, et al. Unique microRNA molecular profiles in lung cancer diagnosis and prognosis. Cancer cell 2006;9:189-98.
159. Schetter AJ, Leung SY, Sohn JJ, et al. MicroRNA expression profiles associated with prognosis and therapeutic outcome in colon adenocarcinoma. JAMA : the journal of the American Medical Association 2008;299:425-36.
160. Liu ZL, Wang H, Liu J, Wang ZX. MicroRNA-21 (miR-21) expression promotes growth, metastasis, and chemo- or radioresistance in non-small cell lung cancer cells by targeting PTEN. Molecular and cellular biochemistry 2013;372:35-45.
161. Garzon R, Marcucci G, Croce CM. Targeting microRNAs in cancer: rationale, strategies and challenges. Nature reviews Drug discovery 2010;9:775-89.
162. Lanford RE, Hildebrandt-Eriksen ES, Petri A, et al. Therapeutic silencing of microRNA-122 in primates with chronic hepatitis C virus infection. Science 2010;327:198-201.
163. Bouchie A. First microRNA mimic enters clinic. Nature biotechnology 2013;31:577.
164. Guan X, Liu Z, Liu H, et al. A functional variant at the miR-885-5p binding site of CASP3 confers risk of both index and second primary malignancies in patients with head and neck cancer. FASEB journal : official publication of the Federation of American Societies for Experimental Biology 2013;27:1404-12.
165. Kozaki K, Imoto I, Mogi S, Omura K, Inazawa J. Exploration of tumor-suppressive microRNAs silenced by DNA hypermethylation in oral cancer. Cancer research 2008;68:2094-105.
166. Lu Z, Liu M, Stribinskis V, et al. MicroRNA-21 promotes cell transformation by targeting the programmed cell death 4 gene. Oncogene 2008;27:4373-9.
167. Liu CJ, Tsai MM, Hung PS, et al. miR-31 ablates expression of the HIF regulatory factor FIH to activate the HIF pathway in head and neck carcinoma. Cancer research 2010;70:1635-44.
168. Hui AB, Lenarduzzi M, Krushel T, et al. Comprehensive MicroRNA profiling for head and neck squamous cell carcinomas. Clinical cancer research : an official journal of the American Association for Cancer Research 2010;16:1129-39.
169. Ivanovska I, Ball AS, Diaz RL, et al. MicroRNAs in the miR-106b family regulate p21/CDKN1A and promote cell cycle progression. Molecular and cellular biology 2008;28:2167-74.
170. Rather MI, Nagashri MN, Swamy SS, Gopinath KS, Kumar A. Oncogenic microRNA-155 down-regulates tumor suppressor CDC73 and promotes oral squamous cell carcinoma cell proliferation: implications for cancer therapeutics. The Journal of biological chemistry 2013;288:608-18.
171. Zhao XD, Zhang W, Liang HJ, Ji WY. Overexpression of miR -155 promotes proliferation and invasion of human laryngeal squamous cell carcinoma via targeting SOCS1 and STAT3. PLoS One 2013;8:e56395.
172. Johnson SM, Grosshans H, Shingara J, et al. RAS is regulated by the let-7 microRNA family. Cell 2005;120:635-47.
173. Childs G, Fazzari M, Kung G, et al. Low-level expression of microRNAs let-7d and miR-205 are prognostic markers of head and neck squamous cell carcinoma. The American journal of pathology 2009;174:736-45.
174. Scott GK, Goga A, Bhaumik D, Berger CE, Sullivan CS, Benz CC. Coordinate suppression of ERBB2 and ERBB3 by enforced expression of micro-RNA miR-125a or miR-125b. The Journal of biological chemistry 2007;282:1479-86.
175. Israelsen WJ, Dayton TL, Davidson SM, et al. PKM2 Isoform-Specific Deletion Reveals a Differential Requirement for Pyruvate Kinase in Tumor Cells. Cell 2013;155:397-409.
176. Kinoshita T, Nohata N, Fuse M, et al. Tumor suppressive microRNA-133a regulates novel targets: moesin contributes to cancer cell proliferation and invasion in head and neck squamous cell carcinoma. Biochemical and biophysical research communications 2012;418:378-83.
177. Korpal M, Lee ES, Hu G, Kang Y. The miR-200 family inhibits epithelial-mesenchymal transition and cancer cell migration by direct targeting of E-cadherin transcriptional repressors ZEB1 and ZEB2. The Journal of biological chemistry 2008;283:14910-4.
178. Avissar M, Christensen BC, Kelsey KT, Marsit CJ. MicroRNA expression ratio is predictive of head and neck squamous cell carcinoma. Clinical cancer research : an official journal of the American Association for Cancer Research 2009;15:2850-5.
179. Ren W, Wang X, Gao L, et al. MiR-21 modulates chemosensitivity of tongue squamous cell carcinoma cells to cisplatin by targeting PDCD4. Molecular and cellular biochemistry 2014;390:253-62.

180. Liu M, Wang J, Huang H, Hou J, Zhang B, Wang A. miR-181a-Twist1 pathway in the chemoresistance of tongue squamous cell carcinoma. Biochemical and biophysical research communications 2013;441:364-70.
181. Sun L, Yao Y, Liu B, et al. MiR-200b and miR-15b regulate chemotherapy-induced epithelial-mesenchymal transition in human tongue cancer cells by targeting BMI1. Oncogene 2012;31:432-45.
182. Joiner MavdK, A. Basic clinical radiobiology. Fourth ed: Hodder Arnold; 2009.
183. Chang TC, Wentzel EA, Kent OA, et al. Transactivation of miR-34a by p53 broadly influences gene expression and promotes apoptosis. Molecular cell 2007;26:745-52.
184. Wang J, He J, Su F, et al. Repression of ATR pathway by miR-185 enhances radiation-induced apoptosis and proliferation inhibition. Cell death & disease 2013;4:e699.
185. Hu H, Du L, Nagabayashi G, Seeger RC, Gatti RA. ATM is down-regulated by N-Myc-regulated microRNA-421. Proceedings of the National Academy of Sciences of the United States of America 2010;107:1506-11.
186. Lal A, Pan Y, Navarro F, et al. miR-24-mediated downregulation of H2AX suppresses DNA repair in terminally differentiated blood cells. Nature structural & molecular biology 2009;16:492-8.
187. Yin E, Nelson DO, Coleman MA, Peterson LE, Wyrobek AJ. Gene expression changes in mouse brain after exposure to low-dose ionizing radiation. International journal of radiation biology 2003;79:759-75.
188. Weidhaas JB, Babar I, Nallur SM, et al. MicroRNAs as potential agents to alter resistance to cytotoxic anticancer therapy. Cancer research 2007;67:11111-6.
189. Josson S, Sung SY, Lao K, Chung LW, Johnstone PA. Radiation modulation of microRNA in prostate cancer cell lines. The Prostate 2008;68:1599-606.
190. Liang Z, Ahn J, Guo D, Votaw JR, Shim H. MicroRNA-302 Replacement Therapy Sensitizes Breast Cancer Cells to Ionizing Radiation. Pharmaceutical research 2012.
191. Niemoeller OM, Niyazi M, Corradini S, et al. MicroRNA expression profiles in human cancer cells after ionizing radiation. Radiat Oncol 2011;6:29.
192. Shiiba M, Shinozuka K, Saito K, et al. MicroRNA-125b regulates proliferation and radioresistance of oral squamous cell carcinoma. British journal of cancer 2013;108:1817-21.
193. Ishigami T, Uzawa K, Higo M, et al. Genes and molecular pathways related to radioresistance of oral squamous cell carcinoma cells. International journal of cancer Journal international du cancer 2007;120:2262-70.
194. Henson BJ, Bhattacharjee S, O'Dee DM, Feingold E, Gollin SM. Decreased expression of miR-125b and miR-100 in oral cancer cells contributes to malignancy. Genes, chromosomes & cancer 2009;48:569-82.
195. de Jong MC, Ten Hoeve JJ, Grenman R, et al. Pretreatment microRNA Expression Impacting on Epithelial-to-Mesenchymal Transition Predicts Intrinsic Radiosensitivity in Head and Neck Cancer Cell Lines and Patients. Clinical cancer research : an official journal of the American Association for Cancer Research 2015.
196. Liu N, Boohaker RJ, Jiang C, Boohaker JR, Xu B. A radiosensitivity MiRNA signature validated by the TCGA database for head and neck squamous cell carcinomas. Oncotarget 2015.
197. Hockel M, Vaupel P. Tumor hypoxia: definitions and current clinical, biologic, and molecular aspects. Journal of the National Cancer Institute 2001;93:266-76.
198. Vaupel P. Tumor microenvironmental physiology and its implications for radiation oncology. Seminars in radiation oncology 2004;14:198-206.
199. Vaupel P, Mayer A. Hypoxia in cancer: significance and impact on clinical outcome. Cancer metastasis reviews 2007;26:225-39.
200. Rademakers SE, Span PN, Kaanders JH, Sweep FC, van der Kogel AJ, Bussink J. Molecular aspects of tumour hypoxia. Molecular oncology 2008;2:41-53.
201. Vaupel P, Schaefer C, Okunieff P. Intracellular acidosis in murine fibrosarcomas coincides with ATP depletion, hypoxia, and high levels of lactate and total Pi. NMR in biomedicine 1994;7:128-36.
202. Thomlinson RH, Gray LH. The histological structure of some human lung cancers and the possible implications for radiotherapy. British journal of cancer 1955;9:539-49.
203. Bayer C, Shi K, Astner ST, Maftei CA, Vaupel P. Acute versus chronic hypoxia: why a simplified classification is simply not enough. International journal of radiation oncology, biology, physics 2011;80:965-8.
204. Harris AL. Hypoxia--a key regulatory factor in tumour growth. Nature reviews Cancer 2002;2:38-47.
205. Rofstad EK, Galappathi K, Mathiesen B, Ruud EB. Fluctuating and diffusion-limited hypoxia in hypoxia-induced metastasis. Clinical cancer research : an official journal of the American Association for Cancer Research 2007;13:1971-8.
206. Sabharwal SS, Schumacker PT. Mitochondrial ROS in cancer: initiators, amplifiers or an Achilles' heel? Nature reviews Cancer 2014;14:709-21.
207. Lu H, Forbes RA, Verma A. Hypoxia-inducible factor 1 activation by aerobic glycolysis implicates the Warburg effect in carcinogenesis. The Journal of biological chemistry 2002;277:23111-5.
208. Warburg O, Wind F, Negelein E. The Metabolism of Tumors in the Body. The Journal of general physiology 1927;8:519-30.

209. Semenza GL. Expression of hypoxia-inducible factor 1: mechanisms and consequences. Biochemical pharmacology 2000;59:47-53.
210. Ferrara N, Gerber HP, LeCouter J. The biology of VEGF and its receptors. Nature medicine 2003;9:669-76.
211. Chandel NS, McClintock DS, Feliciano CE, et al. Reactive oxygen species generated at mitochondrial complex III stabilize hypoxia-inducible factor-1alpha during hypoxia: a mechanism of O2 sensing. The Journal of biological chemistry 2000;275:25130-8.
212. Fang JS, Gillies RD, Gatenby RA. Adaptation to hypoxia and acidosis in carcinogenesis and tumor progression. Seminars in cancer biology 2008;18:330-7.
213. Balamurugan K. HIF-1 at the crossroads of hypoxia, inflammation, and cancer. International journal of cancer Journal international du cancer 2015.
214. Yang MH, Wu MZ, Chiou SH, et al. Direct regulation of TWIST by HIF-1alpha promotes metastasis. Nature cell biology 2008;10:295-305.
215. Krishnamachary B, Zagzag D, Nagasawa H, et al. Hypoxia-inducible factor-1-dependent repression of E-cadherin in von Hippel-Lindau tumor suppressor-null renal cell carcinoma mediated by TCF3, ZFHX1A, and ZFHX1B. Cancer research 2006;66:2725-31.
216. Doedens AL, Stockmann C, Rubinstein MP, et al. Macrophage expression of hypoxia-inducible factor-1 alpha suppresses T-cell function and promotes tumor progression. Cancer research 2010;70:7465-75.
217. Bruning U, Fitzpatrick SF, Frank T, Birtwistle M, Taylor CT, Cheong A. NFkappaB and HIF display synergistic behaviour during hypoxic inflammation. Cellular and molecular life sciences : CMLS 2012;69:1319-29.
218. Jung JE, Lee HG, Cho IH, et al. STAT3 is a potential modulator of HIF-1-mediated VEGF expression in human renal carcinoma cells. FASEB journal : official publication of the Federation of American Societies for Experimental Biology 2005;19:1296-8.
219. Huang X, Ding L, Bennewith KL, et al. Hypoxia-inducible mir-210 regulates normoxic gene expression involved in tumor initiation. Molecular cell 2009;35:856-67.
220. Span PN, Bussink J. Biology of hypoxia. Seminars in nuclear medicine 2015;45:101-9.
221. Wouters BG, Koritzinsky M. Hypoxia signalling through mTOR and the unfolded protein response in cancer. Nature reviews Cancer 2008;8:851-64.
222. Pereira ER, Frudd K, Awad W, Hendershot LM. Endoplasmic reticulum (ER) stress and hypoxia response pathways interact to potentiate hypoxia-inducible factor 1 (HIF-1) transcriptional activity on targets like vascular endothelial growth factor (VEGF). The Journal of biological chemistry 2014;289:3352-64.
223. Wang Y, Alam GN, Ning Y, et al. The unfolded protein response induces the angiogenic switch in human tumor cells through the PERK/ATF4 pathway. Cancer research 2012;72:5396-406.
224. Bi M, Naczki C, Koritzinsky M, et al. ER stress-regulated translation increases tolerance to extreme hypoxia and promotes tumor growth. The EMBO journal 2005;24:3470-81.
225. Hebert C, Norris K, Scheper MA, Nikitakis N, Sauk JJ. High mobility group A2 is a target for miRNA-98 in head and neck squamous cell carcinoma. Molecular cancer 2007;6:5.
226. Kulshreshtha R, Ferracin M, Wojcik SE, et al. A microRNA signature of hypoxia. Molecular and cellular biology 2007;27:1859-67.
227. Guimbellot JS, Erickson SW, Mehta T, et al. Correlation of microRNA levels during hypoxia with predicted target mRNAs through genome-wide microarray analysis. BMC medical genomics 2009;2:15.
228. Bruning U, Cerone L, Neufeld Z, et al. MicroRNA-155 promotes resolution of hypoxia-inducible factor 1alpha activity during prolonged hypoxia. Molecular and cellular biology 2011;31:4087-96.
229. Crosby ME, Kulshreshtha R, Ivan M, Glazer PM. MicroRNA regulation of DNA repair gene expression in hypoxic stress. Cancer research 2009;69:1221-9.
230. Camps C, Saini HK, Mole DR, et al. Integrated analysis of microRNA and mRNA expression and association with HIF binding reveals the complexity of microRNA expression regulation under hypoxia. Molecular cancer 2014;13:28.
231. Wang J, Zhao J, Shi M, et al. Elevated expression of miR-210 predicts poor survival of cancer patients: a systematic review and meta-analysis. PLoS One 2014;9:e89223.
232. Gee HE, Camps C, Buffa FM, et al. hsa-mir-210 is a marker of tumor hypoxia and a prognostic factor in head and neck cancer. Cancer 2010;116:2148-58.
233. Chang W, Lee CY, Park JH, et al. Survival of hypoxic human mesenchymal stem cells is enhanced by a positive feedback loop involving miR-210 and hypoxia-inducible factor 1. Journal of veterinary science 2013;14:69-76.
234. Vaupel P, Hockel M, Mayer A. Detection and characterization of tumor hypoxia using pO2 histography. Antioxidants & redox signaling 2007;9:1221-35.
235. Becker A, Hansgen G, Bloching M, Weigel C, Lautenschlager C, Dunst J. Oxygenation of squamous cell carcinoma of the head and neck: comparison of primary tumors, neck node metastases, and normal tissue. International journal of radiation oncology, biology, physics 1998;42:35-41.
236. Gatenby RA, Kessler HB, Rosenblum JS, et al. Oxygen distribution in squamous cell carcinoma metastases and its relationship to outcome of radiation therapy. International journal of radiation oncology, biology, physics 1988;14:831-8.

237. Nordsmark M, Overgaard M, Overgaard J. Pretreatment oxygenation predicts radiation response in advanced squamous cell carcinoma of the head and neck. Radiotherapy and oncology : journal of the European Society for Therapeutic Radiology and Oncology 1996;41:31-9.
238. Nordsmark M, Overgaard J. A confirmatory prognostic study on oxygenation status and loco-regional control in advanced head and neck squamous cell carcinoma treated by radiation therapy. Radiotherapy and oncology : journal of the European Society for Therapeutic Radiology and Oncology 2000;57:39-43.
239. Brizel DM, Dodge RK, Clough RW, Dewhirst MW. Oxygenation of head and neck cancer: changes during radiotherapy and impact on treatment outcome. Radiotherapy and oncology : journal of the European Society for Therapeutic Radiology and Oncology 1999;53:113-7.
240. Brizel DM, Sibley GS, Prosnitz LR, Scher RL, Dewhirst MW. Tumor hypoxia adversely affects the prognosis of carcinoma of the head and neck. International journal of radiation oncology, biology, physics 1997;38:285-9.
241. Adam MF, Gabalski EC, Bloch DA, et al. Tissue oxygen distribution in head and neck cancer patients. Head & neck 1999;21:146-53.
242. Stadler P, Becker A, Feldmann HJ, et al. Influence of the hypoxic subvolume on the survival of patients with head and neck cancer. International journal of radiation oncology, biology, physics 1999;44:749-54.
243. Dunst J, Stadler P, Becker A, et al. Tumor volume and tumor hypoxia in head and neck cancers. The amount of the hypoxic volume is important. Strahlentherapie und Onkologie : Organ der Deutschen Rontgengesellschaft [et al] 2003;179:521-6.
244. Rudat V, Vanselow B, Wollensack P, et al. Repeatability and prognostic impact of the pretreatment pO(2) histography in patients with advanced head and neck cancer. Radiotherapy and oncology : journal of the European Society for Therapeutic Radiology and Oncology 2000;57:31-7.
245. Nordsmark M, Bentzen SM, Rudat V, et al. Prognostic value of tumor oxygenation in 397 head and neck tumors after primary radiation therapy. An international multi-center study. Radiotherapy and oncology : journal of the European Society for Therapeutic Radiology and Oncology 2005;77:18-24.
246. Gray LH, Conger AD, Ebert M, Hornsey S, Scott OC. The concentration of oxygen dissolved in tissues at the time of irradiation as a factor in radiotherapy. The British journal of radiology 1953;26:638-48.
247. Howard-Flanders P, Moore D. The time interval after pulsed irradiation within which injury to bacteria can be modified by dissolved oxygen. I. A search for an effect of oxygen 0.02 second after pulsed irradiation. Radiation research 1958;9:422-37.
248. Brizel DM, Schroeder T, Scher RL, et al. Elevated tumor lactate concentrations predict for an increased risk of metastases in head-and-neck cancer. International journal of radiation oncology, biology, physics 2001;51:349-53.
249. Sattler UG, Meyer SS, Quennet V, et al. Glycolytic metabolism and tumour response to fractionated irradiation. Radiotherapy and oncology : journal of the European Society for Therapeutic Radiology and Oncology 2010;94:102-9.
250. Bussink J, Kaanders JH, Rijken PF, Raleigh JA, Van der Kogel AJ. Changes in blood perfusion and hypoxia after irradiation of a human squamous cell carcinoma xenograft tumor line. Radiation research 2000;153:398-404.
251. Harada H, Itasaka S, Kizaka-Kondoh S, et al. The Akt/mTOR pathway assures the synthesis of HIF-1alpha protein in a glucose- and reoxygenation-dependent manner in irradiated tumors. The Journal of biological chemistry 2009;284:5332-42.
252. Wozniak AJ, Glisson BS, Hande KR, Ross WE. Inhibition of etoposide-induced DNA damage and cytotoxicity in L1210 cells by dehydrogenase inhibitors and other agents. Cancer research 1984;44:626-32.
253. Tannock IF. Conventional cancer therapy: promise broken or promise delayed? Lancet 1998;351 Suppl 2:SII9-16.
254. Comerford KM, Wallace TJ, Karhausen J, Louis NA, Montalto MC, Colgan SP. Hypoxia-inducible factor-1-dependent regulation of the multidrug resistance (MDR1) gene. Cancer research 2002;62:3387-94.
255. Skovsgaard T. Transport and binding of daunorubicin, adriamycin, and rubidazone in Ehrlich ascites tumour cells. Biochemical pharmacology 1977;26:215-22.
256. Overgaard J. Hypoxic modification of radiotherapy in squamous cell carcinoma of the head and neck--a systematic review and meta-analysis. Radiotherapy and oncology : journal of the European Society for Therapeutic Radiology and Oncology 2011;100:22-32.
257. Fortin A, Wang CS, Vigneault E. Effect of pretreatment anemia on treatment outcome of concurrent radiochemotherapy in patients with head and neck cancer. International journal of radiation oncology, biology, physics 2008;72:255-60.
258. Lee WR, Berkey B, Marcial V, et al. Anemia is associated with decreased survival and increased locoregional failure in patients with locally advanced head and neck carcinoma: a secondary analysis of RTOG 85-27. International journal of radiation oncology, biology, physics 1998;42:1069-75.
259. Hoff CM, Hansen HS, Overgaard M, et al. The importance of haemoglobin level and effect of transfusion in HNSCC patients treated with radiotherapy--results from the randomized DAHANCA 5 study.

Radiotherapy and oncology : journal of the European Society for Therapeutic Radiology and Oncology 2011;98:28-33.
260. Lambin P, Ramaekers BL, van Mastrigt GA, et al. Erythropoietin as an adjuvant treatment with (chemo) radiation therapy for head and neck cancer. The Cochrane database of systematic reviews 2009:CD006158.
261. Bennett M, Feldmeier J, Smee R, Milross C. Hyperbaric oxygenation for tumour sensitisation to radiotherapy: a systematic review of randomised controlled trials. Cancer treatment reviews 2008;34:577-91.
262. Rubin P, Hanley J, Keys HM, Marcial V, Brady L. Carbogen breathing during radiation therapy-the Radiation Therapy Oncology Group Study. International journal of radiation oncology, biology, physics 1979;5:1963-70.
263. Kaanders JH, Pop LA, Marres HA, et al. ARCON: experience in 215 patients with advanced head-and-neck cancer. International journal of radiation oncology, biology, physics 2002;52:769-78.
264. Janssens GO, Rademakers SE, Terhaard CH, et al. Accelerated radiotherapy with carbogen and nicotinamide for laryngeal cancer: results of a phase III randomized trial. Journal of clinical oncology : official journal of the American Society of Clinical Oncology 2012;30:1777-83.
265. Lee DJ, Cosmatos D, Marcial VA, et al. Results of an RTOG phase III trial (RTOG 85-27) comparing radiotherapy plus etanidazole with radiotherapy alone for locally advanced head and neck carcinomas. International journal of radiation oncology, biology, physics 1995;32:567-76.
266. Van den Bogaert W, van der Schueren E, Horiot JC, et al. The EORTC randomized trial on three fractions per day and misonidazole (trial no. 22811) in advanced head and neck cancer: long-term results and side effects. Radiotherapy and oncology : journal of the European Society for Therapeutic Radiology and Oncology 1995;35:91-9.
267. Overgaard J. Clinical evaluation of nitroimidazoles as modifiers of hypoxia in solid tumors. Oncology research 1994;6:509-18.
268. Overgaard J, Hansen HS, Overgaard M, et al. A randomized double-blind phase III study of nimorazole as a hypoxic radiosensitizer of primary radiotherapy in supraglottic larynx and pharynx carcinoma. Results of the Danish Head and Neck Cancer Study (DAHANCA) Protocol 5-85. Radiotherapy and oncology : journal of the European Society for Therapeutic Radiology and Oncology 1998;46:135-46.
269. Bentzen J, Toustrup K, Eriksen JG, Primdahl H, Andersen LJ, Overgaard J. Locally advanced head and neck cancer treated with accelerated radiotherapy, the hypoxic modifier nimorazole and weekly cisplatin. Results from the DAHANCA 18 phase II study. Acta Oncol 2015:1-7.
270. Brown JM. SR 4233 (tirapazamine): a new anticancer drug exploiting hypoxia in solid tumours. British journal of cancer 1993;67:1163-70.
271. Lee DJ, Trotti A, Spencer S, et al. Concurrent tirapazamine and radiotherapy for advanced head and neck carcinomas: a Phase II study. International journal of radiation oncology, biology, physics 1998;42:811-5.
272. Rischin D, Peters L, Hicks R, et al. Phase I trial of concurrent tirapazamine, cisplatin, and radiotherapy in patients with advanced head and neck cancer. Journal of clinical oncology : official journal of the American Society of Clinical Oncology 2001;19:535-42.
273. Rischin D, Peters L, Fisher R, et al. Tirapazamine, Cisplatin, and Radiation versus Fluorouracil, Cisplatin, and Radiation in patients with locally advanced head and neck cancer: a randomized phase II trial of the Trans-Tasman Radiation Oncology Group (TROG 98.02). Journal of clinical oncology : official journal of the American Society of Clinical Oncology 2005;23:79-87.
274. Rischin D, Narayan K, Oza AM, et al. Phase 1 study of tirapazamine in combination with radiation and weekly cisplatin in patients with locally advanced cervical cancer. International journal of gynecological cancer : official journal of the International Gynecological Cancer Society 2010;20:827-33.
275. Rischin D, Hicks RJ, Fisher R, et al. Prognostic significance of [18F]-misonidazole positron emission tomography-detected tumor hypoxia in patients with advanced head and neck cancer randomly assigned to chemoradiation with or without tirapazamine: a substudy of Trans-Tasman Radiation Oncology Group Study 98.02. Journal of clinical oncology : official journal of the American Society of Clinical Oncology 2006;24:2098-104.
276. Hendrickson K, Phillips M, Smith W, Peterson L, Krohn K, Rajendran J. Hypoxia imaging with [F-18] FMISO-PET in head and neck cancer: potential for guiding intensity modulated radiation therapy in overcoming hypoxia-induced treatment resistance. Radiotherapy and oncology : journal of the European Society for Therapeutic Radiology and Oncology 2011;101:369-75.
277. Galvin JM, De Neve W. Intensity modulating and other radiation therapy devices for dose painting. Journal of clinical oncology : official journal of the American Society of Clinical Oncology 2007;25:924-30.
278. Kyzas PA, Cunha IW, Ioannidis JP. Prognostic significance of vascular endothelial growth factor immunohistochemical expression in head and neck squamous cell carcinoma: a meta-analysis. Clinical cancer research : an official journal of the American Association for Cancer Research 2005;11:1434-40.
279. Koukourakis MI, Giatromanolaki A, Sivridis E, et al. Squamous cell head and neck cancer: evidence of angiogenic regeneration during radiotherapy. Anticancer research 2001;21:4301-9.
280. Fury MG, Lee NY, Sherman E, et al. A phase 2 study of bevacizumab with cisplatin plus intensity-modulated radiation therapy for stage III/IVB head and neck squamous cell cancer. Cancer 2012;118:5008-14.

281. Hoang T, Huang S, Armstrong E, Eickhoff JC, Harari PM. Enhancement of radiation response with bevacizumab. Journal of experimental & clinical cancer research : CR 2012;31:37.
282. Willett CG, Boucher Y, di Tomaso E, et al. Direct evidence that the VEGF-specific antibody bevacizumab has antivascular effects in human rectal cancer. Nature medicine 2004;10:145-7.
283. Semenza GL. Defining the role of hypoxia-inducible factor 1 in cancer biology and therapeutics. Oncogene 2010;29:625-34.
284. Schwartz DL, Powis G, Thitai-Kumar A, et al. The selective hypoxia inducible factor-1 inhibitor PX-478 provides in vivo radiosensitization through tumor stromal effects. Molecular cancer therapeutics 2009;8:947-58.
285. Nozue M, Lee I, Yuan F, et al. Interlaboratory variation in oxygen tension measurement by Eppendorf "Histograph" and comparison with hypoxic marker. Journal of surgical oncology 1997;66:30-8.
286. Evans SM, Hahn S, Pook DR, et al. Detection of hypoxia in human squamous cell carcinoma by EF5 binding. Cancer research 2000;60:2018-24.
287. Raleigh JA, Calkins-Adams DP, Rinker LH, et al. Hypoxia and vascular endothelial growth factor expression in human squamous cell carcinomas using pimonidazole as a hypoxia marker. Cancer research 1998;58:3765-8.
288. Varghese AJ, Gulyas S, Mohindra JK. Hypoxia-dependent reduction of 1-(2-nitro-1-imidazolyl)-3-methoxy-2-propanol by Chinese hamster ovary cells and KHT tumor cells in vitro and in vivo. Cancer research 1976;36:3761-5.
289. Raleigh JA, Chou SC, Arteel GE, Horsman MR. Comparisons among pimonidazole binding, oxygen electrode measurements, and radiation response in C3H mouse tumors. Radiation research 1999;151:580-9.
290. Ljungkvist AS, Bussink J, Kaanders JH, van der Kogel AJ. Dynamics of tumor hypoxia measured with bioreductive hypoxic cell markers. Radiation research 2007;167:127-45.
291. Dennis MF, Stratford MR, Wardman P, Watts ME. Cellular uptake of misonidazole and analogues with acidic or basic functions. International journal of radiation biology and related studies in physics, chemistry, and medicine 1985;47:629-43.
292. Nordsmark M, Loncaster J, Aquino-Parsons C, et al. Measurements of hypoxia using pimonidazole and polarographic oxygen-sensitive electrodes in human cervix carcinomas. Radiotherapy and oncology : journal of the European Society for Therapeutic Radiology and Oncology 2003;67:35-44.
293. Nordsmark M, Loncaster J, Aquino-Parsons C, et al. The prognostic value of pimonidazole and tumour pO2 in human cervix carcinomas after radiation therapy: a prospective international multi-center study. Radiotherapy and oncology : journal of the European Society for Therapeutic Radiology and Oncology 2006;80:123-31.
294. Kaanders JH, Wijffels KI, Marres HA, et al. Pimonidazole binding and tumor vascularity predict for treatment outcome in head and neck cancer. Cancer research 2002;62:7066-74.
295. Evans SM, Du KL, Chalian AA, et al. Patterns and levels of hypoxia in head and neck squamous cell carcinomas and their relationship to patient outcome. International journal of radiation oncology, biology, physics 2007;69:1024-31.
296. Sobhanifar S, Aquino-Parsons C, Stanbridge EJ, Olive P. Reduced expression of hypoxia-inducible factor-1alpha in perinecrotic regions of solid tumors. Cancer research 2005;65:7259-66.
297. Aebersold DM, Burri P, Beer KT, et al. Expression of hypoxia-inducible factor-1alpha: a novel predictive and prognostic parameter in the radiotherapy of oropharyngeal cancer. Cancer research 2001;61:2911-6.
298. Koukourakis MI, Giatromanolaki A, Sivridis E, et al. Hypoxia-inducible factor (HIF1A and HIF2A), angiogenesis, and chemoradiotherapy outcome of squamous cell head-and-neck cancer. International journal of radiation oncology, biology, physics 2002;53:1192-202.
299. Kyzas PA, Stefanou D, Batistatou A, Agnantis NJ. Hypoxia-induced tumor angiogenic pathway in head and neck cancer: an in vivo study. Cancer letters 2005;225:297-304.
300. Wachters JE, Schrijvers ML, Slagter-Menkema L, et al. Prognostic significance of HIF-1a, CA-IX, and OPN in T1-T2 laryngeal carcinoma treated with radiotherapy. The Laryngoscope 2013;123:2154-60.
301. Beasley NJ, Leek R, Alam M, et al. Hypoxia-inducible factors HIF-1alpha and HIF-2alpha in head and neck cancer: relationship to tumor biology and treatment outcome in surgically resected patients. Cancer research 2002;62:2493-7.
302. Rademakers SE, Lok J, van der Kogel AJ, Bussink J, Kaanders JH. Metabolic markers in relation to hypoxia; staining patterns and colocalization of pimonidazole, HIF-1alpha, CAIX, LDH-5, GLUT-1, MCT1 and MCT4. BMC cancer 2011;11:167.
303. Mineta H, Miura K, Takebayashi S, et al. Prognostic value of glucose transporter 1 expression in patients with hypopharyngeal carcinoma. Anticancer research 2002;22:3489-94.
304. Oliver RJ, Woodwards RT, Sloan P, Thakker NS, Stratford IJ, Airley RE. Prognostic value of facilitative glucose transporter Glut-1 in oral squamous cell carcinomas treated by surgical resection; results of EORTC Translational Research Fund studies. Eur J Cancer 2004;40:503-7.
305. Jonathan RA, Wijffels KI, Peeters W, et al. The prognostic value of endogenous hypoxia-related markers for head and neck squamous cell carcinomas treated with ARCON. Radiotherapy and oncology : journal of the European Society for Therapeutic Radiology and Oncology 2006;79:288-97.

306. Eckert AW, Lautner MH, Schutze A, Taubert H, Schubert J, Bilkenroth U. Coexpression of hypoxia-inducible factor-1alpha and glucose transporter-1 is associated with poor prognosis in oral squamous cell carcinoma patients. Histopathology 2011;58:1136-47.
307. Wykoff CC, Beasley NJ, Watson PH, et al. Hypoxia-inducible expression of tumor-associated carbonic anhydrases. Cancer research 2000;60:7075-83.
308. Koukourakis MI, Giatromanolaki A, Sivridis E, et al. Hypoxia-regulated carbonic anhydrase-9 (CA9) relates to poor vascularization and resistance of squamous cell head and neck cancer to chemoradiotherapy. Clinical cancer research : an official journal of the American Association for Cancer Research 2001;7:3399-403.
309. Nordsmark M, Eriksen JG, Gebski V, Alsner J, Horsman MR, Overgaard J. Differential risk assessments from five hypoxia specific assays: The basis for biologically adapted individualized radiotherapy in advanced head and neck cancer patients. Radiotherapy and oncology : journal of the European Society for Therapeutic Radiology and Oncology 2007;83:389-97.
310. Eriksen JG, Overgaard J, Danish H, Neck Cancer Study G. Lack of prognostic and predictive value of CA IX in radiotherapy of squamous cell carcinoma of the head and neck with known modifiable hypoxia: an evaluation of the DAHANCA 5 study. Radiotherapy and oncology : journal of the European Society for Therapeutic Radiology and Oncology 2007;83:383-8.
311. Chien CY, Su CY, Chuang HC, et al. Comprehensive study on the prognostic role of osteopontin expression in oral squamous cell carcinoma. Oral oncology 2009;45:798-802.
312. Ahmed M, Behera R, Chakraborty G, et al. Osteopontin: a potentially important therapeutic target in cancer. Expert opinion on therapeutic targets 2011;15:1113-26.
313. Overgaard J, Eriksen JG, Nordsmark M, Alsner J, Horsman MR. Plasma osteopontin, hypoxia, and response to the hypoxia sensitiser nimorazole in radiotherapy of head and neck cancer: results from the DAHANCA 5 randomised double-blind placebo-controlled trial. The Lancet Oncology 2005;6:757-64.
314. Lim AM, Rischin D, Fisher R, et al. Prognostic significance of plasma osteopontin in patients with locoregionally advanced head and neck squamous cell carcinoma treated on TROG 02.02 phase III trial. Clinical cancer research : an official journal of the American Association for Cancer Research 2012;18:301-7.
315. Koong AC, Denko NC, Hudson KM, et al. Candidate genes for the hypoxic tumor phenotype. Cancer research 2000;60:883-7.
316. Denko NC, Fontana LA, Hudson KM, et al. Investigating hypoxic tumor physiology through gene expression patterns. Oncogene 2003;22:5907-14.
317. Chi JT, Wang Z, Nuyten DS, et al. Gene expression programs in response to hypoxia: cell type specificity and prognostic significance in human cancers. PLoS medicine 2006;3:e47.
318. Seigneuric R, Starmans MH, Fung G, et al. Impact of supervised gene signatures of early hypoxia on patient survival. Radiotherapy and oncology : journal of the European Society for Therapeutic Radiology and Oncology 2007;83:374-82.
319. Buffa FM, Harris AL, West CM, Miller CJ. Large meta-analysis of multiple cancers reveals a common, compact and highly prognostic hypoxia metagene. British journal of cancer 2010;102:428-35.
320. Sorensen BS, Toustrup K, Horsman MR, Overgaard J, Alsner J. Identifying pH independent hypoxia induced genes in human squamous cell carcinomas in vitro. Acta Oncol 2010;49:895-905.
321. Toustrup K, Sorensen BS, Nordsmark M, et al. Development of a hypoxia gene expression classifier with predictive impact for hypoxic modification of radiotherapy in head and neck cancer. Cancer research 2011;71:5923-31.
322. Starmans MH, Chu KC, Haider S, et al. The prognostic value of temporal in vitro and in vivo derived hypoxia gene-expression signatures in breast cancer. Radiotherapy and oncology : journal of the European Society for Therapeutic Radiology and Oncology 2012;102:436-43.
323. Eustace A, Mani N, Span PN, et al. A 26-gene hypoxia signature predicts benefit from hypoxia-modifying therapy in laryngeal cancer but not bladder cancer. Clinical cancer research : an official journal of the American Association for Cancer Research 2013;19:4879-88.
324. Toustrup K, Sorensen BS, Lassen P, Wiuf C, Alsner J, Overgaard J. Gene expression classifier predicts for hypoxic modification of radiotherapy with nimorazole in squamous cell carcinomas of the head and neck. Radiotherapy and oncology : journal of the European Society for Therapeutic Radiology and Oncology 2012;102:122-9.
325. Hassan Metwally MA, Ali R, Kuddu M, et al. IAEA-HypoX. A randomized multicenter study of the hypoxic radiosensitizer nimorazole concomitant with accelerated radiotherapy in head and neck squamous cell carcinoma. Radiotherapy and oncology : journal of the European Society for Therapeutic Radiology and Oncology 2015.
326. Turkbey B, Thomasson D, Pang Y, Bernardo M, Choyke PL. The role of dynamic contrast-enhanced MRI in cancer diagnosis and treatment. Diagnostic and interventional radiology 2010;16:186-92.
327. Newbold K, Castellano I, Charles-Edwards E, et al. An exploratory study into the role of dynamic contrast-enhanced magnetic resonance imaging or perfusion computed tomography for detection of intratumoral hypoxia in head-and-neck cancer. International journal of radiation oncology, biology, physics 2009;74:29-37.
328. Jansen JF, Schoder H, Lee NY, et al. Noninvasive assessment of tumor microenvironment using dynamic contrast-enhanced magnetic resonance imaging and 18F-fluoromisonidazole positron emission

tomography imaging in neck nodal metastases. International journal of radiation oncology, biology, physics 2010;77:1403-10.
329. Chopra S, Foltz WD, Milosevic MF, et al. Comparing oxygen-sensitive MRI (BOLD R2*) with oxygen electrode measurements: a pilot study in men with prostate cancer. International journal of radiation biology 2009;85:805-13.
330. Horsman MR, Mortensen LS, Petersen JB, Busk M, Overgaard J. Imaging hypoxia to improve radiotherapy outcome. Nature reviews Clinical oncology 2012;9:674-87.
331. Prekeges JL, Rasey JS, Grunbaum Z, Krohn KH. Reduction of fluoromisonidazole, a new imaging agent for hypoxia. Biochemical pharmacology 1991;42:2387-95.
332. Chapman JD, Baer K, Lee J. Characteristics of the metabolism-induced binding of misonidazole to hypoxic mammalian cells. Cancer research 1983;43:1523-8.
333. Walton MI, Workman P. Nitroimidazole bioreductive metabolism. Quantitation and characterisation of mouse tissue benznidazole nitroreductases in vivo and in vitro. Biochemical pharmacology 1987;36:887-96.
334. Lee NY, Mechalakos JG, Nehmeh S, et al. Fluorine-18-labeled fluoromisonidazole positron emission and computed tomography-guided intensity-modulated radiotherapy for head and neck cancer: a feasibility study. International journal of radiation oncology, biology, physics 2008;70:2-13.
335. Nehmeh SA, Lee NY, Schroder H, et al. Reproducibility of intratumor distribution of (18)F-fluoromisonidazole in head and neck cancer. International journal of radiation oncology, biology, physics 2008;70:235-42.
336. Peeters SG, Zegers CM, Lieuwes NG, et al. A comparative study of the hypoxia PET tracers [(1)(8)F]HX4, [(1)(8)F]FAZA, and [(1)(8)F]FMISO in a preclinical tumor model. International journal of radiation oncology, biology, physics 2015;91:351-9.
337. Lee ST, Scott AM. Hypoxia positron emission tomography imaging with 18f-fluoromisonidazole. Seminars in nuclear medicine 2007;37:451-61.
338. Zimny M, Gagel B, DiMartino E, et al. FDG--a marker of tumour hypoxia? A comparison with [18F]fluoromisonidazole and pO2-polarography in metastatic head and neck cancer. European journal of nuclear medicine and molecular imaging 2006;33:1426-31.
339. Gagel B, Reinartz P, Dimartino E, et al. pO(2) Polarography versus positron emission tomography ([(18)F] fluoromisonidazole, [(18)F]-2-fluoro-2'-deoxyglucose). An appraisal of radiotherapeutically relevant hypoxia. Strahlentherapie und Onkologie : Organ der Deutschen Rontgengesellschaft [et al] 2004;180:616-22.
340. Mortensen LS, Buus S, Nordsmark M, et al. Identifying hypoxia in human tumors: A correlation study between 18F-FMISO PET and the Eppendorf oxygen-sensitive electrode. Acta Oncol 2010;49:934-40.
341. Rajendran JG, Schwartz DL, O'Sullivan J, et al. Tumor hypoxia imaging with [F-18] fluoromisonidazole positron emission tomography in head and neck cancer. Clinical cancer research : an official journal of the American Association for Cancer Research 2006;12:5435-41.
342. Eschmann SM, Paulsen F, Reimold M, et al. Prognostic impact of hypoxia imaging with 18F-misonidazole PET in non-small cell lung cancer and head and neck cancer before radiotherapy. Journal of nuclear medicine : official publication, Society of Nuclear Medicine 2005;46:253-60.
343. Lee N, Nehmeh S, Schoder H, et al. Prospective trial incorporating pre-/mid-treatment [18F]-misonidazole positron emission tomography for head-and-neck cancer patients undergoing concurrent chemoradiotherapy. International journal of radiation oncology, biology, physics 2009;75:101-8.
344. Zips D, Zophel K, Abolmaali N, et al. Exploratory prospective trial of hypoxia-specific PET imaging during radiochemotherapy in patients with locally advanced head-and-neck cancer. Radiotherapy and oncology : journal of the European Society for Therapeutic Radiology and Oncology 2012;105:21-8.
345. Kikuchi M, Yamane T, Shinohara S, et al. 18F-fluoromisonidazole positron emission tomography before treatment is a predictor of radiotherapy outcome and survival prognosis in patients with head and neck squamous cell carcinoma. Annals of nuclear medicine 2011;25:625-33.
346. Lin Z, Mechalakos J, Nehmeh S, et al. The influence of changes in tumor hypoxia on dose-painting treatment plans based on 18F-FMISO positron emission tomography. International journal of radiation oncology, biology, physics 2008;70:1219-28.
347. Okamoto S, Shiga T, Yasuda K, et al. High reproducibility of tumor hypoxia evaluated by 18F-fluoromisonidazole PET for head and neck cancer. Journal of nuclear medicine : official publication, Society of Nuclear Medicine 2013;54:201-7.
348. Tachibana I, Nishimura Y, Shibata T, et al. A prospective clinical trial of tumor hypoxia imaging with 18F-fluoromisonidazole positron emission tomography and computed tomography (F-MISO PET/CT) before and during radiation therapy. Journal of radiation research 2013;54:1078-84.
349. Segard T, Robins PD, Yusoff IF, et al. Detection of hypoxia with 18F-fluoromisonidazole (18F-FMISO) PET/CT in suspected or proven pancreatic cancer. Clinical nuclear medicine 2013;38:1-6.
350. Roels S, Slagmolen P, Nuyts J, et al. Biological image-guided radiotherapy in rectal cancer: is there a role for FMISO or FLT, next to FDG? Acta Oncol 2008;47:1237-48.
351. Souvatzoglou M, Grosu AL, Roper B, et al. Tumour hypoxia imaging with [18F]FAZA PET in head and neck cancer patients: a pilot study. European journal of nuclear medicine and molecular imaging 2007;34:1566-75.

352. Mortensen LS, Johansen J, Kallehauge J, et al. FAZA PET/CT hypoxia imaging in patients with squamous cell carcinoma of the head and neck treated with radiotherapy: results from the DAHANCA 24 trial. Radiotherapy and oncology : journal of the European Society for Therapeutic Radiology and Oncology 2012;105:14-20.
353. Petering HG, Buskirk HH, Underwood GE. The Anti-Tumor Activity of 2-Keto-3-Ethoxybutyraldehyde Bis(Thiosemicarbazone) and Related Compounds. Cancer research 1964;24:367-72.
354. Green MA, Mathias CJ, Welch MJ, et al. Copper-62-labeled pyruvaldehyde bis(N4-methylthiosemicarbazonato)copper(II): synthesis and evaluation as a positron emission tomography tracer for cerebral and myocardial perfusion. Journal of nuclear medicine : official publication, Society of Nuclear Medicine 1990;31:1989-96.
355. Dearling JL, Lewis JS, Mullen GE, Rae MT, Zweit J, Blower PJ. Design of hypoxia-targeting radiopharmaceuticals: selective uptake of copper-64 complexes in hypoxic cells in vitro. European journal of nuclear medicine 1998;25:788-92.
356. Dearling JL, Lewis JS, Mullen GE, Welch MJ, Blower PJ. Copper bis(thiosemicarbazone) complexes as hypoxia imaging agents: structure-activity relationships. Journal of biological inorganic chemistry : JBIC : a publication of the Society of Biological Inorganic Chemistry 2002;7:249-59.
357. Blower PJ, Lewis JS, Zweit J. Copper radionuclides and radiopharmaceuticals in nuclear medicine. Nuclear medicine and biology 1996;23:957-80.
358. Paterson BM, Donnelly PS. Copper complexes of bis(thiosemicarbazones): from chemotherapeutics to diagnostic and therapeutic radiopharmaceuticals. Chemical Society reviews 2011;40:3005-18.
359. Lewis JS, Sharp TL, Laforest R, Fujibayashi Y, Welch MJ. Tumor uptake of copper-diacetyl-bis(N(4)-methylthiosemicarbazone): effect of changes in tissue oxygenation. Journal of nuclear medicine : official publication, Society of Nuclear Medicine 2001;42:655-61.
360. Laforest R, Dehdashti F, Lewis JS, Schwarz SW. Dosimetry of 60/61/62/64Cu-ATSM: a hypoxia imaging agent for PET. European journal of nuclear medicine and molecular imaging 2005;32:764-70.
361. Fujibayashi Y, Taniuchi H, Yonekura Y, Ohtani H, Konishi J, Yokoyama A. Copper-62-ATSM: a new hypoxia imaging agent with high membrane permeability and low redox potential. Journal of nuclear medicine : official publication, Society of Nuclear Medicine 1997;38:1155-60.
362. Obata A, Yoshimi E, Waki A, et al. Retention mechanism of hypoxia selective nuclear imaging/radiotherapeutic agent cu-diacetyl-bis(N4-methylthiosemicarbazone) (Cu-ATSM) in tumor cells. Annals of nuclear medicine 2001;15:499-504.
363. Maurer RI, Blower PJ, Dilworth JR, Reynolds CA, Zheng Y, Mullen GE. Studies on the mechanism of hypoxic selectivity in copper bis(thiosemicarbazone) radiopharmaceuticals. Journal of medicinal chemistry 2002;45:1420-31.
364. Burgman P, O'Donoghue JA, Lewis JS, Welch MJ, Humm JL, Ling CC. Cell line-dependent differences in uptake and retention of the hypoxia-selective nuclear imaging agent Cu-ATSM. Nuclear medicine and biology 2005;32:623-30.
365. Lutsenko S. Human copper homeostasis: a network of interconnected pathways. Current opinion in chemical biology 2010;14:211-7.
366. Yoshii Y, Yoneda M, Ikawa M, et al. Radiolabeled Cu-ATSM as a novel indicator of overreduced intracellular state due to mitochondrial dysfunction: studies with mitochondrial DNA-less rho0 cells and cybrids carrying MELAS mitochondrial DNA mutation. Nuclear medicine and biology 2012;39:177-85.
367. Ikawa M, Okazawa H, Arakawa K, et al. PET imaging of redox and energy states in stroke-like episodes of MELAS. Mitochondrion 2009;9:144-8.
368. Ikawa M, Okazawa H, Kudo T, Kuriyama M, Fujibayashi Y, Yoneda M. Evaluation of striatal oxidative stress in patients with Parkinson's disease using [62Cu]ATSM PET. Nuclear medicine and biology 2011;38:945-51.
369. Donnelly PS, Liddell JR, Lim S, et al. An impaired mitochondrial electron transport chain increases retention of the hypoxia imaging agent diacetylbis(4-methylthiosemicarbazonato)copperII. Proceedings of the National Academy of Sciences of the United States of America 2012;109:47-52.
370. Gottesman MM, Fojo T, Bates SE. Multidrug resistance in cancer: role of ATP-dependent transporters. Nature reviews Cancer 2002;2:48-58.
371. Liu J, Hajibeigi A, Ren G, et al. Retention of the radiotracers 64Cu-ATSM and 64Cu-PTSM in human and murine tumors is influenced by MDR1 protein expression. Journal of nuclear medicine : official publication, Society of Nuclear Medicine 2009;50:1332-9.
372. Yoshii Y, Furukawa T, Kiyono Y, et al. Copper-64-diacetyl-bis (N4-methylthiosemicarbazone) accumulates in rich regions of CD133+ highly tumorigenic cells in mouse colon carcinoma. Nuclear medicine and biology 2010;37:395-404.
373. Hueting R, Kersemans V, Cornelissen B, et al. A comparison of the behavior of (64)Cu-acetate and (64)Cu-ATSM in vitro and in vivo. Journal of nuclear medicine : official publication, Society of Nuclear Medicine 2014;55:128-34.
374. Zowczak M, Iskra M, Torlinski L, Cofta S. Analysis of serum copper and zinc concentrations in cancer patients. Biological trace element research 2001;82:1-8.

375. Lewis JS, Herrero P, Sharp TL, et al. Delineation of hypoxia in canine myocardium using PET and copper(II)-diacetyl-bis(N(4)-methylthiosemicarbazone). Journal of nuclear medicine : official publication, Society of Nuclear Medicine 2002;43:1557-69.
376. Lewis JS, McCarthy DW, McCarthy TJ, Fujibayashi Y, Welch MJ. Evaluation of 64Cu-ATSM in vitro and in vivo in a hypoxic tumor model. Journal of nuclear medicine : official publication, Society of Nuclear Medicine 1999;40:177-83.
377. Obata A, Yoshimoto M, Kasamatsu S, et al. Intra-tumoral distribution of (64)Cu-ATSM: a comparison study with FDG. Nuclear medicine and biology 2003;30:529-34.
378. Tanaka T, Furukawa T, Fujieda S, Kasamatsu S, Yonekura Y, Fujibayashi Y. Double-tracer autoradiography with Cu-ATSM/FDG and immunohistochemical interpretation in four different mouse implanted tumor models. Nuclear medicine and biology 2006;33:743-50.
379. Oh M, Tanaka T, Kobayashi M, et al. Radio-copper-labeled Cu-ATSM: an indicator of quiescent but clonogenic cells under mild hypoxia in a Lewis lung carcinoma model. Nuclear medicine and biology 2009;36:419-26.
380. O'Donoghue JA, Zanzonico P, Pugachev A, et al. Assessment of regional tumor hypoxia using 18F-fluoromisonidazole and 64Cu(II)-diacetyl-bis(N4-methylthiosemicarbazone) positron emission tomography: Comparative study featuring microPET imaging, Po2 probe measurement, autoradiography, and fluorescent microscopy in the R3327-AT and FaDu rat tumor models. International journal of radiation oncology, biology, physics 2005;61:1493-502.
381. Vavere AL, Lewis JS. Examining the relationship between Cu-ATSM hypoxia selectivity and fatty acid synthase expression in human prostate cancer cell lines. Nuclear medicine and biology 2008;35:273-9.
382. Yuan H, Schroeder T, Bowsher JE, Hedlund LW, Wong T, Dewhirst MW. Intertumoral differences in hypoxia selectivity of the PET imaging agent 64Cu(II)-diacetyl-bis(N4-methylthiosemicarbazone). Journal of nuclear medicine : official publication, Society of Nuclear Medicine 2006;47:989-98.
383. Matsumoto K, Szajek L, Krishna MC, et al. The influence of tumor oxygenation on hypoxia imaging in murine squamous cell carcinoma using [64Cu]Cu-ATSM or [18F]Fluoromisonidazole positron emission tomography. International journal of oncology 2007;30:873-81.
384. Dence CS, Ponde DE, Welch MJ, Lewis JS. Autoradiographic and small-animal PET comparisons between (18)F-FMISO, (18)F-FDG, (18)F-FLT and the hypoxic selective (64)Cu-ATSM in a rodent model of cancer. Nuclear medicine and biology 2008;35:713-20.
385. Valtorta S, Belloli S, Sanvito F, et al. Comparison of 18F-fluoroazomycin-arabinofuranoside and 64Cu-diacetyl-bis(N4-methylthiosemicarbazone) in preclinical models of cancer. Journal of nuclear medicine : official publication, Society of Nuclear Medicine 2013;54:1106-12.
386. Carlin S, Zhang H, Reese M, Ramos NN, Chen Q, Ricketts SA. A comparison of the imaging characteristics and microregional distribution of 4 hypoxia PET tracers. Journal of nuclear medicine : official publication, Society of Nuclear Medicine 2014;55:515-21.
387. McCall KC, Humm JL, Bartlett R, Reese M, Carlin S. Copper-64-diacetyl-bis(N(4)-methylthiosemicarbazone) pharmacokinetics in FaDu xenograft tumors and correlation with microscopic markers of hypoxia. International journal of radiation oncology, biology, physics 2012;84:e393-9.
388. Hansen AE, Kristensen AT, Law I, McEvoy FJ, Kjaer A, Engelholm SA. Multimodality functional imaging of spontaneous canine tumors using 64Cu-ATSM and 18FDG PET/CT and dynamic contrast enhanced perfusion CT. Radiotherapy and oncology : journal of the European Society for Therapeutic Radiology and Oncology 2012;102:424-8.
389. Hansen AE, Kristensen AT, Jorgensen JT, et al. (64)Cu-ATSM and (18)FDG PET uptake and (64)Cu-ATSM autoradiography in spontaneous canine tumors: comparison with pimonidazole hypoxia immunohistochemistry. Radiat Oncol 2012;7:89.
390. Bradshaw TJ, Yip S, Jallow N, Forrest LJ, Jeraj R. Spatiotemporal stability of Cu-ATSM and FLT positron emission tomography distributions during radiation therapy. International journal of radiation oncology, biology, physics 2014;89:399-405.
391. Bradshaw TJ, Bowen SR, Deveau MA, et al. Molecular imaging biomarkers of resistance to radiation therapy for spontaneous nasal tumors in canines. International journal of radiation oncology, biology, physics 2015;91:787-95.
392. Clausen MM, Hansen AE, Af Rosenschold PM, et al. Dose escalation to high-risk sub-volumes based on non-invasive imaging of hypoxia and glycolytic activity in canine solid tumors: a feasibility study. Radiat Oncol 2013;8:262.
393. Clausen MM, Hansen AE, Lundemann M, et al. Dose painting based on tumor uptake of Cu-ATSM and FDG: a comparative study. Radiat Oncol 2014;9:228.
394. Takahashi N, Fujibayashi Y, Yonekura Y, et al. Evaluation of 62Cu labeled diacetyl-bis(N4-methylthiosemicarbazone) as a hypoxic tissue tracer in patients with lung cancer. Annals of nuclear medicine 2000;14:323-8.
395. Takahashi N, Fujibayashi Y, Yonekura Y, et al. Copper-62 ATSM as a hypoxic tissue tracer in myocardial ischemia. Annals of nuclear medicine 2001;15:293-6.
396. Dehdashti F, Mintun MA, Lewis JS, et al. In vivo assessment of tumor hypoxia in lung cancer with 60Cu-ATSM. European journal of nuclear medicine and molecular imaging 2003;30:844-50.
397. Wong TZ, Lacy JL, Petry NA, et al. PET of hypoxia and perfusion with 62Cu-ATSM and 62Cu-PTSM using a 62Zn/62Cu generator. AJR American journal of roentgenology 2008;190:427-32.

398. Lohith TG, Kudo T, Demura Y, et al. Pathophysiologic correlation between 62Cu-ATSM and 18F-FDG in lung cancer. Journal of nuclear medicine : official publication, Society of Nuclear Medicine 2009;50:1948-53.
399. Dehdashti F, Grigsby PW, Mintun MA, Lewis JS, Siegel BA, Welch MJ. Assessing tumor hypoxia in cervical cancer by positron emission tomography with 60Cu-ATSM: Relationship to therapeutic response—a preliminary report. International Journal of Radiation Oncology*Biology*Physics 2003;55:1233-8.
400. Dehdashti F, Grigsby PW, Lewis JS, Laforest R, Siegel BA, Welch MJ. Assessing tumor hypoxia in cervical cancer by PET with 60Cu-labeled diacetyl-bis(N4-methylthiosemicarbazone). Journal of nuclear medicine : official publication, Society of Nuclear Medicine 2008;49:201-5.
401. Grigsby PW, Malyapa RS, Higashikubo R, et al. Comparison of molecular markers of hypoxia and imaging with (60)Cu-ATSM in cancer of the uterine cervix. Molecular imaging and biology : MIB : the official publication of the Academy of Molecular Imaging 2007;9:278-83.
402. Lewis JS, Laforest R, Dehdashti F, Grigsby PW, Welch MJ, Siegel BA. An imaging comparison of 64Cu-ATSM and 60Cu-ATSM in cancer of the uterine cervix. Journal of nuclear medicine : official publication, Society of Nuclear Medicine 2008;49:1177-82.
403. Dietz DW, Dehdashti F, Grigsby PW, et al. Tumor hypoxia detected by positron emission tomography with 60Cu-ATSM as a predictor of response and survival in patients undergoing Neoadjuvant chemoradiotherapy for rectal carcinoma: a pilot study. Diseases of the colon and rectum 2008;51:1641-8.
404. Tateishi K, Tateishi U, Sato M, et al. Application of 62Cu-Diacetyl-Bis (N4-Methylthiosemicarbazone) PET Imaging to Predict Highly Malignant Tumor Grades and Hypoxia-Inducible Factor-1alpha Expression in Patients with Glioma. AJNR American journal of neuroradiology 2013;34:92-9.
405. Tateishi K, Tateishi U, Nakanowatari S, et al. (62)Cu-diacetyl-bis (N(4)-methylthiosemicarbazone) PET in human gliomas: comparative study with [(18)F]fluorodeoxyglucose and L-methyl-[(11)C]methionine PET. AJNR American journal of neuroradiology 2014;35:278-84.
406. Chao KS, Bosch WR, Mutic S, et al. A novel approach to overcome hypoxic tumor resistance: Cu-ATSM-guided intensity-modulated radiation therapy. International journal of radiation oncology, biology, physics 2001;49:1171-82.
407. Minagawa Y, Shizukuishi K, Koike I, et al. Assessment of tumor hypoxia by 62Cu-ATSM PET/CT as a predictor of response in head and neck cancer: a pilot study. Annals of nuclear medicine 2011;25:339-45.
408. Sato Y, Tsujikawa T, Oh M, et al. Assessing tumor hypoxia in head and neck cancer by PET with (6)(2)Cu-diacetyl-bis(N(4)-methylthiosemicarbazone). Clinical nuclear medicine 2014;39:1027-32.
409. Kositwattanarerk A, Oh M, Kudo T, et al. Different distribution of (62) Cu ATSM and (18)F-FDG in head and neck cancers. Clinical nuclear medicine 2012;37:252-7.
410. Nyflot MJ, Harari PM, Yip S, Perlman SB, Jeraj R. Correlation of PET images of metabolism, proliferation and hypoxia to characterize tumor phenotype in patients with cancer of the oropharynx. Radiotherapy and oncology : journal of the European Society for Therapeutic Radiology and Oncology 2012;105:36-40.
411. Nyflot MJ, Kruser TJ, Traynor AM, et al. Phase 1 trial of bevacizumab with concurrent chemoradiation therapy for squamous cell carcinoma of the head and neck with exploratory functional imaging of tumor hypoxia, proliferation, and perfusion. International journal of radiation oncology, biology, physics 2015;91:942-51.
412. Grassi I, Nanni C, Cicoria G, et al. Usefulness of 64Cu-ATSM in head and neck cancer: a preliminary prospective study. Clinical nuclear medicine 2014;39:e59-63.
413. Zhang T, Das SK, Fels DR, et al. PET with 62Cu-ATSM and 62Cu-PTSM is a useful imaging tool for hypoxia and perfusion in pulmonary lesions. AJR American journal of roentgenology 2013;201:W698-706.
414. Hino-Shishikura A, Tateishi U, Shibata H, et al. Tumor hypoxia and microscopic diffusion capacity in brain tumors: a comparison of (62)Cu-Diacetyl-Bis (N4-Methylthiosemicarbazone) PET/CT and diffusion-weighted MR imaging. European journal of nuclear medicine and molecular imaging 2014;41:1419-27.
415. Yekta S, Shih IH, Bartel DP. MicroRNA-directed cleavage of HOXB8 mRNA. Science 2004;304:594-6.
416. Magli MC, Barba P, Celetti A, De Vita G, Cillo C, Boncinelli E. Coordinate regulation of HOX genes in human hematopoietic cells. Proceedings of the National Academy of Sciences of the United States of America 1991;88:6348-52.
417. Tanzer A, Amemiya CT, Kim CB, Stadler PF. Evolution of microRNAs located within Hox gene clusters. Journal of experimental zoology Part B, Molecular and developmental evolution 2005;304:75-85.
418. Hu Z, Chen J, Tian T, et al. Genetic variants of miRNA sequences and non-small cell lung cancer survival. The Journal of clinical investigation 2008;118:2600-8.
419. Tian T, Shu Y, Chen J, et al. A functional genetic variant in microRNA-196a2 is associated with increased susceptibility of lung cancer in Chinese. Cancer epidemiology, biomarkers & prevention : a publication of the American Association for Cancer Research, cosponsored by the American Society of Preventive Oncology 2009;18:1183-7.

420. Peng S, Kuang Z, Sheng C, Zhang Y, Xu H, Cheng Q. Association of microRNA-196a-2 gene polymorphism with gastric cancer risk in a Chinese population. Digestive diseases and sciences 2010;55:2288-93.
421. Hu Z, Liang J, Wang Z, et al. Common genetic variants in pre-microRNAs were associated with increased risk of breast cancer in Chinese women. Human mutation 2009;30:79-84.
422. Dou T, Wu Q, Chen X, et al. A polymorphism of microRNA196a genome region was associated with decreased risk of glioma in Chinese population. Journal of cancer research and clinical oncology 2010;136:1853-9.
423. Bloomston M, Frankel WL, Petrocca F, et al. MicroRNA expression patterns to differentiate pancreatic adenocarcinoma from normal pancreas and chronic pancreatitis. JAMA : the journal of the American Medical Association 2007;297:1901-8.
424. Luthra R, Singh RR, Luthra MG, et al. MicroRNA-196a targets annexin A1: a microRNA-mediated mechanism of annexin A1 downregulation in cancers. Oncogene 2008;27:6667-78.
425. Sun M, Liu XH, Li JH, et al. MiR-196a is upregulated in gastric cancer and promotes cell proliferation by downregulating p27(kip1). Molecular cancer therapeutics 2012;11:842-52.
426. Tsai MM, Wang CS, Tsai CY, et al. MicroRNA-196a/-196b promote cell metastasis via negative regulation of radixin in human gastric cancer. Cancer letters 2014;351:222-31.
427. Liu XH, Lu KH, Wang KM, et al. MicroRNA-196a promotes non-small cell lung cancer cell proliferation and invasion through targeting HOXA5. BMC cancer 2012;12:348.
428. Ge J, Chen Z, Li R, Lu T, Xiao G. Upregulation of microRNA-196a and microRNA-196b cooperatively correlate with aggressive progression and unfavorable prognosis in patients with colorectal cancer. Cancer cell international 2014;14:128.
429. Hou T, Ou J, Zhao X, Huang X, Huang Y, Zhang Y. MicroRNA-196a promotes cervical cancer proliferation through the regulation of FOXO1 and p27Kip1. British journal of cancer 2014;110:1260-8.
430. Saito K, Inagaki K, Kamimoto T, et al. MicroRNA-196a is a putative diagnostic biomarker and therapeutic target for laryngeal cancer. PLoS One 2013;8:e71480.
431. Liu CJ, Tsai MM, Tu HF, Lui MT, Cheng HW, Lin SC. miR-196a overexpression and miR-196a2 gene polymorphism are prognostic predictors of oral carcinomas. Annals of surgical oncology 2013;20 Suppl 3:S406-14.
432. Maru DM, Singh RR, Hannah C, et al. MicroRNA-196a is a potential marker of progression during Barrett's metaplasia-dysplasia-invasive adenocarcinoma sequence in esophagus. The American journal of pathology 2009;174:1940-8.
433. Schimanski CC, Frerichs K, Rahman F, et al. High miR-196a levels promote the oncogenic phenotype of colorectal cancer cells. World journal of gastroenterology : WJG 2009;15:2089-96.
434. Yang G, Han D, Chen X, et al. MiR-196a exerts its oncogenic effect in glioblastoma multiforme by inhibition of IkappaBalpha both in vitro and in vivo. Neuro-oncology 2014;16:652-61.
435. Huang F, Tang J, Zhuang X, et al. MiR-196a promotes pancreatic cancer progression by targeting nuclear factor kappa-B-inhibitor alpha. PLoS One 2014;9:e87897.
436. Liu M, Du Y, Gao J, et al. Aberrant expression miR-196a is associated with abnormal apoptosis, invasion, and proliferation of pancreatic cancer cells. Pancreas 2013;42:1169-81.
437. Zhang J, Zheng F, Yu G, Yin Y, Lu Q. miR-196a targets netrin 4 and regulates cell proliferation and migration of cervical cancer cells. Biochemical and biophysical research communications 2013;440:582-8.
438. Mueller DW, Bosserhoff AK. MicroRNA miR-196a controls melanoma-associated genes by regulating HOX-C8 expression. International journal of cancer Journal international du cancer 2011;129:1064-74.
439. Li Y, Zhang M, Chen H, et al. Ratio of miR-196s to HOXC8 messenger RNA correlates with breast cancer cell migration and metastasis. Cancer research 2010;70:7894-904.
440. Braig S, Mueller DW, Rothhammer T, Bosserhoff AK. MicroRNA miR-196a is a central regulator of HOX-B7 and BMP4 expression in malignant melanoma. Cellular and molecular life sciences : CMLS 2010;67:3535-48.
441. Kawasaki H, Taira K. MicroRNA-196 inhibits HOXB8 expression in myeloid differentiation of HL60 cells. Nucleic Acids Symp Ser (Oxf) 2004:211-2.
442. Pin AL, Houle F, Fournier P, et al. Annexin-1-mediated endothelial cell migration and angiogenesis are regulated by VEGF-induced inhibition of miR-196a expression. The Journal of biological chemistry 2012.
443. Coskun E, von der Heide EK, Schlee C, et al. The role of microRNA-196a and microRNA-196b as ERG regulators in acute myeloid leukemia and acute T-lymphoblastic leukemia. Leukemia research 2011;35:208-13.
444. De Martino I, Visone R, Fedele M, et al. Regulation of microRNA expression by HMGA1 proteins. Oncogene 2009;28:1432-42.
445. Lim LH, Pervaiz S. Annexin 1: the new face of an old molecule. FASEB journal : official publication of the Federation of American Societies for Experimental Biology 2007;21:968-75.
446. Gavins FN, Yona S, Kamal AM, Flower RJ, Perretti M. Leukocyte antiadhesive actions of annexin 1: ALXR- and FPR-related anti-inflammatory mechanisms. Blood 2003;101:4140-7.
447. Cheng SX, Tu Y, Zhang S. FoxM1 promotes glioma cells progression by up-regulating Anxa1 expression. PLoS One 2013;8:e72376.

448. Liu YF, Zhang PF, Li MY, Li QQ, Chen ZC. Identification of annexin A1 as a proinvasive and prognostic factor for lung adenocarcinoma. Clinical & experimental metastasis 2011;28:413-25.
449. Garcia Pedrero JM, Fernandez MP, Morgan RO, et al. Annexin A1 down-regulation in head and neck cancer is associated with epithelial differentiation status. The American journal of pathology 2004;164:73-9.
450. Zhang L, Yang X, Zhong LP, et al. Decreased expression of Annexin A1 correlates with pathologic differentiation grade in oral squamous cell carcinoma. Journal of oral pathology & medicine : official publication of the International Association of Oral Pathologists and the American Academy of Oral Pathology 2009;38:362-70.
451. Zhu DW, Yang X, Yang CZ, et al. Annexin A1 down-regulation in oral squamous cell carcinoma correlates to pathological differentiation grade. Oral oncology 2013;49:542-50.
452. Paweletz CP, Ornstein DK, Roth MJ, et al. Loss of annexin 1 correlates with early onset of tumorigenesis in esophageal and prostate carcinoma. Cancer research 2000;60:6293-7.
453. Rodrigo JP, Garcia-Pedrero JM, Fernandez MP, Morgan RO, Suarez C, Herrero A. Annexin A1 expression in nasopharyngeal carcinoma correlates with squamous differentiation. American journal of rhinology 2005;19:483-7.
454. Zeisberg M, Neilson EG. Biomarkers for epithelial-mesenchymal transitions. The Journal of clinical investigation 2009;119:1429-37.
455. Banath JP, Klokov D, MacPhail SH, Banuelos CA, Olive PL. Residual gammaH2AX foci as an indication of lethal DNA lesions. BMC cancer 2010;10:4.
456. Klokov D, MacPhail SM, Banath JP, Byrne JP, Olive PL. Phosphorylated histone H2AX in relation to cell survival in tumor cells and xenografts exposed to single and fractionated doses of X-rays. Radiotherapy and oncology : journal of the European Society for Therapeutic Radiology and Oncology 2006;80:223-9.
457. Kluiver J, Gibcus JH, Hettinga C, et al. Rapid generation of microRNA sponges for microRNA inhibition. PLoS One 2012;7:e29275.
458. Kalluri R, Weinberg RA. The basics of epithelial-mesenchymal transition. The Journal of clinical investigation 2009;119:1420-8.
459. Yang J, Weinberg RA. Epithelial-mesenchymal transition: at the crossroads of development and tumor metastasis. Developmental cell 2008;14:818-29.
460. Kong W, Yang H, He L, et al. MicroRNA-155 is regulated by the transforming growth factor beta/Smad pathway and contributes to epithelial cell plasticity by targeting RhoA. Molecular and cellular biology 2008;28:6773-84.
461. Zeng GQ, Cheng AL, Tang J, et al. Annexin A1: a new biomarker for predicting nasopharyngeal carcinoma response to radiotherapy. Medical hypotheses 2013;81:68-70.
462. Hellweg CE. The nuclear factor kappaB pathway: a link to the immune system in the radiation response. Cancer letters 2015.
463. Bradbury CM, Markovina S, Wei SJ, et al. Indomethacin-induced radiosensitization and inhibition of ionizing radiation-induced NF-kappaB activation in HeLa cells occur via a mechanism involving p38 MAP kinase. Cancer research 2001;61:7689-96.
464. Aravindan N, Madhusoodhanan R, Ahmad S, Johnson D, Herman TS. Curcumin inhibits NFkappaB mediated radioprotection and modulate apoptosis related genes in human neuroblastoma cells. Cancer biology & therapy 2008;7:569-76.
465. Fokas E, Yoshimura M, Prevo R, et al. NVP-BEZ235 and NVP-BGT226, dual phosphatidylinositol 3-kinase/mammalian target of rapamycin inhibitors, enhance tumor and endothelial cell radiosensitivity. Radiat Oncol 2012;7:48.
466. Hu N, Flaig MJ, Su H, et al. Comprehensive characterization of annexin I alterations in esophageal squamous cell carcinoma. Clinical cancer research : an official journal of the American Association for Cancer Research 2004;10:6013-22.
467. Shen D, Chang HR, Chen Z, et al. Loss of annexin A1 expression in human breast cancer detected by multiple high-throughput analyses. Biochemical and biophysical research communications 2005;326:218-27.
468. Silistino-Souza R, Rodrigues-Lisoni FC, Cury PM, et al. Annexin 1: differential expression in tumor and mast cells in human larynx cancer. International journal of cancer Journal international du cancer 2007;120:2582-9.
469. Queiroz CJ, Nakata CM, Solito E, Damazo AS. Relationship between HPV and the biomarkers annexin A1 and p53 in oropharyngeal cancer. Infectious agents and cancer 2014;9:13.
470. Cheng AL, Huang WG, Chen ZC, et al. Identification of novel nasopharyngeal carcinoma biomarkers by laser capture microdissection and proteomic analysis. Clinical cancer research : an official journal of the American Association for Cancer Research 2008;14:435-45.
471. Liu A, Huang W, Zeng G, et al. Expression of the Annexin A1 gene is associated with suppression of growth, invasion and metastasis of nasopharyngeal carcinoma. Molecular medicine reports 2014;10:3059-67.
472. Hsiang CH, Tunoda T, Whang YE, Tyson DR, Ornstein DK. The impact of altered annexin I protein levels on apoptosis and signal transduction pathways in prostate cancer cells. The Prostate 2006;66:1413-24.

473. Maschler S, Gebeshuber CA, Wiedemann EM, et al. Annexin A1 attenuates EMT and metastatic potential in breast cancer. EMBO molecular medicine 2010;2:401-14.
474. Debret R, El Btaouri H, Duca L, et al. Annexin A1 processing is associated with caspase-dependent apoptosis in BZR cells. FEBS letters 2003;546:195-202.
475. Solito E, de Coupade C, Canaider S, Goulding NJ, Perretti M. Transfection of annexin 1 in monocytic cells produces a high degree of spontaneous and stimulated apoptosis associated with caspase-3 activation. British journal of pharmacology 2001;133:217-28.
476. Tabe Y, Jin L, Contractor R, et al. Novel role of HDAC inhibitors in AML1/ETO AML cells: activation of apoptosis and phagocytosis through induction of annexin A1. Cell death and differentiation 2007;14:1443-56.
477. Zhang Z, Huang L, Zhao W, Rigas B. Annexin 1 induced by anti-inflammatory drugs binds to NF-kappaB and inhibits its activation: anticancer effects in vitro and in vivo. Cancer research 2010;70:2379-88.
478. Petrella A, Festa M, Ercolino SF, et al. Induction of annexin-1 during TRAIL-induced apoptosis in thyroid carcinoma cells. Cell death and differentiation 2005;12:1358-60.
479. Alldridge LC, Bryant CE. Annexin 1 regulates cell proliferation by disruption of cell morphology and inhibition of cyclin D1 expression through sustained activation of the ERK1/2 MAPK signal. Experimental cell research 2003;290:93-107.
480. Alldridge LC, Harris HJ, Plevin R, Hannon R, Bryant CE. The annexin protein lipocortin 1 regulates the MAPK/ERK pathway. The Journal of biological chemistry 1999;274:37620-8.
481. Pepinsky RB, Sinclair LK. Epidermal growth factor-dependent phosphorylation of lipocortin. Nature 1986;321:81-4.
482. Croxtall JD, Waheed S, Choudhury Q, Anand R, Flower RJ. N-terminal peptide fragments of lipocortin-1 inhibit A549 cell growth and block EGF-induced stimulation of proliferation. International journal of cancer Journal international du cancer 1993;54:153-8.
483. Kang H, Ko J, Jang SW. The role of annexin A1 in expression of matrix metalloproteinase-9 and invasion of breast cancer cells. Biochemical and biophysical research communications 2012;423:188-94.
484. Cheng TY, Wu MS, Lin JT, et al. Annexin A1 is associated with gastric cancer survival and promotes gastric cancer cell invasiveness through the formyl peptide receptor/extracellular signal-regulated kinase/integrin beta-1-binding protein 1 pathway. Cancer 2012;118:5757-67.
485. de Graauw M, van Miltenburg MH, Schmidt MK, et al. Annexin A1 regulates TGF-beta signaling and promotes metastasis formation of basal-like breast cancer cells. Proceedings of the National Academy of Sciences of the United States of America 2010;107:6340-5.
486. Cote MC, Lavoie JR, Houle F, Poirier A, Rousseau S, Huot J. Regulation of vascular endothelial growth factor-induced endothelial cell migration by LIM kinase 1-mediated phosphorylation of annexin 1. The Journal of biological chemistry 2010;285:8013-21.
487. Pin AL, Houle F, Fournier P, et al. Annexin-1-mediated endothelial cell migration and angiogenesis are regulated by vascular endothelial growth factor (VEGF)-induced inhibition of miR-196a expression. The Journal of biological chemistry 2012;287:30541-51.
488. Becker C, Hammerle-Fickinger A, Riedmaier I, Pfaffl MW. mRNA and microRNA quality control for RT-qPCR analysis. Methods 2010;50:237-43.
489. Boeckx C, Wouters A, Pauwels B, et al. Expression analysis on archival material: comparison of 5 commercially available RNA isolation kits for FFPE material. Diagnostic molecular pathology : the American journal of surgical pathology, part B 2011;20:203-11.
490. Xi Y, Nakajima G, Gavin E, et al. Systematic analysis of microRNA expression of RNA extracted from fresh frozen and formalin-fixed paraffin-embedded samples. RNA 2007;13:1668-74.
491. Doleshal M, Magotra AA, Choudhury B, Cannon BD, Labourier E, Szafranska AE. Evaluation and validation of total RNA extraction methods for microRNA expression analyses in formalin-fixed, paraffin-embedded tissues. The Journal of molecular diagnostics : JMD 2008;10:203-11.
492. Gaken J, Mohamedali AM, Jiang J, et al. A functional assay for microRNA target identification and validation. Nucleic acids research 2012;40:e75.
493. Wang Z, Gerstein M, Snyder M. RNA-Seq: a revolutionary tool for transcriptomics. Nature reviews Genetics 2009;10:57-63.
494. Mutz KO, Heilkenbrinker A, Lonne M, Walter JG, Stahl F. Transcriptome analysis using next-generation sequencing. Current opinion in biotechnology 2013;24:22-30.
495. Anders S, Pyl PT, Huber W. HTSeq--a Python framework to work with high-throughput sequencing data. Bioinformatics 2015;31:166-9.
496. Love MI, Huber W, Anders S. Moderated estimation of fold change and dispersion for RNA-seq data with DESeq2. Genome biology 2014;15:550.
497. Keck MK, Zuo Z, Khattri A, et al. Integrative analysis of head and neck cancer identifies two biologically distinct HPV and three non-HPV subtypes. Clinical cancer research : an official journal of the American Association for Cancer Research 2015;21:870-81.
498. Pyeon D, Newton MA, Lambert PF, et al. Fundamental differences in cell cycle deregulation in human papillomavirus-positive and human papillomavirus-negative head/neck and cervical cancers. Cancer research 2007;67:4605-19.

499. Kong CS, Narasimhan B, Cao H, et al. The relationship between human papillomavirus status and other molecular prognostic markers in head and neck squamous cell carcinomas. International journal of radiation oncology, biology, physics 2009;74:553-61.
500. Hong AM, Martin A, Armstrong BK, et al. Human papillomavirus modifies the prognostic significance of T stage and possibly N stage in tonsillar cancer. Annals of oncology : official journal of the European Society for Medical Oncology / ESMO 2013;24:215-9.
501. Trinkaus ME, Hicks RJ, Young RJ, et al. Correlation of p16 status, hypoxic imaging using [18F]-misonidazole positron emission tomography and outcome in patients with loco-regionally advanced head and neck cancer. Journal of medical imaging and radiation oncology 2014;58:89-97.
502. Sorensen BS, Busk M, Olthof N, et al. Radiosensitivity and effect of hypoxia in HPV positive head and neck cancer cells. Radiotherapy and oncology : journal of the European Society for Therapeutic Radiology and Oncology 2013;108:500-5.
503. Zhang E, Feng X, Liu F, Zhang P, Liang J, Tang X. Roles of PI3K/Akt and c-Jun signaling pathways in human papillomavirus type 16 oncoprotein-induced HIF-1alpha, VEGF, and IL-8 expression and in vitro angiogenesis in non-small cell lung cancer cells. PLoS One 2014;9:e103440.
504. Kersemans V, Cornelissen B, Hueting R, et al. Hypoxia imaging using PET and SPECT: the effects of anesthetic and carrier gas on [Cu]-ATSM, [Tc]-HL91 and [F]-FMISO tumor hypoxia accumulation. PLoS One 2011;6:e25911.
505. Bentzen L, Keiding S, Nordsmark M, et al. Tumour oxygenation assessed by 18F-fluoromisonidazole PET and polarographic needle electrodes in human soft tissue tumours. Radiotherapy and oncology : journal of the European Society for Therapeutic Radiology and Oncology 2003;67:339-44.
506. Rajendran JG, Wilson DC, Conrad EU, et al. [(18)F]FMISO and [(18)F]FDG PET imaging in soft tissue sarcomas: correlation of hypoxia, metabolism and VEGF expression. European journal of nuclear medicine and molecular imaging 2003;30:695-704.
507. Effert PJ, Bares R, Handt S, Wolff JM, Bull U, Jakse G. Metabolic imaging of untreated prostate cancer by positron emission tomography with 18fluorine-labeled deoxyglucose. The Journal of urology 1996;155:994-8.
508. Bowen SR, van der Kogel AJ, Nordsmark M, Bentzen SM, Jeraj R. Characterization of positron emission tomography hypoxia tracer uptake and tissue oxygenation via electrochemical modeling. Nuclear medicine and biology 2011;38:771-80.
509. Adams MC, Turkington TG, Wilson JM, Wong TZ. A systematic review of the factors affecting accuracy of SUV measurements. AJR American journal of roentgenology 2010;195:310-20.
510. Jackson T, Chung MK, Mercier G, Ozonoff A, Subramaniam RM. FDG PET/CT interobserver agreement in head and neck cancer: FDG and CT measurements of the primary tumor site. Nuclear medicine communications 2012;33:305-12.
511. Lodge MA, Chaudhry MA, Wahl RL. Noise considerations for PET quantification using maximum and peak standardized uptake value. Journal of nuclear medicine : official publication, Society of Nuclear Medicine 2012;53:1041-7.
512. Boellaard R. Standards for PET image acquisition and quantitative data analysis. Journal of nuclear medicine : official publication, Society of Nuclear Medicine 2009;50 Suppl 1:11S-20S.
513. Boellaard R, Delgado-Bolton R, Oyen WJ, et al. FDG PET/CT: EANM procedure guidelines for tumour imaging: version 2.0. European journal of nuclear medicine and molecular imaging 2015;42:328-54.
514. Goldenberg D, Begum S, Westra WH, et al. Cystic lymph node metastasis in patients with head and neck cancer: An HPV-associated phenomenon. Head & neck 2008;30:898-903.
515. Skovgaard D, Kjaer M, Madsen J, Kjaer A. Noninvasive 64Cu-ATSM and PET/CT assessment of hypoxia in rat skeletal muscles and tendons during muscle contractions. Journal of nuclear medicine : official publication, Society of Nuclear Medicine 2009;50:950-8.
516. D'Amico F, Skarmoutsou E, Sanfilippo S, Camakaris J. Menkes protein localization in rat parotid acinar cells. Acta histochemica 2005;107:373-8.
517. Melino S, Santone C, Di Nardo P, Sarkar B. Histatins: salivary peptides with copper(II)- and zinc(II)-binding motifs: perspectives for biomedical applications. The FEBS journal 2014;281:657-72.
518. Cobb LM, Hacker T, Nolan J. NAD(P)H nitroblue tetrazolium reductase levels in apparently normoxic tissues: a histochemical study correlating enzyme activity with binding of radiolabelled misonidazole. British journal of cancer 1990;61:524-9.
519. Inoue K, Takano H, Shimada A, Satoh M. Metallothionein as an anti-inflammatory mediator. Mediators of inflammation 2009;2009:101659.
520. Samygina VR, Sokolov AV, Bourenkov G, et al. Ceruloplasmin: macromolecular assemblies with iron-containing acute phase proteins. PLoS One 2013;8:e67145.
521. Shreve PD, Anzai Y, Wahl RL. Pitfalls in oncologic diagnosis with FDG PET imaging: physiologic and benign variants. Radiographics : a review publication of the Radiological Society of North America, Inc 1999;19:61-77; quiz 150-1.
522. Bhargava P, Rahman S, Wendt J. Atlas of confounding factors in head and neck PET/CT imaging. Clinical nuclear medicine 2011;36:e20-9.
523. Stahl A, Ott K, Weber WA, et al. FDG PET imaging of locally advanced gastric carcinomas: correlation with endoscopic and histopathological findings. European journal of nuclear medicine and molecular imaging 2003;30:288-95.

524. de Bruin EC, van de Pas S, Lips EH, et al. Macrodissection versus microdissection of rectal carcinoma: minor influence of stroma cells to tumor cell gene expression profiles. BMC genomics 2005;6:142.
525. von Ahlfen S, Missel A, Bendrat K, Schlumpberger M. Determinants of RNA quality from FFPE samples. PLoS One 2007;2:e1261.
526. Hedegaard J, Thorsen K, Lund MK, et al. Next-generation sequencing of RNA and DNA isolated from paired fresh-frozen and formalin-fixed paraffin-embedded samples of human cancer and normal tissue. PLoS One 2014;9:e98187.
527. Sinicropi D, Qu K, Collin F, et al. Whole transcriptome RNA-Seq analysis of breast cancer recurrence risk using formalin-fixed paraffin-embedded tumor tissue. PLoS One 2012;7:e40092.
528. Lopci E, Grassi I, Rubello D, et al. Prognostic Evaluation of Disease Outcome in Solid Tumors Investigated With 64Cu-ATSM PET/CT. Clinical nuclear medicine 2015.
529. Bai B, Bading J, Conti PS. Tumor quantification in clinical positron emission tomography. Theranostics 2013;3:787-801.
530. Tripathi SC, Matta A, Kaur J, et al. Nuclear S100A7 is associated with poor prognosis in head and neck cancer. PLoS One 2010;5:e11939.
531. Shubbar E, Vegfors J, Carlstrom M, Petersson S, Enerback C. Psoriasin (S100A7) increases the expression of ROS and VEGF and acts through RAGE to promote endothelial cell proliferation. Breast cancer research and treatment 2012;134:71-80.
532. Connor KM, Hempel N, Nelson KK, et al. Manganese superoxide dismutase enhances the invasive and migratory activity of tumor cells. Cancer research 2007;67:10260-7.
533. Shackelford RE, Mayhall K, Maxwell NM, Kandil E, Coppola D. Nicotinamide phosphoribosyltransferase in malignancy: a review. Genes & cancer 2013;4:447-56.
534. Bae SK, Kim SR, Kim JG, et al. Hypoxic induction of human visfatin gene is directly mediated by hypoxia-inducible factor-1. FEBS letters 2006;580:4105-13.
535. Xu TY, Zhang SL, Dong GQ, et al. Discovery and characterization of novel small-molecule inhibitors targeting nicotinamide phosphoribosyltransferase. Scientific reports 2015;5:10043.
536. Yalcin A, Clem BF, Imbert-Fernandez Y, et al. 6-Phosphofructo-2-kinase (PFKFB3) promotes cell cycle progression and suppresses apoptosis via Cdk1-mediated phosphorylation of p27. Cell death & disease 2014;5:e1337.
537. Bando H, Atsumi T, Nishio T, et al. Phosphorylation of the 6-phosphofructo-2-kinase/fructose 2,6-bisphosphatase/PFKFB3 family of glycolytic regulators in human cancer. Clinical cancer research : an official journal of the American Association for Cancer Research 2005;11:5784-92.
538. Lin CI, Merley A, Sciuto TE, et al. TM4SF1: a new vascular therapeutic target in cancer. Angiogenesis 2014;17:897-907.
539. Amin EM, Oltean S, Hua J, et al. WT1 mutants reveal SRPK1 to be a downstream angiogenesis target by altering VEGF splicing. Cancer cell 2011;20:768-80.
540. Lee SH, Bae SC, Kim KW, Lee YM. RUNX3 inhibits hypoxia-inducible factor-1alpha protein stability by interacting with prolyl hydroxylases in gastric cancer cells. Oncogene 2014;33:1458-67.
541. Lee SH, Kim J, Kim WH, Lee YM. Hypoxic silencing of tumor suppressor RUNX3 by histone modification in gastric cancer cells. Oncogene 2009;28:184-94.
542. Lee KM, Nam K, Oh S, Lim J, Lee T, Shin I. ECM1 promotes the Warburg effect through EGF-mediated activation of PKM2. Cellular signalling 2015;27:228-35.
543. Noy R, Pollard JW. Tumor-associated macrophages: from mechanisms to therapy. Immunity 2014;41:49-61.
544. Labiano S, Palazon A, Melero I. Immune response regulation in the tumor microenvironment by hypoxia. Seminars in oncology 2015;42:378-86.
545. Haque I, Banerjee S, Mehta S, et al. Cysteine-rich 61-connective tissue growth factor-nephroblastoma-overexpressed 5 (CCN5)/Wnt-1-induced signaling protein-2 (WISP-2) regulates microRNA-10b via hypoxia-inducible factor-1alpha-TWIST signaling networks in human breast cancer cells. The Journal of biological chemistry 2011;286:43475-85.
546. Lawrie CH, Gal S, Dunlop HM, et al. Detection of elevated levels of tumour-associated microRNAs in serum of patients with diffuse large B-cell lymphoma. British journal of haematology 2008;141:672-5.
547. Mitchell PS, Parkin RK, Kroh EM, et al. Circulating microRNAs as stable blood-based markers for cancer detection. Proceedings of the National Academy of Sciences of the United States of America 2008;105:10513-8.
548. Schwarzenbach H, Nishida N, Calin GA, Pantel K. Clinical relevance of circulating cell-free microRNAs in cancer. Nature reviews Clinical oncology 2014;11:145-56.
549. Kosaka N, Iguchi H, Hagiwara K, Yoshioka Y, Takeshita F, Ochiya T. Neutral sphingomyelinase 2 (nSMase2)-dependent exosomal transfer of angiogenic microRNAs regulate cancer cell metastasis. The Journal of biological chemistry 2013;288:10849-59.
550. Skog J, Wurdinger T, van Rijn S, et al. Glioblastoma microvesicles transport RNA and proteins that promote tumour growth and provide diagnostic biomarkers. Nature cell biology 2008;10:1470-6.
551. Fabbri M, Paone A, Calore F, et al. MicroRNAs bind to Toll-like receptors to induce prometastatic inflammatory response. Proceedings of the National Academy of Sciences of the United States of America 2012;109:E2110-6.

552. Hsu CM, Lin PM, Wang YM, Chen ZJ, Lin SF, Yang MY. Circulating miRNA is a novel marker for head and neck squamous cell carcinoma. Tumour biology : the journal of the International Society for Oncodevelopmental Biology and Medicine 2012;33:1933-42.
553. Zheng Y, Cui L, Sun W, et al. MicroRNA-21 is a new marker of circulating tumor cells in gastric cancer patients. Cancer biomarkers : section A of Disease markers 2011;10:71-7.
554. Lu YC, Chang JT, Huang YC, et al. Combined determination of circulating miR-196a and miR-196b levels produces high sensitivity and specificity for early detection of oral cancer. Clinical biochemistry 2015;48:115-21.
555. Hale A, Lee C, Annis S, et al. An Argonaute 2 switch regulates circulating miR-210 to coordinate hypoxic adaptation across cells. Biochimica et biophysica acta 2014;1843:2528-42.
556. Rosjo H, Dahl MB, Bye A, et al. Prognostic value of circulating microRNA-210 levels in patients with moderate to severe aortic stenosis. PLoS One 2014;9:e91812.
557. Lin SC, Liu CJ, Lin JA, Chiang WF, Hung PS, Chang KW. miR-24 up-regulation in oral carcinoma: positive association from clinical and in vitro analysis. Oral oncology 2010;46:204-8.
558. Wong TS, Liu XB, Wong BY, Ng RW, Yuen AP, Wei WI. Mature miR-184 as Potential Oncogenic microRNA of Squamous Cell Carcinoma of Tongue. Clinical cancer research : an official journal of the American Association for Cancer Research 2008;14:2588-92.
559. Wang K, Yuan Y, Cho JH, McClarty S, Baxter D, Galas DJ. Comparing the MicroRNA spectrum between serum and plasma. PLoS One 2012;7:e41561.
560. Cheng HH, Yi HS, Kim Y, et al. Plasma processing conditions substantially influence circulating microRNA biomarker levels. PLoS One 2013;8:e64795.
561. Fortunato O, Boeri M, Verri C, et al. Assessment of circulating microRNAs in plasma of lung cancer patients. Molecules 2014;19:3038-54.
562. Kirschner MB, Kao SC, Edelman JJ, et al. Haemolysis during sample preparation alters microRNA content of plasma. PLoS One 2011;6:e24145.
563. Appierto V, Callari M, Cavadini E, Morelli D, Daidone MG, Tiberio P. A lipemia-independent NanoDrop((R))-based score to identify hemolysis in plasma and serum samples. Bioanalysis 2014;6:1215-26.
564. McAlexander MA, Phillips MJ, Witwer KW. Comparison of Methods for miRNA Extraction from Plasma and Quantitative Recovery of RNA from Cerebrospinal Fluid. Frontiers in genetics 2013;4:83.
565. Moret I, Sanchez-Izquierdo D, Iborra M, et al. Assessing an improved protocol for plasma microRNA extraction. PLoS One 2013;8:e82753.
566. Kroh EM, Parkin RK, Mitchell PS, Tewari M. Analysis of circulating microRNA biomarkers in plasma and serum using quantitative reverse transcription-PCR (qRT-PCR). Methods 2010;50:298-301.
567. Xiang M, Zeng Y, Yang R, et al. U6 is not a suitable endogenous control for the quantification of circulating microRNAs. Biochemical and biophysical research communications 2014;454:210-4.
568. Studer G, Luetolf UM, Glanzmann C. Locoregional failure analysis in head-and-neck cancer patients treated with IMRT. Strahlentherapie und Onkologie : Organ der Deutschen Rontgengesellschaft [et al] 2007;183:417-23; discussion 24-5.
569. Lawrentschuk N, Poon AM, Foo SS, et al. Assessing regional hypoxia in human renal tumours using 18F-fluoromisonidazole positron emission tomography. BJU international 2005;96:540-6.
570. Eustace A, Mani N, Span PN, et al. A 26-Gene Hypoxia Signature Predicts Benefit from Hypoxia-Modifying Therapy in Laryngeal Cancer but Not Bladder Cancer. Clinical cancer research : an official journal of the American Association for Cancer Research 2013;19:4879-88.
571. Mazurowski MA. Radiogenomics: what it is and why it is important. Journal of the American College of Radiology : JACR 2015;12:862-6.

Appendix I

OPEN

Citation: Cell Death and Disease (2014) 5, e1018; doi:10.1038/cddis.2013.548

www.nature.com/cddis

Review

Clinical update on cancer: molecular oncology of head and neck cancer

Y Suh[1], I Amelio[2], T Guerrero Urbano[3] and M Tavassoli*[,1]

Head and neck cancers encompass a heterogeneous group of tumours that, in general, are biologically aggressive in nature. These cancers remain difficult to treat and treatment can cause severe, long-term side effects. For patients who are not cured by surgery and/or (chemo)radiotherapy, there are few effective treatment options. Targeted therapies and predictive biomarkers are urgently needed in order to improve the management and minimise the treatment toxicity, and to allow selection of patients who are likely to benefit from both nonselective and targeted therapies. This clinical update aims to provide an insight into the current understanding of the molecular pathogenesis of the disease, and explores the novel therapies under development and in clinical trials.

Cell Death and Disease (2014) **5,** e1018; doi:10.1038/cddis.2013.548; published online 23 January 2013
Subject Category: Cancer

Facts

- Head and neck squamous cell carcinoma (HNSCC) is the sixth leading cause of cancer worldwide. Exposure to carcinogens (tobacco and alcohol) and infection with human papillomavirus (HPV) are the most common risk factors.
- The main molecular determinants in HNSCC are the abrogation of p53 and retinoblastoma (pRb) pathways that lead to uncontrolled cell replication.
- Mutations in EGFR-MEK, NOTCH, PI3K, PTEN and AKT pathways are frequently observed in HNSCC. These mutations cooperate to create aberrant mitogenic/survival signalling.
- Changes in metabolism and tumour hypoxia contribute to resistance to current therapies and tumour recurrence.

Open Questions

- Although HNSCC is a heterogeneous disease, the current molecular classification distinguishes only HPV-positive and HPV-negative tumours: further investigation to genetically classify HNSCC subgroups is needed.
- HNSCC metastasises primarily and frequently to regional lymph nodes (more rarely to other organs via haematogenous spread): genetic profiles should aid the identification of causative genes of metastasis.
- Radioresistance has been identified as an important cause of locoregional treatment failure, and identification of molecular mechanisms underpinning this could contribute to better treatment selection and outcome.
- The genetics of HNSCC is complex, especially of HPV-negative cancers: a detailed understanding of the molecular basis and identification of driving mutations and drugable targets should lead to personalised therapies.

Head and neck cancer accounts for ~4% of all malignancies worldwide and 5% mortality of all cancers,[1] and includes the following subsites: oral cavity, nasopharynx, oropharynx, hypopharynx, larynx, paranasal sinuses, nasal cavity and salivary glands. Over 90% are squamous cell carcinomas (head and neck squamous cell carcinoma (HNSCC)), arising from the epithelial cells that line the mucosal surfaces of the head and neck.

More than 75% of cases of HNSCC are attributable to smoking and alcohol consumption. Smoking increases the risk by ~10-fold compared with never smokers, and heavy alcohol intake is an independent risk factor.[2] The combined effect of tobacco and alcohol causes a greater than multiplicative risk.[3] Public health measures have been successful in reducing the use of tobacco, and therefore the incidence of HNSCC overall has been decreasing over the past 30 years in developed countries. However, there has been a dramatic increase in the incidence rates of oropharyngeal (tonsil and base of tongue) cancers because of infection with high-risk human papillomavirus (HPV).[4,5]

[1]Department of Molecular Oncology, King's College London, Guy's Hospital, Hodgkin Building, London SE1 1NU, UK; [2]Medical Research Council, Toxicology Unit, Leicester University, Leicester LE1 9HN, UK and [3]Clinical Oncology Department, Lambeth Wing, St Thomas' Hospital, Westminster Bridge Road, London SE1 7EH, UK
*Corresponding author: M Tavassoli, Department of Molecular Oncology, Head and Neck Oncology Group, Dental Institute, King's College London, Hodgkin Building, London SE1 1UL, UK. Tel: +44 (0)20 7848 6109; Fax: +44 (0)20 7848 6210; E-mail: Mahvash.tavassoli@kcl.ac.uk
Keywords: head and neck squamous cell carcinoma; targeted therapy; HPV; metabolism; hypoxia; biomarkers
Abbreviations: HNSCC, head and neck squamous cell carcinoma; HPV, human papillomavirus; ATM, ataxia telangiectasia mutated; ATR, ataxia telangiectasia and Rad3-related; EGFR, epidermal growth factor receptor; MAPK, mitogen-activated protein kinase; STAT3, signal transducer and activator of transcription 3; JAK, Janus kinase; PI3K, phosphoinositide 3-kinase; mAb, monoclonal antibody; PTEN, phosphatase and tensin homology; mTOR, mammalian target of rapamycin; GDP, guanosine diphosphate; GTP, guanosine triphosphate; VEGF, vascular endothelial growth factor receptor; PDGFR, platelet-derived growth factor receptor; HGF, hepatocyte growth factor; ATP, adenosine triphosphate
Received 04.11.13; revised 04.12.13; accepted 05.12.13; Edited by A Stephanou

At present, treatment of an individual cancer is typically determined in a multidisciplinary setting, with the histological subtype, subsite, staging information, patient fitness, baseline swallow and airway function guiding management decisions. Approximately one-third of patients present with early-stage disease and these patients are treated with either surgery or radiotherapy depending on the primary tumour site, with cure rates of 70–90%.[6] The majority of patients, however, present with locally advanced stage disease. Radical treatment in this situation requires multimodality therapy with surgery, commonly followed by postoperative radiotherapy or chemoradiotherapy, or organ preserving primary radiotherapy, with or without chemotherapy, with reduced cosmetic compromise.[7] These treatments are intensive and associated with severe acute toxicity, such as mucositis, dermatitis and dysphagia, and long-term sequelae, for example, sensorineural hearing loss, permanent xerostomia and altered swallowing function. Despite recent advances in both surgical and radiotherapy delivery techniques, up to 50% of locally advanced tumours relapse usually within the first 2 years after treatment, with limited options for salvage surgery or reirradiation.[6,7] Several chemotherapy agents can be used for inoperable recurrences or metastatic disease, with response rates of only 10–35% and median survival of 6–12 months.[8]

Beyond HPV status, no validated molecular characterisation of the disease has been established. However, preliminary work suggests the existence of several different molecular classes of HNSCC (basal, mesenchymal, atypical and classical), based on the biological characteristics of differentially expressed genes in each subtype.[9] Genetic and molecular advances have revealed new genes and pathways involved in the development and progression of HNSCC, creating opportunities to explore novel therapeutic targets. HNSCC research has shifted to focus on biomarker discovery for diagnosis, prognosis and prediction of treatment response, alongside the development of targeted therapies, with the ultimate goal of personalising therapy for each individual patient.

TP53/RB Pathway

Tumour suppressor protein p53 plays a key role in the regulation of genes involved in cell cycle and growth arrest, DNA repair or apoptosis, thereby maintaining genomic stability.[10] In response to DNA damage, p53 can arrest the cell cycle and activate repair or initiate apoptosis. p53 controls a significant spectrum of genes involved in various pathways;[11] these include recently discovered biochemical pathways, such as the connection of IL-7Ra to telomere erosion,[12] the metabolism of the cell[13] and the silencing of repeats and noncoding RNA.[14] This intense gene expression results in a very fine regulation of life, death or senescence.[15,16] p53 level is regulated by mouse double minute 2 homolog (MDM2), an E3 ubiquitin protein ligase that binds to p53 and causes its degradation. MDM2 is inhibited by $p14^{ARF}$ that is encoded by the gene *CDKN2A*, protecting p53 from degradation.[10,17] Ataxia telangiectasia mutated (ATM) and ataxia telangiectasia and Rad3-related (ATR) pathways sense DNA damage and phosphorylate the cell cycle checkpoint kinases CHK1 and CHK2, resulting in p53 activation. p53 transactivates a number of proteins with roles in cell cycle arrest and apoptosis. Together with p53, its more recently discovered family members, p63 and p73, have also been shown to play important roles in cell cycle regulation and apoptosis, and their link to various types of cancer including HNSCC is being investigated.[18]

The tumour suppressor protein retinoblastoma (pRb) controls the expression of genes involved in cell cycle progression through the G1 restriction point. pRb binds and inhibits E2F transcription factors that induce expression of S-phase genes and cell proliferation. Mitogenic signals activate cyclin D1/CDK4/CDK6 complexes that phosphorylate pRb, resulting in the release of E2F. The cyclin D1-CDK4/6 complexes are inhibited by $p16^{INK4A}$ that is encoded by the gene *CDKN2A*, and also p21 ((cyclin-dependent kinase inhibitor 1 (CDKN1)) that binds to the complexes and prevents them from phosphorylating pRb, thereby halting progression into S phase.[17]

Mutations in p53 and pRb pathways result in limitless replicative potential and immortalisation. *TP53* mutations can occur throughout the entire gene but the majority are because of a missense mutation in the DNA-binding domain. These mutations can result in a number of consequences including inhibition of function, tumour suppressor loss or occasionally gain of function.[19] Mutation of the *TP53* tumour suppressor gene is one of the earliest and most frequently detectable genetic alterations in HNSCC reported in 50–80% of cases,[20,21] and can also be detected in premalignant dysplastic lesions and in histopathologically negative tumour surgical margins.[22,23] A recent mutational screening in 12 types of cancer has revealed mutations of p53 in 69.8% of HNSCC (Figure 1). From this analysis, HNSCC appears the most common p53 mutation-carrying cancer type after ovarian cancer and lung squamous cell carcinoma.[24] Increased *TP53* mutation rate is associated with tobacco and alcohol use in HNSCC and also with increased risk of progression to cancer.[25,26] In p53 wild-type tumours, p53 function may be inactivated by other mechanisms, such as HPV infection, overexpression or amplification of MDM2 and deletion of the $p14^{ARF}$ gene.[10]

pRb is targeted early in the carcinogenesis of HNSCC through inactivation of the tumour-suppressive *CDKN2A* gene, with mutations seen in 7–9% and copy number losses in a further 20–30% of cases.[20,27] The *CCND1* gene, which encodes cyclin D1 on chromosome 11q13, is amplified or overexpressed in over 80% of HNSCC.[28] *TP53* mutation, loss of $p16^{INK4A}$ and overexpression of cyclin D1 are all associated with reduced survival.[21,29] In addition, *TP53* mutation is predictive of poor response to chemotherapy and locoregional recurrence following radiotherapy.[30,31]

Restoring or modulating p53 as targeted therapy has been an area of intensive research for decades, with limited success. Only one phase III study has been completed using adenoviral p53 gene therapy in HNSCC. This showed that patients with wild-type p53 had better response to Ad-p53 gene therapy, whereas mutant p53 patients responded better to methotrexate chemotherapy, suggesting a potential of p53 profile as predictive biomarker of response to specific type of therapy.[32] p53-reactivating small molecules are currently under investigation in HNSCC cell lines,[33] and other

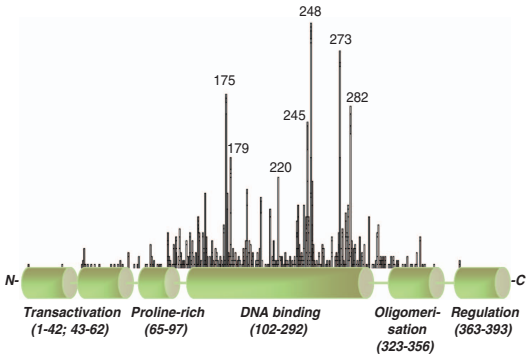

Figure 1 The p53 structure with different protein domains (transactivation domain, proline-rich domain, DNA-binding domain, oligomerisation domain and regulation domain). Vertical lines indicate the occurrence of mutation of the amino acid residues in HNSCC (data from COSMIC website: cancer.sanger.ac.uk/cancergenome/projects/cosmic)

strategies include targeting *CDKN2A* to reactivate $p16^{INK4A}$ and CDK inhibitors. A phase I study of a CDK inhibitor in combination with radiation has recently completed recruitment (NCT00899054, Table 1).

Epidermal Growth Factor Receptor (EGFR) Pathway

EGFR (ErbB1) is a member of the ErbB/HER2 family of transmembrane receptor tyrosine kinases. Other members include HER2 (ErbB2), ErbB3 and ErbB4 and they play a major role in cell proliferation, differentiation, survival and migration. EGFR is composed of an extracellular ligand-binding domain, a transmembrane segment and a cytoplasmic domain with tyrosine kinase activity. It is activated by a number of ligands including EGF, transforming growth factor-α and amphiregulin. Ligand binding results in a conformational change in EGFR and homo- or hetero-dimerisation with other ErbB family members, leading to autophosphorylation and receptor activation. This results in the activation of downstream signal transduction cascades including the Ras/Raf/mitogen-activated protein kinase (MAPK), phosphoinositide 3-kinase (PI3K)/AKT and Janus kinase (JAK)/signal transducer and activator of transcription 3 (STAT3) pathways.[34] The EGF-bound EGFR can also translocate to the nucleus to function as a transcription factor. One of the nuclear targets is *CCND1* that encodes cyclin D1 protein involved in cell cycle progression (Figure 2).[35]

EGFR protein is detected by immunohistochemistry in over 90% of HNSCC cases. EGFR overexpression is mainly at the transcriptional level as there are few EGFR-activating mutations in HNSCC.[36] Approximately 10–30% of HNSCC display *EGFR* gene amplification, and *EGFR* point mutations are reported in only 1–7% of patients.[37,38] A mutant form of EGFR, EGFRvIII, resulting from an in-frame deletion of exons 2–7 in the extracellular domain, has been reported in 42% of HNSCC.[39] The intensity of expression, as assessed by immunohistochemistry, has been shown to indicate poor prognosis, as has *EGFR* gene copy number.[40,41] However, the gene copy number has not been found to be a predictive biomarker of efficacy with EGFR-directed therapy,[41] unlike specific mutations in non-small-cell lung cancer.

EGFR can be targeted either by inhibition of the extracellular ligand binding using monoclonal antibodies (mAbs), such as cetuximab, or by inhibition of the tyrosine kinase domain with a small molecule (TKIs), such as gefitinib, erlotinib and lapatinib. Cetuximab is a chimeric human–murine IgG1 mAb directed specifically against EGFR, resulting in inhibition of cell cycle progression, angiogenesis and metastasis, induction of apoptosis and synergy with radiotherapy and chemotherapy. It remains the only FDA-approved and European Medicines Agency-approved targeted therapy in HNSCC and its use is not dependent on EGFR status. It is used in combination with radiotherapy in locally advanced HNSCC, in combination with platinum-based chemotherapy and 5-fluorouracil for first-line treatment of recurrent/metastatic disease, and as a single agent in recurrent/metastatic disease after failure of platinum-based chemotherapy.[42,43] Skin toxicity is a common side effect with cetuximab treatment and this clinical feature has been suggested as a biomarker for response to cetuximab, with response rates of 33% observed in patients with skin rash compared with 7% in those who do not develop skin toxicities.[44] Panitumumab is a fully humanised mAb against EGFR in use in colorectal cancer. In HNSCC, a phase III trial of panitumumab in combination with chemotherapy did not show an improvement in survival, although retrospective analysis showed that median overall survival in p16 (surrogate marker for HPV)-negative patients was longer in the panitumumab group than in the control group.[45] Other promising mAbs currently in phase III trials include zalutumumab and nimotuzumab (NTC00496652 and NTC00957086). Despite the high expression of EGFR in HNSCC, EGFR inhibition with mAbs has only a modest effect. Preclinical studies investigating resistance to EGFR inhibition have suggested mechanisms such as increased nuclear localisation of EGFR, cross-talk of EGFR with other receptor tyrosine kinases, such as HER2 and ErbB3, as well as upregulation of these receptors and their ligands.[46]

TKIs block the activation and phosphorylation of EGFR, and these drugs are given orally as they are well absorbed across the gastrointestinal tract. Gefitinib and erlotinib, currently used in lung cancer, inhibit only EGFR and have not been shown to be efficacious in HNSCC to date. Because of the potential resistance mechanisms, TKIs that have action against multiple ErbB family receptors are under investigation. Lapatinib has dual specificity for EGFR and HER2 and is in use in breast cancer. In HNSCC trials, it has shown activity in p16-negative tumours in combination with chemoradiation,[47] and is currently being evaluated in the recurrent/metastatic setting in combination with capecitabine chemotherapy (NCT01044433), and in a phase III adjuvant trial (NCT 00424255). Afatinib irreversibly blocks EGFR, HER2 and ErbB4 and is being investigated in the recurrent/metastatic, neoadjuvant and adjuvant settings (NCT 01856478, NCT01538381 and NCT01345669).

NOTCH Pathway

NOTCH1 signalling is involved in a number of biological functions, including regulation of self-renewal capacity,

Table 1 Targeted therapies in HNSCC

Type of drug	Drug	Target	Stage of development	NCT number
Adenovirus gene therapy	Advexin	p53	Phase III	NCT00064103
	ONYX-015	p53	Approved in China	N/A
CDK inhibitor	P276-00	pRb	Phase II	NCT0089954
Monoclonal antibody	Cetuximab	EGFR	In clinical use	N/A
	Panitumumab		Phase II	NCT00756444
				NCT00454779
				NCT00820248
	Zalutumumab		Phase III	NCT00496652
	Nimotuzumab		Phase III	NCT00957086
	Bevacizumab	VEGFR	Phase II	NCT01588431
Tyrosine kinase inhibitor	Gefitinib	EGFR	Phase III	NCT00206219
				NCT00684385
	Erlotinib	EGFR	Phase II	NCT01064479
	Lapatinib	EGFR, HER2	Phase III	NCT00424255
	Afatinib	EGFR, HER2, ErbB4	Phase III	NCT01856478
				NCT01345669
				NCT01345682
	Sorafenib	VEGFR-2, VEGFR-3, Raf, PDGFR	Phase II	NCT00939627
	Sunitinib	VEGFR-1, VEGFR-2, VEGFR-3, PDGFR, RET, c-KIT	Phase II	NCT00387335
	Vandetanib	EGFR, VEGFR, RET	Phase II	NCT00459043
	Pazopanib	VEGFR-1, VEGFR-2, VEGFR-3, PDGFR, c-KIT	Phase II	NCT01377298
	Axitinib	VEGFR-1, VEGFR-2, VEGFR-3, PDGFR, c-KIT	Phase II	NCT01469546
	Nilotinib	BCR-ABL, c-KIT, PDGFR	Phase I	NCT01871311
MEK inhibitor	Trametinib	MEK	Phase I	NCT01725100
PI3K inhibitor	PX866	PI3K	Phase II	NCT01204099
	BKM120	PI3K	Phase II	NCT01527877
	BYL719	PI3K	Phase II	NCT01602315
	Rigosertib	PI3K, PLK	Phase II	NCT01807546
AKT inhibitor	MK2206	AKT	Phase II	NCT01349933
mTOR inhibitor	Rapamycin	mTOR	Phase II	NCT01195922
	Everolimus	mTOR	Phase II	NCT01133678
	Temsirolimus	mTOR	Phase II	NCT01172769
	CC-115	mTOR, DNA-PK	Phase I	NCT01353625
JAK inhibitor	Ruxolitinib	JAK	Phase I	NCT04822756
MET/VEGFR inhibitor	Foretinib	MET, VEGFR-2	Phase II	NCT00725764
	E7050/Golvatinib	MET, VEGFR-2	Phase II	NCT01332266
MET inhibitor	LY2801653	MET	Phase I	NCT01285037
PDK inhibitor	Dichloroacetate	PDK	Phase I	NCT01386632
AMPK activator	Metformin	AMPK	Phase II	NCT01333852

Data source: www.clinicaltrials.gov

survival and promoting terminal differentiation. The NOTCH pathways consist of four receptors bound to the cell membrane, NOTCH 1–4, and two families of ligands, Delta-like (1, 3 and 4) and Jagged (1 and 2). Ligand binding leads to two cleavages of NOTCH1 by TNFα-converting enzyme (TACE) and γ-secretase, resulting in the release of NOTCH1 intracellular domain (NCID). NCID translocates to the nucleus to promote transcription of its target genes, including the HRT and HES families. NOTCH1 is regulated partly by ubiquitination and degradation that involves FBXW7.[48]

One of the novel findings generated from whole-exome sequencing was the discovery that the second most common mutation in HNSCC is in the *NOTCH1* gene, accounting for 14–15%, with mutations in the other NOTCH family members occurring in 3–5% of HNSCC.[20,27] Mutations in the *FBXW7* gene were also identified in 5% of cases that have not been previously observed in HNSCC.[20] Recent integrated analysis has identified the NOTCH pathway to be defective in 66% of HNSCC patients. Along with the mutations in NOTCH itself, chromosomal aberrations were frequent in JAG1, JAG2, MUMB and MAML1, all of which are involved in modulating NOTCH signalling.[49] NOTCH1 signalling has been reported to be oncogenic, as activating mutations and translocations were found in NOTCH receptor genes in haematological malignancies.[50] However, in HNSCC, the majority were nonsense mutations, predicted to result in truncated NOTCH1 proteins lacking the transcriptional activation domains, therefore suggesting a tumour-suppressor role for this pathway in HNSCC.

NOTCH1 signalling promotes terminal differentiation in keratinocytes and skin SCC, and this is negatively regulated by EGFR. Inhibition of EGFR blockade induces keratinocyte

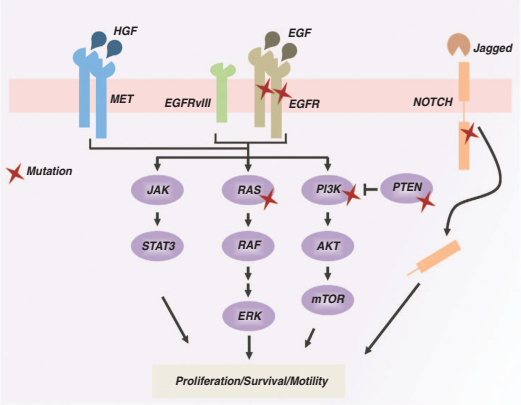

Figure 2 Schematic representation of the major molecular pathways affected in HNSCC. Stars indicate possible mutations in the molecule. EGFR, MET and NOTCH activation can promote molecular signalling through RAS/ERK, PI3K/AKT or JAK/STAT pathways. Aberrant activation of these pathways promotes survival, proliferation and motility of cancer cells, favouring HNSCC tumourigenesis

differentiation.[51] NOTCH1 has also been found to be inhibited in basal epithelial cells by the p53-related transcription factor p63 that becomes downregulated during terminal differentiation coinciding with NOTCH1 upregulation. Overexpression and amplification of *TP63* have been observed in the majority of HNSCC.[52] However, as p63 encodes several isoforms with opposing functions, the precise role of p63 in NOTCH1 signalling and malignant transformation of oral epithelial cells remains to be elucidated.

NOTCH1 signalling has also been linked to suppression of HPV E6 and E7 protein expression in cervical carcinoma cell lines; expression of activated NOTCH1 causes growth inhibition of HPV-positive but not HPV-negative cervical carcinoma cell lines, and results in the downmodulation of HPV-driven transcription of the E6 and E7 viral genes.[53] The role of NOTCH1 in the complex signalling pathway of HNSCC tumourigenesis needs to be further investigated, but could potentially represent another therapeutic target. Both NOTCH1 pathway inhibitors that inhibit γ-secretase and NOTCH1 pathway activators, via inhibition of histone deacetylase, are currently in clinical development.

PI3K/AKT/mTOR Pathway

PI3Ks are a family of enzymes that phosphorylate the 3′OH position of phosphatidylinositols and have important roles in promoting cell growth, differentiation and survival. There are three classes of PI3Ks, each with its own substrate specificity, and class 1A is most frequently associated with cancer. Class 1A PI3Ks are heterodimers and composed of a 110-kDa catalytic subunit and an 85-kDa regulatory subunit, both of which exist in several isoforms. PI3Ks are activated by RTKs, such as EGFR, and the catalytic subunit phosphorylates phosphatidylinositol1,4-bisphosphate (PIP_2) to form phosphatidylinositol1,4,5-triphosphate (PIP_3). PIP_3 recruits pleckstrin-homology domain-containing proteins including phosphoinositide-dependent protein-kinase 1 (PDK1) and AKT to the plasma membrane. Interaction of PIP_3 with the PH (Pleckstrin Homology) domain of AKT results in a conformational change causing phosphorylation of AKT by PKD1 and mammalian target of rapamycin complex 2 (mTORC2). This activates AKT that then phosphorylates proteins involved in cell growth and survival. The tumour-suppressor phosphatase and tensin homology (PTEN) mediates the conversion of PIP_3 to PIP_2, counteracting the activation of AKT.[54] mTOR is a protein kinase that acts downstream of PI3K and AKT and plays an important role in cell growth, survival and protein synthesis regulation. There are two mTOR complexes: mTORC1 activates ribosomal protein S6 kinase 1 (SK6) and inactivates eukaryotic translation initiation factor 4E-binding protein 1 (4E-BP1), resulting in protein translation and cell growth, whereas mTORC2 activates AKT.

Genetic aberrations of the PI3K pathway are common in HNSCC. One of the isoforms of the 110 kDa catalytic subunit, p110α, is encoded by the *PIK3CA* gene. This gene is mutated in 6–20% of HNSCC, especially through the mechanisms of gene amplification and low-level copy number increase.[20,27] It has been found to be particularly common in HPV-positive HNSCC cases, and specific mutations, such as H1047R in exon 20, may predict higher response rates to treatment with PI3K pathway inhibitors.[55,56] In addition, *PTEN* mutations have been reported in 7% of HNSCC, and the mTOR pathway is frequently activated, independent from activation of EGFR or the presence of mutant p53, particularly in HPV-positive tumours.[27,57]

PI3K pathway is an important therapeutic target for cancers and its therapeutic modulation has been assessed in a number of tumour types. The mTOR inhibitor everolimus is in clinical use in renal cell carcinoma, pancreatic neuroendocrine tumours, breast cancer and subependymal giant cell astrocytoma, and temsirolimus can be used in renal cell carcinoma. PI3K inhibitors are being investigated in phase II trials in HNSCC in conjunction with chemotherapy or cetuximab (NCT01252628); AKT inhibitors are being tested in recurrent or metastatic nasopharyngeal cancer (NCT01349933); and the mTOR inhibitors rapamycin, everolimus and temsirolimus are being assessed for HNSCC at the phase II stage in neoadjuvant and recurrent/metastatic settings.

Ras/Raf/MEK/MAPK Pathway

Ras is a guanosine nucleotide binding protein localised on the plasma membrane. There are three Ras genes: *HRAS*, *KRAS* and *NRAS*. In the inactivated state, Ras is bound to guanosine diphosphate (GDP) and activation converts Ras to the guanosine triphosphate (GTP)-bound form; Ras-GTP binds to and activates Raf-1. The targets for phosphorylation of Raf-1 include the kinases MEK1 and MEK2 that in turn activate the MAP kinases ERK1 and ERK2. These translocate to the nucleus and target genes involved in cell growth, proliferation and survival. Ras can also activate the PI3K signalling cascade.[58]

Mutations in the Ras proto-oncogenes are implicated in 20–30% of all cancers.[58] Activating *HRAS* mutations have been found in 4–5% of HNSCC cases.[20,27] *KRAS* mutations occur in 30–50% of colorectal cancers and are predictive of poor response to panitumumab and cetuximab.[59]

The predictive value of KRAS in HNSCC remains unclear and requires further investigation.

Sorafenib is a tyrosine kinase inhibitor that has multiple targets including Raf, VEGF (vascular endothelial growth factor receptor) and PDGFR (platelet-derived growth factor receptor).[60] It is in use in renal cell carcinoma and hepatocellular carcinoma, but has poor results as a single agent in HNSCC. Sorafenib in combination with chemotherapy has shown a response rate of 55% and median overall survival of 22.6 months in a phase II trial in HNSCC.[61] The MEK inhibitor trametinib has recently been approved for use in metastatic melanoma and is under investigation in combination with AKT inhibition in solid tumours including HNSCC (NCT01725100).

MET Pathway

The proto-oncogene *c-MET* encodes mesenchymal–epithelial transition factor (MET), an RTK activated by hepatocyte growth factor (HGF). Ligand binging activates signalling cascades including the RAS, PI3K, STAT3 and NOTCH pathways, resulting in cell morphogenesis, motility, growth and survival. MET and HGF have been found to be overexpressed in over 80% of HNSCC and increased *MET* copy numbers in 13% of HNSCC tumour samples.[62,63] MET expression has been suggested to be a prognostic biomarker in HPV-negative HNSCC with overexpression correlating with reduced disease-free and overall survival.[64,65] It has also been implicated in resistance to radiation, cisplatin and cetuximab.[66–68]

MET overexpression results in enhanced cell motility, angiogenesis and invasion/metastases, and therefore is an important potential therapeutic target. Foretinib is a multi-tyrosine kinase inhibitor that binds to the adenosine triphosphate (ATP) pocket of the receptor. It has been tested in a phase II study in recurrent/metastatic HNSCC but showed disease stabilisation and only minor tumour shrinkage as a single agent.[69] There are several RTK inhibitors and mAbs against MET and HGF in early phase clinical trials.

JAK/STAT Pathway

The JAKs are part of a family of nonreceptor tyrosine kinases. They interact with the cell surface cytokine receptors and activate them by transphosphorylation. Activated cytokine receptors recruit STAT that is phosphorylated by JAKs, mediating dimerisation and translocation to the nucleus to activate transcription of their target genes. JAKs can also be phosphorylated directly by RTKs such as EGFR, activating the RAS and PI3K pathways. The JAK/STAT pathway has a role in promoting cell growth and survival, angiogenesis and suppression of immune surveillance.[70]

STAT proteins are important in mediating EGFR signalling and STAT3 is overexpressed in HNSCC.[71] Ruxolitinib is a JAK inhibitor approved for use in myelofibrosis and is in phase I studies in combination with chemotherapy in advanced solid tumours. A phase 0 trial of a STAT decoy oligonucleotide injected into HNSCC tumours before surgery demonstrated downregulation of STAT3 target gene expression, warranting further investigation of this target in HNSCC.[72]

HPV-Mediated Pathogenesis

HPVs are small, nonenveloped, double-stranded DNA viruses. The genome encodes for early genes (E1–7) and late structural genes (L1, L2). E1 and E2 encode regulatory proteins and E5–7 encode oncoproteins. Over 100 human HPV genotypes have been isolated, and mucosal HPVs can be classified into high and low risk based on their potential to induce malignant transformation. High-risk HPVs include types 16, 18, 31 and 33, with HPV type 16 accounting for over 90% of cases in HNSCC.[73] HPVs enter the host via wounds or abrasions in the mucosa and infect basal epithelial cells, where the host cell DNA replication machinery is used for viral replication. The basal cell nuclei maintain low copy numbers of viral DNA, whereas the virus replicates to high copy numbers in terminally differentiated cells.[74] The E6 protein interacts with E6-associated protein (E6-AP), resulting in a rapid degradation of tumour suppressor p53 via the ubiquitin–proteosome pathway (Figure 3). This leads to inhibition of the proapoptotic functions of p53 and bypassing of the p53-mediated checkpoints.[75] The E7 protein competes with E2F transcription factor for binding to the pRb tumour suppressor, displacing E2F. E2F activates genes responsible for cell cycle progression through the G_1 to S phase, including cyclin A, E and DNA polymerase, causing inactivation of checkpoints and regulatory pathways, and ultimately promoting cellular proliferation and transformation (Figure 3).[76] pRb is a negative regulator of the cyclin-dependent kinase inhibitor p16, and therefore inactivation of pRb results in p16 upregulation. This can be detected using immunohistochemistry in HPV-associated tumour samples and represents a biologically significant surrogate marker for HPV oncoprotein expression.[77]

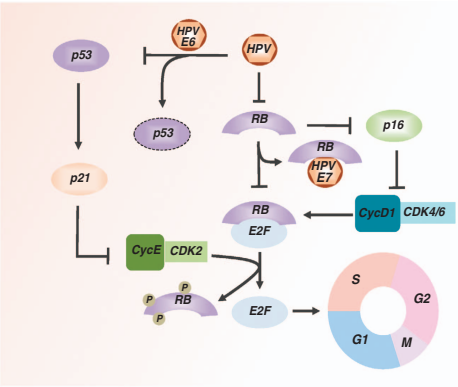

Figure 3 Mechanism of action of the human papillomavirus (HPV) on cell cycle regulation. To progress from G1 to S cell cycle phase, cells have to pass the G1 restriction point that is under the control of the retinoblastoma protein (pRb). pRb binds and represses E2F transcriptional factors. Mitogenic signalling through CyclinD1/CDK4 or CyclinD1/CDK6 phosphorylates pRb, promoting E2F release. CyclinE/CDK2 completes pRb phosphorylation, allowing S-phase entry. HPV affects the cell cycle by using two viral oncoproteins, E6 and E7. The E6 protein binds p53 and promotes its degradation, whereas E7 protein binds and inactivates pRb. These viral oncoproteins determine cell cycle entry and inhibition of p53-mediated apoptosis. HPV-dependent inhibition of pRb promotes p16 accumulation. p16 represents a surrogate marker of HPV-positive HNSCC

Table 2 Clinical features of HPV-positive and -negative HNSCC

	HPV negative	HPV positive	References
Aetiology	Tobacco/alcohol	HPV infection	2,5,78
Age	Above 60 years	Below 60 years	5
p53 mutations	Highly frequent	Infrequent	20,27
Site	Not predictable	Oropharynx	78
Prognosis	Poor	Favourable	77,87

HPV infection in oropharyngeal cancer is now recognised as an aetiological agent, responsible for the significant increase in incidence in Western countries (Table 2).[5,78] These cancers represent a distinct subgroup characterised by specific biological and clinical profiles and improved outcomes. Patients with HPV-associated oropharyngeal squamous cell carcinoma (OPSCC) tend to be white males, on average 5 years younger than HPV-negative patients, have higher socioeconomic status and are less likely to smoke or drink alcohol.[4] Risk factors for HPV-positive HNSCC are related to sexual behaviour, including young age at first intercourse and high number of sexual partners, in particular oral sex partners, and antibodies against HPV16 viral capsid protein and E6 oncoprotein.[79–82] Clinically, these tumours have been found to be present at an earlier stage of the primary cancer but with cystic, multilevel nodal metastases.[83,84] Histologically, the tumours tend to be poorly differentiated basaloid (or nonkeratinising squamous cell) carcinomas.[85] HPV is detected in other subsites such as larynx and nasopharynx but no causal relationship or association with outcome has been established, and therefore the significance in nonoropharyngeal head and neck tumours remains unclear.[86]

HPV-associated OPSCC has a favourable prognosis. Compared with HPV-negative OPSCC, patients have a 60–80% reduction in the risk of death from their cancer after controlling for other factors, highlighting the need for different treatment strategies to reduce the morbidity associated with current treatment.[77,78] The reasons for the improved outcome are unclear but possibilities include host factors such as younger age, fewer smoking-related comorbidities and tumour factors such as increased sensitivity to radiotherapy, absence of field cancerisation mainly seen in smokers, differing response of the host immune system to viral infection, and the presence of wild-type p53 that may become activated in response to radiotherapy and chemotherapy. However, not all HPV-positive patients have the same excellent outcome and they can be further classified into low and intermediate risk of death categories depending on their smoking history.[87] HPV-negative HNSCC are typically characterised by *TP53* and *RB* genetic alterations resulting in genomic instability and resistance to apoptosis. No *TP53* mutations were seen in HPV-positive HNSCC on exome sequencing, and the overall mutation rate was approximately half of that seen in HPV-negative samples. In addition, in contrast to HPV-negative tumours, the expression of *CDKN2A*, encoding $p16^{INK4A}$, is highly upregulated and amplification of cyclin D is infrequent.[88]

At present, treatment is the same regardless of HPV status outside the context of a clinical trial. Two phase III studies currently recruiting (De-ESCaLATE HPV and RTOG 1016) are investigating the replacement of standard cisplatin in concomitant chemoradiation with cetuximab, on the basis that cetuximab may be less toxic with comparable results in retrospective analyses.[89] The results of two studies treating HPV-positive patients with induction chemotherapy followed by reduced dose radiation in responders are awaited. HPV vaccines are under development and investigation, as both preventative and therapeutic applications. Gardasil and Cervarix are HPV vaccines in use for the prevention of cervical cancer, but could afford protection against oral HPV16/18 infection. Reduced prevalence of oral HPV infection was found in women recruited to investigate the efficacy of HPV vaccination against cervical cancer.[90] These vaccines may also cause induction of cell-mediated immunity against HPV-positive tumours, and phase I studies are ongoing investigating the use of HPV16 peptide epitopes in recurrent disease.[91]

Hypoxia and Angiogenesis

Tumour hypoxia is common in HNSCC and is associated with treatment resistance and reduced survival.[92] Under normoxia, the hypoxia-inducible factors HIF1-α and HIF2-α are rapidly degraded by the Von Hippel–Lindau protein (VHL). Hypoxia leads to stabilisation of HIFs that heterodimerise with constitutively expressed HIF2β and translocate to the nucleus. Genes that promote survival in hypoxia, including carbonic anhydrase 9 (*CA9*), glucose transporter 1 (*GLUT1*) and vascular endothelial growth factor (*VEGF*), are upregulated. HIF2-α mediates activation of EGFR, and HIF activation is partly regulated by mTOR signalling.[93] Hypoxia can also drive genomic instability in tumour cells and select for cell populations with a more aggressive phenotype, reduced apoptotic and increased metastatic potential.[94]

Oxygen is required for effective radiation-induced cell damage, as oxygen stabilises the free radicals produced by ionising radiation that causes DNA damage and cell death.[95] To improve their nutrient and oxygen supply, tumours produce angiogenic factors that induce the proliferation of endothelial cells and form new blood vessels. VEGF is the strongest inducer of angiogenesis, and immunohistochemical expression in tumour samples is associated with an increased risk of death.[96]

Strategies to improve tumour oxygenation have included the use of hyperbaric oxygen, carbogen and nicotinamide, radiosensitisation using nitroimidazoles and the hypoxic cytotoxin tirapazamine. However, because of the difficulties in measuring and stratifying for hypoxia, these techniques have not translated into regular clinical practice.[95] There is therefore interest in developing methods to diagnose hypoxia and predict the response to hypoxia-modifying treatments. For example, a 15-gene hypoxia classifier applied retrospectively to HNSCC tissue samples was found to predict for hypoxic modification of radiotherapy with the radiosensitiser nimorazole.[97] More recently, a 26-gene hypoxia signature showed predictive benefit from hypoxia-modifying agents carbogen and nicotinamide in combination with accelerated radiotherapy.[98] Prospective application and validation of these signatures are awaited. The VEGFR-targeting therapies are currently under investigation in HNSCC.

Bevacizumab, a monocloncal antibody against VEGFR, is in clinical use in metastatic colorectal and breast cancer, NSCLC, glioblastoma and renal cell carcinoma. Phase II studies in HNSCC using bevacizumab in combination with pemetrexed, erlotinib or cetuximab have shown response rates of 15–30%.[99–101] The multiple tyrosine kinase inhibitors sunitinib, sorafenib and vandetanib are in clinical use, and sorafenib has shown promise in combination with chemotherapy in recurrent/metastatic HNSCC (Table 1).

Metabolism

Energy in the form of ATP is generated in normal cells via glycolysis or the tricarboxylic acid (TCA) cycle. In glycolysis, glucose is metabolised to pyruvate in the cytosol to produce two ATPs from each molecule of glucose. The TCA cycle utilises pyruvate from glycolysis to produce acetyl-CoA that is catalysed by pyruvate dehydrogenase (PDH) in the mitochondria. Acetyl-CoA is metabolised by oxidative phosphorylation, consuming oxygen and generating 36 ATPs per glucose. In anaerobic conditions, pyruvate is not used in the TCA cycle and is converted to lactate in the cytosol by lactate dehydrogenase (LDH).[102]

Metabolic alterations are common in cancer. The best-characterised metabolic phenotype was originally described by Warburg *et al*.[103] in the 1920s. The Warburg effect is the increase in glycolysis to generate ATP, even in the presence of normal oxygen concentrations. ATP production via glycolysis is much faster but less efficient than oxidative phosphorylation, and cancer cells avidly consume glucose to meet their increased energy and biosynthesis needs.[104] Aerobic glycolysis in tumour cells is regulated by aberrant signalling pathways, including p53, PI3K, HIF1, MYC[105–107] and liver kinase B1 (LKB1)/AMP-activated protein kinase (AMPK) pathways,[108] as well as alterations in metabolic enzymes, such as pyruvate kinase and pyruvate dehydrogenase kinase (PDK).[109]

Aberrant metabolism can be targeted by inhibiting the AKT and mTOR pathways as previously discussed. PDK inhibition with dichloroacetate is being explored in a phase I trial of metabolic reprogramming therapy in recurrent HNSCC (NCT01163487). Metformin is currently used in type II diabetes but also acts as an AMPK activator. Diabetic patients treated with metformin were found to be at lower risk of developing cancer than those on other treatments.[110] Metformin in combination with paclitaxel is being investigated in a phase II trial in metastatic/recurrent HNSCC (NCT01333852).

HNSCC Cancer Stem Cells

HNSCC is highly heterogeneous. This heterogeneity was originally thought to be because of the step-wise accumulation of specific genetic and epigenetic alterations in response to carcinogens, resulting in preneoplastic fields. Clonal divergence and selection within these fields leads to the development of cancer, and the incomplete eradication of these areas are the source of recurrence and secondary tumours after treatment.[111] However, accumulating evidence supports an alternative model for the development and progression of HNSCC involving cancer stem cells (CSCs). This model describes the existence of a hierarchy of cells, where CSCs are a subpopulation within the tumour, capable of initiating and propagating tumourigenesis. These cells have the ability of self-renewal, maintaining the CSC reservoir and differentiate into the heterogeneous progeny.[112] CSCs have been implicated in resistance to treatment, as they are nondividing or slowly dividing, evading the conventional chemotherapy and radiotherapy strategies that target rapidly diving cells.[113] However, they have the potential to become activated resulting in recurrences or metastases.

CD44 is a transmembrane glycoprotein that acts as a receptor for hyaluronic acid and other extracellular matrix molecules, and is involved in cell adhesion and migration. Alternative splicing results in multiple different CD44 variants with a diverse functional repertoire.[114] HNSCC CSCs were first described based on CD44 expression.[115] CD44+ HNSCC cells, but not CD44− cells, initiated tumourigenesis in mice, reproduced the original tumour heterogeneity and demonstrated self-renewal after serial passaging *in vivo*.[115] CD44+ cells were also found to differentially express the *BMI-1* gene,[115] encoding a self-renewal protein found in embryonic stem cells.[116] However, expression of CD44 has also been observed diffusely in normal, benign and malignant epithelia of the head and neck, suggesting CD44 alone cannot identify CSCs.[117]

Aldehyde dehydrogenase (ALDH) is an enzyme involved in detoxifying intracellular aldehydes by oxidation, and converting retinol to retinoic acid.[118] It has been shown that ALDH+ and CD44+ cells form a subpopulation of cells that are highly tumourigenic in immunodeficient mice at very low cell numbers, as well as the ability to self-renew.[119] Therefore, the combination of these two markers are more selective for CSCs. ALDH1+CD44+ cells have also demonstrated increased expression of BMI-1,[119] resistance to chemoradiation and involvement in epithelial–mesenchymal transition.[120]

CSCs represent potential novel diagnostic and therapeutic targets. The concentration of CD44 in the peripheral blood of HNSCC patients has been shown to be significantly higher than healthy controls,[121] and increased CD44+ cell population in the primary tumour correlates with higher rates of recurrence.[122] In addition, CD44 gene expression levels have been found to correlate with response to radiotherapy in laryngeal SCC, suggesting its role as a predictive marker.[123] Targeted elimination of cancer stem cells directly or via their niche, for example, with antiangiogenic agents, are potential treatment strategies under development. Bivatuzumab mertansine, an anti-microtubule agent coupled to a monoclonal antibody against CD44 variant 6, has been tested in metastatic HNSCC. However, two parallel phase I studies were terminated early after a fatal case of toxic epidermal necrolysis.[124] Further investigation is required to fully understand the potential effects of targeting CSCs in HNSCC.

Gene and MicroRNA Expression in HNSCC

There has been a multitude of published studies investigating gene expression profiling to diagnose HNSCC and predict behaviour and sensitivity to treatment.[125–127] The detailed analysis of such studies is beyond the scope of this review; in general, because of tumour heterogeneity and low case numbers in some studies, these studies have not been

Table 3 MicroRNAs in HNSCC

MicroRNA	Targets	Function	References
Upregulated			
miR-21	PTEN, PCDC4	Cell cycle progression, metastasis	129
miR-106b	p21	Cell cycle progression	130
miR-205	PTEN	Prognostic marker, metastasis	131,132
miR-181	not reported in HNSCC	Prognostic factor, metastasis	135
miR-211	not reported in HNSCC	Prognostic factor, metastasis	134
Downregulated			
let-7	KRAS	Prognostic marker, metastasis	131,136
miR-133a/b	PKM2, ARPC5	Cancer metabolism	137,138
miR-200a	ZEB1, ZEB2	EMT, metastasis	139

conclusive. Larger and heterogeneous patient cohorts are therefore needed to obtain an mRNA signature that can be utilised in a clinical setting.

MicroRNAs (miRNAs) are endogenous, small, non-coding RNAs of 18–25 nucleotides that regulate and refine gene expression at both transcriptional and translational levels. Over 1000 miRNAs have so far been identified, with each miRNA influencing the expression of multiple genes and a single mRNA being targeted by several miRNAs. They are involved in the fine-tuning of the expression of many genes involved in a variety of critical biological processes, including cell cycle regulation, differentiation, metabolism and death (Table 3).[128] Consistently altered miRNAs in HNSCC include miR-21 that is negatively correlated with PTEN and the *programmed cell death 4* (*PDCD4*) gene and implicated in cell proliferation, invasion and metastases;[129] the miR-106b family that negatively regulates the p21 CDK inhibitor;[130] and miR-205 that targets PTEN and is suggested as a potential maker for diagnosis, lymph mode metastasis and outcome.[131,132] The ratio of miR-221 to miR-375 can distinguish between normal and malignant tissue,[133] and high expression of miR-181 and miR-211 in oral SCC has been found to be associated with lymph node metastases, vascular invasion and poor outcome.[134,135] Tumour-suppressive miRNAs include let-7 that negatively regulates KRAS, and reduced expression is associated with poor prognosis.[131,136] MiR-133a/b is repeatedly reported to be downregulated in HNSCC and targets pyruvate kinase M2, a key regulator of cancer metabolism.[137] MiR-133a also directly regulates the actin-related protein complex 5 (ARPC5) with inhibition of cell migration and invasion when miR-133a is restored or ARPC5 is repressed.[138] Downregulation of the tumour-suppressive miR-200a is seen in both saliva and tissue samples of HNSCC patients and is known to target ZEB1 and ZEB2 that repress the transcription of E-cadherin and mediate epithelial–mesenchymal transition and tumour cell migration.[139] MiRNAs are also implicated in chemoresistance, with different patterns of expression in resistant HNSCC.[140] Modulation of miRNAs can alter the sensitivity of HNSCC to both drugs and radiation, highlighting the potential for miRNAs in predicting response to treatment and as a therapeutic target.

Conclusion

HNSCC is a group of highly heterogeneous tumours. Their management is likely to change in the near future, moving from treatment as a single disease to tailoring the therapy based on both patient and tumour characteristics. Identification of specific genetic, epigenetic and metabolic aberrations, together with the more traditional techniques in diagnosis, staging and prognostication, will need to inform the individual treatment strategy. It has the potential to provide the clinician with a comprehensive set of diagnostic, prognostic and predictive tools. The paucity of driver mutations in HNSCC and frequent tumour suppressor loss represents a pharmacological challenge, but increased understanding of the molecular biology through the developments in high-throughput technology heralds a future of personalised medicine.

Conflict of Interest

The authors declare no conflict of interest.

Acknowledgements. We thank King's Health Partners, King's College London and the Rosetrees Trust for supporting Dr. Yae-eun Suh. We also thank Mrs. Kathy Doyle for help in the preparation and submission of the manuscript.

1. Ferlay J, Shin HR, Bray F, Forman D, Mathers C, Parkin DM. Estimates of worldwide burden of cancer in 2008: GLOBOCAN 2008. *Int J Cancer* 2010; **127**: 2893–2917.
2. Hashibe M, Brennan P, Benhamou S, Castellsague X, Chen C, Curado MP *et al.* Alcohol drinking in never users of tobacco, cigarette smoking in never drinkers, and the risk of head and neck cancer: pooled analysis in the International Head and Neck Cancer Epidemiology Consortium. *J Natl Cancer Inst* 2007; **99**: 777–789.
3. Hashibe M, Brennan P, Chuang SC, Boccia S, Castellsague X, Chen C *et al.* Interaction between tobacco and alcohol use and the risk of head and neck cancer: pooled analysis in the International Head and Neck Cancer Epidemiology Consortium. *Cancer Epidemiol Biomarkers Prev* 2009; **18**: 541–550.
4. Chaturvedi AK, Anderson WF, Lortet-Tieulent J, Curado MP, Ferlay J, Franceschi S *et al.* Worldwide Trends in incidence rates for oral cavity and oropharyngeal cancers. *J Clin Oncol* 2013; **31**: 4550–4559.
5. Chaturvedi AK, Engels EA, Anderson WF, Gillison ML. Incidence trends for human papillomavirus-related and -unrelated oral squamous cell carcinomas in the United States. *J Clin Oncol* 2008; **26**: 612–619.
6. Argiris A, Karamouzis MV, Raben D, Ferris RL. Head and neck cancer. *Lancet* 2008; **371**: 1695–1709.
7. Pignon JP, le Maitre A, Maillard E, Bourhis J. Group M-NC.. Meta-analysis of chemotherapy in head and neck cancer (MACH-NC): an update on 93 randomised trials and 17,346 patients. *Radiother Oncol* 2009; **92**: 4–14.
8. Brockstein BE. Management of recurrent head and neck cancer: recent progress and future directions. *Drugs* 2011; **71**: 1551–1559.
9. Walter V, Yin X, Wilkerson MD, Cabanski CR, Zhao N, Du Y *et al.* Molecular subtypes in head and neck cancer exhibit distinct patterns of chromosomal gain and loss of canonical cancer genes. *PLoS One* 2013; **8**: e56823.
10. Vogelstein B, Lane D, Levine AJ. Surfing the p53 network. *Nature* 2000; **408**: 307–310.
11. Brady CA, Jiang D, Mello SS, Johnson TM, Jarvis LA, Kozak MM *et al.* Distinct p53 transcriptional programs dictate acute DNA-damage responses and tumor suppression. *Cell* 2011; **145**: 571–583.

12. Kibe R, Zhang S, Guo D, Marrero L, Tsien F, Rodriguez P *et al.* IL-7Ralpha deficiency in p53null mice exacerbates thymocyte telomere erosion and lymphomagenesis. *Cell Death Differ* 2012; **19**: 1139–1151.
13. Boren J, Brindle KM. Apoptosis-induced mitochondrial dysfunction causes cytoplasmic lipid droplet formation. *Cell Death Differ* 2012; **19**: 1561–1570.
14. Leonova KI, Brodsky L, Lipchick B, Pal M, Novototskaya L, Chenchik AA *et al.* p53 cooperates with DNA methylation and a suicidal interferon response to maintain epigenetic silencing of repeats and noncoding RNAs. *Proc Natl Acad Sci USA* 2013; **110**: E89–E98.
15. Cho JH, Kim MJ, Kim KJ, Kim JR. POZ/BTB and AT-hook-containing zinc finger protein 1 (PATZ1) inhibits endothelial cell senescence through a p53 dependent pathway. *Cell Death Differ* 2012; **19**: 703–712.
16. Polager S, Ginsberg D. p53 and E2f: partners in life and death. *Nat Rev Cancer* 2009; **9**: 738–748.
17. Sherr CJ, McCormick F. The RB and p53 pathways in cancer. *Cancer Cell* 2002; **2**: 103–112.
18. Allocati N, Di Ilio C, De Laurenzi V. p63/p73 in the control of cell cycle and cell death. *Exp Cell Res* 2012; **318**: 1285–1290.
19. Morton JP, Timpson P, Karim SA, Ridgway RA, Athineos D, Doyle B *et al.* Mutant p53 drives metastasis and overcomes growth arrest/senescence in pancreatic cancer. *Proc Natl Acad Sci USA* 2010; **107**: 246–251.
20. Agrawal N, Frederick MJ, Pickering CR, Bettegowda C, Chang K, Li RJ *et al.* Exome sequencing of head and neck squamous cell carcinoma reveals inactivating mutations in NOTCH1. *Science* 2011; **333**: 1154–1157.
21. Poeta ML, Manola J, Goldwasser MA, Forastiere A, Benoit N, Califano JA *et al.* TP53 mutations and survival in squamous-cell carcinoma of the head and neck. *N Engl J Med* 2007; **357**: 2552–2561.
22. Brennan JA, Mao L, Hruban RH, Boyle JO, Eby YJ, Koch WM *et al.* Molecular assessment of histopathological staging in squamous-cell carcinoma of the head and neck. *N Engl J Med* 1995; **332**: 429–435.
23. Ebrahimi M, Boldrup L, Coates PJ, Wahlin YB, Bourdon JC, Nylander K. Expression of novel p53 isoforms in oral lichen planus. *Oral Oncol* 2008; **44**: 156–161.
24. Kandoth C, McLellan MD, Vandin F, Ye K, Niu B, Lu C *et al.* Mutational landscape and significance across 12 major cancer types. *Nature* 2013; **502**: 333–339.
25. Boyle JO, Hakim J, Koch W, van der Riet P, Hruban RH, Roa RA *et al.* The incidence of p53 mutations increases with progression of head and neck cancer. *Cancer Res* 1993; **53**: 4477–4480.
26. Brennan JA, Boyle JO, Koch WM, Goodman SN, Hruban RH, Eby YJ *et al.* Association between cigarette smoking and mutation of the p53 gene in squamous-cell carcinoma of the head and neck. *N Engl J Med* 1995; **332**: 712–717.
27. Stransky N, Egloff AM, Tward AD, Kostic AD, Cibulskis K, Sivachenko A *et al.* The mutational landscape of head and neck squamous cell carcinoma. *Science* 2011; **333**: 1157–1160.
28. Smeets SJ, Braakhuis BJ, Abbas S, Snijders PJ, Ylstra B, van de Wiel MA *et al.* Genome-wide DNA copy number alterations in head and neck squamous cell carcinomas with or without oncogene-expressing human papillomavirus. *Oncogene* 2006; **25**: 2558–2564.
29. Bova RJ, Quinn DI, Nankervis JS, Cole IE, Sheridan BF, Jensen MJ *et al.* Cyclin D1 and p16INK4A expression predict reduced survival in carcinoma of the anterior tongue. *Clin Cancer Res* 1999; **5**: 2810–2819.
30. Cabelguenne A, Blons H, de Waziers I, Carnot F, Houllier AM, Soussi T *et al.* p53 alterations predict tumor response to neoadjuvant chemotherapy in head and neck squamous cell carcinoma: a prospective series. *J Clin Oncol* 2000; **18**: 1465–1473.
31. Koch WM, Brennan JA, Zahurak M, Goodman SN, Westra WH, Schwab D *et al.* p53 mutation and locoregional treatment failure in head and neck squamous cell carcinoma. *J Natl Cancer Inst* 1996; **88**: 1580–1586.
32. Nemunaitis J, Clayman G, Agarwala SS, Hrushesky W, Wells JR, Moore C *et al.* Biomarkers predict p53 gene therapy efficacy in recurrent squamous cell carcinoma of the head and neck. *Clin Cancer Res* 2009; **15**: 7719–7725.
33. Roh JL, Kang SK, Minn I, Califano JA, Sidransky D, Koch WM. p53-Reactivating small molecules induce apoptosis and enhance chemotherapeutic cytotoxicity in head and neck squamous cell carcinoma. *Oral Oncol* 2011; **47**: 8–15.
34. Hynes NE, Lane HA. ERBB receptors and cancer: the complexity of targeted inhibitors. *Nat Rev Cancer* 2005; **5**: 341–354.
35. Lin SY, Makino K, Xia W, Matin A, Wen Y, Kwong KY *et al.* Nuclear localization of EGF receptor and its potential new role as a transcription factor. *Nat Cell Biol* 2001; **3**: 802–808.
36. Grandis JR, Tweardy DJ. Elevated levels of transforming growth factor alpha and epidermal growth factor receptor messenger RNA are early markers of carcinogenesis in head and neck cancer. *Cancer Res* 1993; **53**: 3579–3584.
37. Loeffler-Ragg J, Witsch-Baumgartner M, Tzankov A, Hilbe W, Schwentner I, Sprinzl GM *et al.* Low incidence of mutations in EGFR kinase domain in Caucasian patients with head and neck squamous cell carcinoma. *Eur J Cancer* 2006; **42**: 109–111.
38. Temam S, Kawaguchi H, El-Naggar AK, Jelinek J, Tang H, Liu DD *et al.* Epidermal growth factor receptor copy number alterations correlate with poor clinical outcome in patients with head and neck squamous cancer. *J Clin Oncol* 2007; **25**: 2164–2170.
39. Sok JC, Coppelli FM, Thomas SM, Lango MN, Xi S, Hunt JL *et al.* Mutant epidermal growth factor receptor (EGFRvIII) contributes to head and neck cancer growth and resistance to EGFR targeting. *Clin Cancer Res* 2006; **12**: 5064–5073.
40. Ang KK, Berkey BA, Tu X, Zhang HZ, Katz R, Hammond EH *et al.* Impact of epidermal growth factor receptor expression on survival and pattern of relapse in patients with advanced head and neck carcinoma. *Cancer Res* 2002; **62**: 7350–7356.
41. Licitra L, Mesia R, Rivera F, Remenar E, Hitt R, Erfan J *et al.* Evaluation of EGFR gene copy number as a predictive biomarker for the efficacy of cetuximab in combination with chemotherapy in the first-line treatment of recurrent and/or metastatic squamous cell carcinoma of the head and neck: EXTREME study. *Ann Oncol* 2011; **22**: 1078–1087.
42. Bonner JA, Harari PM, Giralt J, Azarnia N, Shin DM, Cohen RB *et al.* Radiotherapy plus cetuximab for squamous-cell carcinoma of the head and neck. *N Engl J Med* 2006; **354**: 567–578.
43. Vermorken JB, Mesia R, Rivera F, Remenar E, Kawecki A, Rottey S *et al.* Platinum-based chemotherapy plus cetuximab in head and neck cancer. *N Engl J Med* 2008; **359**: 1116–1127.
44. Burtness B, Goldwasser MA, Flood W, Mattar B, Forastiere AA. Eastern Cooperative Oncology G. Phase III randomized trial of cisplatin plus placebo compared with cisplatin plus cetuximab in metastatic/recurrent head and neck cancer: an Eastern Cooperative Oncology Group study. *J Clin Oncol* 2005; **23**: 8646–8654.
45. Vermorken JB, Stohlmacher-Williams J, Davidenko I, Licitra L, Winquist E, Villanueva C *et al.* Cisplatin and fluorouracil with or without panitumumab in patients with recurrent or metastatic squamous-cell carcinoma of the head and neck (SPECTRUM): an open-label phase 3 randomised trial. *Lancet Oncol* 2013; **14**: 697–710.
46. Wheeler DL, Huang S, Kruser TJ, Nechrebecki MM, Armstrong EA, Benavente S *et al.* Mechanisms of acquired resistance to cetuximab: role of HER (ErbB) family members. *Oncogene* 2008; **27**: 3944–3956.
47. Harrington K, Berrier A, Robinson M, Remenar E, Housset M, de Mendoza FH *et al.* Randomised Phase II study of oral lapatinib combined with chemoradiotherapy in patients with advanced squamous cell carcinoma of the head and neck: rationale for future randomised trials in human papilloma virus-negative disease. *Eur J Cancer* 2013; **49**: 1609–1618.
48. Egloff AM, Grandis JR. Molecular pathways: context-dependent approaches to Notch targeting as cancer therapy. *Clin Cancer Res* 2012; **18**: 5188–5195.
49. Pickering CR, Zhang J, Yoo SY, Bengtsson L, Moorthy S, Neskey DM *et al.* Integrative genomic characterization of oral squamous cell carcinoma identifies frequent somatic drivers. *Cancer discovery* 2013; **3**: 770–781.
50. Weng AP, Ferrando AA, Lee W, Morris JPt, Silverman LB, Sanchez-Irizarry C *et al.* Activating mutations of NOTCH1 in human T cell acute lymphoblastic leukemia. *Science* 2004; **306**: 269–271.
51. Kolev V, Mandinova A, Guinea-Viniegra J, Hu B, Lefort K, Lambertini C *et al.* EGFR signalling as a negative regulator of Notch1 gene transcription and function in proliferating keratinocytes and cancer. *Nat Cell Biol* 2008; **10**: 902–911.
52. Dotto GP. Crosstalk of Notch with p53 and p63 in cancer growth control. *Nat Rev Cancer* 2009; **9**: 587–595.
53. Talora C, Sgroi DC, Crum CP, Dotto GP. Specific down-modulation of Notch1 signaling in cervical cancer cells is required for sustained HPV-E6/E7 expression and late steps of malignant transformation. *Genes Dev* 2002; **16**: 2252–2263.
54. Engelman JA. Targeting PI3K signalling in cancer: opportunities, challenges and limitations. *Nat Rev Cancer* 2009; **9**: 550–562.
55. Janku F, Wheler JJ, Naing A, Falchook GS, Hong DS, Stepanek VM *et al.* PIK3CA mutation H1047R is associated with response to PI3K/AKT/mTOR signaling pathway inhibitors in early-phase clinical trials. *Cancer Res* 2013; **73**: 276–284.
56. Qiu W, Schonleben F, Li X, Ho DJ, Close LG, Manolidis S *et al.* PIK3CA mutations in head and neck squamous cell carcinoma. *Clin Cancer Res* 2006; **12**: 1441–1446.
57. Molinolo AA, Marsh C, El Dinali M, Gangane N, Jennison K, Hewitt S *et al.* mTOR as a molecular target in HPV-associated oral and cervical squamous carcinomas. *Clin Cancer Res* 2012; **18**: 2558–2568.
58. Bos JL. ras oncogenes in human cancer: a review. *Cancer Res* 1989; **49**: 4682–4689.
59. Bardelli A, Siena S. Molecular mechanisms of resistance to cetuximab and panitumumab in colorectal cancer. *J Clin Oncol* 2010; **28**: 1254–1261.
60. Wilhelm SM, Adnane L, Newell P, Villanueva A, Llovet JM, Lynch M. Preclinical overview of sorafenib, a multikinase inhibitor that targets both Raf and VEGF and PDGF receptor tyrosine kinase signaling. *Mol Cancer Ther* 2008; **7**: 3129–3140.
61. Blumenschein GR Jr, Glisson BS, Lu C, Sabichi AL, Ginsberg LE, Bartos CI *et al.* Final results of a phase II study of sorafenib in combination with carboplatin and paclitaxel in patients with metastatic or recurrent SCCHN. *J Clin Oncol* 2012; **30**(Suppl): abstract 5592.
62. Knowles LM, Stabile LP, Egloff AM, Rothstein ME, Thomas SM, Gubish CT *et al.* HGF and c-Met participate in paracrine tumorigenic pathways in head and neck squamous cell cancer. *Clin Cancer Res* 2009; **15**: 3740–3750.
63. Seiwert TY, Jagadeeswaran R, Faoro L, Janamanchi V, Nallasura V, El Dinali M *et al.* The MET receptor tyrosine kinase is a potential novel therapeutic target for head and neck squamous cell carcinoma. *Cancer Res* 2009; **69**: 3021–3031.
64. Zhao D, Wang SH, Feng Y, Hua CG, Zhao J, Tang XF. Intratumoral c-Met expression is associated with vascular endothelial growth factor C expression, lymphangiogenesis, and lymph node metastasis in oral squamous cell carcinoma: implications for use as a prognostic marker. *Hum Pathol* 2011; **42**: 1514–1523.
65. Lo Muzio L, Farina A, Rubini C, Coccia E, Capogreco M, Colella G *et al.* Effect of c-Met expression on survival in head and neck squamous cell carcinoma. *Tumour Biol* 2006; **27**: 115–121.

66. De Bacco F, Luraghi P, Medico E, Reato G, Girolami F, Perera T *et al.* Induction of MET by ionizing radiation and its role in radioresistance and invasive growth of cancer. *J Natl Cancer Inst* 2011; **103**: 645–661.
67. Sun S, Wang Z. Head neck squamous cell carcinoma c-Met(+) cells display cancer stem cell properties and are responsible for cisplatin-resistance and metastasis. *Int J Cancer* 2011; **129**: 2337–2348.
68. Krumbach R, Schuler J, Hofmann M, Giesemann T, Fiebig HH, Beckers T. Primary resistance to cetuximab in a panel of patient-derived tumour xenograft models: activation of MET as one mechanism for drug resistance. *Eur J Cancer* 2011; **47**: 1231–1243.
69. Seiwert T, Sarantopoulos J, Kallender H, McCallum S, Keer HN, Blumenschein G Jr. Phase II trial of single-agent foretinib (GSK1363089) in patients with recurrent or metastatic squamous cell carcinoma of the head and neck. *Invest New Drugs* 2013; **31**: 417–424.
70. Aaronson DS, Horvath CM. A road map for those who don't know JAK-STAT. *Science* 2002; **296**: 1653–1655.
71. Grandis JR, Drenning SD, Zeng Q, Watkins SC, Melhem MF, Endo S *et al.* Constitutive activation of Stat3 signaling abrogates apoptosis in squamous cell carcinogenesis in vivo. *Proc Natl Acad Sci USA* 2000; **97**: 4227–4232.
72. Sen M, Thomas SM, Kim S, Yeh JI, Ferris RL, Johnson JT *et al.* First-in-human trial of a STAT3 decoy oligonucleotide in head and neck tumors: implications for cancer therapy. *Cancer Discov* 2012; **2**: 694–705.
73. Kreimer AR, Clifford GM, Boyle P, Franceschi S. Human papillomavirus types in head and neck squamous cell carcinomas worldwide: a systematic review. *Cancer Epidemiol Biomark Prev* 2005; **14**: 467–475.
74. Giroglou T, Florin L, Schafer F, Streeck RE, Sapp M. Human papillomavirus infection requires cell surface heparan sulfate. *J Virol* 2001; **75**: 1565–1570.
75. Scheffner M, Werness BA, Huibregtse JM, Levine AJ, Howley PM. The E6 oncoprotein encoded by human papillomavirus types 16 and 18 promotes the degradation of p53. *Cell* 1990; **63**: 1129–1136.
76. Dyson N, Howley PM, Munger K, Harlow E. The human papilloma virus-16 E7 oncoprotein is able to bind to the retinoblastoma gene product. *Science* 1989; **243**: 934–937.
77. Weinberger PM, Yu Z, Haffty BG, Kowalski D, Harigopal M, Brandsma J *et al.* Molecular classification identifies a subset of human papillomavirus–associated oropharyngeal cancers with favorable prognosis. *J Clin Oncol* 2006; **24**: 736–747.
78. Gillison ML, Koch WM, Capone RB, Spafford M, Westra WH, Wu L *et al.* Evidence for a causal association between human papillomavirus and a subset of head and neck cancers. *J Natl Cancer Inst* 2000; **92**: 709–720.
79. Gillison ML, D'Souza G, Westra W, Sugar E, Xiao W, Begum S *et al.* Distinct risk factor profiles for human papillomavirus type 16-positive and human papillomavirus type 16-negative head and neck cancers. *J Natl Cancer Inst* 2008; **100**: 407–420.
80. Kreimer AR, Johansson M, Waterboer T, Kaaks R, Chang-Claude J, Drogen D *et al.* Evaluation of human papillomavirus antibodies and risk of subsequent head and neck cancer. *J Clin Oncol* 2013; **31**: 2708–2715.
81. Mork J, Lie AK, Glattre E, Hallmans G, Jellum E, Koskela P *et al.* Human papillomavirus infection as a risk factor for squamous-cell carcinoma of the head and neck. *N Engl J Med* 2001; **344**: 1125–1131.
82. D'Souza G, Kreimer AR, Viscidi R, Pawlita M, Fakhry C, Koch WM *et al.* Case-control study of human papillomavirus and oropharyngeal cancer. *N Engl J Med* 2007; **356**: 1944–1956.
83. Goldenberg D, Begum S, Westra WH, Khan Z, Sciubba J, Pai SI *et al.* Cystic lymph node metastasis in patients with head and neck cancer: an HPV-associated phenomenon. *Head Neck* 2008; **30**: 898–903.
84. Rischin D, Young RJ, Fisher R, Fox SB, Le QT, Peters LJ *et al.* Prognostic significance of p16INK4A and human papillomavirus in patients with oropharyngeal cancer treated on TROG 02.02 phase III trial. *J Clin Oncol* 2010; **28**: 4142–4148.
85. Begum S, Westra WH. Basaloid squamous cell carcinoma of the head and neck is a mixed variant that can be further resolved by HPV status. *Am J Surg Pathol* 2008; **32**: 1044–1050.
86. Isayeva T, Li Y, Maswahu D, Brandwein-Gensler M. Human papillomavirus in non-oropharyngeal head and neck cancers: a systematic literature review. *Head Neck Pathol* 2012; **6**(Suppl 1): S104–S120.
87. Ang KK, Harris J, Wheeler R, Weber R, Rosenthal DI, Nguyen-Tan PF *et al.* Human papillomavirus and survival of patients with oropharyngeal cancer. *N Engl J Med* 2010; **363**: 24–35.
88. Slebos RJ, Yi Y, Ely K, Carter J, Evjen A, Zhang X *et al.* Gene expression differences associated with human papillomavirus status in head and neck squamous cell carcinoma. *Clin Cancer Res* 2006; **12**(3 Pt 1): 701–709.
89. Mehra R, Cohen RB, Burtness BA. The role of cetuximab for the treatment of squamous cell carcinoma of the head and neck. *Clin Adv Hematol Oncol* 2008; **6**: 742–750.
90. Herrero R, Quint W, Hildesheim A, Gonzalez P, Struijk L, Katki HA *et al.* Reduced prevalence of oral human papillomavirus (HPV) 4 years after bivalent HPV vaccination in a randomized clinical trial in Costa Rica. *PLoS One* 2013; **8**: e68329.
91. Fung C, Grandis JR. Emerging drugs to treat squamous cell carcinomas of the head and neck. *Expert Opin Emerg Drugs* 2010; **15**: 355–373.
92. Nordsmark M, Bentzen SM, Rudat V, Brizel D, Lartigau E, Stadler P *et al.* Prognostic value of tumor oxygenation in 397 head and neck tumors after primary radiation therapy. An international multi-center study. *Radiother Oncol* 2005; **77**: 18–24.
93. Haase VH. The VHL tumor suppressor: master regulator of HIF. *Curr Pharm Des* 2009; **15**: 3895–3903.
94. Hockel M, Vaupel P. Biological consequences of tumor hypoxia. *Semin Oncol* 2001; **28**(2 Suppl 8): 36–41.
95. Overgaard J. Hypoxic radiosensitization: adored and ignored. *J Clin Oncol* 2007; **25**: 4066–4074.
96. Kyzas PA, Cunha IW, Ioannidis JP. Prognostic significance of vascular endothelial growth factor immunohistochemical expression in head and neck squamous cell carcinoma: a meta-analysis. *Clin Cancer Res* 2005; **11**: 1434–1440.
97. Toustrup K, Sorensen BS, Nordsmark M, Busk M, Wiuf C, Alsner J *et al.* Development of a hypoxia gene expression classifier with predictive impact for hypoxic modification of radiotherapy in head and neck cancer. *Cancer Res* 2011; **71**: 5923–5931.
98. Eustace A, Mani N, Span PN, Irlam JJ, Taylor J, Betts GN *et al.* A 26-gene hypoxia signature predicts benefit from hypoxia-modifying therapy in laryngeal cancer but not bladder cancer. *Clin Cancer Res* 2013; **19**: 4879–4888.
99. Argiris A, Kotsakis AP, Hoang T, Worden FP, Savvides P, Gibson MK *et al.* Cetuximab and bevacizumab: preclinical data and phase II trial in recurrent or metastatic squamous cell carcinoma of the head and neck. *Ann Oncol* 2013; **24**: 220–225.
100. Argiris A, Karamouzis MV, Gooding WE, Branstetter BF, Zhong S, Raez LE *et al.* Phase II trial of pemetrexed and bevacizumab in patients with recurrent or metastatic head and neck cancer. *J Clin Oncol* 2011; **29**: 1140–1145.
101. Cohen EE, Davis DW, Karrison TG, Seiwert TY, Wong SJ, Nattam S *et al.* Erlotinib and bevacizumab in patients with recurrent or metastatic squamous-cell carcinoma of the head and neck: a phase I/II study. *Lancet Oncol* 2009; **10**: 247–257.
102. Kim JW, Dang CV. Cancer's molecular sweet tooth and the Warburg effect. *Cancer Res* 2006; **66**: 8927–8930.
103. Warburg O, Wind F, Negelein E. The metabolism of tumors in the body. *J Gen Physiol* 1927; **8**: 519–530.
104. Cairns RA, Harris IS, Mak TW. Regulation of cancer cell metabolism. *Nat Rev Cancer* 2011; **11**: 85–95.
105. Bensaad K, Tsuruta A, Selak MA, Vidal MN, Nakano K, Bartrons R *et al.* TIGAR, a p53-inducible regulator of glycolysis and apoptosis. *Cell* 2006; **126**: 107–120.
106. Dang CV, Kim JW, Gao P, Yustein J. The interplay between MYC and HIF in cancer. *Nat Rev Cancer* 2008; **8**: 51–56.
107. Elstrom RL, Bauer DE, Buzzai M, Karnauskas R, Harris MH, Plas DR *et al.* Akt stimulates aerobic glycolysis in cancer cells. *Cancer Res* 2004; **64**: 3892–3899.
108. Shackelford DB, Shaw RJ. The LKB1-AMPK pathway: metabolism and growth control in tumour suppression. *Nat Rev Cancer* 2009; **9**: 563–575.
109. Kim JW, Tchernyshyov I, Semenza GL, Dang CV. HIF-1-mediated expression of pyruvate dehydrogenase kinase: a metabolic switch required for cellular adaptation to hypoxia. *Cell Metabol* 2006; **3**: 177–185.
110. Libby G, Donnelly LA, Donnan PT, Alessi DR, Morris AD, Evans JM. New users of metformin are at low risk of incident cancer: a cohort study among people with type 2 diabetes. *Diabetes Care* 2009; **32**: 1620–1625.
111. Braakhuis BJ, Leemans CR, Brakenhoff RH. Expanding fields of genetically altered cells in head and neck squamous carcinogenesis. *Semin Cancer Biol* 2005; **15**: 113–120.
112. Reya T, Morrison SJ, Clarke MF, Weissman IL. Stem cells, cancer, and cancer stem cells. *Nature* 2001; **414**: 105–111.
113. Brunner TB, Kunz-Schughart LA, Grosse-Gehling P, Baumann M. Cancer stem cells as a predictive factor in radiotherapy. *Semin Radiat Oncol* 2012; **22**: 151–174.
114. Zoller M. CD44: can a cancer-initiating cell profit from an abundantly expressed molecule? *Nat Rev Cancer* 2011; **11**: 254–267.
115. Prince ME, Sivanandan R, Kaczorowski A, Wolf GT, Kaplan MJ, Dalerba P *et al.* Identification of a subpopulation of cells with cancer stem cell properties in head and neck squamous cell carcinoma. *Proc Natl Acad Sci USA* 2007; **104**: 973–978.
116. Bracken AP, Dietrich N, Pasini D, Hansen KH, Helin K. Genome-wide mapping of Polycomb target genes unravels their roles in cell fate transitions. *Genes Dev* 2006; **20**: 1123–1136.
117. Mack B, Gires O. CD44s and CD44v6 expression in head and neck epithelia. *PLoS One* 2008; **3**: e3360.
118. Ma I, Allan AL. The role of human aldehyde dehydrogenase in normal and cancer stem cells. *Stem Cell Rev* 2011; **7**: 292–306.
119. Krishnamurthy S, Dong Z, Vodopyanov D, Imai A, Helman JI, Prince ME *et al.* Endothelial cell-initiated signaling promotes the survival and self-renewal of cancer stem cells. *Cancer Res* 2010; **70**: 9969–9978.
120. Chen YC, Chen YW, Hsu HS, Tseng LM, Huang PI, Lu KH *et al.* Aldehyde dehydrogenase 1 is a putative marker for cancer stem cells in head and neck squamous cancer. *Biochem Biophys Res Commun* 2009; **385**: 307–313.
121. Faber A, Barth C, Hormann K, Kassner S, Schultz JD, Sommer U *et al.* CD44 as a stem cell marker in head and neck squamous cell carcinoma. *Oncol Rep* 2011; **26**: 321–326.
122. Joshua B, Kaplan MJ, Doweck I, Pai R, Weissman IL, Prince ME *et al.* Frequency of cells expressing CD44, a head and neck cancer stem cell marker: correlation with tumor aggressiveness. *Head Neck* 2012; **34**: 42–49.

123. de Jong MC, Pramana J, van der Wal JE, Lacko M, Peutz-Kootstra CJ, de Jong JM *et al.* CD44 expression predicts local recurrence after radiotherapy in larynx cancer. *Clin Cancer Res* 2010; **16**: 5329–5338.
124. Riechelmann H, Sauter A, Golze W, Hanft G, Schroen C, Hoermann K *et al.* Phase I trial with the CD44v6-targeting immunoconjugate bivatuzumab mertansine in head and neck squamous cell carcinoma. *Oral Oncol* 2008; **44**: 823–829.
125. Braakhuis BJ, Brakenhoff RH, Leemans CR. Gene expression profiling in head and neck squamous cell carcinoma. *Curr Opin Otolaryngol Head Neck Surg* 2010; **18**: 67–71.
126. Roepman P, Wessels LF, Kettelarij N, Kemmeren P, Miles AJ, Lijnzaad P *et al.* An expression profile for diagnosis of lymph node metastases from primary head and neck squamous cell carcinomas. *Nat Genet* 2005; **37**: 182–186.
127. Torres-Roca JF, Eschrich S, Zhao H, Bloom G, Sung J, McCarthy S *et al.* Prediction of radiation sensitivity using a gene expression classifier. *Cancer Res* 2005; **65**: 7169–7176.
128. Bartel DP, Chen CZ. Micromanagers of gene expression: the potentially widespread influence of metazoan microRNAs. *Nat Rev Genet* 2004; **5**: 396–400.
129. Lu Z, Liu M, Stribinskis V, Klinge CM, Ramos KS, Colburn NH *et al.* MicroRNA-21 promotes cell transformation by targeting the programmed cell death 4 gene. *Oncogene* 2008; **27**: 4373–4379.
130. Ivanovska I, Ball AS, Diaz RL, Magnus JF, Kibukawa M, Schelter JM *et al.* MicroRNAs in the miR-106b family regulate p21/CDKN1A and promote cell cycle progression. *Mol Cell Biol* 2008; **28**: 2167–2174.
131. Childs G, Fazzari M, Kung G, Kawachi N, Brandwein-Gensler M, McLemore M *et al.* Low-level expression of microRNAs let-7d and miR-205 are prognostic markers of head and neck squamous cell carcinoma. *Am J Pathol* 2009; **174**: 736–745.
132. Qu C, Liang Z, Huang J, Zhao R, Su C, Wang S *et al.* MiR-205 determines the radioresistance of human nasopharyngeal carcinoma by directly targeting PTEN. *Cell Cycle* 2012; **11**: 785–796.
133. Avissar M, Christensen BC, Kelsey KT, Marsit CJ. MicroRNA expression ratio is predictive of head and neck squamous cell carcinoma. *Clinical cancer research: an official journal of the American Association for Cancer Research* 2009; **15**: 2850–2855.
134. Chang KW, Liu CJ, Chu TH, Cheng HW, Hung PS, Hu WY *et al.* Association between high miR-211 microRNA expression and the poor prognosis of oral carcinoma. *J Dent Res* 2008; **87**: 1063–1068.
135. Yang CC, Hung PS, Wang PW, Liu CJ, Chu TH, Cheng HW *et al.* miR-181 as a putative biomarker for lymph-node metastasis of oral squamous cell carcinoma. *J Oral Pathol Med* 2011; **40**: 397–404.
136. Johnson SM, Grosshans H, Shingara J, Byrom M, Jarvis R, Cheng A *et al.* RAS is regulated by the let-7 microRNA family. *Cell* 2005; **120**: 635–647.
137. Israelsen WJ, Dayton TL, Davidson SM, Fiske BP, Hosios AM, Bellinger G *et al.* PKM2 isoform-specific deletion reveals a differential requirement for pyruvate kinase in tumor cells. *Cell* 2013; **155**: 397–409.
138. Kinoshita T, Nohata N, Fuse M, Hanazawa T, Kikkawa N, Fujimura L *et al.* Tumor suppressive microRNA-133a regulates novel targets: moesin contributes to cancer cell proliferation and invasion in head and neck squamous cell carcinoma. *Biochem Biophys Res Commun* 2012; **418**: 378–383.
139. Korpal M, Lee ES, Hu G, Kang Y. The miR-200 family inhibits epithelial-mesenchymal transition and cancer cell migration by direct targeting of E-cadherin transcriptional repressors ZEB1 and ZEB2. *J Biol Chem* 2008; **283**: 14910–14914.
140. Dai Y, Xie CH, Neis JP, Fan CY, Vural E, Spring PM. MicroRNA expression profiles of head and neck squamous cell carcinoma with docetaxel-induced multidrug resistance. *Head Neck* 2011; **33**: 786–791.

Appendix II

IJC
International Journal of Cancer

MicroRNA-196a promotes an oncogenic effect in head and neck cancer cells by suppressing annexin A1 and enhancing radioresistance

Yae-Eun Suh[1], Nina Raulf[1], Joop Gäken[2], Katherine Lawler[3], Teresa Guerrero Urbano[4], Jessica Bullenkamp[1], Stéphane Gobeil[5], Jacques Huot[6], Eddy Odell[1] and Mahvash Tavassoli[1]

[1] Department of Molecular Oncology, King's College London, Guy's Hospital Campus, London, SE1 1UL, UK
[2] Department of Haematological Medicine, King's College London, the Rayne Institute, London, SE5 9NU, UK
[3] Division of Cancer Studies and Institute of Mathematical and Molecular Biomedicine, King's College London, Guy's Hospital Campus, London, SE1 1UL, UK
[4] Clinical Oncology Department, Lambeth Wing, St Thomas' Hospital, Westminster, Bridge, Road, UKLondon, SE1 7EH
[5] Centre Hospitalier De L'université Laval (CHUL, 2705, Boulevard Laurier, R-4720 Québec, G1V 4G2, Canada
[6] Centre De Recherche Du CHU De Québec Et Centre De Recherche En Cancérologie De L'université Laval, 9 Rue McMahon, Québec, G1R 2J6, Canada

Radiotherapy is a major treatment modality for head and neck squamous cell carcinoma (HNSCC). Up to 50% of patients with locally advanced disease relapse after radical treatment and there is therefore a need to develop predictive bomarkers for clinical use that allow the selection of patients who are likely to respond. MicroRNA (miRNA) expression profiling of a panel of HNSCC tumours with and without recurrent disease after surgery and radiotherapy detected miR-196a as one of the highest upregulated miRNAs in the poor prognostic group. To further study the role of miR-196a, its expression was determined in eight head and neck cancer cell lines. Overexpression of miR-196a in HNSCC cells, with low endogenous miR-196a expression, significantly increased cell proliferation, migration and invasion, and induced epithelial to mesenchymal transition. Conversely, miR-196a knockdown in cells with high endogenous expression levels significantly reduced oncogenic behaviour. Importantly, overexpression of miR-196a increased radioresistance of cells as measured by gamma H2AX staining and MTT survival assay. Annexin A1 (ANXA1), a known target of miR-196a, was found to be directly modulated by miR-196a as measured by luciferase assay and confirmed by Western blot analysis. ANXA1 knockdown in HNSCC exhibited similar phenotypic effects to miR-196a overexpression, suggesting the oncogenic effect of miR-196a may at least be partly regulated through suppression of ANXA1. In conclusion, this study identifies miR-196a as a potential important biomarker of prognosis and response of HNSCC to radiotherapy. Furthermore, our data suggest that miR-196a and/or its target gene ANXA1 could represent important therapeutic targets in HNSCC.

Key words: MicroRNA-196a, annexin A1, head and neck squamous cell carcinoma, biomarkers, radiosensitivity

Abbreviations: **MiRNA**: microRNA; **ANXA1**: annexin A1; **HNSCC**: head and neck squamous cell carcinoma; **OSCC**: oral squamous cell carcinoma; **3'-UTR**: 3' untranslated region; **QRT-PCR**: quantitative real-time polymerase chain reaction; **MTT**: 3-(4: 5-dimethylthiazol-2-yl)-2: 5-diphenyltetrazolium bromide; **IκBα**: nuclear factor kappa-B-inhibitor alpha; **NF-κB**: nuclear factor kappa-B

Additional Supporting Information may be found in the online version of this article.

The authors disclose no potential conflicts of interest

DOI: 10.1002/ijc.29397
History: Received 16 July 2014; Accepted 3 Dec 2014; Online 19 Dec 2014

Corresponding author: Professor Mahvash Tavassoli, Department of Molecular Oncology, King's College London, Hodgkin Building, London SE1 1UL, UK; Tel: +4420784896120;
Email: mahvash.tavassoli@kcl.ac.uk

Introduction

Head and neck squamous cell carcinoma (HNSCC) encompass a group of heterogeneous tumours, the majority of which present with locally advanced disease. Despite recent advances in both surgical and radiotherapy techniques, which are associated with long-term side effects, up to 50% of locally advanced cases relapse after radical therapy. Treatment options at this stage with salvage surgery, re-irradiation or palliative chemotherapy are limited.[1] Therefore, predictive biomarkers and targeted therapies to enable individualisation of treatment are needed to improve outcomes and minimise morbidity.

MicroRNAs (miRNAs) are small non-coding RNAs that regulate and refine gene expression by base pairing with the 3'-untranslated region (3'-UTR) of mRNA targets, resulting in mRNA degradation or inhibition of translation. They function within a complex interactive network, with a single miRNA influencing the expression of multiple genes and a single mRNA being targeted by multiple miRNAs.[2,3] Altered miRNA expression has been reported in almost all types of

What's new?

There is accumulating evidence that miR-196a plays an important role in the pathogenesis of a number of cancers. Through functional studies, here the authors demonstrate that miR-196a confers an oncogenic phenotype in head and neck cancer cells, through the targeting of ANXA1. The results also show that MiR-196a modulation is associated with response to radiation. MiR-196a may therefore represent both a prognostic and a predictive biomarker in head and neck cancer. Furthermore, the data suggest that miR-196a and/or its target gene ANXA1 could represent important therapeutic targets in head and neck cancer.

cancers.[4] MiRNAs can act as oncogenes or tumour suppressor genes and are involved in a variety of pathways in cancer development and progression, such as proliferation, apoptosis, metastasis and resistance to therapy.[5]

MiRNAs have potential roles as biomarkers in HNSCC in tumour diagnosis and prognosis, and as predictors of response to treatment such as radiotherapy.[1,6] Recently, there has been increasing interest in miR-196a as an oncogene in different solid tumours, including oral squamous cell carcinoma (OSCC),[7] glioblastoma,[8] cervical,[9] pancreatic,[10] and gastric cancers.[11] The first identified targets of miR-196a were HOXA and HOXB genes in primary adult acute myeloid leukaemia,[12] and HOXC8 and HOXB7 in malignant melanoma.[13,14] However, HOX genes have not been shown to be regulated by miR-196a in head and neck cancer cell lines such as SCC25 and FaDu.[15] Other validated targets of miR-196a include annexin A1 (ANXA1),[16] S100A9, SPRR2C and KRT5 in oesophageal cancer cells,[17] and ERG in leukaemia,[18] but the precise roles of these targets in regulating the oncogenic effects of miR-196a so far remain unclear.

Here, we studied the miR-196a target ANXA1. A member of the annexin family of calcium-dependent phospholipid-binding proteins, ANXA1 has been shown to exhibit anti-inflammatory and anti-proliferative effects.[19] However, the molecular mechanisms by which ANXA1 modulates these cellular responses have not been fully determined. Due to its anti-proliferative effects, ANXA1 protein has been studied in several types of cancers, but *in vivo* studies have demonstrated that the expression pattern of ANXA1 in human cancers is not well defined. While ANXA1 has been reported to be upregulated in glioma[20] and lung adenocarcinoma,[21] its expression is reduced or lost in other cancer tissues including head and neck,[22–24] oesophageal and prostate.[25] In general, suppression of ANXA1 has been associated with cell line transformation, tumour progression and metastasis. In HNSCC, the expression of ANXA1 has been shown to correlate with higher grades of differentiation, or less aggressive tumours, suggesting a tumour suppressor role.[22,26] ANXA1 has been shown to be a target of miR-196a in oesophageal and breast cancer cells,[16] but the association with miR-196a has not been established in HNSCC.

MiRNA expression profiling of a panel of HNSCC tumours identified miR-196a to be upregulated in a group of patients with HNSCC with recurrent disease after radical treatment. Functional studies demonstrated that miR-196a overexpression induced resistance to irradiation, suggesting an important potential of miR-196a as both a prognostic and predictive biomarker in HNSCC. Amongst the known target genes of miR-196a we studied ANXA1, as it has been shown to have a tumour suppressor role in different tumours including OSCC.[22–24] Here, we show that ANXA1 is a direct target of miR-196a in HNSCC. The overexpression of miR-196a or suppression of ANXA1 in HNSCC cells resulted in similar effects including increased proliferation, migration and invasion. This study suggests that the oncogenic effects of miR-196a in HNSCC are at least partly exerted through targeting ANXA1.

Material and Methods

Tissue samples and miRNA microarray

Sixteen patients with head and neck squamous cell carcinoma were selected based on their long-term outcome to anticancer treatment. All patients were treated with surgery and postoperative radiotherapy and classified as 'good' responders of therapy if they had no evidence of recurrent disease within 5 years of follow up, or 'bad' responders if they had relapsed. Cases were selected as representative stages and sites in each group to include the range of oral carcinoma presentations. All carcinomas were from oral sites with surface origin; those from posterior tongue or soft palate were not of human papillomavirus type. Tissue samples were collected prior to receiving treatment and immediately snap-frozen in liquid nitrogen and stored at -80 °C until RNA extraction. Ethics approval was covered by an existing project (REC reference 04/02/10). The samples were profiled for miRNA gene expression using Illumina v2 miRNA Beadchip (Illumina, Inc., San Diego, CA, USA) according to manufacturer's instructions. Bead summary data were exported from GenomeStudio (GSGX V1.9.0; no background subtraction, no normalisation) and imported into R/Bioconductor. Arrays were log2-transformed and quantile normalized using the beadarray package.[27] Differential expression of miRNAs between the two patient groups ('good' and 'bad' responders) was estimated by fitting a linear model and empirical Bayes moderated *t*-tests using the limma package for R/Bioconductor.[28] Log_2 fold-change, unadjusted and adjusted *p*-values were inspected.[29] There was insufficient power to detect significantly differentially expressed genes after adjustment for multiple testing ($p < 0.05$, adjusted), which may be due to the biopsy origin of samples. Therefore the unadjusted *p* -values ($p < 0.05$) were used to define the top-ranked miRNAs for

differential expression (Fig. 1A) and the fold-change between "good" and "bad" responders was inspected (Fig. 1B).

Cell lines and culture

Eight head and neck cancer cell lines were profiled for expression of miR-196a. HN5, HN30, SCC11B and SCC22B were selected to further investigate the effects of miR-196a modulation. HN5 was obtained from Professor Barry Gusterson, Department of Pathology, University of Glasgow, UK and HN30 from Dr Andrew Yeudall, Department of Craniofacial Development, King's College London, UK. SCC11B and 22B were obtained from Dr Thomas Carey, University of Michigan, USA. HEK293T cells were provided by Dr Lucas Chan, Rayne Institute, King's College London, UK and MDA-MB-231 were obtained from Prof Joy Burchell, Breast Cancer Biology Group, King's College London, UK. All cells were maintained in Dulbecco's Modified Eagle's Medium (DMEM; GE Healthcare, Chalfont St. Giles, UK) supplemented with 10% fetal bovine serum (FBS), 20 µl/ml penicillin and 10 µl/ml streptomycin, and 1 mM sodium pyruvate.

RNA extraction and quantitative real-time RT-PCR (qRT-PCR)

Total RNA was extracted from tissue samples using the miRNeasy kit (Qiagen, Hilden, Germany) and from cells using TRIzol (Life Technologies, Paisley, UK) according to the manufacturer's instructions. Complementary DNA was created from 10 ng of RNA using TaqMan miRNA reverse transcription kit (Life Technologies, Paisley, UK). Quantitative RT-PCR was performed using TaqMan Small RNA Assay (Life Technologies, Paisley, UK), with each 10µl reaction consisting of 1.5µl cDNA, 0.5µl miRNA primer, 5 µl of TaqMan mastermix and 3 µl RNA free water. Samples were run in triplicate according to the manufacturer's recommendations, and the standard curve method was used to quantitate miRNA expression levels relative to the level of the housekeeping gene RNU48. All mature miRNA primers were purchased from Life Technologies. QRT-PCR analysis was carried out on three independent RNA samples.

Plasmids and transfection

MiR-196a expression plasmids were prepared by PCR amplification of a 630 bp genomic DNA fragment containing mir-196a using the following forward and reverse primers; CAGGCTTGTGCCTGTGTCTA and GTGCCTCGGGAGAGTTGAC. The PCR product was sequence verified and cloned into the retroviral expression vector pBabe-puro. HN5 cells at 70–80% confluency were transfected with miR-196a or empty vector pBabe-puro using X-tremeGENE DNA transfection reagent (Roche Applied Science, West Sussex, UK) and stable populations were selected using puromycin. A mixed population of cells and a population grown from a single surviving colony after selection were used. MiR-196a sponge and sponge control were gifts from Dr Sebastian Herzog, Division of Developmental Immunology, Medical University of Innsbruck, Austria. The sponge plasmid was produced using HEK293T cells as the packaging cell line and the retrovirus-containing supernatant was harvested at 24 and 48 hrs. HN30 cells were infected with the supernatant and stable cells selected using puromycin. This was repeated using SCC11B and SCC22B cells. Lentiviral ANXA1 shRNA and control were gifts from Dr Stéphane Gobeil, CHUL Research Centre, Laval University, Canada. ANXA1 shRNA was produced using HEK293T cells as the packaging cell line. HN5 cells were infected and a stable population selected with puromycin.

Cell proliferation assays

Stably transfected cells were seeded in triplicate in 6-well plates (10^5 cells per well) and left for 24 hrs. Cells were trypsinized and counted over the next 7 days. Cell proliferation was also assessed using the 3–(4,5-dimethylthiazol-2-yl)-2,5-diphenyltetrazolium bromide (MTT) cell viability assay. Cells were seeded in 96-well plates (3000 cells per well), 6 wells per time point, and left overnight. On days 1 to 5, 20µl of MTT (5 mg/ml, Calbiochem, Watford, UK) solution was added to each well and incubated for 2 hrs, after which 150µl of solubilisation solution (50% dimethylformamide, 0.2% glacial acetic acid, 20 mM HCl, 20% SDS) was added. After further incubation for 24 hrs, the optical density was measured at a wavelength of 595 nm on a LT-4000 microplate reader.

Scratch assay

To investigate the migratory ability of the modulated cells, cells were seeded to confluence in 6-well plates with perpendicular markings on the bottom surface as reference points for imaging. Confluent cells were serum starved for 24 hrs, before creating a straight scratch along the diameter of the well using a p200 pipette tip. Floating cells were removed by washing the well twice with media. Images were taken at 0 and 16 to 24 hrs. The assay was performed in triplicate in two independent experiments and the area between the scratch was imaged, analyzed using ImageJ (NIH, Bethesda, MD, USA) and the percentage of the scratch area closed between the two time points calculated.

Invasion assay

The invasion potential of the cells was assessed using Matrigel invasion chambers (BD Biosciences, San Jose, CA, USA), according to the manufacturer's instructions. Briefly, the optimal seeding density of the parental cell lines was determined before the $2x10^5$/ml and $4x10^5$/ml cells were prepared for HN5 and HN30 modulated cells respectively. Cells were placed in the invasion chambers, which were placed in a 24-well plate, and chemoattractant (medium containing 5% FBS) was added to the wells. Cells were incubated for 22 hrs, after which the non-invading cells on the upper surface of the chamber were scrubbed off with a cotton swab, and the invading cells on the lower surface were fixed, stained and

counted. Five random images from each membrane were counted and invasion expressed as the percent invasion through the Matrigel membrane relative to the migration through the control membrane. Invasion assays were performed in duplicate and repeated in an independent experiment.

Vimentin immunofluorescence

Forty thousand cells were seeded in duplicate into 8-chamber slides (BD Biosciences, San Jose, CA, USA) and allowed to attach overnight. Cells were then washed with PBS, fixed with 4% paraformaldehyde for 15 min, washed and permeabilized with 0.2% Triton X-100 for 15 min, washed and blocked for 30 min with 3% bovine serum albumin in TBS-tween. Cells were then incubated overnight at 4 °C with rabbit anti-vimentin antibody (Cell Signaling, Danvers, MA, USA; 1:100 dilution). Cells were washed again and incubated for 90 min with secondary fluorescein isothiocyanate (FITC)-conjugated goat anti-rabbit antibody (Sigma-Aldrich, Poole, UK; 1:100 dilution). The chambers were removed from the slide and cells mounted in Vectashield mounting medium containing 4',6-diamidin-2-phenylindole (DAPI; Vector Laboratories, Burlingame, CA, USA). Images were acquired at 60× magnification using a fluorescence microscope.

Radiation assays

Radiosensitivity of the miR-196a overexpressing cells was assessed using gamma H2AX immunofluorescence. Forty thousand cells were seeded into 8-chamber slides in duplicate and incubated overnight prior to irradiation with 0 (control), 0.5 Gy, 1 Gy and 2 Gy using a Noridon GC-1000S v2.9 cell irradiator, which contains a caesium source at a dose rate of $250 \pm 0.59\%$ Gy/hour. Cells were fixed, permeabilized and blocked as above at 30 min or 24 hrs post-irradiation, and incubated overnight with rabbit phospho-histone H2AX (Ser139) antibody (Cell Signaling, Danvers, MA, USA; 1:100 dilution), followed by secondary anti-rabbit FITC antibody. The number of gamma H2AX foci in each nucleus was analyzed using BlobFinder software (Center for Image Analysis, Uppsala University, Sweden) and expressed relative to the control cells. A minimum of 100 cells were imaged and analyzed for each dose and time point. Radiosensitivity of the miR-196a cells and the other modulated cells was also assessed by MTT cell viability assay. Cells were irradiated in 25 cm^2 flasks when 70–80% confluent, irradiated at 0 (control), 2, 4, and 6 Gy, and incubated overnight. Cells were seeded in a 96-well plate (3000 cells per well, 6 wells per dose, two independent experiments) and incubated for five days, at which point the control cells were confluent. The MTT assay was then carried out as above and measurements expressed relative to the control cells.

Western blot analysis

The concentration of proteins extracted was determined using the Bradford assay (Bio-Rad, Hercules, CA). Equal amounts of protein were separated by 10% SDS-PAGE and transferred to a nitrocellulose membrane (Sigma-Aldrich, Poole, UK). The membrane was blocked in 5% milk and incubated with rabbit anti-ANXA1 (Cell Signaling, Danvers, MA, USA; 1:1000), rabbit anti-cleaved PARP (Cell Signaling; 1:1000), mouse anti-caspase-3 (Cell Signaling; 1:1000), or mouse anti-tubulin (Sigma-Aldrich; 1:2000) as a loading control. Primary antibody binding was detected using secondary anti-rabbit (GE Healthcare, Chalfont St. Giles, UK; 1:2000) or anti-mouse (Sigma-Aldrich; 1:2000) antibodies linked to horseradish peroxidase and enhanced chemoluminescence.

Luciferase reporter assay

The ANXA1 luciferase reporter construct was a gift from Professor Jacques Huot, Laval University Cancer Research Centre, Canada. Cells were seeded in 96-well plates at a density of 10^4 cells per well and transfected with 0.1 μg of ANXA1 luciferase construct the following day using FuGENE HD transfection reagent (Promega, Madison, WI, USA). The cells were incubated for 48 hrs before the luciferase assay was performed using the Dual-Glo Luciferase Assay System according to the manufacturer's instructions (Promega). Measurements from untransfected cells were used as negative controls and the data was normalized by dividing the Firefly activity by the Renilla activity. Each experiment was carried out in repeated triplicates.

Statistical analysis

The data is presented as the mean ± standard deviation unless otherwise stated, and compared using one-way ANOVA or unpaired student's *t*-test. Statistical analysis was performed using GraphPad Prism version 6.0 (Graphpad Software Inc, La Jolla, CA, USA). *p* values less than 0.05 were considered statistically significant.

Results

MiR-196a is overexpressed in patients with worse outcome

Gene expression profiling of the sixteen patient samples with differing outcomes identified 41 miRNAs to be differentially expressed between the patients with "good" and "bad" outcomes (threshold $p < 0.05$; limma, unadjusted *p*; Fig. 1A). MiR-196a was selected as being highly upregulated in the "bad" responders group compared with the "good" responders group ($\log_2$ fold-change $= -1.8$; $p = 0.014$; limma, unadjusted P; Fig. 1B). To investigate the function of miR-196a, eight HNSCC cell lines were evaluated for the expression of miR-196a (Fig. 1C). Only the cell line HN5 was found to have low endogenous expression of miR-196a and was therefore selected for ectopic overexpression functional studies, while HN30, SCC11B and SCC22B, with high miR-196a levels, were selected for miR-196a suppression experiments. The cell proliferation rate of representative cell lines with low (HN5) or high (HN30) miR-196a levels was compared by

daily cell counting over seven days. HN30 showed a significantly faster proliferation rate (Fig. 1D).

Exogenous miR-196a overexpression promotes cell proliferation, migration and invasion

MiR-196a overexpression plasmid was transfected into HN5 cells and a stable population selected using puromycin. QRT-PCR analysis demonstrated successful upregulation, with an approximate 50-fold increase in the expression in the mixed population of miR-196a overexpressing cells (Fig. 2A). The effect of this modulation on cell proliferation was assessed using two different methods: daily cell counting and MTT cell viability assay. Both methods demonstrated significant enhancement in the rate of growth in the miR-196a overexpressing cells compared with control vector transfected cells (Fig. 2B). The impact of miR-196a on cell migration and invasion was analyzed using the scratch and Matrigel invasion assays, respectively. MiR-196a overexpression clearly increased cell migration when the scratch assay was analyzed at 16 hrs, with an average of 78% of the scratch area closed in the miR-196a cells *versus* 28% in the control cells ($p < 0.01$, Fig. 2C). Invasion was also enhanced with the upregulation of miR-196a, with the mean percentage invasion relative to the control membrane of 53% compared with 16% in the empty vector control cells ($p = 0.01$, Fig. 2D). Vimentin immunofluorescence was used as a marker for epithelial-mesenchymal transition (EMT). The pattern of vimentin expression was significantly altered after overexpressing miR-196a, with appearances resembling the known mesenchymal breast cancer cell line MDA-MB-231 (Fig. 2E), suggesting miR-196a contributes to the change in vimentin configuration in preparation for transition into the mesenchymal phenotype. To validate the functional effect of miR-196a overexpression, single colonies were selected and expanded. The miR-196a level was approximately 45-fold higher, shown in a representative clone, compared to control cells (Supporting Information Fig. S1A). Importantly, cell cultures derived from single miR-196a overexpressing clones or a mixed population of cells showed similar oncogenic characteristics. These results confirm that the phenotypic changes induced by miR-196a are unlikely to be due to clonal effects (Supporting Information Fig. S1B–C).

MiR-196a alters radiosensitivity of head and neck cancer cells

The patients with disease recurrence after treatment had higher levels of miR-196a than patients who remained disease free after treatment. This observation prompted further investigation into whether this miRNA could alter the sensitivity of HNSCC to radiation. First, the miR-196a overexpressing cells and empty vector transfected control cells were irradiated at low doses and stained for the presence of gamma H2AX foci within the nucleus as a biomarker for double-stranded DNA breaks. Gamma H2AX foci rapidly accumulated and peaked at 30 min after irradiation, with foci remaining at 24 hr representing persistent damage and therefore increased radiosensitivity.[30] The miR-196a overexpressing cells demonstrated similar numbers of gamma H2AX foci per nucleus (relative to the unirradiated cells, Supporting Information Fig. S2) compared with empty vector control cells at 30 min. However, at 24 hr significantly fewer foci were detected in miR-196a overexpressing cells, indicating more efficient repair and increased radioresistance (Fig. 3A). This was confirmed by MTT assay, where the cells were irradiated at higher doses and enhanced cell viability was demonstrated after five days in the miR-196a overexpressing cells (Fig. 3B).

MiR-196a knockdown results in decreased cell proliferation, migration and invasion

MiRNA sponges are transcripts that contain multiple target sites complementary to the miRNA under investigation and sequester endogenous miRNAs, resulting in functional inhibition of the mature miRNA.[31] MiR-196a sponge infection in HN30 cell lines resulted in approximately 60% suppression of the expression level measured by qRT-PCR (Fig. 4A). The effect of this downregulation led to the opposite functional consequence of miR-196a overexpression on cell proliferation (Fig. 4B), migration (Fig. 4C) and invasion (Fig. 4D). The mean percentage of the scratch closed at 24 hrs was 39% in the knockdown cells compared with 76% in the sponge control cells ($p < 0.01$). The mean percentage invasion relative to the control membrane was 18% in the knockdown cells *versus* 46% in the control cells ($p = 0.02$). Response to radiation was assessed using the MTT assay, which showed reduced cell viability at 2, 4 and 6 Gy, suggesting increased radiosensitivity in the miR-196a knockdown cells (Fig. 4E). MTT and scratch assays were also performed on two other cell lines with high miR-196a levels, SCC11B and SCC22B. Inhibition of miR-196a using miR-196a sponge induced similar effects observed with HN30 miR-196a knockdown cells, with consistent inhibition of cell proliferation and migration (Supporting Information Fig. S3A–E). To investigate whether the inhibition of growth and cellular migration was due to induction of apoptosis, HN30 cells were transiently transduced with miR-196a sponge or control vector, and cell lysates were analyzed for apoptotic markers at 48 and 72 hr. Western blot analysis confirmed similar levels of cleaved PARP and cleaved caspase-3 between miR-196a knockdown and vector control cells suggesting that the observed effects of miR-196a downregulation on suppressing proliferation and migration are unlikely to be due to increased apoptosis (Fig. 4F).

ANXA1 is a direct target of miR-196a in HNSCC

We explored the mechanisms by which miR-196a exerts its oncogenic effect in HNSCC cell lines. As described several cellular genes have been shown to be targeted by miR-196a. In this study, ANXA1 was further analyzed due to its role as a tumour suppressor and potential prognostic marker in head and neck cancers.[22–24] MiR-196a overexpression in

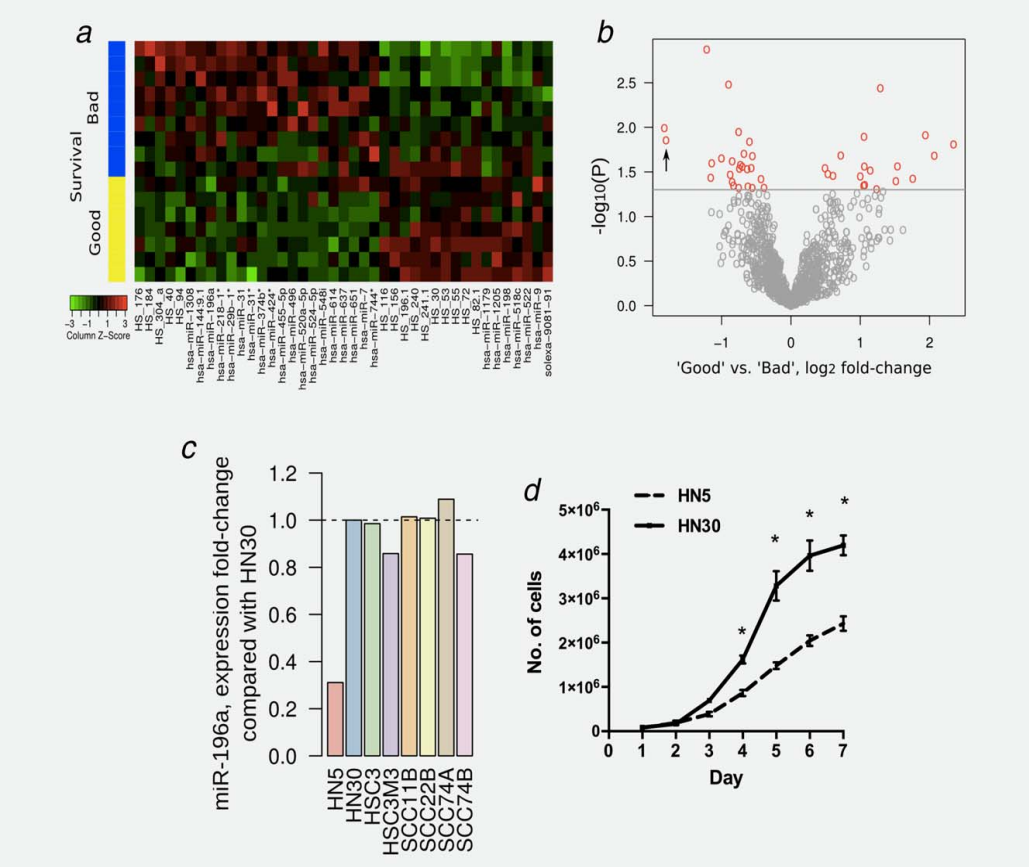

Figure 1. MiRNA expression pattern in head and neck cancers. (a) heatmap displaying miRNA expression in samples with "good" (yellow) and "bad" (blue) survival following anticancer therapy from a panel of 16 fresh tissue specimens. The 41 top-ranked miRNAs for differential expression between "good" and "bad" survival groups are shown (threshold $p < 0.05$; limma, unadjusted p). Rows (samples) are ordered by expression score (sum of expression weighted by the sign of the fold-change, $\sum_{probes,g}[expression_g \times sign\ of\ fold\text{-}change_g]$). Columns (miRNAs) are ordered by the direction of fold-change then alphabetically. (B) volcano plot for 'good' *versus* 'bad' survival showing $\log_2$ fold-change *versus* significance ($-\log_{10}$ p; limma, unadjusted p) for all probes. The arrow indicates miR-196a, which shows increased expression in the "bad" survival group compared with the "good" survival group ($\log_2 FC = -1.8$, $p = 0.014$; limma, unadjusted p). Red points: $p < 0.05$ (limma, unadjusted p). (C) MiR-196a gene expression levels in eight head and neck cancer cell lines, displayed as expression fold-change compared with HN30. Cell line expression values are shown as the mean of two duplicate samples. The cell lines HN5 and HN30, with low and high endogenous levels of miR-196a respectively, were selected for further investigation. (D) cell proliferation in HN5 and HN30 cells assessed by daily counting over 7 days.

HN5 cells induced suppression of ANXA1 protein (Fig. 5A), while its knockdown induced increased ANXA1 protein expression in HN30 cells, compared with their respective empty vector controls. Using a luciferase reporter plasmid containing the 3'-UTR of the ANXA1 gene demonstrated that there was direct interaction between ANXA1 and miR-196a, with a clear reduction in relative luciferase activity in the miR-196a overexpressing cells compared with controls ($p < 0.01$, Fig. 5C). Similarly, increased relative luciferase activity was observed in the miR-196a knockdown cells compared with their empty vector control ($p < 0.01$, Fig. 5D). Importantly, a reverse association between the endogenous levels of miR-196a and ANXA1 in the HNSCC cell lines tested was observed (Supporting Information Fig. S4).

ANXA1 silencing reproduces the oncogenic phenotype of mir-196a overexpression

The role of ANXA1 in HNSCC cell lines was further investigated by stably downregulating ANXA1 expression in the HN5 cell line with ANXA1 shRNA (Fig. 6A). Similar to the behaviour of the miR-196a overexpressing HN5 cells, ANXA1 knockdown resulted in enhanced cell proliferation assessed by growth rate over seven days, as well as cell survival measured by MTT assay over five days (Fig. 6B). Cell

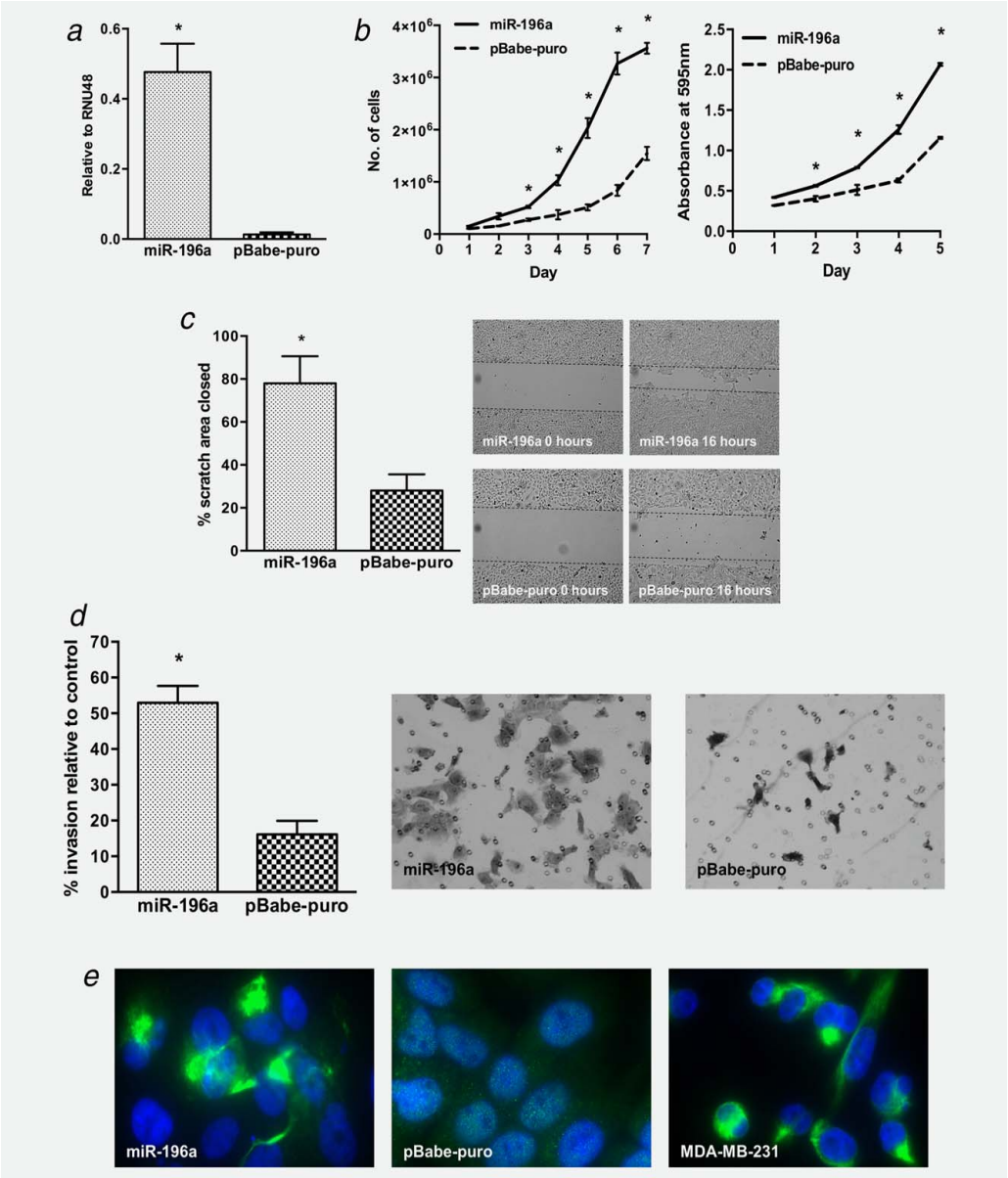

Figure 2. Overexpression of miR-196a increases cell proliferation, migration and invasion. (a) Mir-196a expression level by qRT-PCR after stable transfection of HN5 cells with miR-196a plasmid. (B) cell proliferation of miR-196a overexpressing cells was assessed by daily counting (left) and MTT cell viability assay (right). (C) cell migration by scratch assay at 16 hrs of miR-196a overexpressing cells compared with empty vector pBabe-puro, with representative images at 0 and 16 hrs at 4× magnification. Data shown as mean percentage scratch area closed after 16 hr. (D) invasion through matrigel in the miR-196a cells compared with control. Data represents mean number of invaded cells through the matrigel membrane relative to migration through the control membrane. Images are representative of cells fixed and stained on the invasion membrane at 10× magnification. (E) vimentin immunofluorescence of miR-196a cells compared with empty vector pBabe-puro and the mesenchymal breast cancer cell line MDA-MB-231. Images taken at 60× magnification. * $p < 0.05$. [Color figure can be viewed in the online issue, which is available at wileyonlinelibrary.com.]

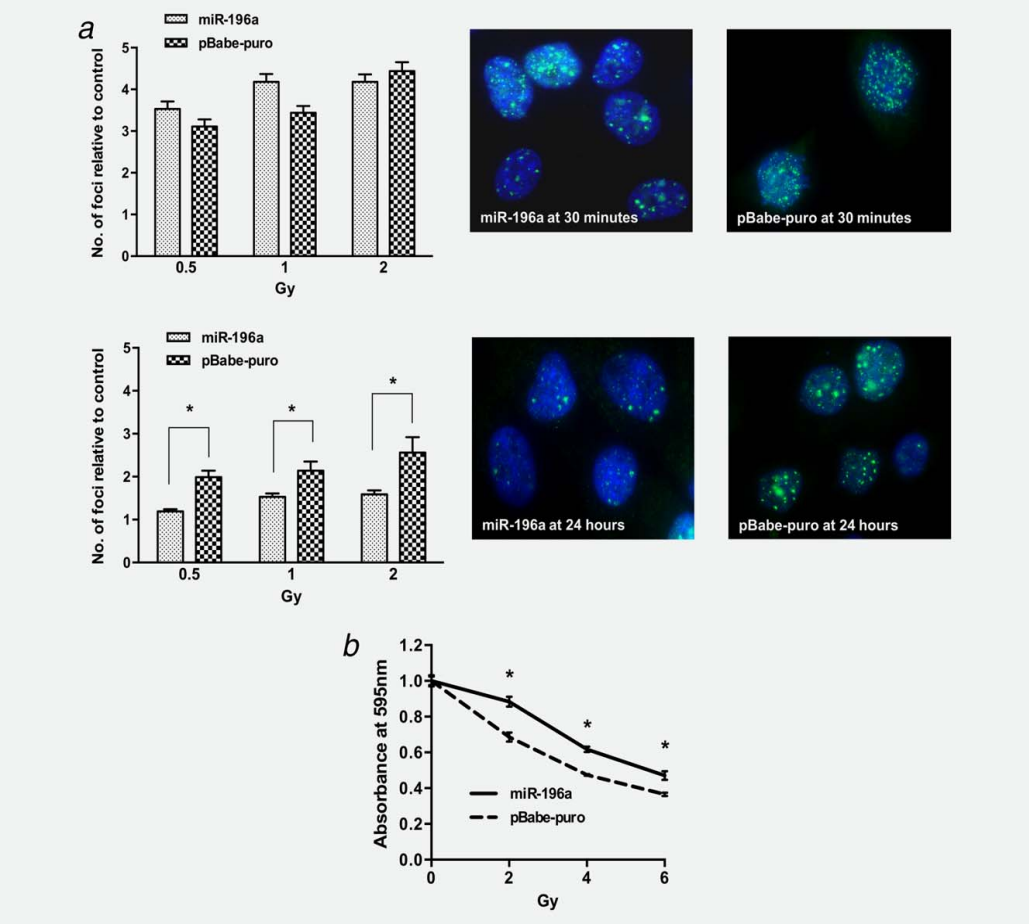

Figure 3. MiR-196a overexpression and response to irradiation. (a) MiR-196a overexpressing HN5 cells were irradiated at 0.5, 1 and 2 gy and stained for gamma H2AX foci at 30 min (top) and 24 hrs (bottom) post irradiation. The number of foci was analyzed in a minimum of 100 cells at each dose point and data is presented as the mean number of foci relative to unirradiated cells. Error bars represent standard error. Images are representative of cells irradiated at 0.5 gy at 60× magnification. (B) MTT cell viability of miR-196a and empty vector control HN5 cells five days after irradiation with 2, 4 and 6 gy. * $p < 0.05$. [Color figure can be viewed in the online issue, which is available at wileyonlinelibrary.com.]

migration was also significantly increased after 20 hr, with a mean percentage scratch area closed by 59% in the ANXA1 knockdown compared with 26% in control cells ($p < 0.01$, Fig. 6C). The mean percentage invasion relative to control was 41% in the ANXA1 knockdown cells and 20% in the ANXA1 empty vector control cells ($p < 0.01$, Fig 6D). Immunofluorescence analysis of ANXA1 knockdown cells also revealed similar changes in vimentin configuration to that of miR-196a overexpressing cells (Fig. 6E). ANXA1 silencing resulted in some resistance to irradiation (Fig. 6F). However, this was lower than that observed with miR-196a overexpression, suggesting that the miR-196a-induced radioresistance in HNSCC cells may not be entirely through ANXA1 suppression, and additional targets are likely to be involved.

Discussion

It has become clear that miRNAs play important roles in cancer development and metastasis and are potential predictive biomarkers and therapeutic targets. Expression profiling of a small exploratory cohort of HNSCC biopsy samples identified several miRNAs, which were differentially expressed, amongst which miR-196a was found to be highly upregulated in patients with poor outcome. Functional analysis demonstrated that overexpression of miR-196a in HNSCC cells with low endogenous levels significantly promoted cell proliferation, migration, invasion, and radioresistance, whereas knockdown of miR-196a in cells with high endogenous levels led to the opposite effects. Moreover, the antiproliferative effect of miR-196a is unlikely to be due to

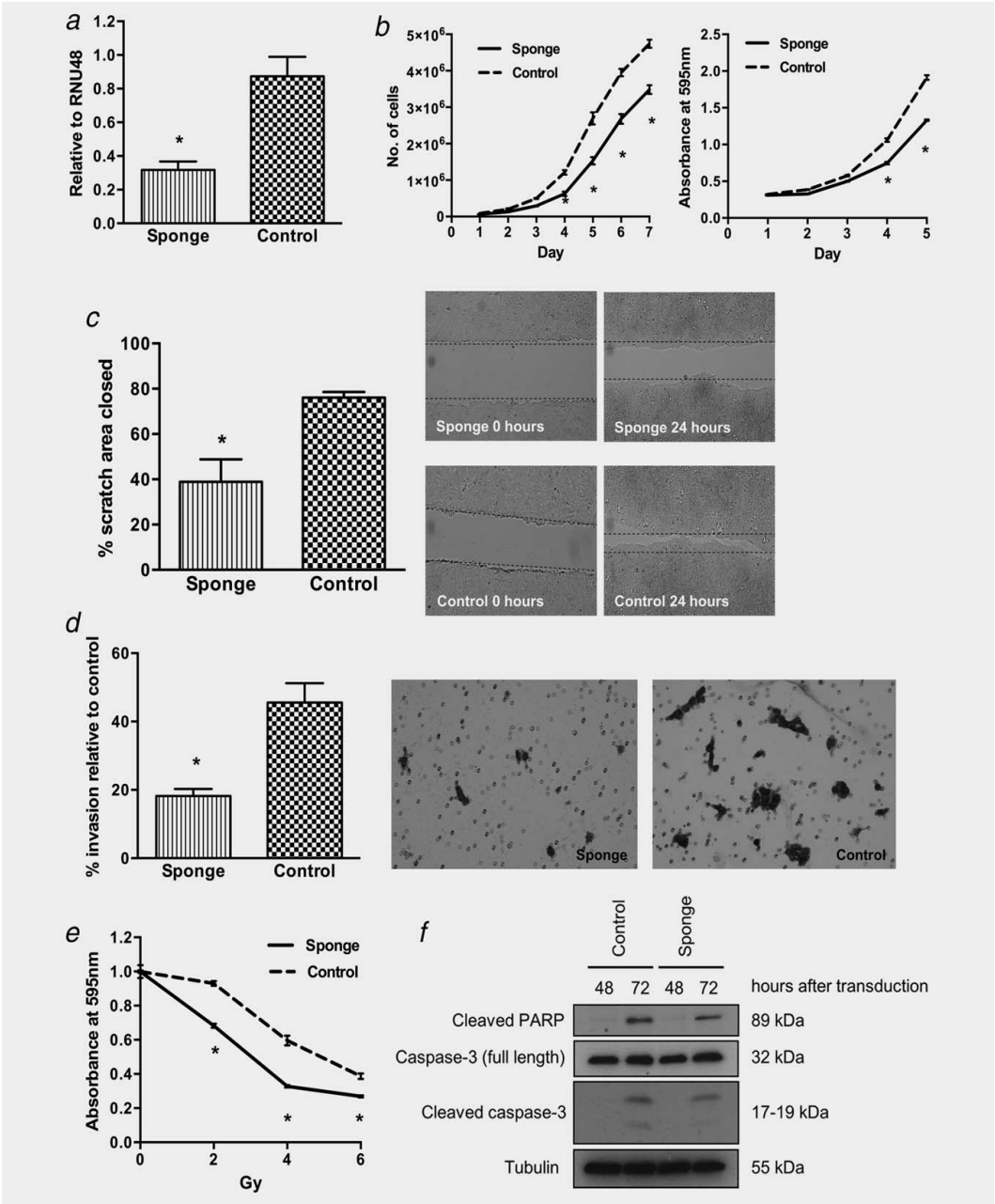

Figure 4. MiR-196a knockdown with miRNA sponge inhibits cell proliferation, migration, invasion and increases sensitivity to radiation compared with control. (a) HN30 cells were stably infected with miR-196a sponge to inhibit the expression of miR-196a and assessed by qRT-PCR. (B) cell proliferation of miR-196a downregulated HN30 cells was assessed by daily counting (left) and MTT cell viability assay (right). (C) cell migration by scratch assay of miR-196a sponge cells compared with empty vector control. Bar graph shows mean percentage of scratch area closed after 24 hrs incubation. Representative images are shown at 0 and 24 hrs, at 4× magnification. (D) invasion through matrigel in the miR-196a sponge cells compared with empty vector control. Bar graph represents the mean number of invaded cells through the matrigel membrane relative to migration through the control membrane. Images are representative of cells fixed and stained on the invasion membrane at 10× magnification. (E) assessment of response to radiation by MTT cell viability assay. Cells were irradiated at 2, 4 and 6 gy and data are expressed relative to unirradiated control cells. (F) western blot of proapoptotic markers cleaved PARP and caspase-3 in HN30 cells 48 and 72 hr after transient miR-196a knockdown using miR-196a sponge or empty vector control.

Int. J. Cancer: **137**, 1021–1034 (2015) © 2014 UICC

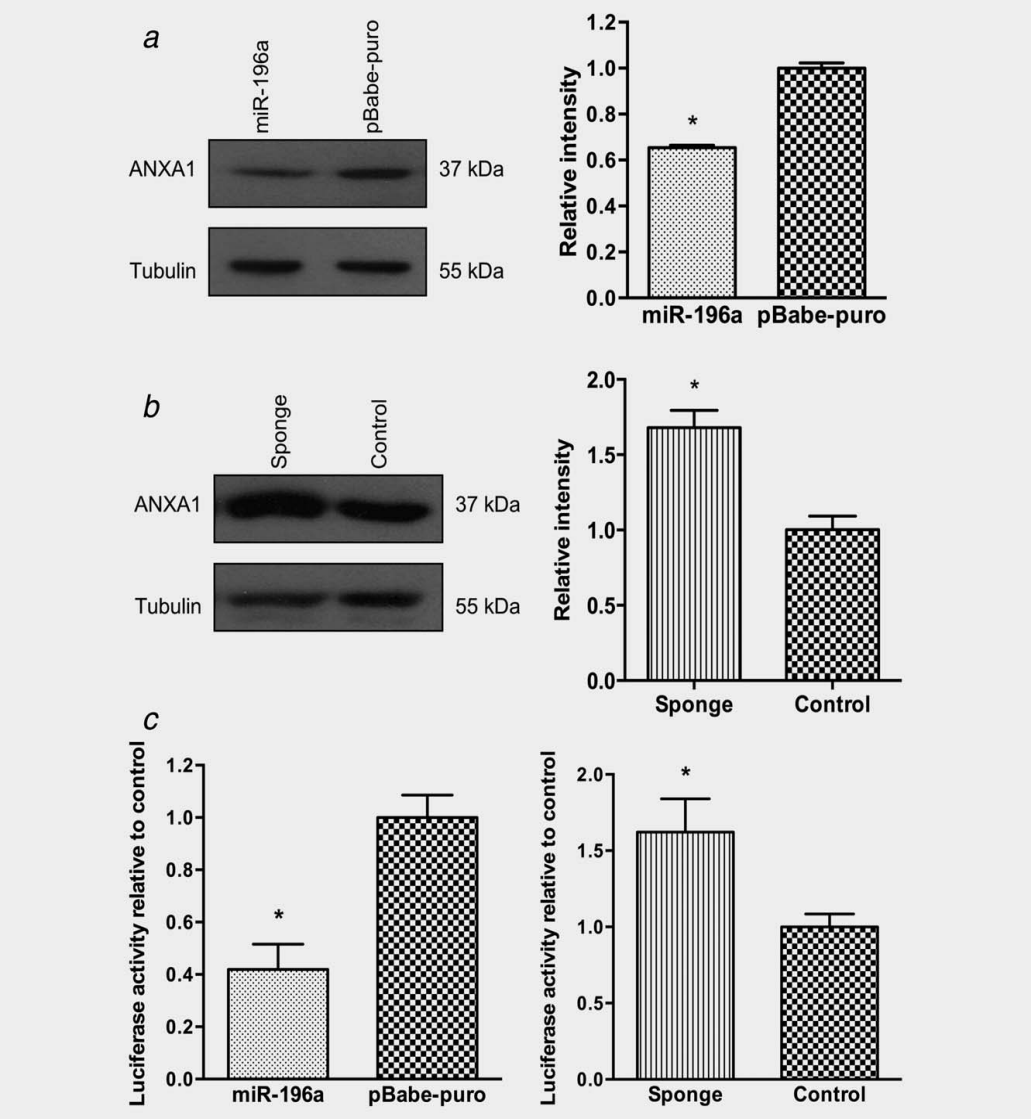

Figure 5. ANXA1 is a direct target of miR-196a. (a) western blot of ANXA1 protein levels in miR-196a overexpressing cells and pBabe-puro control, with tubulin as loading control. Bar graph shows mean quantification of the intensity of the bands by ImageJ. (B) western blot of ANXA1 protein level in miR-196a knockdown sponge and empty vector control. (C) luciferase reporter plasmid containing ANXA1 3'UTR was transfected into HN5 miR-196a overexpressing cells and the relative luciferase activity measured using the dual luciferase assay. (D) luciferase reporter plasmid containing ANXA1 3'UTR was transfected into HN30 miR-196a knockdown cells and the relative luciferase activity measured using the dual luciferase assay. * $p < 0.05$.

increased apoptosis, further suggesting a role for this miRNA in tumour invasiveness and resistance to therapy. However this requires further investigation.

Although overexpression of miR-196a has been demonstrated in several types of tumours, and in general is linked with a more aggressive, metastatic, tumour phenotype,[10,32] it has not previously been linked to radioresistance. The patient samples in this study were derived from cases that required radiotherapy, with patients developing recurrent disease demonstrating higher levels of pretreatment miR-196a. One of the important findings of our study was the significant effect of miR-196a overexpression on reducing radiation-induced gamma H2AX foci after 24 hrs, indicating more efficient repair of radiation-induced DNA damage, as well as

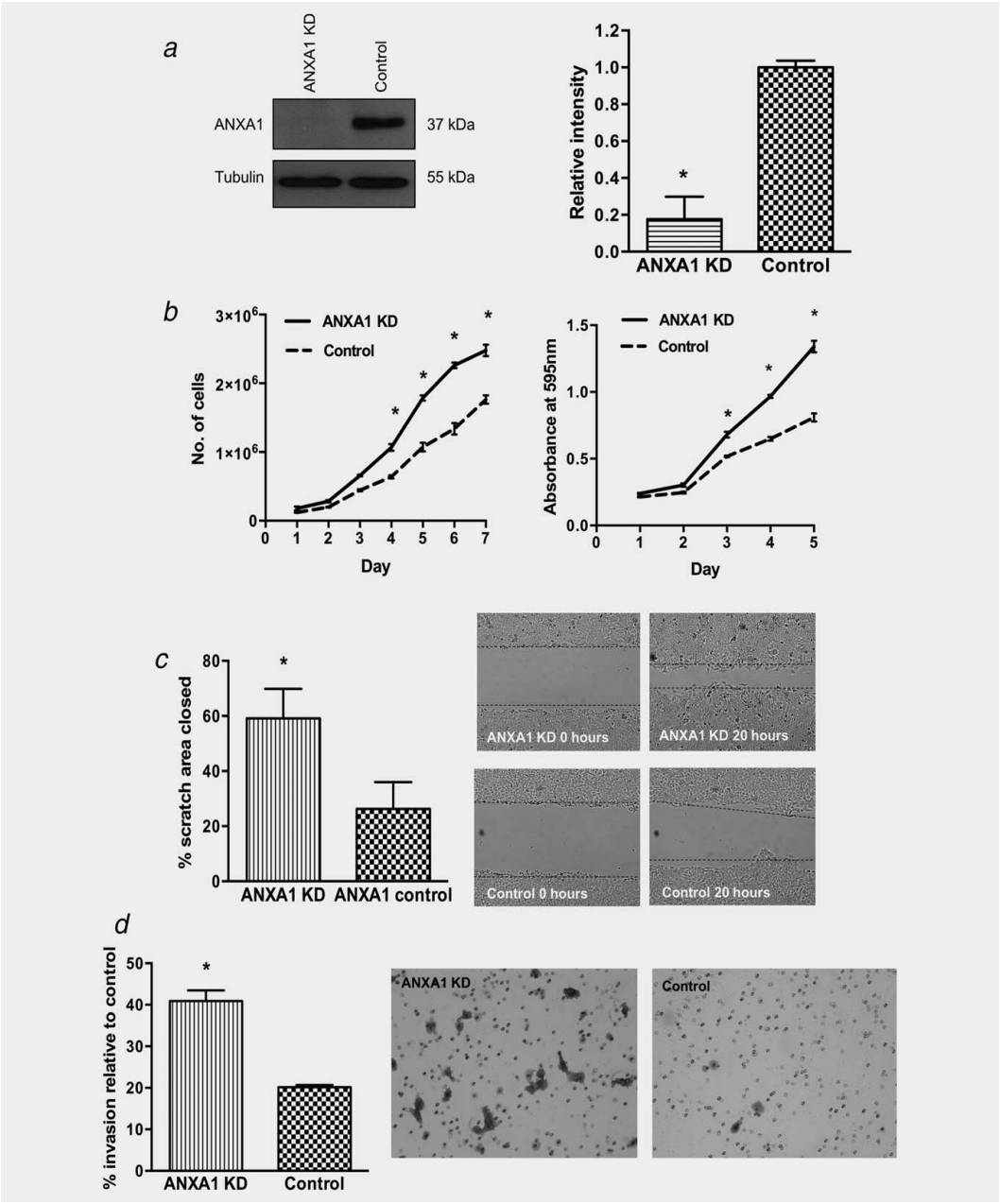

Figure 6. ANXA1 knockdown (ANXA1 KD) with shRNA increases cell proliferation, migration, invasion and alters vimentin immunofluorescence. (a) western blot of ANXA1 KD with shRNA in HN5 cells compared with empty vector control. (B) cell proliferation in ANXA1 KD measured by daily counting and MTT cell viability. (C) scratch assay to assess the effect of ANXA1 KD on migration. Data is expressed as mean percentage scratch area closed after 20 hrs of incubation and representative images at 0 and 20 hrs at 4× magnification are shown. (D) matrigel invasion assay. Data shown as mean percentage invasion relative to control membrane without matrigel. Images of the invasion membrane in ANXA1 KD and empty vector control cells, taken at 10x magnification. (E) vimentin immunofluorescence staining in ANXA1 KD cells compared with empty vector control. Images at 60x magnification. (F) analysis of response to radiation of ANXA1 knockdown HN5 cells as assessed using MTT cell viability assay 5 days after irradiation. * $p < 0.05$. [Color figure can be viewed in the online issue, which is available at wileyonlinelibrary.com.]

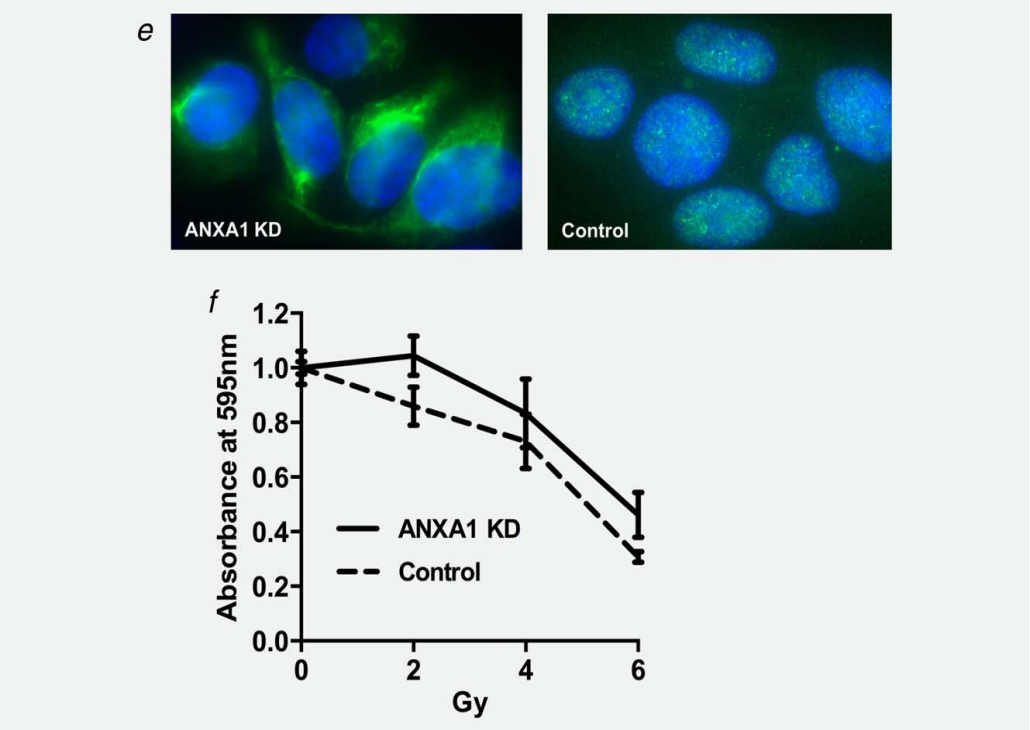

Figure 6. Continued.

increased cell viability after irradiation. These data suggest that miR-196a could have potential value as a predictive biomarker of radiation response, identifying patients at diagnosis who are more likely to fail conventional radiation treatments. In addition, the modulation of miR-196a and/or its target genes could have a therapeutic potential as a radiation sensitising agent. In agreement with our data Liu *et al.*also demonstrated an association between higher miR-196a expression in tumours and worse disease free survival in patients with OSCC.[7] However, it is unclear how many patients in the Liu *et al.* study received radiotherapy, and whether the worse survival could be due to increased radioresistance.

Several cellular genes with important roles in proliferation, adhesion and apoptosis have been shown to be targets of miR-196a.[33] Of these targets there is strong evidence that ANXA1 expression decreases during the development and progression of cancer. In oral cancer tissues, low ANXA1 expression is associated with poorer differentiation status,[22–24] with forced ANXA1 overexpression significantly reducing cell proliferation in oral squamous cell carcinoma lines and nude mice, whereas downregulation increased proliferation.[24] These effects are consistent with the phenotypic characteristics of our miR-196a overexpressing cells, prompting further investigation into ANXA1 as a target of interest in this study. An inverse correlation between miR-196a and ANXA1 expression has been previously shown in oesophageal, breast and endometrial cancer cell lines, but not in HNSCC.[16] Here, we show that ANXA1 is a direct target of miR-196a in head and neck cancer cell lines, and that knockdown of ANXA1 resulted in a more aggressive tumour cell phenotype. Interestingly, we observed that overexpression of miR-196a in HNSCC cell lines had a clear effect on the expression pattern of vimentin, a known marker of EMT. ANXA1 downregulation by shRNA reproduced similar changes in vimentin expression as observed by miR-196a upregulation. ANXA1 overexpression has been shown to attenuate EMT and metastasis in breast cancer, with knockdown resulting in stimulation of EMT.[34] We demonstrate a similar role of EMT promotion by ANXA1 knockdown in HNSCC, which may occur through suppression mediated by miR-196a.

Several mechanisms for the anti-proliferative function of ANXA1 have been suggested. In myelo-monocytic cells and broncho-alveolar epithelial cells ANXA1 has been shown to stimulate apoptosis.[35,36] ANXA1 can bind to NF-κB, suppressing its transcriptional activity, leading to enhancement of apoptotic cell death and inhibition of cell growth.[37,38] In addition, ANXA1 expression is strongly induced in thyroid carcinoma cells during tumour necrosis factor-related

apoptosis inducing ligand (TRAIL)-induced apoptosis.[39] Another possible mechanism for the anti-proliferative action of ANXA1 could be due to the activation of the extracellular receptor kinase (ERK) signalling cascade, as demonstrated in a variety of cell types. This results in disruption of the actin cytoskeleton, inhibition of cyclin D1 and subsequent suppression of cell proliferation.[40,41] Furthermore, ANXA1 is a substrate for the tyrosine kinase activity of the epidermal growth factor (EGF) receptor,[42] which is expressed in over 90% of HNSCC,[43] and has been shown to block EGF-induced cell proliferation.[44] Interestingly, both activation of EGFR signalling and overexpression of cyclin D1 are strongly implicated in head and neck cancer progression. It would therefore be interesting to explore whether miR-196a through its target ANXA1 influences EGFR signalling and the cell cycle pathway on HNSCC tumour behaviour. It is important to mention that although the majority of evidence indicates a tumour suppressor role for ANXA1, an oncogenic role has also been reported in cancers such as lung[21] and stomach.[45] ANXA1 has also been shown to be a major regulator of endothelial cell migration, and thereby angiogenesis in response to vascular endothelial growth factor (VEGF).[46,47] Additionally, apoptosis-induced externalization of endogenous cytosolic ANXA1 was found to initiate an anti-inflammatory effector mechanism that suppressed the immune response against antigens of apoptotic cells.[48] The opposing functions of ANXA1 are likely to be cell type specific and may also depend on other factors including tissue microenvironment and immune response.

Downregulation of ANXA1 has been hypothesised to increase radioresistance in nasopharyngeal carcinoma.[49] We observed a trend towards radioresistance in ANXA1 knockdown cells, whereas miR-196a modulation had a more profound effect on radioresistance. MiR-196a has several cellular targets, and it is likely that other target proteins play roles in the response to radiation. Recent reported targets of miR-196a include IκBα, an inhibitor of NF-κB. In glioblastoma multiforme miR-196a, which is upregulated and associated with poor outcome, has been shown to directly interact with IκBα 3'-UTR to suppress IκBα expression and subsequently promote NF-κB activation, enhance proliferation and suppress apoptosis.[8] Similar results have also been demonstrated in pancreatic cancer.[10] In cervix and gastric cancers increased miR-196a expression has shown to be associated with advanced tumour stage and poor outcome,[9,11] and $p27^{kip1}$, a cyclin-dependent kinase inhibitor known to prevent cell cycle progression, was identified as a direct target. These findings highlight that there are multiple targets of miR-196a which may contribute to the behaviour and response to therapy, and these targets may depend on the tumour type.

In conclusion, miR-196a is an oncogene in HNSCC and its overexpression is associated with increased tumourigenic potential and radioresistance. ANXA1 is a direct target of miR-196a and acts as a tumour suppressor in these cells. The clear association between ANXA1 and cancer suggests that its suppression by miR-196a may be an important step in the oncogenesis of HNSCC. Expression levels of miR-196a may represent a predictive biomarker for selecting patients for individualized therapy, and its target ANXA1 could be an important focus for future targeted therapy in HNSCC. Confirmation in a larger number of patient samples and *in vivo* studies are required in order to establish a clinical application for miR-196a and ANXA1 in cancers of head and neck.

Acknowledgments

Yae-eun Suh is funded by the King's Health Partner's Research and Development Challenge Fund and The Rosetrees Trust. Yae-eun Suh and Katherine Lawler also receive funding from the CRUK and EPSRC Comprehensive Cancer Imaging Centre at KCL and UCL (C1519/10331 and C1519/A16463) and the European Framework Programme 7 HEALTH-2010 grant entitled Imagin (grant number 259881). We would like to thank Dr Sebastian Herzog, Division of Developmental Immunology, Medical University of Innsbruck, Austria, for microRNA sponge constructs, Dr Anne-Laure Pin for constructing the Annexin A1 plasmids in Dr. Jacques Huot's laboratory, which were used in this study. Also, the authors would like to thank Dr Loris De Cecco, Fondazione IRCCS Istituto Nazionale dei Tumori, Milan, for important contribution to the microRNA expression profiling data.

Patient tissue samples and data were provided by Guy's & St Thomas' Head & Neck Biobank – part of the KHP Cancer Biobank, which is supported by the Department of Health *via* the National Institute for Health Research (NIHR) comprehensive Biomedical Research Centre award and Guy's & St Thomas' NHS Foundation Trust.

References

1. Suh Y, Amelio I, Guerrero Urbano T, Tavassoli M. Clinical update on cancer: molecular oncology of head and neck cancer. *Cell Death Dis* 2014; 5: e1018.
2. Lewis BP, Shih IH, Jones-Rhoades MW, Bartel DP, Burge CB. Prediction of mammalian microRNA targets. *Cell* 2003; 115:787–98.
3. Bartel DP. MicroRNAs: genomics, biogenesis, mechanism, and function. *Cell* 2004; 116:281–97.
4. Lu J, Getz G, Miska EA, Alvarez-Saavedra E, Lamb J, Peck D, Sweet-Cordero A, Ebert BL, Mak RH, Ferrando AA, Downing JR, Jacks T, Horvitz HR, Golub TR. MicroRNA expression profiles classify human cancers. *Nature* 2005; 435: 834–8.
5. Chen CZ. MicroRNAs as oncogenes and tumor suppressors. *N Engl J Med* 2005; 353:1768–71.
6. Shiiba M, Shinozuka K, Saito K, Fushimi K, Kasamatsu A, Ogawara K, Uzawa K, Ito H, Takiguchi Y, Tanzawa H. MicroRNA-125b regulates proliferation and radioresistance of oral squamous cell carcinoma. *Br J Cancer* 2013; 108: 1817–21.
7. Liu CJ, Tsai MM, Tu HF, Lui MT, Cheng HW, Lin SC. miR-196a overexpression and miR-196a2 gene polymorphism are prognostic predictors of oral carcinomas. *Ann Surg Oncol* 2013; 20(Suppl 3):S406–14.
8. Yang G, Han D, Chen X, Zhang D, Wang L, Shi C, Zhang W, Li C, Liu H, Kang J, Peng F, Liu Z, Qi J, Gao X, Ai J, Zhao S. MiR-196a exerts its oncogenic effect in glioblastoma multiforme by inhibition of IkappaBalpha both in vitro and in vivo. *Neuro Oncol* 2014; 16:652–61.
9. Hou T, Ou J, Zhao X, Huang X, Huang Y, Zhang Y. MicroRNA-196a promotes cervical cancer proliferation through the regulation of FOXO1 and p27Kip1. *Br J Cancer* 2014; 110:1260–8.
10. Huang F, Tang J, Zhuang X, Zhuang Y, Cheng W, Chen W, Yao H, Zhang S. MiR-196a promotes pancreatic cancer progression by targeting nuclear factor kappa-B-inhibitor alpha. *PLoS One* 2014; 9:e87897.
11. Sun M, Liu XH, Li JH, Yang JS, Zhang EB, Yin DD, Liu ZL, Zhou J, Ding Y, Li SQ, Wang ZX,

Cao XF, De W. MiR-196a is upregulated in gastric cancer and promotes cell proliferation by downregulating p27(kip1). *Mol Cancer Ther* 2012; 11:842–52.
12. Debernardi S, Skoulakis S, Molloy G, Chaplin T, Dixon-McIver A, Young BD. MicroRNA miR-181a correlates with morphological sub-class of acute myeloid leukaemia and the expression of its target genes in global genome-wide analysis. *Leukemia* 2007; 21:912–6.
13. Braig S, Mueller DW, Rothhammer T, Bosserhoff AK. MicroRNA miR-196a is a central regulator of HOX-B7 and BMP4 expression in malignant melanoma. *Cell Mol Life Sci* 2010; 67:3535–48.
14. Mueller DW, Bosserhoff AK. MicroRNA miR-196a controls melanoma-associated genes by regulating HOX-C8 expression. *Int J Cancer* 2011; 129:1064–74.
15. Severino P, Bruggemann H, Andreghetto FM, Camps C, Klingbeil Mde F, de Pereira WO, Soares RM, Moyses R, Wunsch-Filho V, Mathor MB, Nunes FD, Ragoussis J, Tajara EH. MicroRNA expression profile in head and neck cancer: HOX-cluster embedded microRNA-196a and microRNA-10b dysregulation implicated in cell proliferation. *BMC Cancer* 2013; 13:533
16. Luthra R, Singh RR, Luthra MG, Li YX, Hannah C, Romans AM, Barkoh BA, Chen SS, Ensor J, Maru DM, Broaddus RR, Rashid A, Albarracin CT. MicroRNA-196a targets annexin A1: a microRNA-mediated mechanism of annexin A1 downregulation in cancers. *Oncogene* 2008; 27: 6667–78.
17. Maru DM, Singh RR, Hannah C, Albarracin CT, Li YX, Abraham R, Romans AM, Yao H, Luthra MG, Anandasabapathy S, Swisher SG, Hofstetter WL, Rashid A, Luthra R. MicroRNA-196a is a potential marker of progression during barrett's metaplasia-dysplasia-invasive adenocarcinoma sequence in esophagus. *Am J Pathol* 2009; 174: 1940–8.
18. Coskun E, von der Heide EK, Schlee C, Kuhnl A, Gokbuget N, Hoelzer D, Hofmann WK, Thiel E, Baldus CD. The role of microRNA-196a and microRNA-196b as ERG regulators in acute myeloid leukemia and acute T-lymphoblastic leukemia. *Leuk Res* 2011; 35:208–13.
19. Lim LH, Pervaiz S. Annexin 1: the new face of an old molecule. *FASEB J* 2007; 21:968–75.
20. Cheng SX, Tu Y, Zhang S. FoxM1 promotes glioma cells progression by up-regulating Anxa1 expression. *PLoS One* 2013; 8:e72376
21. Liu YF, Zhang PF, Li MY, Li QQ, Chen ZC. Identification of annexin A1 as a proinvasive and prognostic factor for lung adenocarcinoma. *Clin Exp Metastasis* 2011; 28:413–25.
22. Garcia Pedrero JM, Fernandez MP, Morgan RO, Herrero Zapatero A, Gonzalez MV, Suarez Nieto C, Rodrigo JP. Annexin A1 down-regulation in head and neck cancer is associated with epithelial differentiation status. *Am J Pathol* 2004; 164:73–9.
23. Zhang L, Yang X, Zhong LP, Zhou XJ, Pan HY, Wei KJ, Li J, Chen WT, Zhang ZY. Decreased expression of annexin A1 correlates with pathologic differentiation grade in oral squamous cell carcinoma. *J Oral Pathol Med* 2009; 38:362–70.
24. Zhu DW, Yang X, Yang CZ, Ma J, Liu Y, Yan M, Wang LZ, Li J, Zhang CP, Zhang ZY, Zhong LP. Annexin A1 down-regulation in oral squamous cell carcinoma correlates to pathological differentiation grade. *Oral Oncol* 2013; 49:542–50.
25. Paweletz CP, Ornstein DK, Roth MJ, Bichsel VE, Gillespie JW, Calvert VS, Vocke CD, Hewitt SM, Duray PH, Herring J, Wang QH, Hu N, Linehan WM, Taylor PR, Liotta LA, Emmert-Buck MR, Petricoin EF. 3rd. Loss of annexin 1 correlates with early onset of tumorigenesis in esophageal and prostate carcinoma. *Cancer Res* 2000; 60: 6293–7.
26. Rodrigo JP, Garcia-Pedrero JM, Fernandez MP, Morgan RO, Suarez C, Herrero A. Annexin A1 expression in nasopharyngeal carcinoma correlates with squamous differentiation. *Am J Rhinol* 2005; 19:483–7.
27. Dunning MJ, Smith ML, Ritchie ME, Tavare S. beadarray: R classes and methods for illumina bead-based data. *Bioinformatics* 2007; 23:2183–4.
28. Smyth GK. Linear models and empirical bayes methods for assessing differential expression in microarray experiments. *Stat Appl Genet Mol Biol* 2004; 3:Article3
29. Benjamini Y, Hochberg Y. Controlling the false discovery rate: a practical and pawerful approach to multiple testing. *Journal of the Royal Statistical Society: Series B (Statistical Methodology)* 1995; 57:289–300.
30. Bouquet F, Muller C, Salles B. The loss of gamma H2AX signal is a marker of DNA double strand breaks repair only at low levels of DNA damage. *Cell Cycle* 2006; 5:1116–22.
31. Kluiver J, Gibcus JH, Hettinga C, Adema A, Richter MK, Halsema N, Slezak-Prochazka I, Ding Y, Kroesen BJ, van den Berg A. Rapid generation of microRNA sponges for microRNA inhibition. *PLoS One* 2012; 7:e29275
32. Tsai MM, Wang CS, Tsai CY, Chen CY, Chi HC, Tseng YH, Chung PJ, Lin YH, Chung IH, Chen CY, Lin KH. MicroRNA-196a/-196b promote cell metastasis via negative regulation of radixin in human gastric cancer. *Cancer Lett* 2014; 351:222–31.
33. Chen C, Zhang Y, Zhang L, Weakley SM, Yao Q. MicroRNA-196: critical roles and clinical applications in development and cancer. *J Cell Mol Med* 2011; 15:14–23.
34. Maschler S, Gebeshuber CA, Wiedemann EM, Alacakaptan M, Schreiber M, Custic I, Beug H. Annexin A1 attenuates EMT and metastatic potential in breast cancer. *EMBO Mol Med* 2010; 2:401–14.
35. Solito E, de Coupade C, Canaider S, Goulding NJ, Perretti M. Transfection of annexin 1 in monocytic cells produces a high degree of spontaneous and stimulated apoptosis associated with caspase-3 activation. *Br J Pharmacol* 2001; 133:217–28.
36. Debret R, El Btaouri H, Duca L, Rahman I, Radke S, Haye B, Sallenave JM, Antonicelli F. Annexin A1 processing is associated with caspase-dependent apoptosis in BZR cells. *FEBS Lett* 2003; 546:195–202.
37. Tabe Y, Jin L, Contractor R, Gold D, Ruvolo P, Radke S, Xu Y, Tsutusmi-Ishii Y, Miyake K, Miyake N, Kondo S, Ohsaka A, Nagaoka I, Andreeff M, Konopleva M. Novel role of HDAC inhibitors in AML1/ETO AML cells: activation of apoptosis and phagocytosis through induction of annexin A1. *Cell Death Differ* 2007; 14:1443–56.
38. Zhang Z, Huang L, Zhao W, Rigas B. Annexin 1 induced by anti-inflammatory drugs binds to NF-kappaB and inhibits its activation: anticancer effects in vitro and in vivo. *Cancer Res* 2010; 70: 2379–88.
39. Petrella A, Festa M, Ercolino SF, Zerilli M, Stassi G, Solito E, Parente L. Induction of annexin-1 during TRAIL-induced apoptosis in thyroid carcinoma cells. *Cell Death Differ* 2005; 12: 1358–60.
40. Alldridge LC, Bryant CE. Annexin 1 regulates cell proliferation by disruption of cell morphology and inhibition of cyclin D1 expression through sustained activation of the ERK1/2 MAPK signal. *Exp Cell Res* 2003; 290:93–107.
41. Alldridge LC, Harris HJ, Plevin R, Hannon R, Bryant CE. The annexin protein lipocortin 1 regulates the MAPK/ERK pathway. *J Biol Chem* 1999; 274:37620–8.
42. Pepinsky RB, Sinclair LK. Epidermal growth factor-dependent phosphorylation of lipocortin. *Nature* 1986; 321:81–4.
43. Ang KK, Berkey BA, Tu X, Zhang HZ, Katz R, Hammond EH, Fu KK, Milas L. Impact of epidermal growth factor receptor expression on survival and pattern of relapse in patients with advanced head and neck carcinoma. *Cancer Res* 2002; 62:7350–6.
44. Croxtall JD, Waheed S, Choudhury Q, An R, Flower RJ. Nterminal peptide fragments of lipocortin-1 inhibit A549 cell growth and block EGF-induced stimulation of proliferation. *Int J Cancer* 1993; 54:153–8.
45. Cheng TY, Wu MS, Lin JT, Lin MT, Shun CT, Huang HY, Hua KT, Kuo ML. Annexin A1 is associated with gastric cancer survival and promotes gastric cancer cell invasiveness through the formyl peptide receptor/extracellular signal-regulated kinase/integrin beta-1-binding protein 1 pathway. *Cancer* 2012; 118:5757–67.
46. Cote MC, Lavoie JR, Houle F, Poirier A, Rousseau S, Huot J. Regulation of vascular endothelial growth factor-induced endothelial cell migration by LIM kinase 1-mediated phosphorylation of annexin 1. *J Biol Chem* 2010; 285:8013–21.
47. Pin AL, Houle F, Fournier P, Guillonneau M, Paquet ER, Simard MJ, Royal I, Huot J. Annexin-1-mediated endothelial cell migration and angiogenesis are regulated by VEGF-induced inhibition of miR-196a expression. *J Biol Chem* 2012; 287: 30541–51.
48. Weyd H, Abeler-Dorner L, Linke B, Mahr A, Jahndel V, Pfrang S, Schnolzer M, Falk CS, Krammer PH. Annexin A1 on the surface of early apoptotic cells suppresses CD8+ T cell immunity. *PLoS One* 2013; 8:e62449.
49. Zeng GQ, Cheng AL, Tang J, Li GQ, Li MX, Qu JQ, Cao C, Liao L, Xiao ZQ. Annexin A1: a new biomarker for predicting nasopharyngeal carcinoma response to radiotherapy. *Med Hypotheses* 2013; 81:68–70.